

Genome-wide analysis of gene expression
and alternative splicing in
human medulloblastoma

FRANCESCA MENGHI

A thesis submitted for the Degree of Doctor of Philosophy

Institute of Child Health
University College London

2010

Declaration

I, Francesca Menghi, confirm that the work presented in this thesis is my own. Where work has been derived from other sources, I confirm that this has been indicated in the thesis.

Signed

Date

*To my grandmother,
who always thought I was a Doctor*

*Alla mia nonna,
che ha sempre pensato fossi un Dottore*

Acknowledgments

I would first like to thank my supervisor, Dr. Jonathan Ham, for giving me the opportunity to work on this PhD project and for his confidence in my abilities and his enthusiasm. I am equally grateful to my secondary supervisor, Dr. Thomas Jacques, for his guidance and essential contribution to this project. My gratitude also goes to Dr. Mike Hubank, whose insight during the first stages of the microarray study as well as throughout its realisation was extremely valuable.

For giving me their support, encouragement and friendship, I am extremely grateful to previous and current members of the Molecular Haematology and Cancer Biology Unit at ICH. In particular, I would like to thank Susy, who introduced me to the mouse cerebellum, and Martino, whose mathematical wit has been enlightening in many occasions. Olesya is the best companion you would want to have on a late night at work, and although we often ended up chatting about science rather than doing science, those evenings were always a source of inspiration. I would like to thank Daisy for welcoming me to the lab from the very beginning and for having been such a good friend since. I'm grateful to Jasper for his most generous help and for his genuine interest in my neurons and their little legs. My PhD wouldn't have been such an enjoyable experience hadn't Rosie and Mark been there. I will be forever grateful for their support, their patience with my frequent enquires about science and English grammar and their great sense of humour.

This project was funded by the Olivia Hodson Cancer Fund and the Annabel McEnery Children's Cancer Fund. My sincere gratitude goes to Olivia's and Annabel's families and friends and all of the charities' trustees. In particular, I would like to express my appreciation for Michael and Maria McEnery, for having so much faith in me and for giving me the most valuable reasons to keep doing what I do.

Abstract

Medulloblastoma is a malignant embryonal tumour of the cerebellum which most commonly affects children. A subset of tumours is thought to arise from cerebellar granule cell precursors (GCPs) that fail to undergo normal neuronal development, following the hyper-activation of the Sonic hedgehog (Shh) signalling pathway.

To identify candidate genes that might be important for medulloblastoma pathogenesis, I investigated patterns of gene expression and alternative splicing in 14 paediatric medulloblastoma and five normal cerebellar samples using Affymetrix Human Exon arrays. Statistical analysis of the gene expression data identified a group of medulloblastomas with a molecular signature of Shh pathway activation. These tumours showed higher expression levels of genes involved in spindle formation, cytokines, and cell cycle regulation. Further studies using an *in vitro* mouse GCP cell culture model, in which Shh is necessary for the maintenance of the progenitor state, showed that a selection of candidate genes was also over-expressed when GCPs were cultured in the presence of Shh, as compared to control cells, as well as in human medulloblastoma cell lines. Ongoing and future *in vitro* experiments will investigate the potential role of candidate genes in sustaining the growth of precursor and tumour cells.

Exon-level analysis of gene expression showed that abnormal expression of different transcript variants is likely to occur in medulloblastoma. I selected several examples of differential exon usage and validated these using an independent set of normal and tumour specimens. Tumour-associated splicing alterations were highly consistent, enabling clear separation of normal and cancer samples and in some cases of different medulloblastoma molecular subgroups. Interestingly, Shh-treated GCPs recapitulated the

splicing patterns observed in the tumour samples for six out of the eight genes analysed, suggesting that the preferential expression of specific transcript forms is regulated during normal cerebellar development. The possible relationship between inappropriate splicing and medulloblastoma pathogenesis will be the subject of future investigation.

Table of Contents

DECLARATION	2
ACKNOWLEDGMENTS	4
ABSTRACT	5
TABLE OF CONTENTS	7
LIST OF FIGURES	12
LIST OF TABLES	14
ABBREVIATIONS	15
CHAPTER 1: INTRODUCTION	16
1.1. MEDULLOBLASTOMA	16
1.2. MEDULLOBLASTOMA PATHOLOGY	17
1.2.1. <i>Classic medulloblastoma</i>	17
1.2.2. <i>Desmoplastic medulloblastoma</i>	19
1.2.3. <i>Large cell/anaplastic medulloblastoma</i>	19
1.3. MEDULLOBLASTOMA CYTOGENETICS.....	19
1.4. THE STRUCTURE OF THE MATURE CEREBELLUM	22
1.5. OVERVIEW OF CEREBELLAR DEVELOPMENT	23
1.6. CONTROL OF GCP PROLIFERATION IN THE POST-NATAL CEREBELLUM.....	25
1.6.1. <i>The Sonic hedgehog signalling pathway</i>	25
1.6.2. <i>Shh effectors</i>	27
1.6.2.1. <i>Mycn</i>	28
1.6.2.2. <i>Mad3</i>	30
1.6.2.3. <i>Bmi1</i>	30
1.6.2.4. <i>The IGF pathway and Irs1</i>	31
1.6.2.5. <i>Yap1</i>	31
1.6.3. <i>Atoh1</i>	32
1.6.4. <i>Bone morphogenetic proteins</i>	33
1.6.5. <i>Fibroblast growth factor</i>	34
1.6.6. <i>REN</i>	35
1.7. THE ORIGIN OF SHH-DRIVEN MEDULLOBLASTOMA	35
1.8. SHH-INDEPENDENT MEDULLOBLASTOMAS	38

1.9. GENE EXPRESSION PROFILING OF MEDULLOBLASTOMA	40
1.10. MOLECULAR CLASSIFICATION OF HUMAN MEDULLOBLASTOMA BASED ON GENE EXPRESSION PROFILES	46
1.11. ALTERNATIVE mRNA SPLICING	50
1.11.1 <i>Alternative splicing in cancer biology</i>	53
1.11.2 <i>Relevance of alternative splicing in medulloblastoma</i>	56
1.11.2.1. The <i>ErbB-4</i> gene	56
1.11.2.2. <i>Survivin</i>	57
1.11.2.3. The <i>Ptch</i> gene	57
1.11.2.4. The <i>Mtss1</i> gene	58
1.12. AIM OF THIS STUDY	59
CHAPTER 2: MATERIALS AND METHODS	60
2.1. HUMAN SPECIMEN COLLECTION AND CLASSIFICATION	60
2.1.1. <i>Samples for Exon array analysis</i>	60
2.1.2. <i>Samples for validation of differential splicing</i>	60
2.1.3. <i>Tumour histopathology</i>	61
2.2. EXON ARRAY STUDY	62
2.2.1. <i>RNA processing and array hybridisation</i>	62
2.2.2. <i>Affymetrix Human Exon 1.0 ST array</i>	64
2.2.3. <i>Exon array analysis software</i>	64
2.2.4. <i>Gene level summary, quality control and analysis</i>	66
2.2.5. <i>Alternative splicing analysis</i>	67
2.3. CELL BIOLOGY	68
2.3.1. <i>Cell lines</i>	68
2.3.1.1. <i>Daoy</i>	68
2.3.1.2. <i>UW228-2</i>	69
2.3.1.3. <i>D425 Med</i>	69
2.3.1.4. <i>293FT</i>	70
2.3.2. <i>Cell culture conditions</i>	70
2.3.3. <i>Subculture</i>	71
2.3.4. <i>Freezing cultured cells</i>	71
2.3.5. <i>Recovery of frozen cells</i>	71
2.3.6. <i>Isolation and culture of mouse granule cell precursors</i>	72
2.3.6.1. <i>Granule cell precursor preparation</i>	72
2.3.6.2. <i>Poly-D-lysine coating of culture plates</i>	73

2.3.6.3. Preparation of <i>Shh</i> and mock supernatants	73
2.3.7. Producing lentivirus in 293FT cells	74
2.3.8. Lentiviral transduction of immortalised cell lines	75
2.3.9. Flow cytometry	75
2.3.9.1. Detection of EGFP-positive cells	76
2.3.9.2. Cell cycle analysis	76
2.3.9.3. Bromodeoxyuridine staining for flow cytometry analysis	77
2.3.10. Immunocytochemistry	78
2.3.10.1. Coverslip preparation	78
2.3.10.2. Intracellular antigen staining	78
2.3.10.3. Bromodeoxyuridine staining for immunocytochemistry	79
2.3.10.4. Image capture and processing	80
2.4. MOLECULAR BIOLOGY	80
2.4.1. Total RNA isolation	80
2.4.1.1. RNA isolation from frozen tissues using the RNeasy mini kit	80
2.4.1.2. RNA isolation using the TRIzol reagent	80
2.4.1.3. RNA quality control	81
2.4.2. First strand cDNA synthesis	81
2.4.3. Polymerase Chain Reaction (PCR)	82
2.4.3.1. Primer design	82
2.4.3.2. Semi-quantitative PCR	83
2.4.3.3. Estimation of the ratio between cassette-exon splice variants	83
2.4.3.4. Real Time PCR	84
2.4.4. Preparation of protein extracts from cells in culture	85
2.4.5. Western blotting	85
2.5. MOLECULAR CLONING	87
2.5.1. Plasmid vectors	87
2.5.1.1. Rat <i>ShhN</i> expression plasmid	87
2.5.1.2. pGIPZ lentiviral vector	87
2.5.1.3. pGIPZ-SFFV lentiviral vector	88
2.5.2. Restriction digestion	89
2.5.3. Blunting reaction	89
2.5.4. Agarose gel electrophoresis	89
2.5.5. Purification of DNA from agarose gels	91
2.5.6. Ligation of DNA fragments	91
2.5.7. Bacterial transformation	91

2.5.8. Isolation of Plasmid DNA	92
2.5.9. PCR subcloning	93
2.5.10. Sequencing.....	93
2.6. STATISTICS	94
2.7. BUFFERS AND SOLUTIONS.....	94
CHAPTER 3: EXON ARRAY ANALYSIS OF PAEDIATRIC MEDULLOBLASTOMAS.....	95
3.1. INTRODUCTION.....	95
3.2. HISTOPATHOLOGICAL CLASSIFICATION AND SAMPLE PROCESSING	96
3.3. EXON ARRAY QUALITY CONTROL AND FILTERING	103
3.4. SAMPLE SUB-GROUPING BASED ON THE SHH GENE EXPRESSION SIGNATURE	109
3.5. DISCUSSION.....	111
CHAPTER 4: ANALYSIS OF DIFFERENTIAL GENE EXPRESSION IN PAEDIATRIC MEDULLOBLASTOMA	113
4.1. INTRODUCTION.....	113
4.2. IDENTIFICATION OF GENES DIFFERENTIALLY EXPRESSED IN SHH-DRIVEN MEDULLOBLASTOMAS.....	115
4.3. SELECTION OF MEDULLOBLASTOMA ASSOCIATED CANDIDATE GENES.....	124
4.4. <i>IN VITRO</i> CULTURE OF MOUSE CEREBELLAR GRANULE CELL PROGENITORS	128
4.5. ANALYSIS OF CANDIDATE GENE EXPRESSION IN GCP CULTURES	135
4.6. ANALYSIS OF CANDIDATE GENE EXPRESSION IN HUMAN MEDULLOBLASTOMA CELL LINES	140
4.7. FUNCTIONAL ANALYSIS OF CANDIDATE GENES BY shRNA-MEDIATED KNOCKDOWN IN MEDULLOBLASTOMA CELL LINES	142
4.7.1. Initial characterisation of the shRNA expression system.....	143
4.7.2. Screening of candidate genes	149
4.7.3. Optimisation of a viral transduction protocol for the D425 Med cell line	158
4.8. DISCUSSION.....	162
CHAPTER 5: ANALYSIS OF DIFFERENTIAL SPLICING IN PAEDIATRIC MEDULLOBLASTOMA	169
5.1. INTRODUCTION.....	169
5.2. IDENTIFICATION OF TUMOUR-ASSOCIATED SPLICING EVENTS	171
5.3. IDENTIFICATION OF NOVEL SPLICE FORMS	183
5.4. VALIDATION OF DIFFERENTIAL SPLICING IN AN INDEPENDENT SET OF PRIMARY MEDULLOBLASTOMAS AND IN MEDULLOBLASTOMA CELL LINES	185
5.5. TUMOUR-ASSOCIATED SPLICING PATTERNS ARE OBSERVED DURING THE NORMAL DEVELOPMENT OF MOUSE CEREBELLUM.....	190

5.6. ANALYSIS OF <i>MADD</i> DIFFERENTIAL SPLICING	194
5.7. AN EXAMPLE OF ALTERNATIVE TRANSCRIPT TERMINATION SITES: ANALYSIS OF <i>QKI</i> DIFFERENTIAL SPLICING	198
5.8. DISCUSSION.....	204
CHAPTER 6: GENERAL DISCUSSION AND FUTURE DIRECTIONS.....	209
REFERENCES.....	219
APPENDIXES	237
APPENDIX 1. PRIMER SETS FOR PCR ANALYSIS OF GENE EXPRESSION AND ALTERNATIVE SPLICING.	237
APPENDIX 2. LIST OF GENES SIGNIFICANTLY UP-REGULATED IN SHH-DRIVEN MEDULLOBLASTOMAS.	239
APPENDIX 3. LIST OF GENES SIGNIFICANTLY DOWN-REGULATED IN SHH-DRIVEN MEDULLOBLASTOMAS.	242

List of Figures

Figure 1.1. Schematic overview of common chromosomal gains and losses in medulloblastoma.	21
Figure 1.2. Structure of the adult mouse cerebellum.	24
Figure 1.3. Shh signalling in the post-natal cerebellum.	26
Figure 1.4. Control of GCP proliferation in the post-natal cerebellum.	29
Figure 1.5. Alternative modes of splicing.	52
Figure 1.6. Causes and consequences of splicing pattern alterations.	55
Figure 2.1. Schematic representation of the whole transcript sense target labelling assay.	63
Figure 2.2. Affymetrix Exon array design.	65
Figure 2.3. Schematic representation of the pGIPZ shRNAmir lentiviral vector.	90
Figure 3.1. Histopathological grading of anaplasia in medulloblastoma.	98
Figure 3.2. Medulloblastoma features of nodularity and desmoplasia, and normal cerebellum.	100
Figure 3.3. Histology of medulloblastoma frozen sections.	102
Figure 3.4. Sample signal distribution.	105
Figure 3.5. Schematic overview of low level analysis and filtering of the exon array data.	106
Figure 3.6. Filter on gene expression.	107
Figure 3.7. Unsupervised hierarchical cluster analysis.	108
Figure 3.8. A medulloblastoma subgroup is characterised by the Shh-gene signature.	110
Figure 4.1. Schematic overview of gene-level analysis.	117
Figure 4.2. Top 50 genes up- and down-regulated in Shh-driven medulloblastomas.	118
Figure 4.3. Functional enrichment analysis of Gene Ontology terms.	119
Figure 4.4. Functional enrichment analysis of tissue annotation.	121
Figure 4.5. Selection of candidate genes up-regulated in Shh-driven medulloblastomas.	126
Figure 4.6. <i>In vitro</i> culture of mouse cerebellar granule cell precursors.	129
Figure 4.7. ShhN induces expression of granule precursor markers and proliferation of GCPs.	132
Figure 4.8. ShhN-treated cultures are a mixture of mature granule neurons and granule precursors.	134
Figure 4.9. Genes over-expressed in Shh-driven medulloblastomas are also up-regulated in GCPs in the presence of Shh.	136
Figure 4.10. Shh induced the expression of Pou3f2 in GCP cultures.	138
Figure 4.11. Shh induced the expression of Ube2c in GCP cultures.	139
Figure 4.12. Expression of selected candidate genes in human medulloblastoma cell lines.	141
Figure 4.13. Experimental outline for the screening of candidate genes by shRNA silencing.	144
Figure 4.14. <i>BMI1</i> knockdown in Daoy cells.	146
Figure 4.15. Cell cycle analysis of Daoy cells transduced with <i>BMI1</i> shRNAs.	148

Figure 4.16. Analysis of <i>DLG7</i> knockdown in Daoy cells.....	150
Figure 4.17. Analysis of <i>UBE2C</i> knockdown in Daoy and UW228-2 cells.....	151
Figure 4.18. Cell cycle analysis of Daoy and UW228-2 cells transduced with <i>UBE2C</i> shRNAs.....	152
Figure 4.19. Analysis of <i>KIF4A</i> knockdown in Daoy and UW228-2 cells.....	154
Figure 4.20. Analysis of <i>PLK1</i> knockdown in Daoy and UW228-2 cells.....	156
Figure 4.21. Transduction of D425 Med cells with different lentiviral constructs.....	160
Figure 4.22. <i>GAPDH</i> knockdown in D425 Med cells.....	161
Figure 5.1. Schematic overview of exon-level analysis.....	172
Figure 5.2. <i>TJPI</i> and <i>DAAMI</i> probe set expression plots.....	173
Figure 5.3. <i>MADD</i> and <i>MAGI1</i> probe set expression plots.....	175
Figure 5.4. Differential splicing of the <i>WHSC1</i> , <i>TRRAP</i> and <i>WASF3</i> genes.....	177
Figure 5.5. RT-PCR validation of differentially spliced cassette exons.....	181
Figure 5.6. Visualisation of splicing patterns using the Splicing Indicator formula.....	182
Figure 5.7. Examples of splice variant sequence analysis.....	184
Figure 5.8. RT-PCR analysis of differential splicing in an independent set of samples and in medulloblastoma cell lines.....	187
Figure 5.9. Cluster analysis of normal and tumour samples based on splicing patterns.....	189
Figure 5.10. Splicing variants characteristic of human medulloblastomas are expressed during normal mouse cerebellar development.....	192
Figure 5.11. <i>MADD/IG20</i> splice forms.....	196
Figure 5.12. Analysis of <i>MADD/IG20</i> mRNA splicing in human medulloblastomas and during mouse cerebellar development.....	197
Figure 5.13. <i>QKI</i> probe set expression profile.....	200
Figure 5.14. <i>QKI5/QKI7</i> expression ratio assessed by exon arrays and Real Time PCR.....	201
Figure 5.15. Validation of <i>QKI</i> differential splicing in an independent set of samples.....	202
Figure 5.16. <i>QKI5</i> and <i>QKI7</i> splice variants are differentially expressed during normal mouse cerebellar development.....	203
Figure 6.1. Gene-level expression analysis for genes encoding splicing factors.....	215
Figure 6.2. <i>PTBPI</i> is over-expressed in medulloblastomas compared to normal adult cerebella.....	217

List of Tables

Table 1.1. Summary of medulloblastoma histology.	18
Table 1.2. Gene expression profiling of medulloblastoma.	42
Table 1.3. Genetic, transcriptional and clinical associations of medulloblastoma molecular subgroups.	50
Table 1.4. Examples of disruptions in mRNA splicing mechanisms that are associated with malignant disease.	54
Table 2.1. Antibodies used for immunocytochemistry.	79
Table 2.2. Antibodies used for western blotting.	87
Table 2.3. Buffers and solutions.	94
Table 3.1. Patients and tumour features of the sample series used for the exon array study.	97
Table 4.1. Biological functions and potential tumorigenic roles of selected genes significantly up-regulated in Shh-driven medulloblastomas.	127
Table 5.1. Genes alternatively spliced in medulloblastoma identified by exon array analysis and validated by RT-PCR.	180
Table 5.2. Patients and tumour features of the sample series used for independent validation of differential splicing.	186
Table 5.3. Mouse cassette exons analysed by RT-PCR and their human equivalents.	191

Abbreviations

AS - Alternative splicing

BrdU - Bromodeoxyuridine

CB - Cerebellum

CMV - Cytomegalovirus

CNS - Central nervous system

CTNNB1 - *Catenin (cadherin-associated protein), beta 1 gene*

DABG - Detection above background

DCN - Deep cerebellar nuclei

DEG - Differentially expressed gene

EGL - External germinal layer

FDR - False discovery rate

GCP - Granule cell precursor

IGL - Internal granule layer

LC/A - Large cell/anaplastic

LIMMA - Linear models for microarray data

MB - Medulloblastoma

MB2 - Non Shh-driven medulloblastoma

ML - Molecular layer

MOI - Multiplicity of infection

PCR - Polymerase chain reaction

PL - Purkinje cell layer

PLIER - Probe logarithmic intensity error

PTCH - *Patched 1 gene*

RT-PCR - Reverse transcription PCR

SAGE - Serial analysis of gene expression

SFFV-LTR - Spleen focus forming virus long terminal repeat

SHH - Shh-driven medulloblastoma

Shh - Sonic hedgehog

ShhN - Sonic hedgehog N-terminal peptide

Chapter 1

Introduction

1.1. Medulloblastoma

Medulloblastoma is a highly malignant embryonal tumour of the cerebellum. It represents the most common brain cancer in children, with an incidence of 0.48 for girls and 0.75 for boys in every 100,000 paediatric patients/year [1]. Medulloblastoma mainly occurs within the first decade of life, with a peak in incidence between 4 and 7 years of age. However cases in the young adult and adult populations have also been described [2]. Despite advances in the clinical management of this disease, approximately one third of patients remain incurable and the majority of survivors suffer from severe long-term side effects caused by therapeutic treatments [3]. The outcome of medulloblastoma is significantly related to the age of the patient and the extent of disease at diagnosis [4, 5]. Children younger than 3 years of age have a poorer prognosis than older children partly because their treatment regime does not include radiotherapy. This is because cranial irradiation to the developing brain can cause severe neurological sequelae [3]. Also, evidence of metastatic spread within the central nervous system (CNS) at diagnosis, which occurs in one third of patients, is indicative of unfavourable prognosis [4, 6].

Novel therapies and prognostic markers are necessary to reduce mortality rate of medulloblastoma and to improve the quality of life of survivors in the long-term. A better understanding of the molecular pathogenesis of medulloblastoma is essential for the development of new therapeutic approaches which are likely to derive from the investigation of key cellular pathways implicated in tumour initiation and growth. A

concerted effort is currently being undertaken to improve medulloblastoma classification based on the integration of both clinical and molecular parameters, which will allow a better prediction of disease outcome and lead to the development of disease risk stratification schemes [7-9].

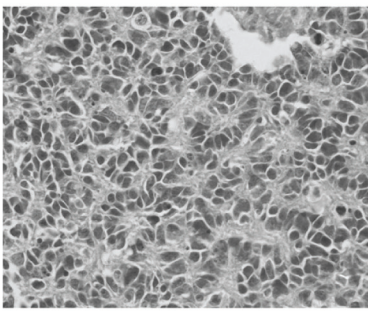
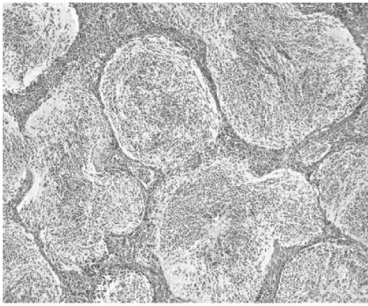
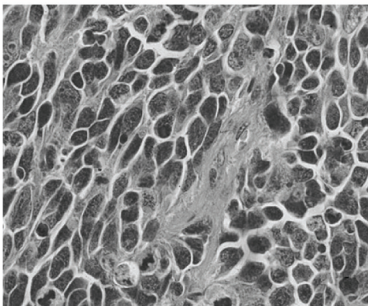
1.2. Medulloblastoma pathology

According to the 2007 World Health Organisation (WHO) classification of CNS tumours, medulloblastomas are classified as one of five histological variants: classic, desmoplastic/nodular, medulloblastoma with extensive nodularity (MBEN), large cell medulloblastoma and anaplastic medulloblastoma [2]. However, in most clinico-pathological and molecular studies, desmoplastic/nodular medulloblastomas and MBEN are combined into a single category of desmoplastic tumours, as they share many fundamental histological features. Similarly, the large cell/anaplastic histological category includes both anaplastic and large cell medulloblastomas, both of which are characterised by cytological features of anaplasia [7].

1.2.1. Classic medulloblastoma

The classic histological subtype is the most frequent, accounting for up to 75% of cases [3-5]. Classic medulloblastomas grow as sheets of generally small round cells with a high nuclear:cytoplasmic ratio and an ability to invade adjacent brain tissue and meninges. Less than half of these cases form neuroblastic (Homer-Wright) rosettes, which consist of circular columns of tumour cell nuclei arranged around a central core of cytoplasmic processes (Table 1.1) [10].

Table 1.1. Summary of medulloblastoma histology.

Histological category	Frequency	5-year OS	Histology
CLASSIC MEDULLOBLASTOMA	All children 73%	73.6%	
	< 3 years 26%		
	3-16 years 78%		
DESMOPLASTIC MEDULLOBLASTOMA	All children 10%	87.1%	
	< 3 years 57%		
	3-16 years 5%		
LARGE CELL/ ANAPLASTIC MEDULLOBLASTOMA	All children 17%	54.7%	
	< 3 years 17%		
	3-16 years 17%		

The table shows frequency and 5-year overall survival (OS) for the three major medulloblastoma histological categories. The data in this table has been derived from McManamy *et al.* [11] and, unless otherwise stated, refers to the entire paediatric population. Histological images reproduced from Gulino *et al.*[12] are shown for comparison.

1.2.2. Desmoplastic medulloblastoma

Desmoplastic medulloblastomas account for approximately 15% of the tumours, but represent up to 60% of the tumours occurring in children of less than three years of age and adults [11]. Desmoplastic medulloblastomas are associated with a better overall prognosis, which is particularly relevant for disease risk stratification within the infant population [9, 13]. They display a characteristic biphasic architecture consisting of nodular areas of more differentiated cells surrounded by reticulin-rich internodular regions, featuring densely packed, highly proliferating cells, and pericellular deposition of collagen (Table 1.1).

1.2.3. Large cell/anaplastic medulloblastoma

Large-cell/anaplastic medulloblastomas have been reported to account for approximately 5-15% of medulloblastomas [11, 14], although features of moderate or severe anaplasia have been identified in up to 24% of cases [15]. These tumours are characterised by marked nuclear pleomorphism, cellular wrapping, extensive apoptosis and intense mitotic activity (Table 1.1). The patients often present with metastatic disease and this type of medulloblastoma is generally associated with a poor prognosis [14, 15].

1.3. Medulloblastoma cytogenetics

Medulloblastomas are not characterised by any single defining chromosomal abnormality, but rather show a range of cytogenetic alterations (Figure 1.1) [16]. The presence of an isochromosome 17q (i17q), which combines the loss of 17p and duplication of 17q, has been widely acknowledged as the most frequent chromosomal abnormality in medulloblastomas, affecting approximately 40% of cases [16-18]. The

individual loss of the short arm of chromosome 17 has also been frequently reported [16-18]. These abnormalities are found in all of the medulloblastoma histological variants and have been significantly associated with a poor outcome for patients [8, 18]. However, little is known about the individual genes mapping to these chromosomal regions whose loss/amplification might favour medulloblastoma development.

Another frequently observed chromosomal abnormality in medulloblastoma is the loss of an entire copy of chromosome 6. Interestingly, this aberration is exclusively found in medulloblastomas with abnormal activation of the Wntless (Wnt) signalling pathway (assessed by identifying mutation in the *CTNNB1* gene encoding β -catenin, β -catenin nucleo-positivity, or gene expression profiling), and is a strong biomarker of good prognosis [8, 19, 20]. Other regions of extensive chromosomal gain and loss include loss of chromosomes 8, 9q, 10q, 11 and 16q; and gain of chromosomes 1q, and 7; all of which are observed in up to 40% of cases [16, 21]. Still, it is unclear whether the disruption of individual genes in these regions might be relevant to medulloblastoma pathogenesis.

Double minutes, fragments of extra-chromosomal DNA generated by gene amplification, have also been commonly observed in cytogenetic studies of medulloblastoma primary tumours and cell lines [22, 23]. *MYCN* (at 2p24) and *MYC* (at 8q24) are the most frequently amplified *loci* in medulloblastomas. Their amplification has been found in up to 10% of tumours, and is strongly associated with the large cell/anaplastic phenotype and unfavourable patient outcome [8, 18, 24].

Recently, Pizer and colleagues proposed a scheme of disease risk stratification based on a combination of histological and molecular tumour features, with the aim of improving medulloblastoma survival rates while reducing the long-term side effects of

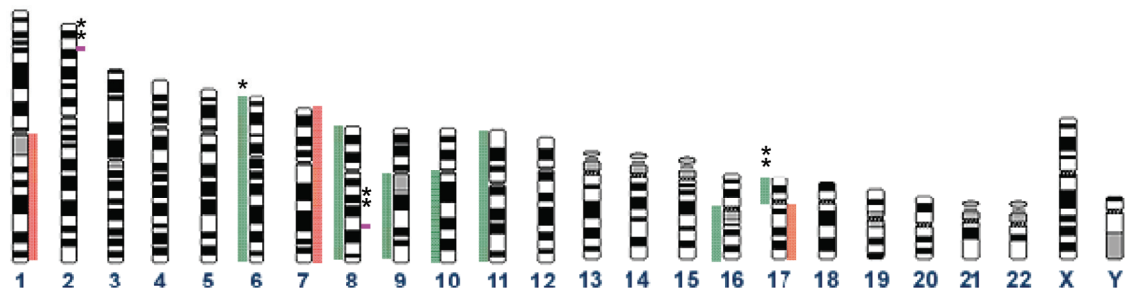


Figure 1.1. Schematic overview of common chromosomal gains and losses in medulloblastoma.

The red and green bars shown on the right and left of each chromosome indicate common chromosomal gains and losses, respectively. Amplifications of the *MYCN* and *MYC* genes are represented as narrow pink bars matching their genomic location on chromosomes 2 and 8. Asterisks designate chromosomal abnormalities which have been associated with a favourable (single asterisk) or poor (double asterisk) outcome for patients. Adapted from Ellison [7] and Northcott *et al.* [25].

treatment [9]. A large-cell/anaplastic histology as well as evidence of metastatic disease, suboptimal surgical resection and amplification of the *MYC* or *MYCN* oncogenes are all considered independent high risk biomarkers. Absence of any of these high risk disease features is associated with a standard risk. Finally, the presence of positive biomarkers, among which is the activation of the Wnt pathway, is predictive of a better outcome [9]. On this basis, two European clinical trials are currently being implemented, which will test whether alternative treatment options could be used for different disease risk groups to improve the outcome for patients with medulloblastoma.

Although histological and cytological studies of medulloblastomas have provided important biomarkers for the clinical management of the disease, there is a general consensus that our ability to predict the clinical behaviour of medulloblastoma and to counteract its growth and relapse depends on a better understanding of the molecular mechanisms that drive oncogenesis in the cerebellum. Therefore, the pathways and molecules which regulate normal and abnormal cerebellar development are being intensively studied since they represent potential targets of novel therapeutic approaches [26-28].

1.4. The structure of the mature cerebellum

In mammals, the cerebellum is largely responsible for the coordination of motor activities in the brain [29]. It is located in the posterior fossa of the skull and it consists of a central vermis, flanked by two lateral hemispheres (Figure 1.2A). Both the vermis and the hemispheres are folded into lobules, and each lobule is subdivided into folia by a series of parallel fissures (Figure 1.2B). The cerebellum is also divided into a cortex and a mass of centrally located neurons known as the deep cerebellar nuclei. The functions of the cerebellum depend on the activities of at least five neuronal types [30],

located in specific layers within the cerebellum. The most abundant are the granule neurons, which regulate the activity of the underlying Purkinje cells. Purkinje neurons are the only output neurons of the cerebellar cortex and they form an orderly single cell layer (Purkinje cell layer, PL) in the mature cerebellar cortex, interspersed between the internal granule cell layer (IGL) and the molecular layer (ML) (Figure 1.2C). Granule neurons project their ascending axons from the IGL into the ML, where they form synapses with Purkinje cells and ML interneurons, *i.e.* stellate and basket cells. The IGL also contains Golgi neurons and astrocytes, while the Bergman glia are predominantly located in the PL [30, 31].

1.5. Overview of cerebellar development

The development of the cerebellum occurs over a long period of time, from the early embryonic period until the first two post-natal weeks in mice [32]. The cerebellum arises from the most anterior rhombomere of the hindbrain. The isthmus, a signalling centre located at the boundary separating the midbrain and hindbrain, has been shown to play an essential role in the establishment of the cerebellar territory during early embryonic development and the specification of the different cerebellar cell types [33]. Cells in the cerebellum arise at different times of development from two distinct germinal zones: the ventricular zone, which gives rise to multipotent precursors of both cerebellar neurons and glial cells, and the more dorsally located rhombic lip, from which granule neurons originate [34]. The first cells to be formed in the developing cerebellum migrate radially from the ventricular zone to evolve into the deep cerebellar nuclei and Purkinje neurons of the cerebellar cortex. Subsequently, stellate, basket and Golgi interneurons are generated from the same germinal matrix [34]. Conversely, granule cell precursors (GCPs) originate from the rhombic lip. They

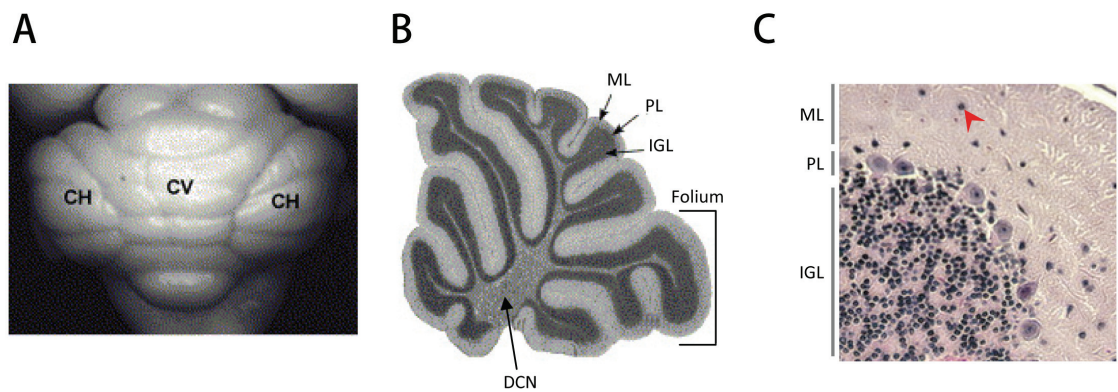


Figure 1.2. Structure of the adult mouse cerebellum.

A) Dorsal view of the adult mouse cerebellum. The cerebellar vermis (CV) and the cerebellar hemispheres (CH) are indicated. Adapted from Chizhikov and Millen [35].

B) Para-sagittal section of the cerebellar vermis. Black arrows indicate the three distinct layers of the mature cerebellar cortex: the molecular layer (ML), the Purkinje cell layer (PL), and the internal granule cell layer (IGL). A red arrow indicates deep cerebellar nuclei (DCN). One of the folia is labelled by a bracket. Adapted from Chizhikov and Millen [35].

C) Hematoxylin and Eosin staining of a section of mouse cerebellum. The three layers of the mature cerebellar cortex are indicated: ML, molecular layer; PL, Purkinje cell layer; IGL, internal granule layer. Stellate neurons are detectable in the ML (arrowhead), while Purkinje neurons and granule cells are located in the PL and IGL, respectively. Adapted from Oliver *et al.* [36].

then migrate across the outer surface of the cerebellum to form the external germinal layer (EGL). During post-natal development, precursor cells in the EGL undergo extensive proliferation generating a large pool of GCPs. As new GCPs are generated, older precursors exit the cell cycle, differentiate into mature neurons and migrate inward, past the Purkinje cell layer, to their final destination, the IGL (Figure 1.3A). At about three weeks of age, the mouse cerebellum is completely developed. The EGL disappears and the IGL is populated with mature granule neurons. The same process occurs in the human cerebellum and continues during the first eleven post-natal months [34].

Recently, a new stem cell population was identified in the white matter of the adult mouse cerebellum [37]. These cells express the neural stem cell marker prominin-1 (CD133), are able to form self-renewing neurospheres *in vitro* and can differentiate into astrocytes, oligodendrocytes and neurons *in vivo*. Thus, the mouse cerebellum contains at least three different neural precursor cell populations from which medulloblastoma and its variants might develop.

1.6. Control of GCP proliferation in the post-natal cerebellum

1.6.1. The Sonic hedgehog signalling pathway

Cerebellar granule neurons are the most abundant cell type in the brain and constitute the main cell population in the cerebellum. The observation that mutations in genes that encode components of the Sonic hedgehog (Shh) signalling pathway could result in the formation of cerebellar tumours in mice and humans suggested that this pathway might have a major role in the regulation of granule cell precursor proliferation and differentiation [38-40]. Indeed, several studies have demonstrated that the Shh mitogen is an essential regulator of GCP post-natal expansion. Addition of recombinant

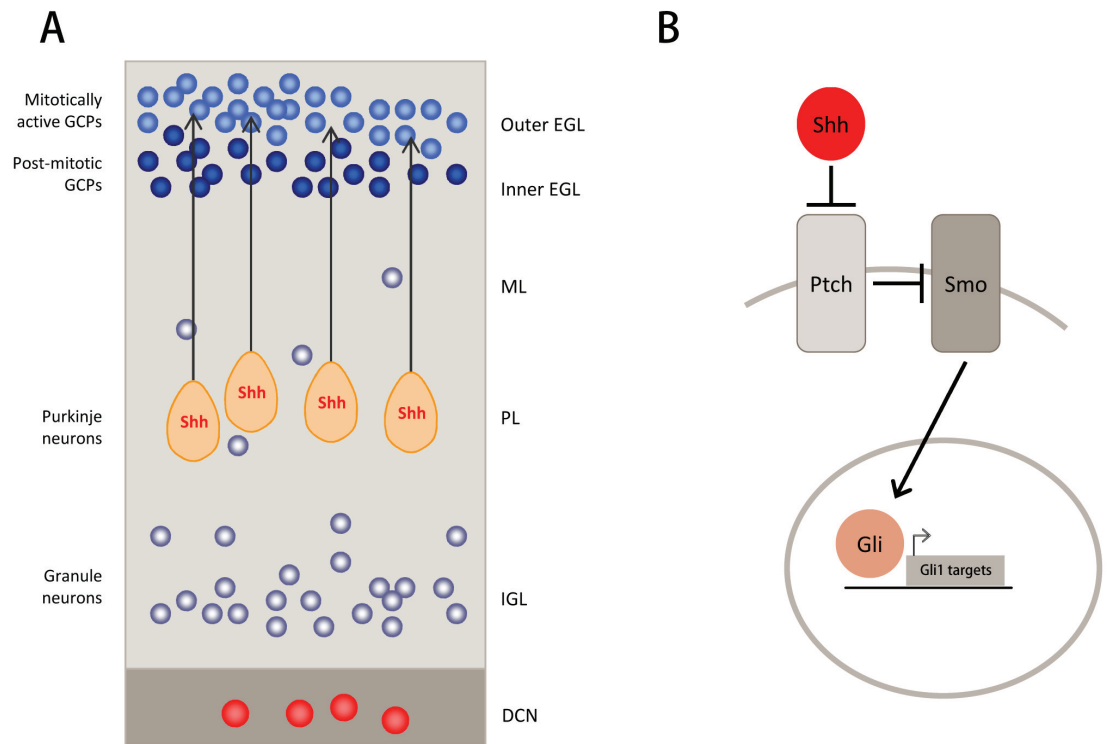


Figure 1.3. Shh signalling in the post-natal cerebellum.

A) Schematic representation of the mouse cerebellum during the post-natal expansion of GCPs. Mitotically active GCPs are found in the outer EGL, and Shh secreted from Purkinje neurons sustains their proliferation. As new GCPs are generated, older GCPs exit the cell cycle, differentiate into neurons and migrate inward, through the Purkinje cell layer, to reach the internal granule layer (IGL). EGL, external germinal layer; ML, molecular layer; PL, Purkinje cell layer; DCN, deep cerebellar nuclei. Adapted from Ruiz i Altaba [41].

B) Shh signalling pathway. Binding of Shh to the trans-membrane receptor Ptch inhibits the repression of Smo by Ptch. Smo can in turn activate an intracellular signalling pathway that increases the nuclear activity of the Gli family of transcription factors, which regulate the expression of target genes.

Shh protein to mouse GCPs in culture induces a significant increase in their proliferation rate, as measured by thymidine and bromodeoxyuridine (BrdU) incorporation assays. Conversely, blocking the Shh signalling pathway *in vivo* with an anti-Shh antibody causes a decrease in GCP proliferation resulting in a significantly thinner EGL and defects in cerebellar foliation [42, 43]. During normal cerebellar development, Shh is produced and secreted by Purkinje neurons. GCPs express all of the downstream elements of the Shh pathway, which allows them to respond to it [43]. Binding of Shh to the receptor Patched (Ptch) on the surface of GCPs results in Ptch inhibition and consequently in the release of the Ptch-partner receptor Smoothed (Smo). Smo in turn activates downstream effectors of the pathway, leading to the nuclear translocation of the Gli transcription factors and eventually the transcriptional activation of target genes, which induce a pro-proliferative response (Figure 1.3B) [43]. Although three Gli proteins have been described that can mediate the cellular response to Shh signalling in vertebrates, it has been shown that Gli2 is the major effector of the Shh mitogenic signal during cerebellar development. Indeed, depletion of Gli2 but not Gli1 results in a thinner EGL and reduced cerebellar foliation [42].

1.6.2. Shh effectors

While the role of Shh in promoting GCP proliferation has been widely established, the mechanisms underlying this mitogenic effect remain to be elucidated. To identify target genes activated by Shh, several groups over the last few years have used whole-genome approaches to investigate changes in gene expression induced by Shh in mouse GCPs both *in vitro* and *in vivo* [44-46]. Consistent with the mitogenic effects of Shh, many of the genes whose expression increases after Shh stimulation are

involved in the regulation of cell cycle progression, DNA replication and the negative regulation of differentiation [45, 47].

1.6.2.1. *Mycn*

The *Mycn* gene, which encodes a basic helix-loop-helix (bHLH) transcription factor, has been identified as one of the early transcriptional targets of the Shh pathway (Figure 1.4). Overexpression of *Mycn* alone is sufficient to induce GCP proliferation *in vitro*, even in the absence of Shh [45, 48], whereas the conditional disruption of *Mycn* in the developing mouse brain results in impaired GCP proliferation in the EGL [49]. Interestingly, in the *Ptch*^{+/-} mouse model of medulloblastoma, loss of the *Ptch* gene has been associated with an increased stability of the *Mycn* protein, suggesting that Shh can increase the level of *Mycn* activity through both transcriptional and post-transcriptional mechanisms [50]. The *MYCN* gene is overexpressed in the majority of human medulloblastomas [51] and its amplification, together with the amplification of the *MYC* oncogene, is seen in almost 10% of cases [25]. Overexpression of *Mycn* in the developing cerebellum induces the formation of classic and nodular desmoplastic medulloblastomas in genetically engineered mice [51]. Furthermore, dexamethasone treatment of genetically modified mice with Shh-induced medulloblastomas leads to the proteasomal degradation of the *Mycn* protein via the activation of glycogen synthase kinase 3 β (Gsk-3 β). This eventually results in the inhibition of tumour growth and increased survival of tumour-prone transgenic mice [52]. This suggests that *Mycn* is required for the Shh-induced proliferation of GCPs in the normal developing cerebellum as well as for the initiation and maintenance of medulloblastoma. In Shh-treated cultured GCPs, the increased expression of *Mycn* is followed by an increase in the level

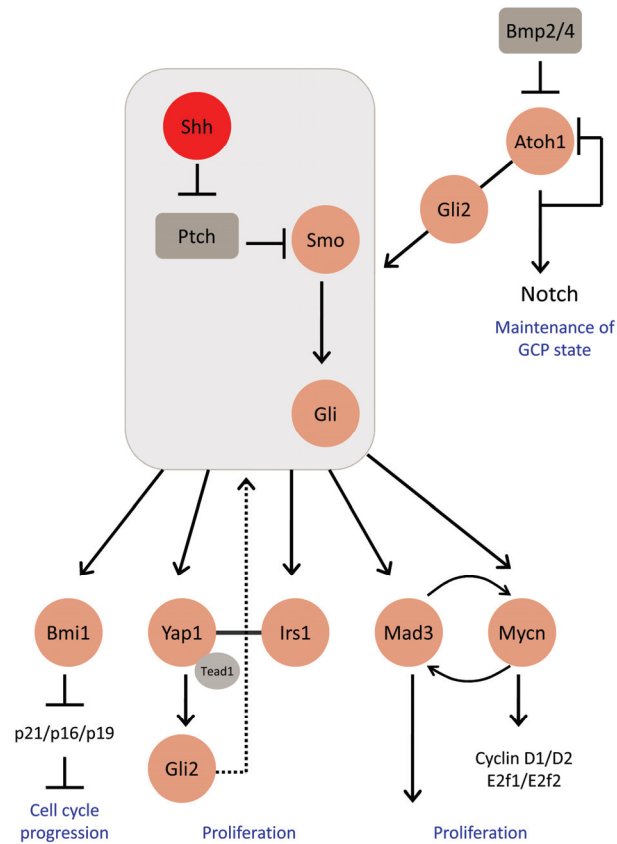


Figure 1.4. Control of GCP proliferation in the post-natal cerebellum.

In the post-natal cerebellum, Shh plays an essential role in triggering GCP proliferation by inducing downstream effectors that favour GCP progression through the cell cycle. Among these, *Mycn* and *Mad3* regulate each other and induce the expression of type D Cyclins and E2F transcription factors. *Bmi1* represses the expression of negative regulators of the cell cycle, including p16, p19 and p21, and this favours GCP proliferation. Yap1 has been shown to form a complex with Irs1 and translocate to the nucleus where it binds its transcriptional partner Tead1 to induce the expression of target genes. A possible positive feedback loop has been suggested, in which *Gli2* expression is induced by the Yap1-Tead1 complex. The expression of *Bmp2* and *Bmp4* in the maturing GCPs as well as the accumulation of Notch downstream effectors (e.g. Hes5) counteract Atoh1 positive enhancement of Shh signalling and eventually favor GCP differentiation.

of expression of Cyclin D1 and of the E2F1 and E2F2 transcription factors, all of which are positive regulators of the cell cycle [45].

1.6.2.2. *Mad3*

Mad3, which encodes a bHLH transcription factor transiently expressed in proliferating GCPs during post-natal cerebellar development, is also up-regulated as a result of *Mycn* expression [53]. *Mad3* is essential for sustained Shh-dependent GCP proliferation and when expressed by itself *Mad3* can trigger GCP proliferation and *Mycn* gene expression *in vitro* [53]. Like *Mycn*, *Mad3* is overexpressed in medulloblastomas derived from *Ptch*^{+/-} mice compared to normal cerebellum. It has been suggested that the *Mycn* and *Mad3* proteins positively regulate each other's transcription but induce the expression of different sets of genes that are required for the post-natal expansion of GCPs (Figure 1.4) [53].

1.6.2.3. *Bmi1*

The polycomb group gene *Bmi1* is another target of the Shh signalling pathway that contributes to the proliferation of GCPs both *in vitro* and *in vivo* [54]. The *Bmi1* protein is expressed in the EGL during the post-natal development of the cerebellum and deletion of the *Bmi1* gene impairs GCP survival and expansion *in vivo*, resulting in the depletion of the IGL. It has been suggested that *Bmi1* regulates Shh-dependent GCP proliferation by repressing the transcription of genes that inhibit cell proliferation (Figure 1.4) [55].

1.6.2.4. The IGF pathway and *Irs1*

An additional molecule identified as an effector of the Shh mitogenic signal in GCPs is insulin receptor substrate 1 (*Irs1*) (Figure 1.4) [56]. The *Irs1* protein was shown to be essential for insulin-like growth factor (IGF)-induced proliferation of different cell types [57] although its role in GCP proliferation has only recently been investigated. Components of the IGF signalling pathway are expressed both in the developing and the mature cerebellum, and activation of the pathway is required for the proliferation of GCPs and medulloblastoma cells *in vitro* [58]. Interestingly, the IGF pathway has been shown to enhance Shh signalling in cultured mouse GCPs by inhibiting Gsk-3 β , which blocks GCP cell cycle progression by targeting the *Mycn* protein for degradation via the proteasome [58]. *Irs1* is a downstream effector of the IGF signalling pathway and is expressed in the EGL of the developing mouse cerebellum. Shh treatment of GCPs favours *Irs1* protein stability via the inhibition of mTOR-mediated *Irs1* protein turnover. Moreover, overexpression of *Irs1* can promote GCP proliferation *in vitro* in the absence of Shh [56].

1.6.2.5. *Yap1*

The oncogenic transcriptional coactivator yes-associated protein 1 (*Yap1*) has recently been found to have a role in Shh-induced GCP proliferation [59]. *Yap1* was initially identified as being overexpressed and occasionally amplified in human medulloblastomas characterised by hyper-activation of the Shh signalling pathway [59]. Immunofluorescence staining of mouse cerebellar sections at different developmental stages showed that *Yap1* is strongly expressed in the EGL at the peak of GCP expansion (post-natal day 7), but is also detected in the mature cerebellum suggesting that it may play multiple roles at different stages of cerebellar development. In *in vitro*

GCP cultures, an increase in the levels of *Yap1* mRNA and its protein is observed in the presence of Shh [59]. Furthermore, Shh is able to induce the translocation of the Yap1 protein from the cytoplasm to the nucleus, possibly by favouring its interaction with the Irs1 protein, as the two molecules are found in the same protein complex in Shh-treated GCPs as well as in a mouse model of Shh-induced medulloblastoma [59]. As is the case for *Irs1*, the ectopic expression of *Yap1* in cultured GCPs strongly increases cell cycle progression even in the absence of Shh, while its depletion causes a dramatic decrease in Shh-induced GCP proliferation. Yap1 interacts with and activates different transcription factors, which in turn induce the expression of cell cycle related genes. Immunoprecipitation analysis showed that Yap1 binds to its transcriptional partner Tead1 in Shh-treated GCPs and *in silico* analysis suggests that the *Gli2* gene is one of the putative targets of the Yap1/Tead1 complex (Figure 1.4) [59].

1.6.3. *Atoh1*

The control of GCP proliferation results from the balanced interaction of different signalling pathways. While Shh plays a major role in promoting the clonal expansion of GCPs in the developing cerebellum, additional signals are essential for the regulation of GCP differentiation. The *Atoh1* gene, which encodes a bHLH transcription factor expressed in neuronal precursors in the rhombic lip and subsequently in the EGL, is the earliest marker of the GCP lineage and is essential to maintain GCPs in a proliferative state [60]. GCPs derived from the rhombic lip of *Atoh1* null mice are normal in their specification and viability, but are unable to differentiate into mature granule neurons. Components of the Notch signalling pathway are significantly down-regulated in *Atoh1* null GCPs compared to control cells, suggesting that *Atoh1* controls GCP differentiation, at least in part, by regulating Notch signalling [60]. Moreover,

Atoh1 modulates a negative feedback loop which results in its own repression following the activation of the Notch downstream effector Hes5, which inhibits *Atoh1* transcription. Therefore, accumulation of the Atoh1 protein eventually reduces its own expression consequently blocking Notch signalling, which allows GCPs to differentiate [60]. More recently, *Atoh1* has been shown to directly sustain Shh signalling through the direct transcriptional regulation of *Gli2*, which in turn controls the activity of the Shh pathway (Figure 1.4) [61]. Consistent with this, *Atoh1* deletion prevents the formation of Shh-driven medulloblastomas in mice which bear an oncogenic constitutively active allele of the *Smo* gene [61].

1.6.4. Bone morphogenetic proteins

The bone morphogenetic protein (Bmp) family is also implicated in the regulation of GCP cell cycle exit, migration and differentiation during early cerebellar development. Bmps are secreted members of the transforming growth factor β super-family which, upon interaction with their receptors, activate an intracellular signalling cascade leading to the nuclear translocation of Smad effector proteins and the transcriptional activation of a variety of target genes [62]. During the embryonic development of the cerebellum, *Bmp6* and *Bmp7* are expressed by dorsal midline cells, which are adjacent to the rhombic lip primordium and are implicated in the proliferation and migration of GCPs [63]. Addition of Bmp6 or Bmp7 to rhombic lip cerebellar progenitors in culture induces the expression of GCP markers, including *Atoh1* [63], and constant *Bmp7* expression antagonises GCP differentiation by inducing the expression of *Atoh1* and sustaining cell cycle progression [64, 65]. In contrast, *Bmp2* and *Bmp4* are expressed in GCPs in the EGL and in mature granule neurons in the IGL. Both Bmp2 and Bmp4, but not Bmp7, are able to induce cell cycle arrest and

differentiation of cultured GCPs [65, 66]. More interestingly, Bmp2 and Bmp4 have been shown to antagonise Shh-dependent proliferation of GCPs and medulloblastoma cells *in vitro* and *in vivo* by triggering the post-transcriptional down-regulation of the Atoh1 protein (Figure 1.4) [65].

1.6.5. Fibroblast growth factor

Fibroblast growth factors (FGFs) and their receptors play diverse roles during mammalian development. In the CNS, they are involved in the regulation of neurogenesis, axon growth, differentiation, as well as neuronal survival in the developing and adult brain [67]. Genes encoding several FGF ligands and receptors are expressed in the mouse cerebellum during both late embryogenesis and early post-natal development [68]. Interestingly, basic FGF (bFGF or FGF2) has been suggested to act as a negative regulator of Shh-induced GCP proliferation, both *in vitro* and *in vivo* [43, 69]. Addition of bFGF to cultured GCPs causes a 90% reduction in thymidine incorporation [43] and prevents the induction of Shh target genes (*Gli1*, *Mycn*, *cyclin D1*) [69]. Also, bFGF suppresses the Shh-dependent activation of a Gli1-responsive promoter in fibroblasts, which suggests that FGF can block Shh signalling upstream of Gli1-mediated transcription. GCPs treated with bFGF *in vitro* undergo morphological changes indicative of cell differentiation and express lower levels of proliferation markers, such as Ki67 [69]. Furthermore, intracisternal injection of bFGF into the developing mouse cerebellum accelerates the differentiation of GCPs resulting in a significantly thinner EGL by post-natal day 7 (P7) and an increase in NeuN-positive post-mitotic neurons in the inner EGL and in the molecular layer. [69]. Of note, immunohistochemical analysis of the expression of Fgfs during mouse cerebellar morphogenesis revealed that the Fgf2 protein is detectable from P0 in a few GCPs

located in the inner EGL as well as in some migrating GCPs in the molecular layer. By P7, Fgf2 is expressed by some of the granule neurons in the IGL [68]. This is compatible with a role for Fgf2 in modulating GCP cell cycle exit and differentiation *in vivo*. However, Fgf2 knockout mice do not display any cerebellar phenotype suggesting a possible redundant role for several Fgfs in the control of GCP proliferation and differentiation [70].

1.6.6. REN

The *REN* gene has been recently identified as a putative tumour suppressor which is frequently lost in human medulloblastoma [71]. Indeed, *REN* maps to chromosome 17p13.2, the most commonly deleted chromosomal region in medulloblastoma, and its level of expression significantly decreases in both diploid and hemizygous tumours compared to the normal cerebellum [71]. Interestingly, in the developing mouse cerebellum, the highest levels of *REN* mRNA and protein expression are detected in the inner EGL and in the IGL. Consistently, *REN* expression increases as GCPs undergo differentiation *in vitro*; whereas *REN* overexpression causes a block in GCP proliferation, even in the presence of Shh, and an up-regulation in the level of expression of the p27 protein [72]. In addition, *REN* overexpression significantly suppresses Gli-dependent gene transcription and causes a decrease in the level of *Gli1* mRNA, possibly by interfering with the nuclear translocation of Gli1 in response to Shh signalling [72].

1.7. The origin of Shh-driven medulloblastoma

Medulloblastomas often originate on the surface of the cerebellum, where GCPs are proliferating during embryonic and early post-natal development and they express

several of the genes which sustain GCP proliferation [28]. Therefore, it has been hypothesised that medulloblastomas originate from GCPs following the abnormal activation of signalling pathways which control GCP progression through the cell cycle [26-28].

The Shh signalling pathway is one of the best characterised regulatory pathways implicated in medulloblastoma initiation and maintenance. Initial evidence for a role of the Shh pathway in medulloblastoma came from the observation that patients affected by Gorlin's syndrome had inherited an inactivating mutation in the *PTCH* gene [73, 74]. Gorlin's syndrome (also known as nevoid basal-cell carcinoma syndrome) is a hereditary condition characterized by a range of developmental abnormalities and an increased predisposition to nevoid basal cell carcinoma and medulloblastoma [75]. Subsequent studies found that mutations affecting the *PTCH* gene are also present in up to 10% of sporadic medulloblastomas, predominantly in those with a desmoplastic histology [39, 40]. In addition, alterations in other components of the Shh pathway occur in approximately a further 15 % of cases [76-78]. Moreover, approximately 15% of mice carrying a single allele of the *Ptch* gene develop tumours of the cerebellum which resemble human medulloblastomas [38]. Even when they do not develop malignancies, the majority of *Ptch*^{+/-} mutant mice display an abnormal accumulation of pre-neoplastic, GCP-like cells at the cerebellar surface by 4 to 6 weeks of age [79, 80]. When *Ptch*^{+/-} mice were crossed with mice expressing the GFP protein under the control of the *Atoh1* promoter, both tumours and pre-neoplastic cells which developed in the cerebellum of transgenic mice expressed the GFP protein, strongly supporting the hypothesis that they were derived from the granule cell lineage [36].

Similar approaches have been used to generate alternative medulloblastoma mouse models, as well as to demonstrate the implication of other tumour-related genes

in the development of medulloblastoma from mouse GCPs. Hatton *et al.* generated a transgenic mouse in which a constitutively active mutant form of the *Smo* gene (*SmoA1*) was regulated by the *NeuroD2* promoter, which is primarily expressed in GCPs [81]. More than 90% of *Smo^{A1/A1}* homozygous mice had an abnormal expansion of cells in the EGL by two weeks of age, and developed medulloblastomas as early as one month after birth [81].

Using the Cre-LoxP system, Marino *et al.* developed genetically engineered mice in which the *Rb* and *p53* genes were specifically deleted in the *GFAP*-expressing cell populations, including GCPs [82]. All of the mice examined developed Atoh1-positive tumours on the surface of the cerebellum which closely resembled human large cell/anaplastic medulloblastomas [82]. In a follow up study, the authors demonstrated that the combined loss of the *Rb* and *p53* tumour suppressor genes predisposed target cells to the accumulation of additional genomic mutations [83]. These included the amplification and consequent overexpression of the *Mycn*, *Gli2* and *Ptch2* genes, suggesting Rb/p53-mediated oncogenesis may occur via the abnormal activation of the Shh signalling pathway [83].

Interestingly, *p53* has been shown to enhance Shh-induced tumorigenesis in other mouse models of medulloblastoma. The loss of the *p53* gene significantly accelerated medulloblastoma formation in *Ptch^{+/-}* mice [84], while the overexpression of either *Mycn* or *Cyclin D1* in primary GCPs isolated from *p53* and *Ink4c* double knockout mice induced medulloblastoma formation when the cells were injected into the brains of immuno-compromised animals [85].

Recent experiments have shown that Shh is required for the control of stem cell growth and maintenance in the adult brain [86], and that primary medulloblastomas express markers of neural stem cells and can differentiate into both neuronal and glial

cell types [87-89]. This suggested that additional cerebellar cell types other than GCPs may also be transformed as a result of the aberrant activation of the Shh pathway and give rise to medulloblastoma. To investigate this hypothesis, Yang *et al.* developed a conditional allele of the *Ptch* gene which allowed its specific inactivation in either *Atoh1*-expressing GCPs or *GFAP*-expressing multipotent stem cells located in the ventricular zone of the embryonal mouse cerebellum [90]. The authors observed that in both cases the transgenic animals developed medulloblastomas with 100% penetrance. However, tumours initiating from multipotent stem cells grew more rapidly, suggesting that the cells from which medulloblastomas develop do have an impact on the clinical course of the disease. Interestingly, although neural stem cells of the ventricular zone have the potential to differentiate along both the neuronal and the glial lineages, they only gave rise to medulloblastomas [90], suggesting that a neuronal specification is essential for Shh to induce its oncogenic effects in the cerebellum. In agreement with these observations, Schüller *et al.* demonstrated that following the activation of the Shh signalling pathway, both multipotent and unipotent cells within the GCP lineage were able to generate medulloblastomas, but not other brain cancers, and that the tumour growth rate varied according to the cell type which was targeted [91]. Importantly, these studies demonstrated that GCPs are not the only cell type from which medulloblastoma can originate, and that the Shh signalling pathway can exert its oncogenic potential at different stages of cerebellar development, but it requires its target cells to commit along the GCP lineage.

1.8. Shh-independent medulloblastomas

Although increasing evidence supports a role for Shh in medulloblastoma formation, a majority of human medulloblastomas do not show alterations in the Shh

pathway and are likely to be Shh-independent [20, 92]. Approximately 25% of the tumours are characterised by alterations in the Wnt signalling pathway [20, 92], but very little is known about their possible cell of origin. Wnt signalling is essential for the proliferation of neural stem and precursor cells during brain development [93]. The activity of the Wnt pathway is directly related to the amount of free cytosolic β -catenin, a downstream component of the pathway which interacts with other transcription factors to regulate gene expression. In normal cells, the cytosolic level of the β -catenin protein is kept low by the interaction of β -catenin with a multiprotein complex which favours its phosphorylation and degradation via the proteasome. When Wnt ligands bind to their receptors on the cell surface, the β -catenin multiprotein complex is inactivated allowing β -catenin to translocate to the nucleus where it can activate gene transcription. Loss of *Wnt-1*, a member of the *Wnt* gene family, can block mouse cerebellar development by inhibiting the specification of the midbrain-hindbrain junction from which the cerebellum originates [94]. Furthermore, conditional *β -catenin* knockout mice in which the Wnt pathway is inhibited at mid-gestation also display defects of the midbrain-hindbrain region as well as cerebellar vermis hypoplasia [95]. It has been suggested that early multipotent precursor cells which depend on Wnt signals in the cerebellum, rather than unipotent GCPs, might be the cells of origin of medulloblastomas that have alterations in the Wnt pathway [96, 97]. As yet, no mouse models of medulloblastoma in which the Wnt pathway is altered have been developed. However the overexpression of a constitutively active form of the β -catenin protein in GCPs *in vivo* or *ex vivo* does not alter cerebellar development, nor does it induce malignant transformation (unpublished observations by M. Thompson and colleagues, and Y. Pei and R. Wechsler-Reya, reported in [97]). This suggests that GCPs may not be susceptible to mutations affecting the Wnt pathway.

Earlier this year, Sutter *et al.* reported the development of medulloblastoma in immuno-compromised mice injected with CD133-positive neural stem cells obtained from the post-natal mouse cerebellum and genetically engineered *in vitro* to inactivate both the *p53* and the *Rb* tumour suppressor genes [89]. The same group had previously shown that the combined loss of *p53* and *Rb* in cerebellar GCPs gave rise to medulloblastoma with 100% penetrance [82]. A comparison of gene expression between medulloblastomas originating from the two different cell types showed significant differences, with GCP-derived tumours expressing high levels of markers of the GCP lineage (*e.g. Atoh1, Gli1, Mycn, Ptch2*), and stem cell-derived tumours strongly expressing genes typically associated with a neural stem cell phenotype (*e.g. Sox2, Nestin*) [89]. This was the first study in which non-GCP cerebellar cells have been genetically engineered to give rise to medulloblastoma independently of Shh signalling. It suggests that the disruption of the same key regulatory pathways can trigger medulloblastoma formation from different cell types and at different stages of cerebellar development. This type of approach is likely to provide significant insights into the putative cell of origin of Shh-independent medulloblastomas.

1.9. Gene expression profiling of medulloblastoma

To identify novel genes involved in medulloblastoma, several investigators have performed gene expression analysis of human primary tumours and normal brain or cerebellum [98-103]. One of the earliest studies of this kind was carried out by Michiels and colleagues in 1999 [98], who used the serial analysis of gene expression (SAGE) technique to compare expression profiles between a human medulloblastoma and a sample of normal fetal brain. SAGE exploits DNA sequencing to measure the frequency with which specific short nucleotide sequence tags corresponding to unique gene

transcripts are represented within a cDNA library generated from the tissue of interest [104]. The major advantage of this technique is that it does not require prior knowledge of the genome under investigation and is therefore completely unbiased. The authors identified 138 sequence tags with significantly different counts in the two samples examined. Among these, sequences corresponding to the *ZIC1* and *OTX2* genes were expressed at a higher level in the tumour sample compared to normal brain. *ZIC1* and *OTX2* gene expression was verified by Northern blot analysis and found to be increased in a set of six independent medulloblastoma samples compared to fetal brain [98]. As the two genes are normally expressed in the germinal zones of the developing cerebellum, this study provided initial evidence supporting the hypothesis that medulloblastoma may originate from cerebellar precursor cells. Table 1.2 contains a summary of the major findings of this and the following studies.

Approaching the problem from a different perspective, MacDonald *et al.* used DNA microarrays to identify differences in gene expression between metastatic and non-metastatic medulloblastomas [99]. Approximately one-third of medulloblastoma patients present with metastatic disease at the time of diagnosis and up to two-thirds will display dissemination of neoplastic cells to the brain and spine by the time of relapse [6]. Moreover, the evidence of metastatic disease at diagnosis is among the most powerful independent indicators of poor medulloblastoma prognosis [9]. Thus, the investigation of changes in gene expression that are associated with metastatic medulloblastoma could provide useful prognostic markers as well as putative targets for new therapeutic strategies directed against tumour dissemination. MacDonald and colleagues identified an 85-gene signature which allowed an accurate classification of medulloblastomas into either the metastatic or the non-metastatic subgroup [99]. The gene coding for the platelet-derived growth factor receptor (*PDGFR*) was one of the

Table 1.2. Gene expression profiling of medulloblastoma.

Study	Technology	Experimental outline	Major findings
Michiels <i>et al.</i> 1999 [98]	SAGE	MB <i>versus</i> fetal CB	Markers of cerebellar precursors (<i>e.g.</i> <i>ZIC1</i> and <i>OTX2</i>) are highly expressed in MB
MacDonald <i>et al.</i> 2001 [99]	Affymetrix microarray	Metastatic MBs <i>versus</i> non-metastatic MBs	An 85-gene signature distinguishes metastatic from non-metastatic MBs. <i>PDGFR</i> as a biomarker of tumour aggressiveness.
Pomeroy <i>et al.</i> 2002 [100]	Affymetrix microarray	Comparison of different CNS tumour types	Despite sharing histological features, MBs and PNETs can be distinguished based on gene expression profiles.
		Classic MBs <i>versus</i> desmoplastic MBs	Desmoplastic MBs express a specific gene signature indicative of Shh signalling pathway activation.
		Poor outcome MBs <i>versus</i> good outcome MBs	Genes associated with cerebellar differentiation (<i>e.g.</i> <i>TRKC</i>) are predictive of good outcome. Genes implicated in cell proliferation and metabolism (<i>e.g.</i> <i>MYBL2</i>) are predictive of poor outcome.
Boon <i>et al.</i> 2003 [101]	SAGE	MBs <i>versus</i> normal brain	Identification of tumour-associated genes (<i>e.g.</i> <i>PRAME</i> , <i>CD24</i> , <i>PRL</i> , <i>TOP2A</i> , and <i>MYCN</i>).
Park <i>et al.</i> 2003 [102]	cDNA microarray	MBs <i>versus</i> normal cerebellum	MBs overexpress genes implicated in cell proliferation and migration (<i>e.g.</i> <i>Cyclin D2</i> , <i>Ezrin</i>) and share expression profiles with cells in the EGL.
Neben <i>et al.</i> 2004 [103]	Two colour cDNA microarray	Poor outcome MBs <i>versus</i> good outcome MBs	Identification of 54 genes whose increased level of expression is predictive of unfavourable outcome (<i>e.g.</i> <i>AURKA</i>).
Kho <i>et al.</i> 2004 [105]	Affymetrix microarray	Integrated analysis of human MBs (from Pomeroy <i>et al.</i> [100]) and mouse cerebellum at post-natal days 1 to 60.	Gene expression similarities between: Human MBs and mouse P1-P10 CB. Human CB and mouse P30-P60 CB. Human metastatic MBs and mouse P5 CB.

The table summarises the experimental outline of the major studies of gene expression in human medulloblastomas and their main findings. MB, medulloblastoma; CB, normal cerebellum; CNS, central nervous system.

genes which most strongly correlated with a metastatic phenotype. *In vitro* studies demonstrated an essential role for *PDGFR* in promoting MAPK-dependent cell migration of Daoy medulloblastoma cells [99], suggesting that it might represent an important biomarker of tumour aggressiveness.

In 2002, Pomeroy *et al.* used an Affymetrix GeneChip array representing over 6,000 human genes to analyse a large cohort of CNS malignancies, including primitive neuro-ectodermal tumours (PNETs), atypical teratoid/rhabdoid tumours and medulloblastomas [100]. Their aim was to provide molecular evidence that the different tumour types constituted distinct entities, despite similarities in their histology [100]. Indeed they found that each one of the different tumour types expressed a defining set of genes which were indicative of their putative cells of origin. In particular, medulloblastomas, as opposed to PNETs, expressed genes characteristic of cerebellar granule neurons (*e.g.* *ZIC1* and *NSCL1*). This suggests that despite having been classified under the same broad category of embryonal brain tumours for a long time, medulloblastomas and PNETs represent distinct molecular and biological tumour types, in which different transcriptional programmes are activated [100].

In the same study, the authors addressed the possibility that the diverse histologies within the medulloblastoma tumour type were associated with different molecular profiles. They compared gene expression profiles of classic and desmoplastic medulloblastomas and identified a specific gene signature for the desmoplastic histology. This signature included genes belonging to the Shh signalling pathway (*e.g.* *GLII*, *PTCH*, *MYCN*, *IGF2*), providing early evidence linking abnormal activation of the Shh pathway to sporadic desmoplastic medulloblastomas [100].

Regardless of their possible role in the aetiology of medulloblastoma, differentially expressed genes may be useful biomarkers of disease course and responsiveness to therapy. Pomeroy *et al.* analysed gene expression in a series of 60 primary medulloblastomas from patients who underwent similar post-surgical treatment to identify candidate genes whose level of expression correlated with patient outcome. Among the best predictors of favourable outcome were genes related to cerebellar

differentiation (e.g. *TRKC* and *NSCL1*), whereas genes implicated in cell proliferation and metabolism (e.g. *MYBL2*, *E2F5*, *CENPF*) were expressed at higher levels in tumours associated with a poor prognosis [100]. Although the molecular mechanisms by which the genes identified might affect prognosis are not clear, the identification of a gene expression signature which can predict patient outcome undoubtedly represents an extremely valuable tool in clinical practice.

More studies investigating medulloblastoma gene expression profiles followed the work by Pomeroy and colleagues. In 2003, Boon *et al.* reported how they used SAGE to profile a series of 20 primary medulloblastomas and samples from multiple regions of the human adult and paediatric brain [101]. They identified 30 transcripts expressed at high levels in the tumour samples but with little or no expression in the normal brain. These included the cancer-testis antigen *PRAME*, *CD24*, *PRL*, *TOP2A*, and *MYCN* [101]. In same year, Park *et al.* applied cDNA microarray technology to compare the expression of 1,200 genes between six samples of paediatric medulloblastoma and total normal cerebellum [102]. Among the genes expressed at higher level in the tumour samples were genes implicated in cell proliferation and migration, e.g. *Cyclin D2*, *Ezrin*. Interestingly, they identified a larger number of genes whose expression decreased in medulloblastomas compared to normal cerebellum, and which included *Tenascin-C*, *GABBR1*, encoding the GABA-B receptor subunit 1, and *TRKB*. They also performed immunocytochemical analysis for some of the candidate genes using sections of normal human fetal cerebellum and found that medulloblastomas shared similar expression profiles with precursor cells in the EGL [102].

Another study on medulloblastoma gene expression was carried out by Neben *et al.* to identify genes whose expression level could be indicative of patient survival

[103]. A cohort of newly diagnosed medulloblastomas was analysed by two-colour cDNA microarrays using a sample of universal human RNA derived from ten human cancer cell lines as a reference. The array included approximately 2,600 genes with relevance to mitosis, cell cycle control, oncogenesis or apoptosis. Analysis of individual gene hazard ratios identified 54 genes whose increased level of expression was predictive of unfavourable outcome [103]. The expression of nine of these genes was verified on a larger series of 180 medulloblastomas using tumour tissue microarrays. Positive staining for aurora kinase A (*AURKA/STK15*), which is implicated in the regulation of chromosome segregation during mitosis, was identified as an independent prognostic factor for overall survival. Moreover, amplification of the *AURKA* gene was detected in 32.5% of the medulloblastoma samples by fluorescent *in situ* hybridisation and was associated with poor survival [103].

An interesting approach to the molecular characterisation of human medulloblastoma was developed by Kho *et al.*, who applied principal component analysis to summarise and compare gene expression profiles associated with human medulloblastomas and different post-natal stages of normal mouse cerebellum [105]. Using this statistical tool, they observed that human medulloblastoma samples shared similar patterns of gene expression with mouse cerebellum at post-natal days 1-10 (P1-P10), whereas normal human cerebellar samples were more similar to mouse P30-P60 cerebella. They also found a strong association between metastatic medulloblastomas and mouse P5 cerebella, and between less aggressive tumour samples and mouse cerebella of more than five post-natal days, suggesting that tumour clinical behaviour can be predicted by the expression profile of development-related genes [105]. This study represents one of the first genome-wide analyses providing a developmental perspective on tumorigenesis, and strongly emphasises the importance of studying the

molecular programmes regulating normal cerebellar development for a better understanding of medulloblastoma pathogenesis.

These early analyses of medulloblastoma gene expression demonstrated the use of large scale approaches for the unbiased identification of genes affecting tumour clinical behaviour. They also provided strong evidence of the profound connections between normal cerebellar development and medulloblastoma oncogenesis, indicating that the same genes are implicated in both processes, so that the combined study of the two systems can be used to investigate human medulloblastoma aetiology.

1.10. Molecular classification of human medulloblastoma based on gene expression profiles

Over the last few years, continuous improvements in microarray technology have boosted the scale of gene expression analysis up to the whole-genome-level [106]. Several groups have exploited the high resolution capacity of novel microarray platforms to perform genome-wide analysis of human medulloblastoma gene expression and detailed the existence of discrete tumour molecular subgroups, making a large contribution to our understanding of medulloblastoma molecular heterogeneity [20, 92].

The first of a series of seminal papers in the field was published by Thompson *et al.* in 2006 [20]. The authors profiled a cohort of 46 paediatric medulloblastomas of the classic, desmoplastic and large cell/anaplastic histological subtypes. They applied unsupervised cluster analysis to subgroup the tumour samples according to the expression patterns of the most variable genes, with the assumption that differences in gene expression would be caused by distinct sets of genetic alterations that caused the tumour to form in the first place. Five distinct subgroups were identified, each of which expressed a unique gene signature indicative of the presence of key molecular

alterations, as verified by gene sequence analysis and FISH [20]. The authors found subgroup-specific alterations affecting the Shh signalling pathway (mutations of *PTCH* and *SUFU*) in tumours that showed overexpression of genes belonging to the same pathway (SHH tumours). Similarly, a second molecular subgroup displayed a gene expression profile and a pattern of genetic alterations suggestive of Wnt signalling pathway activation (WNT tumours). Importantly, these two sets of combined genetic and transcriptional alterations appeared to be mutually exclusive, clearly suggesting that tumours belonging to the two molecular subgroups originated from alternative oncogenic processes. In contrast, the other three molecular subgroups did not clearly associate with any specific regulatory pathway [20].

Two years later, Kool *et al.* used an even more comprehensive approach to investigate the associations between gene expression profiles and genetic abnormalities of medulloblastomas characterised by distinct clinico-pathological features. A total of 62 human medulloblastomas were profiled using Affymetrix microarrays, and 52 of them were also analysed by comparative genomic hybridisation (CGH) to search for copy number alterations [92]. The authors initially performed an unsupervised clustering of the samples included in the microarray experiment and found that they recapitulated the five molecular clusters previously identified by Thompson *et al.* [20]. Indeed, the tumours in the SHH subgroup showed increased levels of transcripts encoded by genes involved in Shh signalling, such as *PTCH*, *BOC*, *GLI1* and *GLI2*. These tumours also had a significantly higher frequency of 9q loss [92]. Conversely, WNT tumours overexpressed several of the Wnt pathway genes, including *AXIN2*, *LEF1*, *WNT11* and *WNT16*. They all also carried mis-sense mutations of the *CTNNB1* gene resulting in single amino acid changes in the β -catenin protein, and all of the cases

examined showed monosomy of chromosome 6, in agreement with data from Thompson *et al.* [20] and Clifford *et al.* [19].

The authors also provided a more detailed description of the molecular features characterising the remaining three medulloblastoma subgroups (subgroups C, D and E). Tumours in these three clusters were closely related and showed increased levels of expression of genes implicated in neuronal (subgroups C and D) and retinal differentiation (subgroups D and E). In contrast with SHH and WNT tumours, clusters C, D and E often showed gain of chromosome 18. Gain of chromosome 17q, frequently in the form of *i17q*, was strongly associated with tumours in clusters C and D [92].

Interestingly, the five medulloblastoma molecular subgroups also differed in terms of clinical and histological features. Evidence of metastatic disease at diagnosis was significantly more frequent in tumours of the C, D and E clusters. SHH tumours occurred more frequently in patients younger than three or older than 25 years of age, whereas the age of the patients with the other tumour subgroups generally ranged between 3 and 20 years. Moreover, all of the WNT tumours were of classic histology, whereas most of the SHH tumours were desmoplastic medulloblastomas [92].

More recently, Northcott *et al.* applied a similar whole-genome approach to study the molecular heterogeneity of human medulloblastoma [107]. The investigators profiled a total of 90 primary medulloblastomas. Unsupervised hierarchical clustering of the most differentially expressed genes across the entire data set generated four discrete subgroups. As had been described by Thompson *et al.* [20] and Kool *et al.* [92], the investigators clearly identified the SHH and WNT subgroups, whereas they only observed two additional clusters, which they called C and D. In agreement with previous observations, SHH tumours showed the frequent loss of chromosome 9q,

whereas most of the WNT tumours carried a single copy of chromosome 6. Isochromosome 17q was only found in clusters C and D [107].

These studies significantly advanced our knowledge of the molecular background characterising human medulloblastomas. Whether the four/five tumour molecular subgroups identified originate from the same cell lineage via the accumulation of different genetic alterations, or whether they arise from distinct cell types remains to be elucidated. Nevertheless, the importance of a detailed molecular classification of medulloblastomas is indisputable. Potential stratification schemes for medulloblastoma patients that take into account molecular parameters as well as clinical and histological features have been recently proposed and are likely to be implemented for clinical practice in the near future [7]. Table 1.3 summarises the major genetic, transcriptional and clinical features defining the different medulloblastoma molecular subgroups.

Table 1.3. Genetic, transcriptional and clinical associations of medulloblastoma molecular subgroups.

	Medulloblastoma molecular subgroups		
	WNT	SHH	Non-WNT/SHH
Proportion of medulloblastomas	15%	25%	65%
Age at diagnosis	Median age ~ 10 years (range 6-20)	Median age ~ 3 years (range 1.5-35.3) Uncommon between 5 and 15 years of age	Median age ~ 8 years (range 2-25.6)
Histological variant	Mainly classic MBs No desmoplastic MBs	Mainly desmoplastic MBs 50% of LC/A MBs	Mainly classic MBs 50% of LC/A MBs
Metastatic disease at diagnosis	Rare	Rare	Frequent
Chromosomal abnormalities	Monosomy of chromosome 6	Loss of chromosome 9q Rare MYCN amplification	Loss of chromosome 17p Isochromosome 17q Rare MYC/MYCN amplification
Gene mutations	Frequent <i>β-catenin</i> mutations	<i>PTCH</i> mutations in some MBs Rare <i>SUFU</i> mutations	
Gene expression patterns	Wnt signalling pathway	Shh Signalling pathway Markers of GCPs	Neuronal differentiation Retinal differentiation
Prognosis	Very good	Good if desmoplastic MB Poor if LC/A MB	Poor if metastatic Poor if LC/A MB

MB, medulloblastoma; LC/A, Large cell/anaplastic. Adapted from Ellison [7], with data derived from Thompson *et al.* [20], Kool *et al.* [92], Northcott *et al.* [107].

1.11. Alternative mRNA splicing

Changes in gene expression are necessary for cells to differentiate and respond to extracellular and environmental signals, as well as for cell death, proliferation and malignant transformation. In prokaryotic organisms, the combined activation and repression of different sets of genes is the main mechanism which defines the identity of a cell. However, the discovery of introns in the eukaryotic genome and of the process of splicing, which removes them from immature mRNAs, introduced another level of

complexity in the way gene expression is modulated to generate a large variety of protein products [108].

Intron sequences must be precisely excised to form mature mRNAs, or frame shift alterations would be introduced, which could result in inappropriate protein translation [109]. Introns are much longer than exons, reaching up to tens of thousands of nucleotides in length, and they contain several regulatory elements, including splice donor and acceptor consensus signals, the branching sequence preceding the acceptor site, splicing enhancers and silencers [109-111]. The combination of all of these cis-acting elements, together with their counterparts located within the exon sequences and RNA secondary structures, defines which sequences will be included in the mature mRNA product [109, 112].

The spliceosome is a complex of specialised RNA and protein subunits, containing at least five types of small nuclear ribonucleoproteins (snRNPs) and a large number of auxiliary proteins. It is responsible for intron excision and exon joining during each one of the splice events that are necessary to generate a mature mRNA molecule [109, 113]. Depending on the availability and relative abundance of the trans-acting regulatory proteins, there is variability in the selection of certain splice sites, so that the same precursor molecule can be processed in different ways giving rise to alternative mature mRNA forms [112].

At the most basic level, it is possible to distinguish between two modes of splicing: constitutive splicing refers to the usage of certain exons which are always included in the final mRNA products; whereas, alternative splicing occurs when two or more splice sites compete so that the corresponding exons can be either retained in or removed from the mature mRNA. In addition, alternative splicing is subclassified into several modes (Figure 1.5). The extent of any individual exon inclusion or exclusion

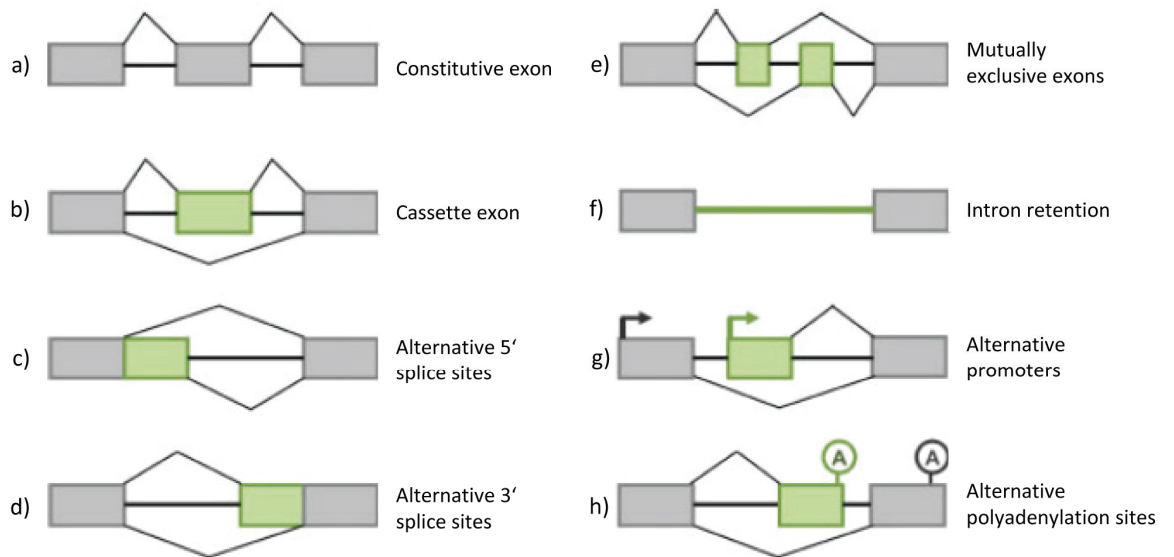


Figure 1.5. Alternative modes of splicing.

Constitutive exons are always included in the mature mRNA (a) and therefore do not affect the quality of the final mRNA product. A consistent increase in the variety of mRNA molecules is obtained through the alternative usage of exons, introns, promoters and polyadenylation sites (b-h). Cassette exons are individual exons which can be independently included or excluded from the mature mRNA (b). Alternative 5' and 3' splice sites allow the inclusion/exclusion of only part of an exon (c, d). Mutually exclusive splicing involves the selection of only one from an array of two or more exon variants (e). Finally, intron retention (f), alternative promoters (*i.e.* alternative 5' ends of the transcript) (g) and alternative polyadenylation sites (*i.e.* alternative 3' ends of the transcript) (h) all contribute to mRNA diversity. Reproduced from Ward and Cooper [114].

depends on the strength of the cis-regulatory sequences as well as on the presence of specific trans-acting splicing proteins which in turn are modulated by a variety of cellular stimuli [112].

1.11.1 Alternative splicing in cancer biology

The presence of any individual exon in a mature mRNA can significantly influence the final protein product, in terms of translation efficiency, protein stability, subcellular localisation, protein-protein interaction and protein activity [108]. It is easy to imagine how a change in exon inclusion rates could result in the disruption of protein functions and eventually lead to a pathological cell response. Indeed, it has been estimated that up to 50% of human disease-causing mutations affect the splicing process [115]. Inappropriate splicing can be generated either from mutations in the cis-acting elements within individual genes, or changes in the trans-acting factors that are required for normal splicing or splicing regulation [114, 115].

Defects in mRNA splicing are commonly found in a variety of human cancers [116-118]. Mutations that alter cis-acting splicing sequences can affect the pattern of mRNA isoforms that are expressed and, as a consequence, protein function. Activation of signalling pathways that regulate the expression and activity of trans-acting splicing factors can result in a change in the proportion of normal mRNA splice variants. Both cases can lead to a significant change in the global pattern of protein expression within a cell and cause the deregulation of critical cellular processes, including cell proliferation and differentiation, all of which contribute to cancer initiation and growth (Table 1.4 and Figure 1.6) [119]. Several studies have documented the expression of tumour-specific splice forms in a variety of systems, and suggested that they may represent useful biomarkers for tumour classification and prognosis as well as novel targets for

cancer therapy (reviewed in [117, 120, 121]). Moreover, there is evidence for numerous genes that participate in the regulation of mRNA processing to be causally implicated in cancer (Table 1.4) [117].

As our knowledge of the mechanisms regulating alternative mRNA splicing in higher eukaryotes improves, it becomes increasingly clear that an exon-level approach to the study of human cancer is likely to reveal a completely novel range of candidate events critically implicated in tumorigenesis.

Table 1.4. Examples of disruptions in mRNA splicing mechanisms that are associated with malignant disease.

Gene (function)	Mechanism of splicing disruption	Molecular consequences	Biological implications	Reference
CD44 (multifunctional receptor)	Splice form imbalance	High levels of CD44v6 induced by RAS signalling	CD44v6 sustains late RAS signalling and mitogenic progression.	Cheng <i>et al.</i> 2006 [122]
KLF6 (tumour suppressor)	Splice form imbalance	High levels of KLF6-sv1	KLF6-sv1 antagonises the tumour suppressor function of KLF6 and promotes tumour growth and dissemination in both ovarian and prostate cancer models. Biomarker of poor prognosis in prostate, lung, and ovarian cancer.	DiFeo <i>et al.</i> 2009 [123]
KLK8 (peptidase)	Splice form imbalance	High levels of KLK8-T4	Biomarker of poor prognosis in lung cancer.	Planque <i>et al.</i> 2010 [124]
KIT (oncogene)	Mutation in cis-acting sequence	Deletion of intron 10 3' splice site	Aberrant splicing resulting in constitutive protein activation.	Chen <i>et al.</i> 2005 [125]
BRCA1 (tumour suppressor)	Mutation in cis-acting sequence	Nonsense mutation exon 18 skipping	Predisposes to breast and ovarian cancer.	Mazoyer <i>et al.</i> 1998 [126]
SFRS1 (splicing factor)	Overexpression of trans-acting splicing factor	Inappropriate splicing of <i>BIN1</i> , <i>MNK2</i> and <i>S6K1</i> target genes	<i>BIN1</i> loses its tumour suppressor properties, <i>MNK2</i> and <i>S6K1</i> acquire transforming functions.	Karni <i>et al.</i> 2007 [127]

The table illustrates some examples of alterations affecting the splicing process and which have been described in association with human cancer.

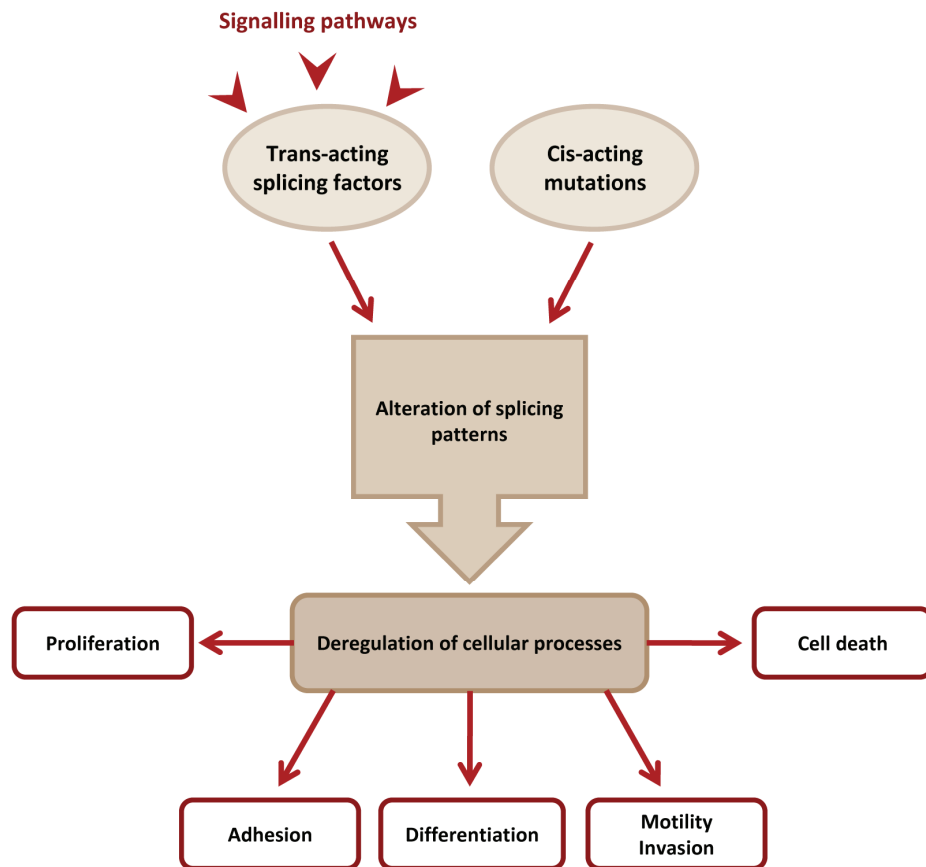


Figure 1.6. Causes and consequences of splicing pattern alterations.

Defects in mRNA splicing can result from mutations affecting the cis-regulatory elements or the deregulation of trans-acting splicing factors. Both can lead to the alteration of critical cellular processes and initiate or sustain tumour growth. Adapted from Srebrow and Kornblihtt [118].

1.11.2. Relevance of alternative splicing in medulloblastoma

During the last couple of years, a few studies have investigated specific alternative splicing events occurring in medulloblastoma [128-131]. These studies suggested that differential expression of specific splice isoforms might alter medulloblastoma biology and provide new clues for the investigation of the signalling pathways involved in tumorigenesis.

1.11.2.1. The *ErbB-4* gene

Ferretti *et al.* analysed the expression pattern of *ErbB-4* splice variants in human medulloblastomas [128]. ErbB-4 is a member of the ErbB family of receptors which are implicated in both development and tumorigenesis [132]. In particular, ErbB-4 is highly expressed during the development of the cerebellum and its levels decrease into adulthood [133]. Two major cytoplasmic splice variants of the *ErbB-4* gene have been described, CYT-1 and CYT-2, which differ in their C-terminal domain. CYT-1 includes a phosphatidylinositol 3-kinase (PI3K)-binding site that is missing in CYT-2 [134]. By analysing medulloblastoma tissues derived from *Ptch*^{+/+} mice, mouse GCP cultures and human medulloblastoma cell lines, the investigators observed a negative correlation between the levels of expression of the *ErbB-4* and *Gli1* genes, suggesting that activation of the Shh signalling pathway negatively regulates *ErbB-4* expression [128]. Interestingly, in primary human medulloblastomas, low levels of Gli1 are associated with increased levels of the ErbB-4 CYT-1 form [128]. *In vitro* studies using medulloblastoma cell lines showed that activation of the ErbB-4 receptor with its ligand neuregulin resulted in enhanced resistance to starvation and to etoposide-dependent apoptosis only when the CYT-1 isoform was expressed. In contrast, expression of CYT-2 inhibited cell proliferation [128]. Moreover, the authors measured CYT-1:CYT-2

ratios in a series of human medulloblastomas and found that higher values were characteristic of large cell/anaplastic tumours and were associated with a poorer prognosis for patients [128].

1.11.2.2. *Survivin*

Survivin is a member of the inhibitor of apoptosis protein family, and it is overexpressed in most human cancers [135]. In addition to the full length survivin protein, three alternatively spliced forms have been described, which differ in their subcellular localisation and unique functions [136]. In particular, full length survivin and survivin-deltaEx3 have been shown to possess anti-apoptotic properties in human tumours, whereas survivin-2B counteracts this anti-apoptotic activity [136]. Expression analysis of survivin splice variants in human medulloblastoma showed that all of the described forms were expressed at higher levels relative to normal adult brain and cerebellum [130, 137]. More importantly, high levels of survivin protein, and especially of the deltaEx3 variant, were indicative of a poor prognosis for patients [130, 137].

1.11.2.3. The *Ptch* gene

Using a specifically designed oligonucleotide microarray containing exon junction probes for the *PTCH* gene, Nagao and colleagues identified exon 12b as a novel alternative exon located between exons 12 and 13, and expressed in the heart and brain, particularly in the cerebellum, of both humans and mice [138]. Exon 12b contains a stop codon which results in a truncated PTCH protein [138]. In a subsequent study, the authors used a Gli-luciferase reporter construct to investigate the biological activity of the PTCH12b truncated protein. They found that, in contrast to the wild type PTCH protein, PTCH12b was unable to repress luciferase activity. However, when the two

proteins were co-expressed, PTCH12b reversed PTCH-mediated luciferase suppression, suggesting that it has a dominant negative effect on wild type PTCH [129]. Interestingly, two cases of Gorlin's syndrome were described, in which inclusion of exon 12b in the *PTCH* transcript followed the activation of cryptic splice donor sites which resulted from the partial disruption of the authentic splice donor site due to point mutations [138]. This suggests that mutations in the *PTCH* gene which favour the imbalanced expression of the *PTCH12b* isoform could initiate tumorigenesis [138]. Moreover, *PTCH12b* was found to be expressed in medulloblastoma cell lines and primary tumours [129].

1.11.2.4. The *Mtss1* gene

Metastasis suppressor 1, *Mtss1*, encodes an actin-binding protein which has been shown to regulate actin filament assembly [139]. In the epidermis, *Mtss1* has been identified as a Shh-responsive gene which participates in the regulation of Gli-dependent transcription [140]. Glassmann *et al.* described a splicing shift occurring during the maturation of GCPs in the developing mouse cerebellum, in which *Mtss1* exon 12 is replaced by the CNS-specific exon 12a [131]. Of note, the authors found that, besides being expressed in immature GCPs, exon 12 is also preferentially expressed in primary human medulloblastomas, indicating that expression of the alternative exon 12a may be associated with cellular differentiation [131]. Bioinformatic analysis of the *Mtss1* gene suggested a possible role for exon 12a in favouring the interaction of the Mtss1 protein with tyrosine kinases implicated in the regulation of cerebellar cell migration and histogenesis [131].

1.12. Aim of this study

The aim of this project is to investigate global patterns of differential gene expression and alternative splicing in medulloblastoma samples isolated from a cohort of paediatric patients treated at Great Ormond Street Hospital and normal cerebellar samples. I will initially analyse the gene expression profiles of primary tumour tissues to classify them into one of the molecular subgroups described in the literature. I will then compare gene expression patterns between medulloblastoma subgroups and normal cerebellum with the aim of identifying biologically interesting candidate genes whose level of expression correlates with a malignant phenotype. Putative tumour-related genes will be further investigated using *in vitro* cultures of mouse cerebellar granule cell precursors as well as human medulloblastoma cell lines to assess their possible role in regulating cerebellar cell proliferation and malignant transformation.

I will also perform a statistical analysis of differential exon expression for the identification of splice variants which associate with medulloblastoma. Technical validation of a selection of candidate events will be carried out to confirm the reliability of the methodology. I will then look for possible similarities between splicing patterns characteristic of human medulloblastomas and normal cerebellar development, to investigate whether alterations in splicing programmes regulated in the cerebellum may be relevant to the pathogenesis of medulloblastoma.

Chapter 2

Materials and methods

2.1. Human specimen collection and classification

2.1.1. Samples for exon array analysis

The array study included 14 snap-frozen paediatric medulloblastoma samples (a mix of female and male samples between 1 and 14 years of age) obtained from the Histopathology Department of Great Ormond Street Hospital (GOSH), with the approval of the local research ethics committee (LREC ref. no. 06/Q0508/57). In addition, a sample of normal cerebellar tissue was obtained from a juvenile patient who had undergone brain surgery at GOSH for the removal of a pilocytic astrocytoma of the posterior fossa. Additional normal cerebellar total RNA samples to be used as controls for the study were purchased from commercial sources and included one adult cerebellar RNA (Applied Biosystems/Ambion), one pool of 24 individual adult cerebellar RNAs (Clontech Laboratories), and two fetal cerebellar RNAs (BioChain Institute). A detailed description of all samples included in this study is reported in Table 3.1, on page 97.

2.1.2. Samples for validation of differential splicing

Twenty human primary medulloblastoma RNA samples were kindly provided by Professor Steve Clifford from the Northern Institute for Cancer Research, Newcastle upon Tyne, UK. All samples had been profiled using Affymetrix 3' arrays and classified into medulloblastoma molecular subgroups as reported in Kool *et al.* [92].

Six frozen specimens of normal adult cerebellum were obtained from the UCL Institute of Neurology Queen Square Brain Bank (QSBB), following ethical committee approval. A further four normal cerebellar total RNA samples were obtained from commercial sources and included two adult and one fetal cerebellar RNAs (all purchased from BioChain Institute), and one pool of 10 individual adult cerebellar RNAs (Clontech Laboratories). Sample clinical information can be found in Table 5.2, on page 186.

2.1.3. Tumour histopathology

A histopathological review of the selected medulloblastoma cases for the array study was undertaken by a clinical neuropathologist (Dr. Thomas Jacques). Haematoxylin and eosin (H&E) slides from the original diagnosis were re-evaluated and tumour features of anaplasia, nodularity and desmoplasia (collagen deposition) were graded for each tumour sample according to published criteria [15, 141]. Anaplasia was graded as none, slight, moderate or severe according to increasing levels of nuclear enlargement and pleomorphism, extensive mitosis, extensive apoptosis and cell wrapping. The extent of anaplasia was considered diffuse when anaplasia was present in all fields examined; otherwise, it was designated focal. Nodularity was graded according to the percentage of tumour area that consisted of nodules: extensive (96-100% of the area contained nodules), widespread (51-95%), moderate (11-50%), slight (1-10%), or none (no nodules). Desmoplasia was scored as being present or absent. According to this histological grading, each tumour was classified into one of the major medulloblastoma variants: classic (no or slight anaplasia, no or slight nodularity), desmoplastic (presence of desmoplasia and nodularity) or anaplastic (moderate or severe anaplasia).

Prior to RNA extraction, a 10 µm tissue section was cut from each frozen tumour sample using a cryostat and H&E staining was performed by Sian Gibson in the histopathology laboratory of GOSH. Stained sections were then examined to confirm that the frozen specimen was representative of the tumour.

2.2. Exon array study

2.2.1. RNA processing and array hybridisation

Total RNA was extracted from frozen tissue specimens as described in section 2.4.1.1. Two µg of each RNA sample was processed by Nipurna Jina and Sean Barry at the ICH Gene Microarray Centre at UCL using the Affymetrix GeneChip Whole Transcript Sense Target Labelling Assay [142]. The majority of ribosomal RNA was depleted from each RNA sample to increase sensitivity, then an *in vitro* transcription-based linear amplification was carried out and finally, single stranded DNA targets were generated in the sense orientation. A schematic representation of the major steps of the procedure is shown in Figure 2.1. Fragmented and labelled DNA was applied to the Affymetrix GeneChip Human Exon 1.0 ST arrays. Hybridisation was performed for 16 hours at 45 °C with constant rotation. The following day chips were washed and stained with SAPE (Streptavidin Phycoerythrin) according to the manufacturer's recommendations and then scanned. GeneChip Operating System software was used to read image files and to convert them into workable .CEL intensity files.

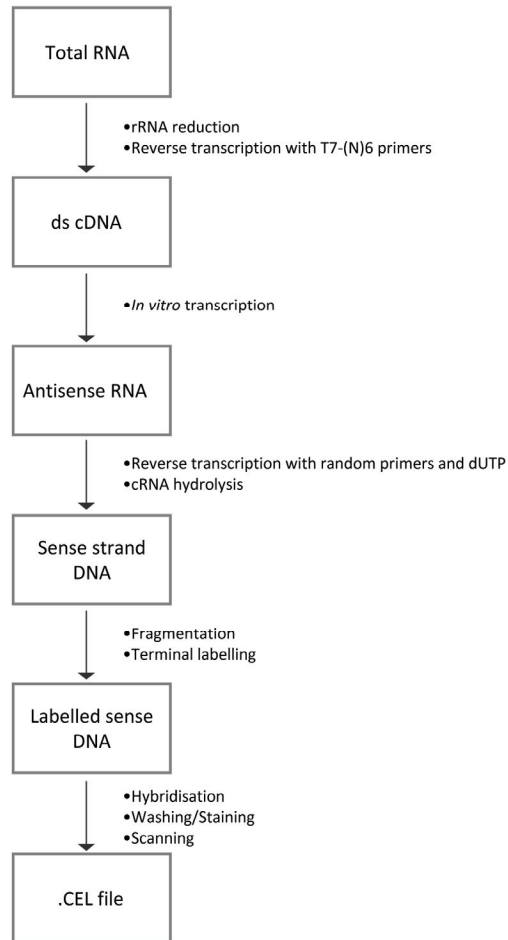


Figure 2.1. Schematic representation of the whole transcript sense target labelling assay.

To increase the assay sensitivity, most of the ribosomal RNA was removed from the total RNA samples. The remaining RNA was reverse-transcribed into double-stranded cDNA using short random oligonucleotide primers linked to a T7 promoter. Antisense RNA (cRNA) was generated by *in vitro* transcription, before a second cycle of cDNA synthesis was carried out through random priming and addition of dUTP to the nucleotide substrates. The cRNA template was digested by RNase H treatment, and the remaining sense strand cDNA was fragmented using a combination of uracil-DNA glycosylase and human apurinic/apyrimidinic endonuclease, which cut the DNA where dUTP has been incorporated. Finally, DNA fragments were terminally labelled with biotin molecules and hybridised to the Affymetrix chip. Unbound DNA was washed from the chip and Streptavidin Phycoerythrin was added followed by biotinylated anti-streptavidin antibody to stain the hybridised DNA molecules before scanning.

2.2.2. Affymetrix Human Exon 1.0 ST array

The Affymetrix Human Exon arrays consist of approximately 5.5 million probes, targeting the whole length of protein coding transcripts across the entire genome. The expression signals obtained from these probes are summarised into probe set signals, which provide a measure of expression of individual exons. The collection of probe sets mapping to the same gene structure constitutes a transcript cluster (gene). By combining the expression signals of all of the probe sets that belong to one transcript cluster, it is possible to calculate an accurate estimate of gene expression as well as to identify events of differential exon inclusion or skipping (Figure 2.2).

Statistical analysis of exon array data was carried out at two levels: firstly, at the gene level, to identify genes differentially expressed between normal and tumour samples; secondly, at the exon level, to investigate patterns of alternative splicing.

2.2.3. Exon array analysis software

Exon array data analysis was performed with the help of two main tools: the Affymetrix Expression Console software, which is freely available from the Affymetrix website; and Bioconductor, an open source software project primarily based on the R programming language. I used Expression Console to read .CEL files and generate gene and exon expression values, whereas I used R and Bioconductor for the subsequent statistical analysis.

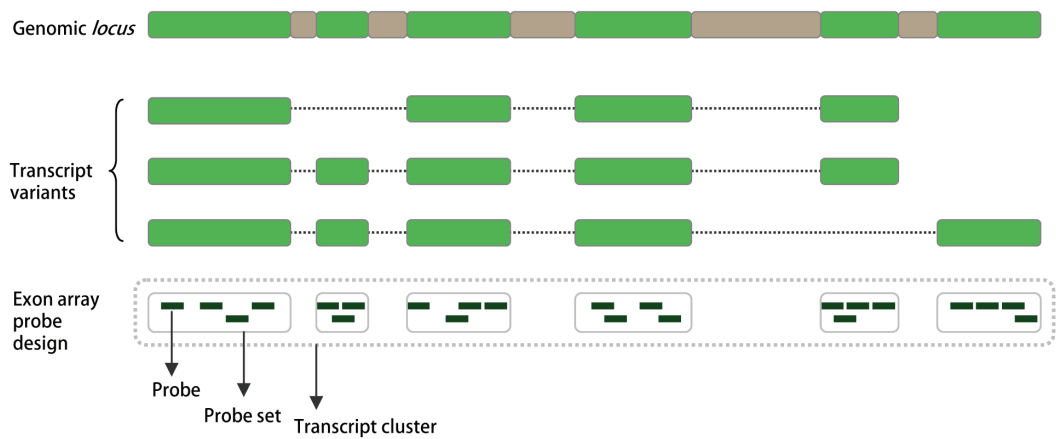


Figure 2.2. Affymetrix Exon array design.

Probes are distributed along the entire length of the gene. On average, four different probes map to each individual exon and their expression signals are summarised into a single probe set signal (exon expression value). Probe sets, in turn, can be assembled into virtual transcript clusters to provide the expression signal of all the transcripts encoded by the same gene (gene expression value). Two levels of analysis can be performed: one at the probe set level, to provide information about alternative splicing; and one at the transcript cluster level, to investigate differential gene expression. Green boxes represent exons. Grey boxes are introns which are removed during mRNA splicing. Adapted from the Affymetrix datasheet [143].

2.2.4. Gene level summary, quality control and analysis

Gene-level signal estimates were calculated by applying the PLIER (Probe Logarithmic Intensity Error) algorithm [144], and including only those probe sets that map to well-annotated exons (core probe sets). Variance stabilisation was obtained by adding the small constant 16 to all the data points, followed by \log_2 transformation [144].

As a quality control analysis, I drew box plots and density plots which described the overall signal distribution of every individual sample within the dataset. Samples whose intensity signals deviated from the common distribution of the set were excluded from further analysis.

Prior to statistical analysis, a filter based on expression was applied to remove any genes not expressed across the entire dataset. I used the detection above background (DABG) algorithm, which is implemented in Expression Console, to generate a detection p-value for every individual probe set based on the background signal distribution of control probes on the array. I considered a gene to be expressed in any given sample if at least 75% of its targeting probe sets had a detection p-value < 0.05 . Genes considered to be expressed in less than three samples were filtered out.

Once filtered, the gene-level dataset was analysed to identify differentially expressed genes (DEGs) between sample subgroups, using the moderated t-statistic of the LIMMA package [145] and applying False Discovery Rate (FDR) to correct for multiple testing. The LIMMA moderated t-statistic differs from the ordinary Student's t-statistic in the way it estimates a moderated standard error for every gene by taking into account information from all other genes. This procedure shrinks estimated standard errors towards a pooled estimate, relatively increasing and decreasing small and large sample variances respectively, to reduce the likelihood that significant

statistics arise merely from under-estimated sample variances. Moderated statistics such as the one in the LIMMA package have been reported to work particularly well with small microarray datasets [145]. FDR controls the expected proportion of false positives within the collection of significant observations. For example, if 100 observations were considered to be significantly different between two sample groups with a maximum FDR value of 0.05, we would expect 5 of these observations to be false positives.

Lists of significantly up- and down-regulated genes obtained from statistical comparisons were subjected to functional enrichment analysis using DAVID functional annotation tools [146].

2.2.5. Alternative splicing analysis

Alternatively spliced exons were identified by Dr. Sonia Shah at the Bloomsbury Centre for Bioinformatics, UCL. Following the removal of cross-hybridising probe sets, as according to Affymetrix annotation, exon- and gene-level signal estimates were generated through the Robust Multichip Average (RMA) algorithm [147]. To reduce false positives caused by non-expressed genes or non-expressed exons across all samples, background noise was filtered out. This was achieved by excluding probe sets and transcript clusters from the dataset which fell into the lowest quartile of the expression signal distribution in all samples.

The Splicing Index algorithm was applied to identify alternative splicing events between sample subgroups. This method aims to identify those exons that show significantly different inclusion rates between two groups of samples. It assumes that in the absence of splicing, the observed signal from each exon would have a constant ratio with the observed signal from its gene across all samples. A ratio that differed significantly between two groups of samples would be indicative of differential

splicing. For every probe set a gene-level normalized intensity (NI) value (probe set signal / gene signal) was calculated and NI average values across sample subgroups were compared through the LIMMA moderated t-statistic and FDR correction to identify statistically significant differences. A splicing index value was also calculated as the \log_2 ratio between NI values in different subgroups.

Statistical analysis of differential splicing has been reported to be particularly prone to the generation of false positives [148, 149]. Filtering of potential false positives was done through manual inspection of the data using expression plots. For example, I discarded probe sets whose expression value strongly and uniformly deviated from the profile of adjacent probe sets, as they most probably indicated cross-hybridising, poorly performing probes or non-expressed exons [150]. Finally, I selected the most promising splicing patterns by visualising probe sets in their genomic context using the publicly available annotation database X:MAP [151]. This database provides information about the location of each exon within the gene, known alternative splicing events, presence of overlapping transcripts and potential artefacts of Affymetrix transcript annotations, such as multiple genes being combined into a single transcript cluster. I evaluated all of this information and selected a subset of most promising alternative splicing events for further analysis.

2.3. Cell biology

2.3.1. Cell lines

2.3.1.1. Daoy

The Daoy cell line was established in 1985 by Jacobsen *et al.* from a portion of a desmoplastic medulloblastoma of a 4-year-old boy [152]. Daoy cells are adherent in culture and display a polygonal shape with prominent nuclei and multiple nucleoli. The

Daoy cell line is hyper-tetraploid, with the majority of cells possessing between 93 and 99 chromosomes. We purchased the Daoy cell line from the American Type Culture Collection.

2.3.1.2. UW228-2

The UW228-2 cell line was established by Keles *et al.* in 1995 from the surgical specimen of a primary medulloblastoma in the posterior fossa of a 9-year-old female patient [153]. UW228-2 cells are adherent in culture and are not sensitive to cell-contact inhibition. They display multiple chromosomal aberrations, among which is the loss of heterozygosity for a distal sequence on the short arm of chromosome 17. The UW228-2 cell line was the kind gift of Professor Silvia Marino from Barts and The London School of Medicine and Dentistry, London.

2.3.1.3. D425 Med

The D425 Med cell line was established in the late 1980s by Friedman *et al.* from the resected tumour tissue of a 5-year-old boy with medulloblastoma [23]. Chromosomal analysis revealed that the D425 Med cell line is near-diploid and displays some of the structural abnormalities most commonly described in human medulloblastoma, such as isochromosome 17q and abundant double minutes, which have been associated with amplification of the *c-Myc* gene [23]. D425 Med cells are semi-adherent in culture and display spheroid morphology. The D425 Med cell line was the kind gift of Professor Silvia Marino from Barts and The London School of Medicine and Dentistry, London.

2.3.1.4. 293FT

The 293FT cell line is a fast growing variant of the HEK 293 cell line, a permanent line established by Graham *et al.* in 1977 by exposing primary human embryonic kidney cells to sheared fragments of adenovirus type 5 DNA [154]. 293FT cells constitutively express the SV40 large T antigen under the control of the human cytomegalovirus promoter. Overexpression of the large T antigen favours the replication of packaging and lentiviral expression plasmids containing the SV40 origin of replication and generally enhances lentiviral production [155]. The 293FT cell line is therefore an ideal host for the production of non-replicating lentiviral particles. We purchased the 293FT cell line from Invitrogen.

2.3.2. Cell culture conditions

Unless otherwise stated, cells were cultured in complete culture medium consisting of Dulbecco's Modified Eagle Medium (DMEM) supplemented with 10% fetal bovine serum, 2 mM L-glutamine and 1% penicillin-streptomycin (all from Invitrogen). Cell cultures were kept in an incubator at 37 °C in an atmosphere of 5% CO₂.

Cell cultures were regularly checked for mycoplasma contamination using a MycoProbe mycoplasma detection assay (R&D Systems) according to the manufacturer's instructions. The MycoProbe assay detects approximately 95% of all of the mycoplasma contaminants using a colorimetric signal amplification system which targets the mycoplasma 16S ribosomal RNA.

2.3.3. Subculture

When cells reached approximately 80% confluence, the culture medium was discarded and the cells were rinsed with PBS to remove any residual serum and incubated for a few minutes at 37 °C with 1 ml of trypsin-EDTA per 10 cm dish. When starting to detach from the dish, the cells were harvested in fresh complete medium and centrifuged at 1,200 rpm in an Eppendorf 5810 R bench-top centrifuge (Eppendorf UK Ltd) for 5 minutes. The resulting cell pellet was resuspended in culture medium and replated at 1:4 to 1:20 dilutions, depending on cell density.

2.3.4. Freezing cultured cells

Cells were harvested and pelleted as described in section 2.3.3. The cell pellet was resuspended in a small volume of culture medium and cells were counted using a Neubauer haemocytometer. Cells were diluted in freezing medium (culture medium plus 10% cell culture grade DMSO) at a concentration of 1×10^6 cells/ml and 1ml aliquots were dispensed into cryovials and transferred to a -80 °C freezer in a Nalgene freezing container (Nalgene Labware) to assure the optimal cooling rate of -1 °C per minute which avoids the formation of intracellular ice crystals. After 24 hours, cells were transferred to liquid nitrogen for longer storage.

2.3.5. Recovery of frozen cells

A vial of frozen cells was rapidly thawed in a water bath at 37 °C. The cells were then transferred to a centrifuge tube containing 10 ml of culture medium and centrifuged at 1,200 rpm for 5 minutes to remove the DMSO. Cells were resuspended in complete culture medium, plated in a 10 cm dish and maintained in an incubator at 37 °C with 5% CO₂. Cells were re-fed with fresh complete medium after 24 hours.

2.3.6. Isolation and culture of mouse granule cell precursors

2.3.6.1. Granule cell precursor preparation

Granule cell precursors (GCPs) were isolated from 7 or 8-day-old C57Bl/6 mice according to the procedure described by Wechsler-Reya *et al.* [43]. Cerebella were dissected, stripped of their meninges, cut into small pieces, and digested for 30 minutes at 37 °C in a solution containing 10 U/ml of papain (Lorne Laboratories Ltd), 200 µg/ml L-cysteine (Sigma Aldrich) and 250 U/ml of DNase I (Sigma Aldrich). A single-cell suspension was obtained by triturating the cerebella in PBS containing 8 mg/ml of chicken egg white trypsin inhibitor (Roche Diagnostics Corporation), 8 mg/ml of bovine serum albumin (BSA, Sigma Aldrich) and 250 U/ml of DNase I. The cells were then centrifuged, resuspended in PBS containing 200 µg/ml of BSA (PBS-BSA), and passed through a cell strainer to remove debris. GCPs were selectively isolated by centrifugation through a step gradient of 35% and 65% Percoll (Sigma Aldrich) and harvested from the 35%-65% interface. After a wash in PBS-BSA, the cells were resuspended in neurobasal medium supplemented with 2% B-27 serum free supplement, 1 mM sodium pyruvate, 2 mM L-glutamine and 1% penicillin/streptomycin (all from Invitrogen). GCPs were plated on poly-D-lysine-coated plasticware or glass coverslips at a density of 1×10^6 cells/ml and incubated at 37 °C in 5% CO₂.

To maintain the precursor state, 3 µg/ml of recombinant ShhN (R&D Systems) was added to the cell culture medium immediately after plating. Alternatively, ShhN supernatant, generated as described in section 2.3.6.3 was added to the cell culture medium at 20% v/v. A similar amount of mock supernatant was used for the control culture.

2.3.6.2. Poly-D-lysine coating of culture plates

To favour the adhesion of mouse GCPs to culture surfaces, glass coverslips (placed in 24-well plates) and plastic culture plates were treated with a solution of 70-150 kDa poly-D-lysine (Sigma Aldrich) at a concentration of 0.2 mg/ml and 0.02 mg/ml respectively. A suitable volume of poly-D-lysine solution was used to completely coat the culture surface. After two hours, the solution was removed by aspiration and the surface was washed three times with tissue culture grade water. Coated plates were air-dried, sealed with parafilm and stored at 4 °C until needed.

2.3.6.3. Preparation of Shh and mock supernatants

293FT cells were cultured in 10 cm dishes in antibiotic-free medium until they reached 40-60% confluence. To prepare the transfection mixture, 25 µl of FuGene 6 reagent (Roche Diagnostics Corporation) was added to 600 µl of DMEM and incubated at room temperature for five minutes. Nine µg of plasmid DNA, either rat ShhN expression plasmid (described in section 2.5.1.1) or pcDNA 3.1 control plasmid (Invitrogen), was added to the mixture and incubated at room temperature for a further 30 minutes. The transfection mixture was then added to the cells in culture in a drop-wise fashion. After 24 hours, culture medium was discarded and replaced with 8 ml of fresh complete culture medium. Culture medium was then harvested every 24 hours for 72 hours and stored at 4 °C. After each harvest 8 ml of fresh medium was added to the culture and the cells were discarded on the third day. ShhN supernatants from the three consecutive harvests were combined, filtered through 0.45 µm filters and stored at -80 °C in 5 ml aliquots. Similarly, frozen aliquots were generated for the mock supernatant. To confirm the presence of ShhN in the ShhN supernatant, western blots were carried

out using serial dilutions of ShhN and mock supernatants, and recombinant ShhN as a control.

2.3.7. Producing lentivirus in 293FT cells

To produce lentiviral particles, 6×10^6 293FT cells were plated in a 10 cm dish in 10 ml of culture medium and co-transfected with 5 μg of lentiviral transgene expression plasmid, 3.75 μg of packaging plasmid and 1.5 μg of envelope expression plasmid, using 36 μl of Lipofectamine 2000 reagent (Invitrogen) diluted in Opti-MEM I medium without serum (Invitrogen). Transfection was carried out overnight at 37 °C with 5% CO₂. The following day, the transfection supernatant was replaced with 8 ml of fresh complete culture medium. 48 hours after transfection, the virus-containing supernatant was harvested and cells were discarded. Floating cells and cell debris were removed by filtering the supernatant through 0.45 μm filters and 1 ml viral aliquots were prepared and stored at -80 °C until use.

To determine viral titre, serial dilutions of the viral preparations were used to transduce 293FT cells seeded in 6-well plates. Transduction was carried out as described in section 2.3.8. The cell culture medium was changed every 24 hours for 72 hours, at which time, the proportion of transduced cells (*i.e.* EGFP expressing cells) was measured on a BD FACSAarray bioanalyser system as described in section 2.3.9.1 and data corresponding to the viral dilution factor yielding about 10-15% of transduced cells was used to calculate viral titre as follows:

$$T = (F \times C_0 / V) \times 1000$$

where T is the titre (number of infectious particles per ml of viral preparation), F is the frequency of transduced cells, C₀ is the number of cells at the time of transduction and V is the volume of virus added to the cells [μl].

2.3.8. Lentiviral transduction of immortalised cell lines

Target cells were plated in 6-well plates at a density of 50,000 cells/well (Daoy and UW228-2 cell lines) or 100,000 cells/well (D425 Med cell line) and allowed to grow overnight. Typically cells were inoculated with defrosted viral aliquots at a multiplicity of infection (MOI) of 0.1 (Daoy and UW228-2) or 0.5 (D425 Med) in a final volume of 2 ml. This would normally give a transduction efficiency ranging between 50% and 80%. Cells were spin-infected by centrifuging the plates at 1,800 rpm for 45 minutes at room temperature and then incubated overnight at 37 °C / 5% CO₂. After 24 hours, the culture medium was replaced with fresh complete medium. 48 hours after transduction, the cells were ready to be assayed for transgene expression and functional studies.

When a 100% proportion of transgene-expressing cells was required, a puromycin selection protocol was applied to remove the non-transduced cells from the culture. At least 48 hours post-transduction, cell culture medium was replaced with fresh medium containing 0.5 µg/ml (D425 Med cells) or 1 µg/ml (Daoy and UW228-2 cells) of puromycin antibiotic (Sigma Aldrich). Puromycin treatment was carried out for four to five days, using a sample of non-transduced cells to monitor how efficiently the antibiotic caused cell death. Following puromycin treatment, the percentage of transduced cells was measured by flow cytometry as the proportion of EGFP expressing cells. Cultures were kept in puromycin-free medium for an additional week before performing any other assays.

2.3.9. Flow cytometry

Flow cytometry assays were performed at the flow cytometry core facility at the UCL Institute of Child Health using either the BD LSRII or the BD FACSAarray

bioanalyser system (both from BD Biosciences). Fcs files generated by cytometry analysis were analysed using the Summit v4.3 software (Beckman Coulter).

2.3.9.1. Detection of EGFP-positive cells

Transduced cells were washed in PBS, incubated in Trypsin-EDTA at 37 °C for 2 minutes and harvested in 1 ml of complete medium directly into flow cytometry tubes. A non-transduced sample was used to set up voltage parameters and define a threshold for the autofluorescence signal. A gate was applied to include only live cells and at least 10,000 events/sample were recorded. A histogram showing EGFP signal on the *x*-axis and cell count on the *y*-axis was used to visualise the distribution of EGFP fluorescence.

2.3.9.2. Cell cycle analysis

Flow cytometry cell cycle analysis was performed by labelling nuclear DNA with Propidium Iodide (PI). PI is a fluorescent dye which intercalates between nucleic acid bases and is commonly used to quantitatively assess cellular DNA content. The assay is based on the principle that as cells progress through the cell cycle their DNA content doubles from 2n in G1, gradually increasing through the S phase, up to 4n in G2/M. PI labelling of fixed cells can therefore be used to analyse the cell cycle distribution of whole cell populations. Because PI can also bind to RNA, an RNase treatment is necessary to allow the selective labelling of nuclear DNA.

Cells were harvested, washed in PBS and pelleted through centrifugation. One ml of ice-cold 70% ethanol was added dropwise to the cell pellet while vortexing to ensure homogeneous fixation of all cells. The sample was incubated for at least 30 minutes at 4 °C and spun at 2,000 rpm for 5 minutes. The supernatant was discarded

and cells were washed twice in PBS. The cell pellet was treated with 50 μ l of ribonuclease A (Sigma Aldrich) at 100 μ g/ml to get rid of RNA. 400 μ l of a 50 μ g/ml PI solution (Sigma Aldrich) in PBS was added to the pellet and the sample was incubated in the dark for 30 minutes prior to flow cytometry analysis.

A dot plot showing PI signal area *versus* PI signal width was used to gate on single cells and filter out doublets and cell clumps. A second plot representing PI signal on the *x*-axis and cell count on the *y*-axis was then used to estimate the percentage of cells in each cell cycle phase.

2.3.9.3. Bromodeoxyuridine staining for flow cytometry analysis

Bromodeoxyuridine (BrdU) is a thymidine analogue which is readily incorporated into DNA by cells undergoing DNA synthesis during the S phase of the cell cycle. Flow cytometry analysis of BrdU incorporation allows cell cycle studies to be performed which add a dynamic dimension to the PI analysis described above, since only cells that are actively cycling will incorporate BrdU.

For the last 30 minutes to 3 hours of culture, cells were incubated with fresh medium containing 10 μ M BrdU (Roche Diagnostics Corporation). Cells were then harvested using trypsin, washed in PBS and fixed in 1 ml of ice cold 70% ethanol. After 30 minutes at 4 $^{\circ}$ C, cells were centrifuged at 2,000 rpm for 5 minutes and washed twice in 1 ml of PBS. To unwind the DNA, cells were resuspended in 1 ml of 2N hydrochloric acid and left at room temperature for 30 minutes with occasional mixing. Two more washes in PBS were performed, followed by a third wash in PBS-T (PBS, 0.2% Tween 20, 1% BSA). Two μ l of anti-BrdU antibody (Abcam) was added directly to the cell pellet and incubated for 30 minutes at room temperature. Following one wash in PBS-T, cells were incubated in a 1:10 dilution of fluorescein-conjugated anti-rat-IgG

antibody (Roche Diagnostics Corporation) for 30 minutes at room temperature, in the dark. Cells were then washed in PBS-T and incubated for 30 minutes in 50 µl RNase A (100 µg/ml) and 400 µl of PI (50 µg/ml) prior to flow cytometry analysis.

Single cells were gated on a dot plot graph showing PI signal area *versus* PI signal width. A second dot plot showing PI signal on the x-axis and BrdU signal on the y-axis was used to visualise cell cycle distribution. The cell scatter plot formed a characteristic horseshoe profile, allowing the distinction of G1, S and G2/M phases.

2.3.10. Immunocytochemistry

2.3.10.1. Coverslip preparation

Glass coverslips were placed in a centrifuge tube containing 2N NaOH for sterilisation and incubated for two hours on a tube roller to assure constant rotation. Coverslips were rinsed thoroughly with tissue culture grade water and stored in sterile 70% ethanol. Before use, coverslips were allowed to air dry inside a class I tissue culture hood.

2.3.10.2. Intracellular antigen staining

For immunocytochemistry analysis, cells were cultured on sterilised glass coverslips in 24-well plates and then fixed with 4% paraformaldehyde (PFA) at room temperature for 15 minutes. Following three washes in PBS, cells were blocked and permeabilised for an hour in a solution of 10% sheep serum (Sigma Aldrich) and 0.1% Triton X-100 (Sigma Aldrich) in PBS. Cells were incubated with primary antibodies diluted in 1% sheep serum in PBS overnight at 4 °C. A negative control was incubated in 1% sheep serum in PBS in the absence of primary antibody to check for any auto-fluorescence of the secondary antibody. Three more washes in PBS were performed

before incubating cells with fluorochrome-conjugated secondary antibodies diluted in 1% sheep serum in PBS for 2 hours at room temperature. Cells were carefully rinsed with PBS and coverslips were mounted on slides using ProLong Gold antifade reagent with DAPI (Invitrogen). All antibodies used for immunocytochemistry analysis are listed in Table 2.1.

Table 2.1. Antibodies used for immunocytochemistry.

Antibody	Company/Cat. number	Source	Working dilution
Anti-NeuN	Millipore/Chemicon MAB377	Mouse	1:250
Anti-GFAP	Millipore/Chemicon MAB360	Mouse	1:250
Anti-Brn2 (Pou3F2)	Santa Cruz Biotechnology sc-28594	Rabbit	1:250
Anti-Ube2C (UbcH10)	Boston Biochem A-650	Rabbit	1:400
Anti-BrdU	Abcam Ab6326	Rat	1:400
Fluorescein-conjugated anti-rat IgG	Jackson ImmunoResearch Laboratories 712-095-153	Donkey	1:500
Rhodamine-conjugated anti-mouse IgG	Jackson ImmunoResearch Laboratories 715-025-150	Donkey	1:500
Rhodamine-conjugated anti-rabbit IgG	Jackson ImmunoResearch Laboratories 711-025-152	Donkey	1:500

2.3.10.3. Bromodeoxyuridine staining for immunocytochemistry

Cells growing on coverslips were incubated with 10 μ M bromodeoxyuridine (BrdU, Roche Diagnostics Corporation) for the last 30 minutes to 3 hours of culture depending on the experiment. Cells were washed and fixed in 4% PFA as described in section 2.3.10.2. Cells were permeabilised in ice-cold methanol for 1 minute at -20 $^{\circ}$ C, before being incubated for one hour in a blocking solution containing 10% sheep serum, 0.1% Triton X-100 and DNaseI at 10 μ g/ml (Roche Diagnostics Corporation) to unwind the DNA. Cells were then stained and mounted as described in section 2.3.10.2.

This same protocol was applied for both single-labelling of BrdU and double-labelling of intracellular antigens and BrdU.

2.3.10.4. Image capture and processing

Fluorochrome-labelled cells mounted on slides were visualised on a Zeiss Axioplan fluorescence microscope (Carl Zeiss Ltd) using a x63 objective with Immersol oil, and images were captured using a Quantix digital camera and Smart Capture VP software. Image files were processed using the ImageJ software.

2.4. Molecular biology

2.4.1. Total RNA isolation

2.4.1.1. RNA isolation from frozen tissues using the RNeasy mini kit

Up to 30 mg of frozen tissue was disrupted in 600 µl of RLT buffer (RNeasy mini kit, QIAGEN) using a disposable plastic pestle. The suspension was finely homogenised through a QIAshredder homogenizer (QIAGEN) and transferred to an RNeasy spin column for total RNA isolation with an RNeasy mini kit, according to the manufacturer's instructions. An on-column DNase digestion was performed to eliminate genomic DNA contamination. RNA was stored at -80 °C.

2.4.1.2. RNA isolation using the TRIzol reagent

Up to 5×10^6 cells growing in culture were washed with ice-cold PBS and harvested in 1ml of TRIzol reagent (Invitrogen). Alternatively, up to 30 mg of frozen tissue was ground up in 1ml of TRIzol reagent using a disposable plastic pestle. Homogenised samples were incubated at room temperature for 5 minutes to allow the complete dissociation of nucleo-protein complexes before adding 200 µl of chloroform.

Tubes were vigorously shaken for 15 seconds and centrifuged at 11,000 rpm in an Eppendorf tabletop centrifuge for 15 minutes at 4 °C. The upper aqueous phase was collected in a fresh tube and RNA was precipitated with isopropanol. After 10 minutes at room temperature, RNA was pelleted by centrifuging at 11,000 rpm for 10 minutes at 4 °C, washed in ice-cold 70% ethanol, and resuspended in 20 µl of RNase-free water.

To remove contaminating DNA, up to 1 µg of total RNA was incubated for 15 minutes at room temperature with 1 unit of DNase I (Invitrogen). The reaction was stopped by adding EDTA to 2.5 mM and heating at 65 °C for 10 minutes. RNA was stored at -80 °C.

2.4.1.3. RNA quality control

RNA purity and concentration were assessed by measuring sample absorbance at 260 and 280 nm using the NanoDrop spectrophotometer (Thermo Fisher Scientific). An A_{260}/A_{280} ratio higher than 1.8 was considered indicative of highly purified RNA. RNA samples to be used for the exon array study were profiled using the Agilent Bioanalyser (Agilent Technologies) to assess total RNA integrity.

2.4.2. First strand cDNA synthesis

Total RNA was reverse transcribed into first strand cDNA using SuperScript II reverse transcriptase (RT, Invitrogen), a modified version of the Moloney Murine Leukemia Virus RT, and oligo(dT).

Up to 1 µg of DNase-treated total RNA was heated to 65 °C for 5 minutes in the presence of oligo(dT) at a final concentration of 25 µg/ml and dNTPs, each at a final concentration of 0.5 mM. 5X RT buffer and DTT (10 mM final concentration) were then added and a pre-incubation at 42 °C for 2 minutes was carried out. Finally, 200

units of SuperScript II RT were added to the reaction before incubating at 42 °C for 50 minutes. The enzyme was then heat-inactivated at 70 °C for 15 minutes and samples were stored at -20 °C.

2.4.3. Polymerase Chain Reaction (PCR)

2.4.3.1. Primer design

PCR primers were designed using the online open access Primer3 software developed at the Whitehead Institute for Biomedical Research [156]. Whenever possible, forward and reverse primers were chosen to selectively amplify cDNA templates. As a general rule, primer pairs with no or very low self-complementarity were chosen to reduce the probability of primer dimer formation.

For the validation of cassette-exon splicing events, primers were designed to recognise sequences located upstream and downstream of the candidate cassette exon, so as to generate PCR products of different sizes depending on the inclusion or exclusion of the target exon from the spliced transcript. Alternative ends of the transcript were discriminated using two independent pairs of primers, each specifically targeting one individual splicing variant. Primers for whole gene expression analysis were chosen to amplify regions of the target gene common to all Ensembl-annotated transcript variants (<http://ensembl.genomics.org.cn/index.html>).

To confirm target specificity, primer sequences were aligned against whole organism nucleotide databases using the NCBI nucleotide blast program (<http://blast.ncbi.nlm.nih.gov/Blast.cgi>). A complete list of the primer sequences used for this project can be found in Appendix 1.

Desalted primer oligonucleotides were purchased from Sigma Aldrich.

2.4.3.2. Semi-quantitative PCR

Approximately 5 ng of cDNA template was mixed with 1X CoralLoad PCR buffer (QIAGEN), a mix of dNTPs (Promega) at 200 μ M each, 0.5 μ M of forward and reverse primers and one unit of Taq DNA polymerase (QIAGEN). Following an initial 5-minute heating step at 95 °C, the PCR reaction was performed for 26 to 34 cycles, each of which consisted of a 30 second denaturation step at 95 °C, followed by a 30 second annealing step at 60 °C and a 30 second extension step at 72 °C. The reaction was completed with a final elongation step at 72 °C for 5 minutes before cooling down to 4 °C. For cDNA amplicons of more than 600 base pairs, the extension step was prolonged to 45 seconds.

Generally, PCR products were analysed at least twice, at increasing numbers of cycles. Each time 5 μ l of PCR product was directly loaded on a 2% agarose gel and DNA electrophoresis was performed as described in section 2.5.4.

2.4.3.3. Estimation of the ratio between cassette-exon splice variants

After electrophoresis, agarose gels were photographed using a UVI-doc gel documentation system and the PCR-amplified DNA bands corresponding to the two alternatively spliced transcript forms were quantified using the ImageQuant TL v2005 software (GE Healthcare).

A simple formula was developed to quantify the prevalence of one or the other form in each individual sample. The formula computes the ratio between the difference and the average of the signal intensities of the two alternative splice forms (Splicing Indicator). The outcome is a number which only ranges from -2 to 2. A Splicing Indicator value of 2 is obtained when only the band corresponding to target exon

inclusion is visible on the gel. Conversely, a value of -2 indicates the exclusive amplification of the splice form in which the target exon is excluded.

2.4.3.4. Real Time PCR

To validate alternative end of transcript splicing events, Real Time PCR was performed using the SYBR Green chemistry. Reactions containing 1X SYBR Green PCR master mix (Applied Biosystems), 0.5 μ M of forward and reverse primers and approximately 5 ng of cDNA template were run in triplicate or quadruplicate on a 7900HT Fast Real-Time PCR System (Applied Biosystems). The amplification protocol included an initial step at 95 °C for 10 minutes, followed by 40 cycles of both a denaturation step at 95 °C for 15 seconds and an annealing/extension step at 60 °C for 1 minute. To confirm the absence of primer-dimers, a dissociation curve analysis was performed at the end of the run.

To verify the equal amplification efficiency of different primer pairs, an initial optimisation protocol was carried out to generate standard curves based on increasing concentrations of a cDNA template. Amplification rates for the different primer pairs were compared through the Δ Ct method and PCR efficiencies were calculated based on the slope of the standard curves [157]. Following this initial analysis, the $2^{-\Delta\Delta C_t}$ relative quantitation method could be applied to measure the relative abundance of one transcript form relative to the other, using one of the samples as the internal calibrator.

TaqMan chemistry was used for Real Time PCR analysis of whole gene expression. Optimised individual assays containing gene specific primers and probe were purchased from Applied Biosystems. Reaction mixes contained 1X TaqMan PCR master mix (Applied Biosystems), 1X primer/probe solution and approximately 5 ng of cDNA template. A fast PCR protocol was performed, consisting of 40 cycles of

denaturation at 95 °C for 1 second followed by annealing/extension at 60 °C for 20 seconds. Transcript abundance relative to housekeeping gene expression was calculated by applying the $2^{-\Delta\Delta Ct}$ method.

2.4.4. Preparation of protein extracts from cells in culture

Cells growing in culture were rinsed in ice-cold PBS and harvested using a cell scraper. Following one more wash in ice-cold PBS, cells were pelleted by centrifugation, lysed in SDS buffer containing 10 mM Tris-HCl, 150 mM NaCl, 0.5 mM EDTA, 1 mM EGTA, 1% SDS, 0.5 mM phenylmethylsulfonyl fluoride (PMSF) and 2% v/v of a mammalian protease inhibitor cocktail (Sigma Aldrich) and incubated for 20 minutes at 90 °C. Cell debris was pelleted by high speed centrifugation for 20 minutes, the protein-containing supernatant was collected in a fresh tube and protein concentration was determined using a Bio-Rad protein assay (Bio-Rad Laboratories) with known concentrations of gamma globulin protein to generate a standard curve.

2.4.5. Western blotting

Protein samples were mixed with 5X SDS sample buffer to obtain a final concentration of 62.5 mM Tris-Cl pH 6.8, 10% glycerol, 2% SDS, 0.1% β -mercaptoethanol and 0.0005% bromophenol blue. Samples were then boiled for 5 minutes, vortexed and spun before loading on the gel.

Denatured proteins were separated by SDS polyacrylamide gel electrophoresis on gels cast with concentrations of acrylamide ranging from 8% to 13% depending on the size of the protein to be resolved (for a detailed composition of stacking and resolving gels, see Table 2.3, on page 94). Acrylamide gels were usually run at 80 Volts for two hours in SDS running buffer (Table 2.3), in a Mini-PROTEAN electrophoresis

chamber (Bio-Rad Laboratories). Proteins were then transferred to an Immobilon-P membrane (Millipore Ltd), by electroblotting in 1X transfer buffer (Table 2.3) using a Mini-PROTEAN blotting module (Bio-Rad Laboratories) and applying a constant voltage of 35 Volts for 3 hours. To prevent non-specific binding, the membrane was incubated for 45 minutes in a blocking solution of 5% non-fat dry milk and 0.05% v/v Tween 20 in TBS (Table 2.3).

Primary antibody incubation was carried out at 4 °C overnight in blocking solution. The membrane was then washed thoroughly in TBS containing 0.05% v/v Tween 20 (TBS-T) and incubated with a peroxidase-conjugated secondary antibody in 5% non-fat dry milk in TBS-T for one hour at room temperature. Following a 60-minute long series of washes in TBS-T, proteins were detected using the ECL Plus Western Blotting detection system (GE Healthcare) and protein bands were visualised by exposing the blot to an ECL hyperfilm (GE Healthcare). For protein quantitation, films were scanned and analysed using the Bio-Rad Quantity One analysis software (Bio-Rad Laboratories).

Membranes to be re-probed were dipped in methanol to drive out the water and allowed to dry on a paper sheet before being re-activated by soaking in methanol for 15 seconds and washing in water for 2 minutes. A list of the primary antibodies used for western blotting experiments can be found in Table 2.2.

Table 2.2. Antibodies used for western blotting.

Antibody	Company/Cat. number	Source	Working dilution
Anti-Gli1	Santa Cruz Biotechnology sc-20687	Rabbit	1:1000
Anti-Shh	Cell Signaling Technology 2287	Rabbit	1:1000
Anti-Brn2 (Pou3F2)	Santa Cruz Biotechnology sc-28594	Rabbit	1:1000
Anti-Pttg1 (Securin)	Abcam Ab3305	Mouse	1:1000
Anti-Bmi	Abcam Ab14389	Mouse	1:500
Anti-Ube2C (UbcH10)	Boston Biochem A-650	Rabbit	1:1000
Anti-Gapdh	Cell Signaling Technology 2118	Rabbit	1:1000
Anti- β -actin	Cell Signaling Technology 3700	Mouse	1:1000

2.5. Molecular cloning

2.5.1. Plasmid vectors

2.5.1.1. Rat ShhN expression plasmid

The rat ShhN expression plasmid was kindly provided by Dr. Robert Wechsler-Reya, Duke University Medical Center, Durham, North Carolina. The DNA sequence encoding amino acid residues Met 1 – Gly 198 of rat Sonic hedgehog (Shh) is cloned within the pMT21 parent plasmid. The 198 amino acid residue protein encoded by the plasmid corresponds to the 20 kDa N-terminal domain of rat Shh, which is generated through an autocatalytic reaction required for Shh signalling activity. The Shh N-terminal domain (ShhN) is secreted from the cell and is responsible for all known Shh signalling functions.

2.5.1.2. pGIPZ lentiviral vector

The pGIPZ lentiviral vector was developed by Open Biosystems in collaboration with Dr. Gregory Hannon (Cold Spring Harbour Laboratory, NY) and Dr. Stephen

Elledge (Harvard University Medical School, Boston, MA), with the aim to achieve effective messenger-RNA silencing in a wide variety of cell types, including primary and non-dividing cells. The pGIPZ vector is designed to express short hairpin RNA constructs (shRNAs) within the context of the human microRNA-30 (miR30). The shRNA consists of a 22-nucleotide double-stranded RNA (sense and antisense strands) and a 19-nucleotide loop from human miR30, embedded in 125 nucleotides of miR30 flanking sequence on either side (Figure 2.3A). This design allows the expression of the shRNA from an RNA polymerase II promoter and was shown to increase the ability of shRNAs to down-regulate their target genes, by enhancing shRNA processing by the RNase III enzymes Drosha and Dicer [158].

The shRNA is transcribed as part of a multicistronic mRNA for the co-expression of the EGFP reporter gene and a mammalian selectable marker (puromycin resistance gene), thereby allowing the tracking and selection of shRNA producing cells (Figure 2.3B).

In order to generate replication-defective lentiviral particles, pGIPZ vectors expressing the shRNA of interest were co-transfected into 293FT cells together with the psPAX2 vector, expressing the gag and pol viral packaging proteins, and the pMD2.G vector, containing the VSV-G viral envelope expression cassette (both vectors were a kind gift from Professor Didier Trono, Ecole Polytechnique Federale de Lausanne, Lausanne, Switzerland).

2.5.1.3. pGIPZ-SFFV lentiviral vector

The pGIPZ-SFFV lentiviral vector is a modified version of the pGIPZ vector in which the cytomegalovirus (CMV) promoter was substituted for the spleen focus forming virus (SFFV) long terminal repeat (LTR) sequence. A pGIPZ recipient vector was generated by removing the CMV-EGFP cassette by XbaI restriction digestion

followed by 5' overhang blunting and NotI digestion. Similarly, an SFFV-EGFP insert was generated from the pHR-SIN-CSGW vector [159] by EcoRI digestion, 5' overhang blunting and NotI digestion. Finally the SFFV-EGFP insert was subcloned into the pGIPZ recipient vector.

2.5.2. Restriction digestion

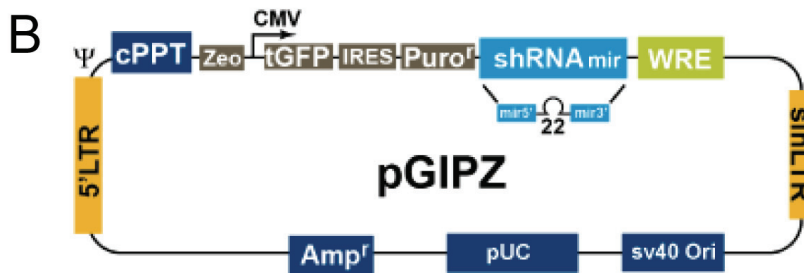
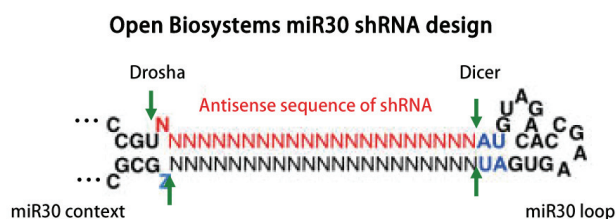
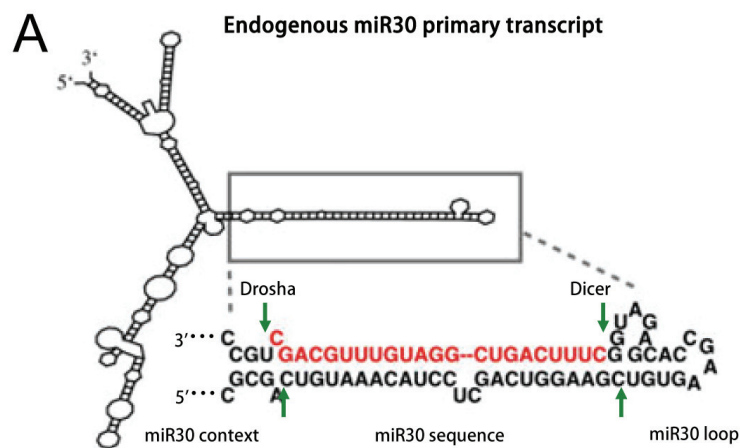
A reaction mix containing up to 3 µg of plasmid DNA, restriction enzymes at 10 units per µg of DNA and 1X optimal restriction buffer was incubated at 37 °C for 2-4 hours. Digested products were then mixed with 6X orange loading dye (15% Ficoll, 0.25% Orange G in distilled water) and analysed by agarose gel electrophoresis as described in section 2.5.4.

2.5.3. Blunting reaction

Following restriction enzyme digestion, 5 units of T4 DNA polymerase/µg of plasmid DNA was added to the reaction tube, together with dNTPs at a final concentration of 100 µM and a compatible restriction enzyme 10X buffer in a final volume of 50 µl. The reaction was incubated at 37 °C for 10 or 5 minutes to blunt 5'- or 3'-overhangs respectively.

2.5.4. Agarose gel electrophoresis

Plasmid DNA from restriction enzyme digestion were resolved on 1% agarose gels, whilst PCR products, normally within the range of 100-700 bps, were resolved on 2% agarose gels. Molecular biology grade Agarose (Invitrogen) was weighed out and then microwaved in 1X TAE buffer (Table 2.3). Ethidium bromide was added to a final concentration of 0.5 µg/ml. Once set, the gel was placed in a Horizon 11.14



Vector Element	Function
CMV promoter	RNA Polymerase II promoter
WRE	Enhances transcript stability and translation
Turbo GFP	Marker to track shRNA expression
IRES-Puro resistance	Mammalian selectable marker
Amp resistance	Bacterial selectable marker
5' LTR	Long terminal repeat
SIN-LTR	3' Self inactivating long terminal repeat

Figure 2.3. Schematic representation of the pGIPZ shRNAmir lentiviral vector.

(A) Secondary structure fold of endogenous miR30 microRNA and miR30-based shRNAs. In pGIPZ, the mature miR30 coding sequence (upper hairpin) is replaced with sequences encoding shRNAs which target any gene of choice (lower hairpin). Adapted from Stegmeier *et al.* [160].

(B) A diagram of the pGIPZ lentiviral vector and its main features. Adapted from the Open Biosystem website [161].

electrophoresis chamber (Biometra) filled with 1X TAE buffer and DNA samples containing 1X loading buffer were loaded into the wells. One well was loaded with a DNA ladder of known size, 1 kb Plus DNA ladder (Invitrogen) or GeneRuler 50 bp DNA ladder (Fermentas Life Sciences) for restriction enzyme digests or PCR products respectively. Typically, a constant voltage of 100 Volts was applied to the gel for 30-60 minutes. After electrophoresis, the DNA bands were visualised under UV light.

2.5.5. Purification of DNA from agarose gels

Following electrophoresis, the DNA bands of interest were excised from the agarose gel using a disposable scalpel. DNA was purified from the gel using a QIAquick Gel Extraction kit (QIAGEN) according to the manufacturer's guidelines.

2.5.6. Ligation of DNA fragments

Typically, 100 ng of plasmid vector DNA was mixed with insert DNA at 1:3 and 1:1 molar ratios. Three units of T4 DNA ligase and 2X rapid ligation buffer (both from Promega) were added to the ligation mix to give a 10 µl final volume. The ligation reaction was incubated at room temperature for 15 minutes.

2.5.7. Bacterial transformation

For routine molecular cloning, I used subcloning efficiency DH5α competent cells (Invitrogen). Briefly, 50 µl of E.coli DH5α cells were mixed in a tube with 4 µl of ligation reaction or 1 ng of plasmid DNA and incubated on ice for 30 minutes. Cells were then heat shocked for precisely 20 seconds at 42 °C and cooled on ice for 2 minutes. Each sample was diluted in 900 µl of pre-warmed LB medium (Table 2.3) and incubated for 1 hour at 37 °C with constant shaking. Up to 200 µl from each

transformation was spread on pre-warmed LB-agar plates (Table 2.3) containing the appropriate selection antibiotic (either ampicillin at 100 µg/ml or kanamycin at 50 µg/ml, depending on the plasmid). Plates were incubated overnight at 37 °C.

For transformation of large or problematic plasmids, I used library efficiency DH5α competent cells (Invitrogen), following the protocol described above except that there was a 45-second heat shock step.

2.5.8. Isolation of Plasmid DNA

Small scale preparations of plasmid DNA (mini preps) for colony screening were obtained by picking single well-isolated transformation colonies from an agar plate and transferring them to individual tubes containing 5 ml of LB medium with the appropriate antibiotic for selection. The small cultures were grown overnight at 37 °C with constant shaking. Bacterial cells were harvested by centrifugation at 4,000 rpm for 15 minutes at room temperature and plasmid DNA was purified using a QIAprep spin miniprep kit (QIAGEN) and a microcentrifuge, according to the manufacturer's instructions.

For transfection experiments, larger preparations of purified plasmid DNA (maxi preps) were generated. A single transformation colony containing the plasmid of interest was transferred to a starter 5 ml culture of LB medium containing the selective antibiotic. The culture was allowed to grow for 7-8 hours at 37 °C in a shaking incubator after which it was transferred to a larger flask containing 400 ml of selective LB medium and was incubated for 14-16 hours at 37 °C with constant shaking. Bacterial cells were centrifuged in a Sorvall RC5B plus ultra-centrifuge at 10,000 rpm for 20 minutes at 4 °C. Plasmid DNA was purified using a Genopure plasmid maxi kit

(Roche Diagnostics Corporation) following the procedure for high copy number plasmids as per manufacturer's instructions.

2.5.9. PCR subcloning

PCR products were subcloned into the pGEM-T Easy vector (Promega). The pGEM-T Easy vector is a linearised vector with 3' thymidine-overhangs at both ends which facilitate the insertion of 3' adenine-tailed PCR products generated by some thermostable DNA polymerases. Briefly, the PCR fragment of interest was purified from the agarose gel as described in section 2.5.5. A 10 µl ligation reaction was set up containing 3 µl of PCR insert, 25 ng of plasmid vector, 3 units of T4 DNA ligase and 2X rapid ligation buffer (both from Promega). After 1 hour incubation at room temperature, 4 µl of the reaction was used to transform subcloning efficiency DH5α competent cells as described in section 2.5.7. To allow for blue/white colony selection, 100 µl of 0.1 M IPTG (Insight Biotechnology Ltd) and 50 µl of 20 mg/ml Xgal (Promega) were spread on top of the ampicillin agar plates before seeding the bacteria.

2.5.10. Sequencing

To confirm the DNA sequence of plasmid constructs or PCR products, a small amount of purified DNA was sent to The Wolfson Institute for Biomedical Research DNA sequencing facility at UCL to be analysed on an Applied Biosystems 3730xl Genetic Analyser. Sequencing results were provided in the form of .ab1 files which were then examined using FinchTV analysis software (Geospiza). Sequence comparison was performed using the NCBI nucleotide BLAST tools.

2.6. Statistics

Unless otherwise stated, data were analysed using two-tailed Student's t-test and comparisons were considered statistically significant for p-values < 0.05. In cases where other statistical tools were more appropriate, details of the analysis were described in the individual figure legends.

2.7. Buffers and solutions

The composition of all buffers and solutions used for this project are listed in Table 2.3.

Table 2.3. Buffers and solutions.

Buffer/Solution	Components
LB (Luria-Bertani) medium	1% w/v bacto-tryptone (BD Biosciences) 0.5% w/v bacto-yeast extract (BD Biosciences) 17 mM NaCl
LB agar	1.5% w/v bacto-agar (BD Biosciences) in LB medium
TAE (Tris-acetate-EDTA electrophoresis buffer)	40 mM Tris-acetate 1 mM EDTA
Stacking gel	13% v/v 30% acrylamide/0.8% bis-acrylamide solution (National Diagnostics) to obtain a final concentration of 3.9% acrylamide 125 mM Tris-HCl pH 6.8 0.1% SDS 0.05% ammonium persulfate 0.2% TEMED
Resolving gel	33% v/v 30% acrylamide/0.8% bis-acrylamide solution (National Diagnostics) for a 10% acrylamide gel 375 mM Tris-HCl pH 8.8 0.1% SDS 0.05% ammonium persulfate 0.2% TEMED
SDS running buffer	25 mM Tris Base 250 mM glycine 0.1% SDS
Transfer buffer	25 mM Tris Base 250 mM glycine 20% v/v methanol
TBS (Tris Buffered Saline)	100 mM Tris-HCl pH 7.6 150 mM NaCl

Chapter 3

Exon array analysis of paediatric medulloblastomas

3.1. Introduction

During the past decade, a few seminal papers have described the use of genome-wide approaches to classify large cohorts of medulloblastomas into discrete molecular subgroups characterised by alterations in specific signalling pathways [20, 92, 100]. These studies largely contributed to the notion that medulloblastoma is a heterogeneous disease and that different clinical outcomes might be associated with particular tumour molecular fingerprints.

In the light of these findings, it became interesting to look at the molecular profile of medulloblastoma patients treated at GOSH, and to generate a novel expression data set providing an additional level of analysis of the molecular complexity of human medulloblastoma.

Within our group, we decided to use the novel Affymetrix Human Exon 1.0 ST array platform to measure the expression level of more than one million exons in human medulloblastoma and normal cerebellum. With more than 5.5 million individual probes mapping to both cDNA-supported transcripts (*e.g.* RefSeq mRNAs) and *in silico* predicted gene structure sequences (*e.g.* from Ensembl), Affymetrix exon arrays are among the most powerful expression tools currently available (Figure 2.2). At the gene level, an average of 40 probes are distributed across the entire length of the gene, generating a more sensitive and robust measurement of gene expression compared to traditional 3'-based approaches where probes exclusively cover the 3'-end of genes. At

the exon level, approximately four probes per exon provide an estimate of individual exon expression and support the detection of alternative splicing.

This chapter contains a description of the samples used for microarray profiling and a summary of low level data analysis, including sample molecular classification according to specific gene signatures.

3.2. Histopathological classification and sample processing

A total of 14 snap-frozen paediatric medulloblastoma samples (median age of 7.3 years) were obtained from the Histopathology Department of GOSH and the original H&E stains were evaluated by a clinical neuropathologist (Dr. Thomas Jacques) as described in section 2.1.3. On review, four cases were classified as classic medulloblastoma and ten as anaplastic medulloblastoma. The spectrum of histology is shown in Figures 3.1 and 3.2.

H&E staining performed on frozen tissue sections confirmed that all of the medulloblastoma samples used in this project consisted predominantly of tumour cells and that they were representative of the diagnosed tumours (two examples are shown in Figure 3.3). Sections of the normal cerebellum sample obtained from GOSH did not show evidence of neoplasia, except for a small area at the periphery where astrocytoma cells were detectable, and that was eventually cut off before RNA extraction. Table 3.1 summarises histological and clinical features of the 19 samples included in the array study.

Table 3.1. Patients and tumour features of the sample series used for the exon array study.

Medulloblastoma samples							
Sample Id	Sex	Age at surgery (years)	Pathology (CLA, classic; ANA, anaplastic)	Nodularity	Desmoplasia	Anaplasia Grade	Anaplasia Extent
T1	F	6.5	ANA	Slight	-	Severe	Diffuse
T3	F	2.7	CLA	Slight	-	None	--
T7	M	14.7	ANA	None	-	Severe	Diffuse
T8	F	5.7	ANA	Slight	+	Severe	Diffuse
T9	M	5.8	CLA	None	+	Slight	Focal
T10	M	5.7	CLA	None	+	Slight	Focal
T11	F	8.1	ANA	None	-	Moderate	Diffuse
T12	M	1.9	ANA	None	-	Severe	Diffuse
T13	M	10.3	ANA	None	-	Moderate	Focal
T15	M	8.3	ANA	None	-	Moderate	Focal
T16	F	9.7	ANA	Slight	-	Severe	Diffuse
T17	M	7.8	ANA	None	-	Moderate	Focal
T18	F	6.8	ANA	None	-	Severe	Diffuse
T19	M	11.3	CLA	Slight	-	Slight	Focal
Normal cerebellar samples							
Sample Id	Sex	Age (years)		Source		Notes	
CB1	na	na		GOSH			
CB2	F/M	16-70		Clontech		pool of 24 individuals	
CB3	M	63		Ambion			
CBF1	F	Fetus (37 weeks gestation)		BioChain			
CBF2	F	Fetus (40 weeks gestation)		BioChain			

The table illustrates histological and clinical parameters for the 19 samples used in the exon array study. The upper part lists medulloblastoma samples; the lower part describes normal cerebellar samples. F, female; M, male; GOSH, Great Ormond Street Hospital; na, not available.

Figure 3.1. Histopathological grading of anaplasia in medulloblastoma.

Anaplasia was graded as none (A), slight (B), moderate (C) or severe (D) according to increasing levels of nuclear enlargement and pleomorphism, extensive mitosis, extensive apoptosis and cell wrapping. A-D show H&E stains performed on paraffin-embedded sections of medulloblastoma samples. Insets are enlarged to the right of each panel.

(A) The medulloblastoma with no anaplasia is composed of small, morphologically uniform cells with a high nuclear-cytoplasmic ratio.

(B) A representative field of a medulloblastoma with slight anaplasia showing nuclear enlargement. Patterns resembling Homer-Wright rosettes are formed in this tumour (inset).

(C) Large areas of abundant apoptosis and polyhedral cell morphology are typical features of medulloblastomas with moderate anaplasia. Arrow heads point to apoptotic cells.

(D) Severely anaplastic medulloblastomas feature larger, pleomorphic cells with high mitotic index and occasional cell wrapping (arrow head).

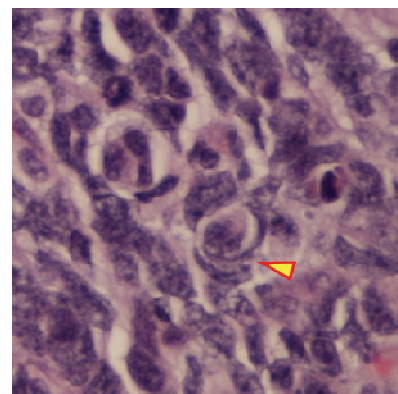
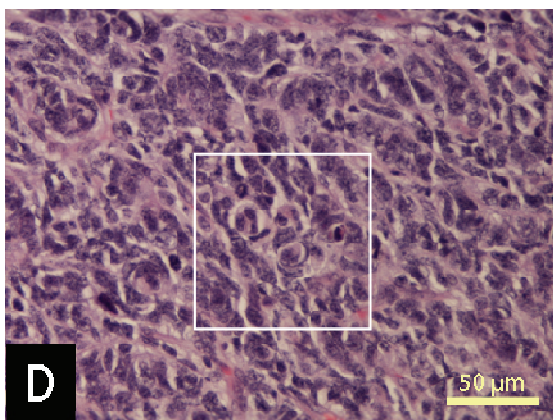
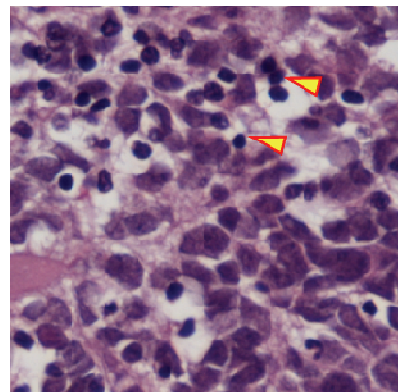
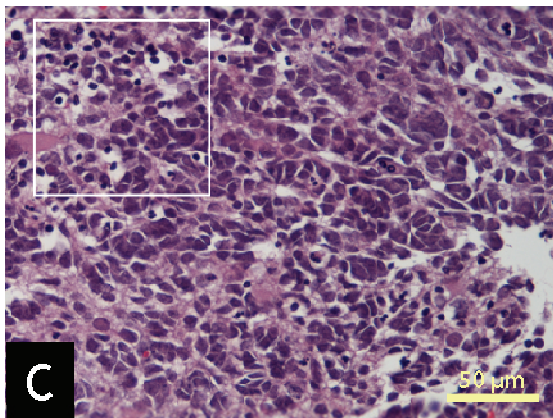
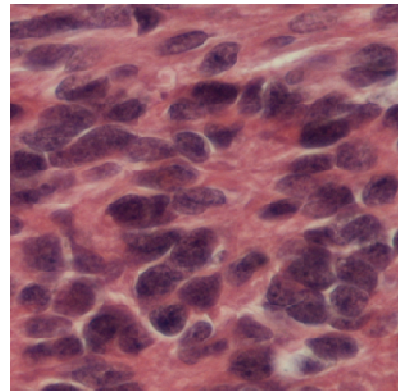
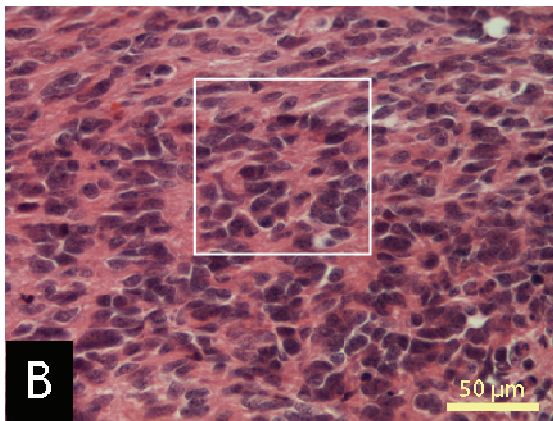
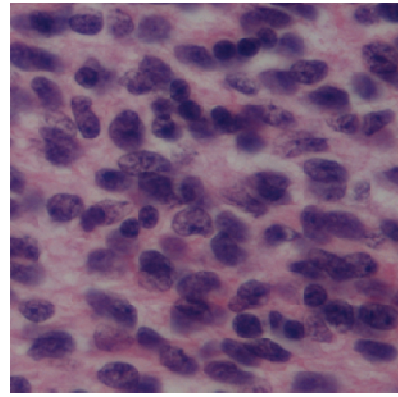
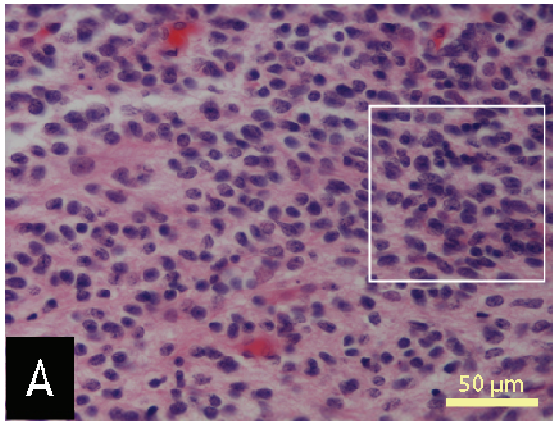


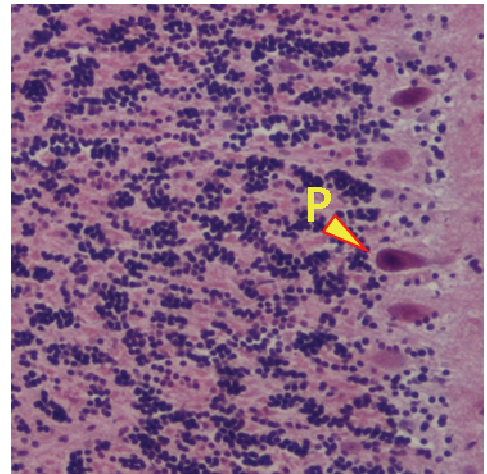
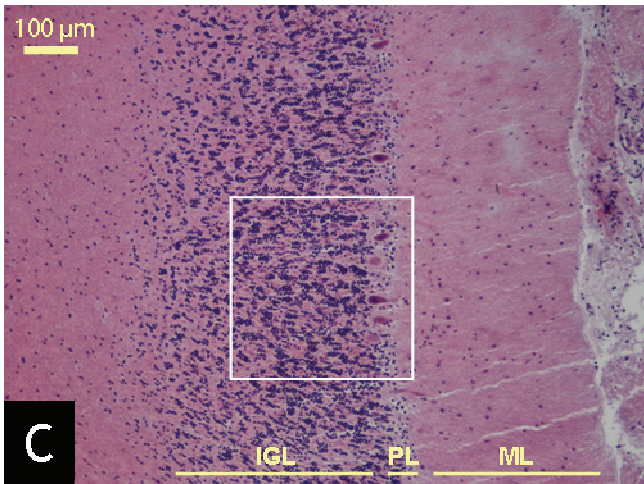
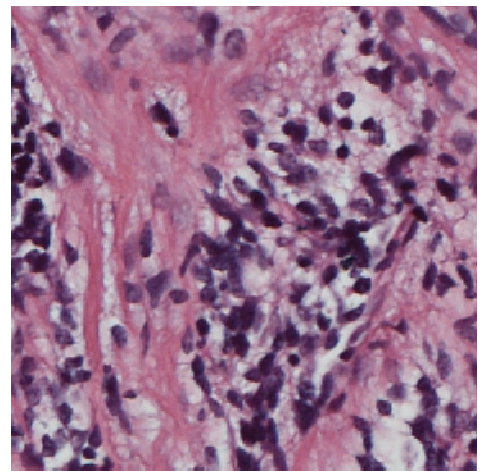
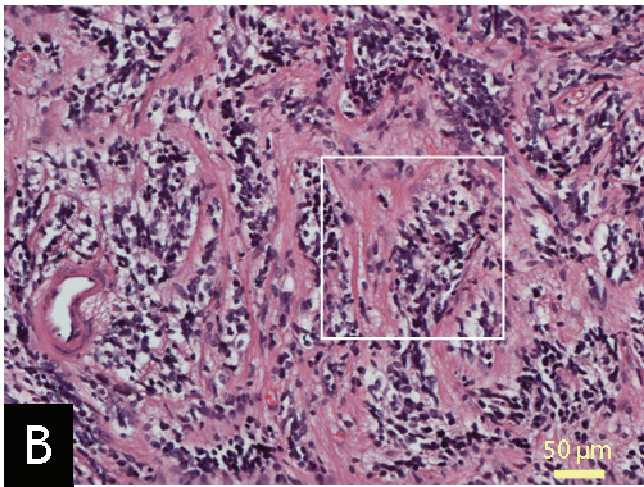
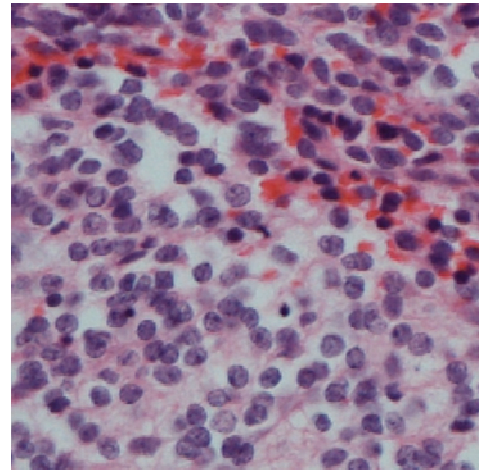
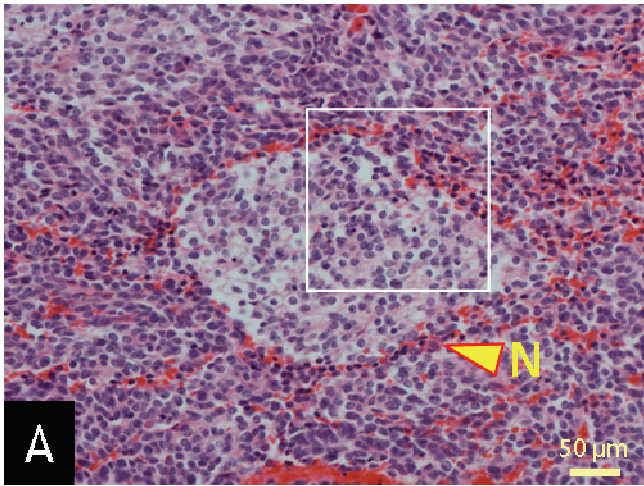
Figure 3.2. Medulloblastoma features of nodularity and desmoplasia, and normal cerebellum.

A-B show H&E stains performed on paraffin-embedded sections of medulloblastoma samples. C is a stained section of snap frozen normal cerebellum. Insets are enlarged to the right of each panel.

(A) An example of a classic medulloblastoma showing a slight degree of nodularity. The nodular area (N) contains small neurocytic cells with abundant cytoplasm and is surrounded by moderately pleomorphic cells with higher nuclear-cytoplasmic ratios.

(B) A region of desmoplasia characterised by abundant pericellular collagen deposition.

(C) A section of normal adult cerebellum showing a fine structured cortex with a completely formed mature internal granule layer (IGL), a Purkinje cell layer (PL) and a molecular layer (ML). P, Purkinje neuron.



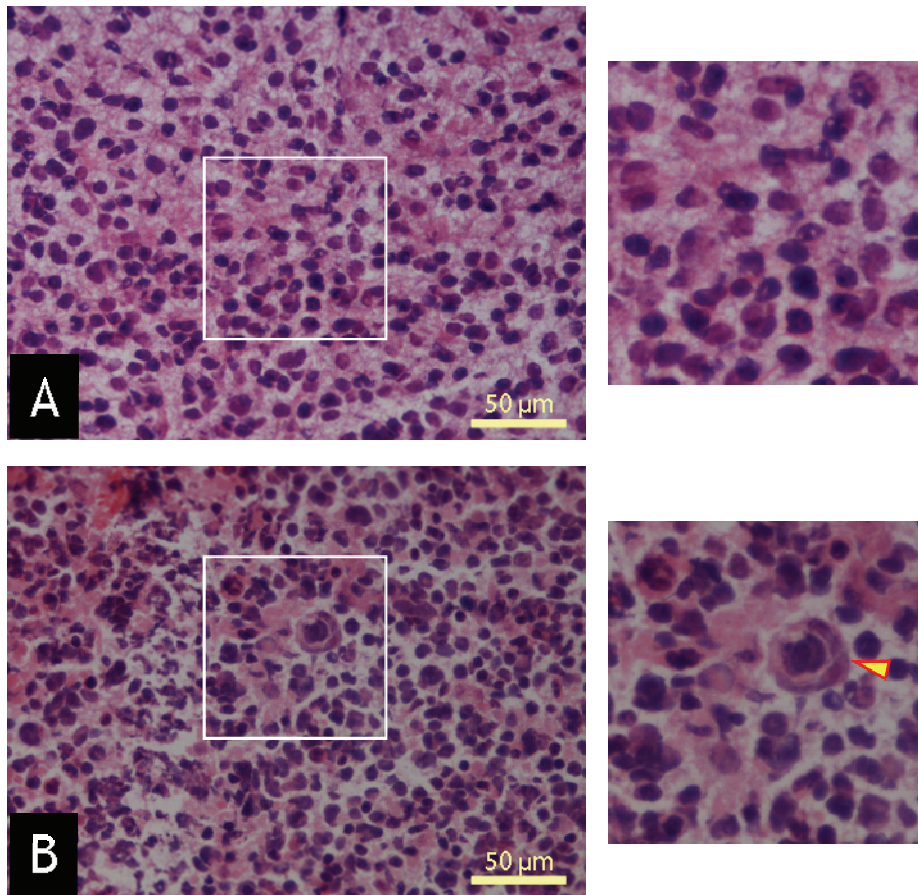


Figure 3.3. Histology of medulloblastoma frozen sections.

H&E staining performed on frozen tissue sections confirmed that the specimens used for the exon array study consisted predominantly of tumour cells and were representative of the diagnosed medulloblastomas. Two examples are shown. Insets are enlarged to the right of each panel.

(A) Frozen section H&E stain of the classic medulloblastoma with no anaplasia described in Figure 3.1A.

(B) Frozen section H&E stain of the medulloblastoma with severe anaplasia described in Figure 3.1D. An example of cell wrapping is indicated by the arrow head.

3.3. Exon array quality control and filtering

Total RNA was extracted from all tissue samples (14 medulloblastomas and one normal cerebellum obtained from GOSH). One μg of each RNA sample, including the four samples of normal cerebellum obtained from commercial sources, was then processed and hybridised to the exon array.

Low level array analysis was initially applied to assess the overall experiment performance and to identify potential sample outliers. Briefly, gene level signal estimates were generated and box plots were drawn to visualise signal variation among different arrays. As shown in Figure 3.4, individual array signal distributions largely overlapped, which excluded any general hybridisation problems. A filter based on expression was applied to remove genes with very low expression across the entire data set and which contributed to the background signal noise potentially affecting subsequent analysis. This led to the generation of a final data set consisting of 12,160 genes, which appeared to be significantly expressed in at least three out of the 19 total samples. Figure 3.5 represents a schematic overview of the initial analysis workflow while in Figure 3.6 density curves illustrate the effect of the filtering step on signal distribution.

I used unsupervised clustering as an explorative method to assess the overall quality of the microarray experiment. Samples with the most similar expression profiles are grouped together; therefore, biological replicates belonging to the same histological category are expected to cluster together. As expected, normal and tumour samples segregated into two discrete clusters (Figure 3.7). Within the normal cerebellum cluster, it was possible to distinguish fetal from adult samples. The four medulloblastomas designated as classic clustered in the same tumour subgroup, together with four anaplastic medulloblastomas, mostly characterised by lower degrees of anaplasia. A

second tumour cluster contained six anaplastic medulloblastomas, five of which displayed severe anaplasia (Figure 3.7). Although clinical and histological parameters did not completely explain the molecular variability observed within the data set, normal and malignant tissues significantly diverged (p-value < 0.0001), and I could see a trend for more anaplastic tumours to cluster together (p-value = 0.057), which strongly supported the good quality of the data.

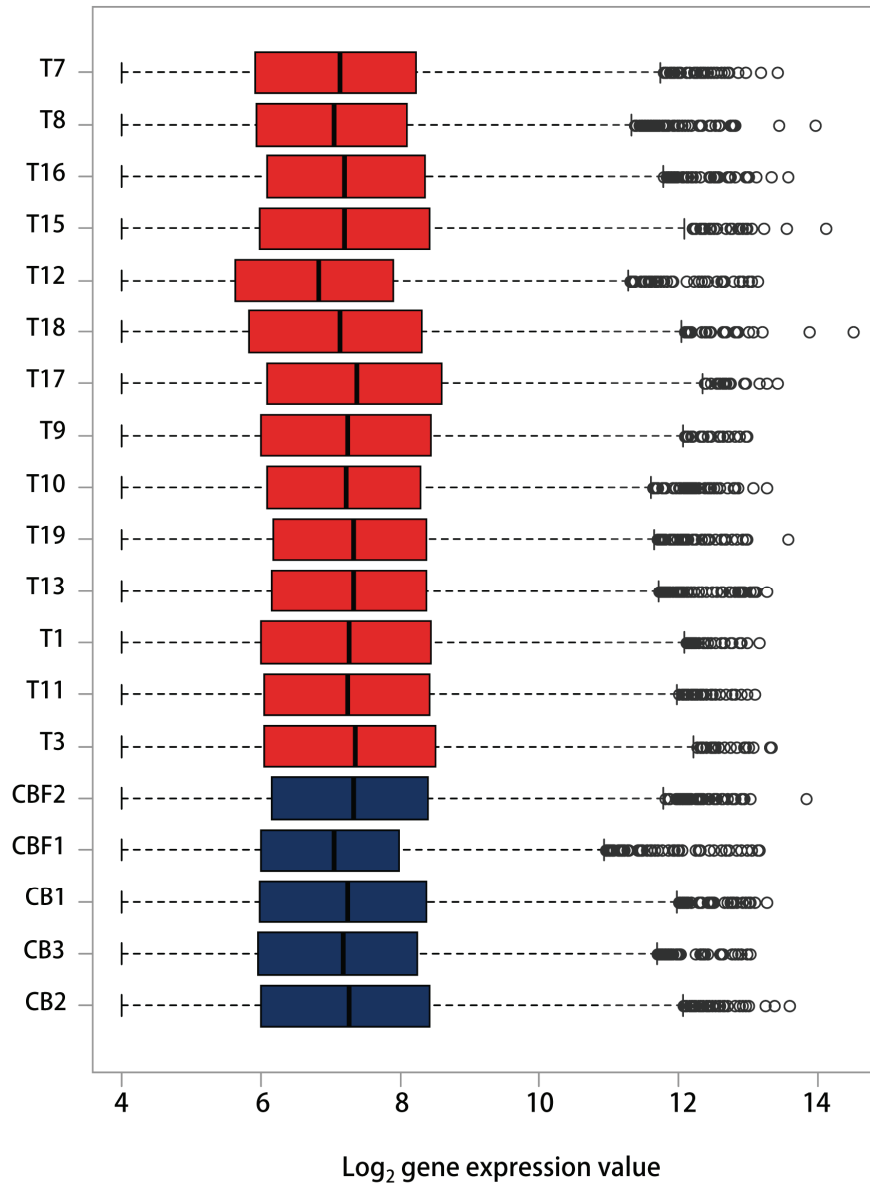


Figure 3.4. Sample signal distribution.

Box plots were used to describe the overall gene signal distribution for each individual sample within the dataset. The left and right edges of each box correspond to the 25th percentile and 75th percentile, respectively. The median value is shown as a vertical line through each box. Whiskers extend to 1.5 times the inter-quartile range (defined as the difference between the 75th and 25th percentiles), and outliers are marked with circles. Individual signal distributions appeared to consistently overlap, which indicated an overall good performance of the microarray experiments. Red, medulloblastoma samples; blue, normal cerebellum samples.

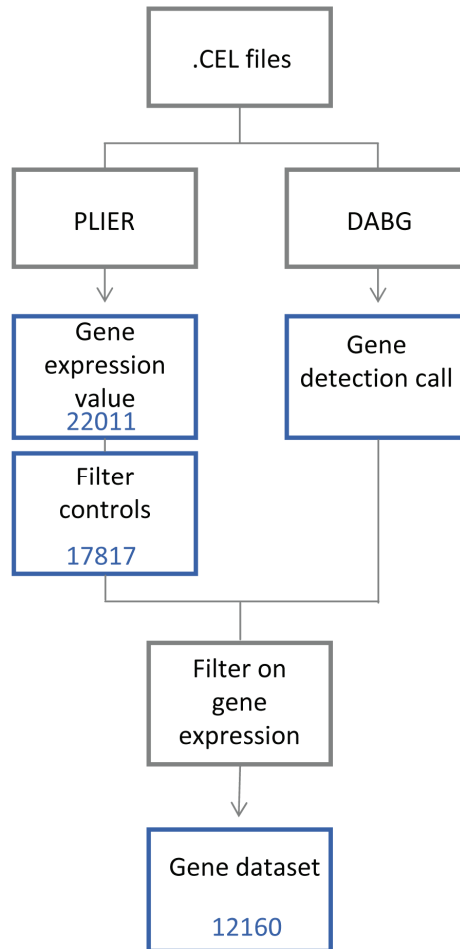


Figure 3.5. Schematic overview of low level analysis and filtering of the exon array data.

Intensity files (.CEL files) were generated with the GeneChip Operating System software following exon array hybridisation and scanning and were loaded into the Expression Console software for low-level analysis. The probe logarithmic intensity error estimate (PLIER) algorithm was used to summarise probe intensities into gene-level signal estimates for the 22,011 genes represented on the array. Background noise was detected with the detection above background (DABG) algorithm and the resulting probe set signal detection p-values were used to assign a detection call to each gene. Following the removal of all control features, a filter based on gene expression was applied to the remaining 17,817 genes, generating a final dataset of 12,160 genes to be used for the subsequent gene-level analysis.

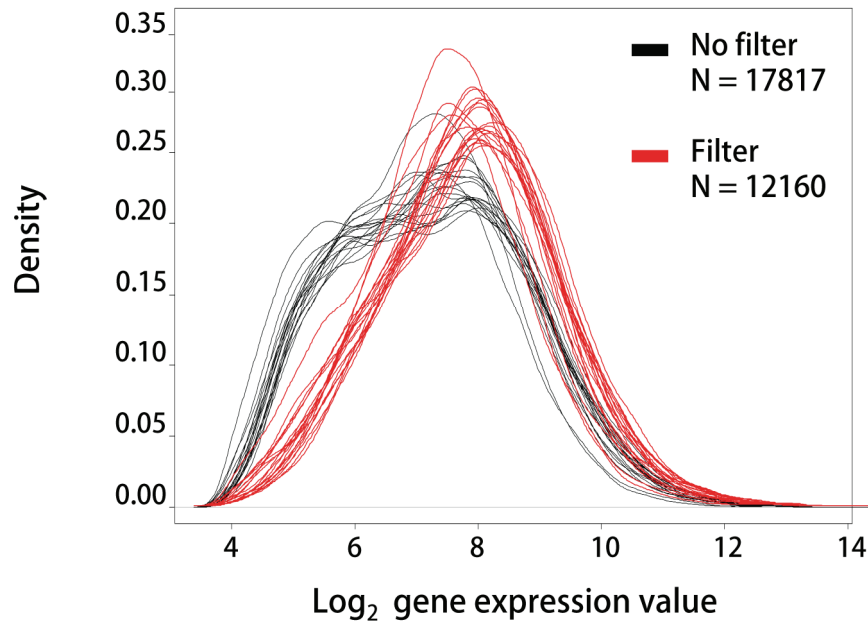


Figure 3.6. Filter on gene expression.

A filter based on expression was applied to remove genes not expressed across the entire dataset. A gene was considered expressed if at least 75% of its targeting probe sets had a detection p-value < 0.05 . Only genes expressed in at least three out of 19 samples were selected for further analysis. The density plots illustrated above show the dataset signal distribution before (black) and after (red) applying the filter. Each line corresponds to an individual sample. After filtering, the minor peak on the left of the graph corresponding to genes expressed at a low level disappeared.

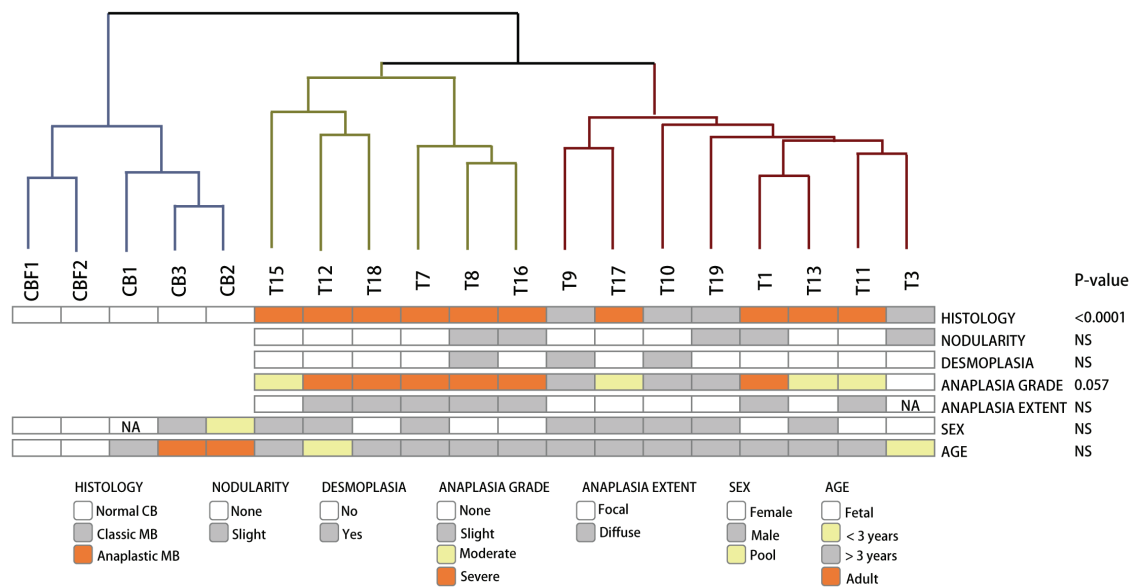


Figure 3.7. Unsupervised hierarchical cluster analysis.

The dendrogram was computed on the expression levels of 624 genes with a variance value across all samples higher than 2. Distances between samples were calculated using the Euclidean distance metric and are measured on the graph along the vertical axis. The shorter the bar to the junction node between two samples, the more similar the samples are. The three major clusters are colour-coded as follows: blue bars, normal cerebella; green bars, anaplastic medulloblastomas, mainly characterised by severe anaplasia; brown bars, a mix of classic and mostly moderate anaplastic medulloblastomas. The Pearson Chi-Square test was used to assess the significance of clinical differences across clustering subgroups. Differences in age distributions were tested using the Kruskal-Wallis test. The Pearson Chi-Square test on histology performed on the two tumour clusters only (*i.e.* testing classic vs anaplastic histology) generated a significant p-value of 0.04. NS, non significant, NA, not available.

3.4. Sample subgrouping based on the Shh gene expression signature

Before performing statistical analysis for differential gene expression, I used gene-level expression profiles to identify samples expressing gene signatures characteristic of previously described medulloblastoma molecular subgroups. I performed an unsupervised hierarchical clustering of the 523 genes corresponding to the Shh-signature genes reported in Thompson's data series [20], as supported by the Affymetrix Best Match array comparison spreadsheet (www.affymetrix.com). Three anaplastic medulloblastoma samples segregated in a discrete cluster (Figure 3.8) and, when compared to the other samples, showed significant overexpression of genes typically belonging to the Shh signalling pathway or associated with a cerebellar granule cell precursor state, such as *GLII*, *MYCN* and *ATOH1* (Figure 3.8). These three samples were therefore classified as Shh-driven tumours (SHH).

Similarly, I applied cluster analysis using the other gene lists identified by Thompson *et al.*, but none of the samples seemed to express any distinctive gene signatures, therefore I grouped all of the remaining tumour samples together as medulloblastoma subset 2 (MB2).

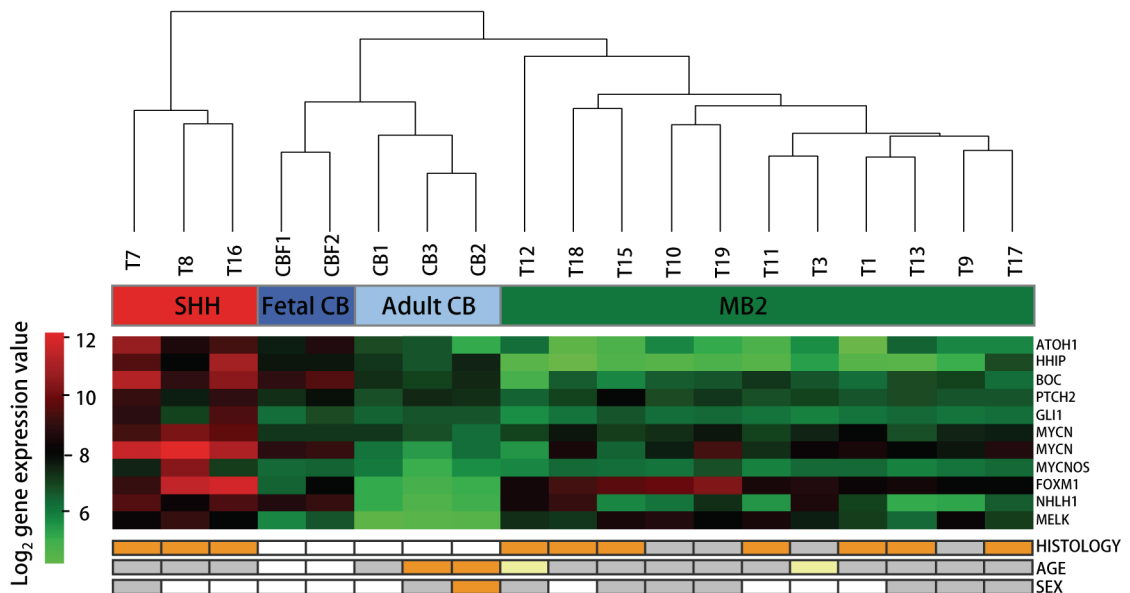


Figure 3.8. A medulloblastoma subgroup is characterised by the Shh-gene signature.

The clustering was computed on the expression levels of 523 genes which corresponded to the Shh-signature genes in Thompson's data series. The Euclidean distance metric was used as a measure of distance between samples. Three medulloblastoma samples formed a discrete cluster and were classified as Shh-driven medulloblastomas (SHH). Abnormal activation of the Shh signalling pathway in these samples was confirmed by the significant overexpression of Shh-related genes (FDR adjusted p-value < 0.01), as shown in the heatmap. Two different transcript clusters for the *MYCN* gene are shown. All remaining medulloblastoma samples were subgrouped together for further analysis (MB2). A summary of the major clinical parameters is reported at the bottom. Histology: white = normal CB, grey = classic MB, orange = anaplastic MB; Age: white = fetal, yellow = <3 years, grey = >3 years, orange = adult; Sex: white = female, grey = male, orange = pool.

3.5. Discussion

In this chapter I have described the collection, processing and hybridisation of a set of paediatric medulloblastomas and normal cerebellar samples to the Affymetrix Human Exon arrays, and the initial steps of array data analysis.

Tumour samples displayed features of either classic or anaplastic histological subtype and were classified accordingly. Following array hybridisation and an initial assessment of experiment performance, I applied a filter on gene expression level and obtained a workable data set for subsequent analysis (Figure 3.5). Unsupervised hierarchical clustering of the most informative genes confirmed that samples from the same biological classification shared similar expression profiles (normal cerebellum vs tumour, p -value < 0.0001 ; classic vs anaplastic medulloblastomas, p -value = 0.04). However, histological features of nodularity, desmoplasia and anaplasia extent did not appear to affect the overall clustering results (Figure 3.7). Although previous studies had described specific molecular subgroups to strongly associate with the infant patient population (< 3 years) [20, 92], I did not find any significant correlation between age and clustering subgroups (Figure 3.7). Still, this result might have been biased due to the limited number of younger patients in my medulloblastoma cohort.

I performed one more unsupervised cluster analysis using a well characterised list of Shh-associated genes (Figure 3.8). Remarkably, although none of the tumours in my cohort belonged to the desmoplastic histological subtype, which is significantly over-represented among Shh-driven medulloblastomas; three samples of anaplastic medulloblastoma formed a discrete cluster and expressed significantly higher levels of genes involved in Shh signalling, such as *PTCH2*, *GLII*, *BOC*, and *HHIP*. Known targets of the Shh signalling pathway such as *MYCN*, *FOXMI* and *MELK* were also overexpressed in this cluster, as well as the GCP marker *ATOHI* (Figure 3.8). Of note,

these three Shh-activated tumour samples were also subgrouped together in the previous analysis, in which samples were clustered according to the expression profile of the most variable genes (samples T7, T8 and T16 in Figure 3.7).

The percentage of Shh-activated tumours in my sample set (21%) was in line with previously published studies (24% in Kool *et al.* [92], 19.5% in Thompson *et al.* [20], 30% in Northcott *et al.* [107]). Even so, I failed to identify tumours matching any of the other four gene signatures described in Thompson *et al.*, probably because of the relatively small size of my sample set. Since several studies agree on a few genetic features characterising medulloblastomas with activated WNT signalling pathway, such as mutations in the *CTNNB1* gene encoding the β -catenin protein [19], it would be interesting to perform mutation analysis as an alternative method to identify samples belonging to the WNT medulloblastoma subtype. It will also be important to update patients' clinical information with details regarding their clinical course, as medulloblastoma patients' outcome significantly differs as a function of the tumour molecular features [9].

To summarise, initial array data analysis showed evidence of good experimental performance and a significant association between the biological classification of the samples and similarities in gene expression. A group of three Shh-driven medulloblastomas was identified based on the expression profile of well characterised Shh-related genes, which would allow the investigation of Shh-mediated differential gene expression and splicing. On the other hand, the remaining medulloblastoma samples did not demonstrate a similarly distinct gene signature and were therefore grouped together for subsequent analysis.

Chapter 4

Analysis of differential gene expression in paediatric medulloblastoma

4.1. Introduction

In recent years, the use of sophisticated microarray technologies has greatly improved our understanding of the molecular alterations underlying human cancer [106]. The use of integrated genomic approaches has led to significant advances in the molecular characterisation of human medulloblastoma. These approaches provide a more accurate classification of tumour subtypes when compared to histological analysis alone. Furthermore, they can also identify additional genes involved in medulloblastoma pathogenesis and this will lead to the development of new therapeutic regimens, specifically designed to address a heterogeneous patient population [7, 25, 162].

Because medulloblastoma originates from immature precursor cells in the cerebellum, functional analysis of putative tumour-associated genes typically involves the investigation of gene-regulated biological processes in the context of normal cerebellar development [27, 28, 163]. Primary cultures of mouse granule cell precursors (GCPs) constitute one of the best characterised *in vitro* models for the analysis of candidate gene function [163]. In a seminal paper published in 1999, Wechsler-Reya and Scott described the *in vitro* culture of Shh-dependent mouse GCPs [43]. While granule cell cultures had been used for a long time to study cerebellar cell biology [164, 165], the use of Shh to promote cell proliferation and maintain an undifferentiated state represented a fundamental step forward in our understanding of the mechanisms

regulating growth and oncogenesis in the cerebellum. Since then, GCP cultures have been used in numerous studies investigating the role of candidate genes in the regulation of cell cycle progression [44-46, 48, 53, 54, 59, 66, 166], leading to the generation of genetically engineered mice in which specific genetic alterations targeting the GCP lineage favour the development of cerebellar tumours [36, 81, 82, 85].

The functional characterisation of putative tumour genes also relies on the use of human medulloblastoma cell lines [167]. Because these cells can be indefinitely propagated *in vitro* and injected into the flank or brain of immuno-compromised mice to recapitulate the tumour of origin, human tumour cell lines constitute a useful model of human cancer and are used in the majority of preclinical studies [168]. In contrast to other cancer types which are readily established as immortalised cell lines, only a small percentage of human medulloblastomas successfully give rise to cell lines in culture [169, 170]. In addition, a recent study by Sasai *et al.* showed that medulloblastoma cell cultures established from Shh-dependent tumours developed in *Ptch*^{+/-} *p53*^{-/-} mice down-regulate Shh pathway activity and are therefore unable to respond to hedgehog antagonists [171]. The authors suggested that the propagation of tumour cells in culture leads to permanent epigenetic changes which induce Shh pathway silencing [171]. Based on these findings, caution should be used when working with medulloblastoma cell lines as models of the primary tumours from which they are derived. Nevertheless, several studies have successfully used a variety of well characterised cell lines to gain insights into the molecular pathogenesis of human medulloblastoma, highlighting the value of medulloblastoma cells as an *in vitro* model for the preliminary functional analysis of candidate genes [172-177].

For my project, I cultured both mouse primary GCPs and human medulloblastoma cell lines to assess the importance of candidate gene expression for the proliferation of normal cerebellar precursor and medulloblastoma cells, respectively.

In this chapter, I compared gene-level expression profiles of medulloblastoma and normal cerebellar tissues and identified a selection of genes overexpressed in Shh-driven medulloblastomas. As an initial step in the characterisation of the selected genes, I analysed their expression patterns in *in vitro* cultures of GCPs maintained in the presence or absence of Shh, as well as in human medulloblastoma cell lines. This chapter also describes preliminary studies in which I used a lentiviral expression system to study the biological effects of candidate gene knockdown in medulloblastoma cell lines.

4.2. Identification of genes differentially expressed in Shh-driven medulloblastomas

Following the identification of a subset of Shh-driven medulloblastoma samples within my data set (SHH tumours), I was interested in characterising their gene expression profile in more detail. I therefore compared gene expression values between the SHH tumour subset and three other sample subgroups, that is the entire set of five normal cerebellar samples (all CB), the subset of adult normal cerebella (adult CB), or the remaining subset of non-Shh-associated tumours (MB2), as shown in Figure 4.1A. Each individual comparison generated a list of differentially expressed genes (DEGs), which were either up- or down-regulated in SHH tumours. Figure 4.1A shows a schematic description of gene-level analysis, including the number of DEGs identified for each individual comparison. As expected, SHH and MB2 tumours shared more similar expression profiles compared to normal cerebella. As a result, I obtained a

workable number of DEGs for the SHH *versus* MB2 comparison at the higher significance threshold of 0.01, as opposed to the 0.001 significance level applied for the other two comparisons (Figure 4.1A). In total, 278 and 300 unique genes were identified as being respectively up- and down-regulated in SHH tumours. The 50 most significantly differentially expressed genes for each list are shown in Figure 4.2. The complete lists can be found in Appendices 2 and 3. In Figure 4.1B a Venn diagram was drawn representing the intersections between the three lists of DEGs identified. Of note, six genes were significantly deregulated in all three comparisons. These include the *MYCN* gene, one of the best characterised Shh-driven medulloblastoma signature genes.

For a general description of the biological relevance of DEGs, I performed functional enrichment analysis of Gene Ontology (GO) terms and tissue annotations (Figures 4.3 and 4.4). This type of analysis identifies annotation terms which are significantly over-represented in any individual gene list with reference to a background list, generally consisting of all of the annotated genes represented on the array platform in use. I analysed the two lists of genes that were up- and down-regulated in SHH tumours independently. Genes overexpressed in SHH tumour samples appeared to be involved in cell cycle related processes corresponding to GO terms such as spindle organisation, chromosome segregation, DNA replication and mitosis (Figure 4.3, right bars). In contrast, the down-regulated genes were typical of a more differentiated phenotype, being implicated in specialised cell functions such as synaptic transmission and cell-cell signalling (Figure 4.3, left bars). I then looked at the enrichment in tissue annotation terms and found that genes up-regulated in SHH tumours were expressed at higher levels in normal embryonic and malignant tissues, including medulloblastomas (Figure 4.4, right bars). In contrast, down-regulated genes were mostly expressed in normal brain tissues, including cerebellum and cerebral cortex (Figure 4.4, left bars).

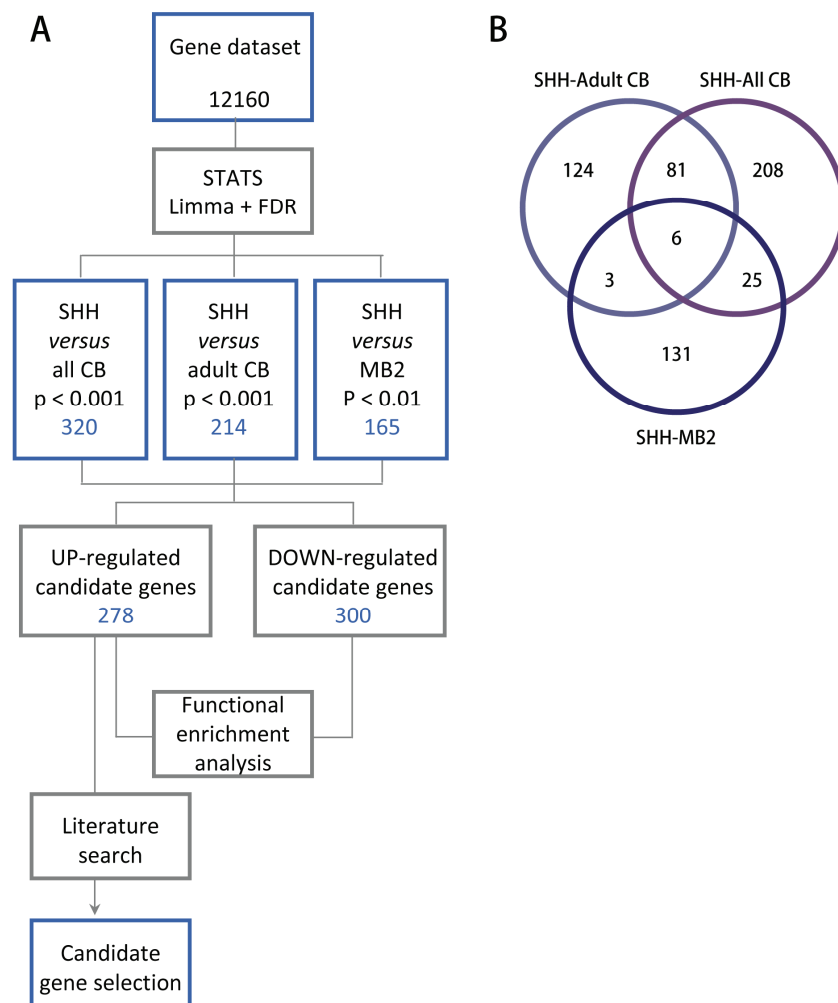


Figure 4.1. Schematic overview of gene-level analysis.

(A) Statistical analysis of differential gene expression was carried out using the moderated t-statistic of the LIMMA package in R, and applying false discovery rate (FDR) to correct for multiple testing. Shh-driven medulloblastomas (SHH) were compared to the five normal cerebellar samples (all CB), the adult cerebellar samples (adult CB), or the second tumour subset (MB2). In each case, a significance threshold was set based on FDR adjusted p-values, as detailed in the flow chart. Numbers in boxes refer to the number of genes which were selected at any particular step of the analysis. In total, 278 and 300 unique genes were identified as being respectively up- and down-regulated in SHH tumours. Functional enrichment analysis was performed on the two lists of up- and down-regulated genes. Candidate genes for following studies were selected from the up-regulated gene set.

(B) Venn diagram of DEG lists identified by different subgroup comparisons.

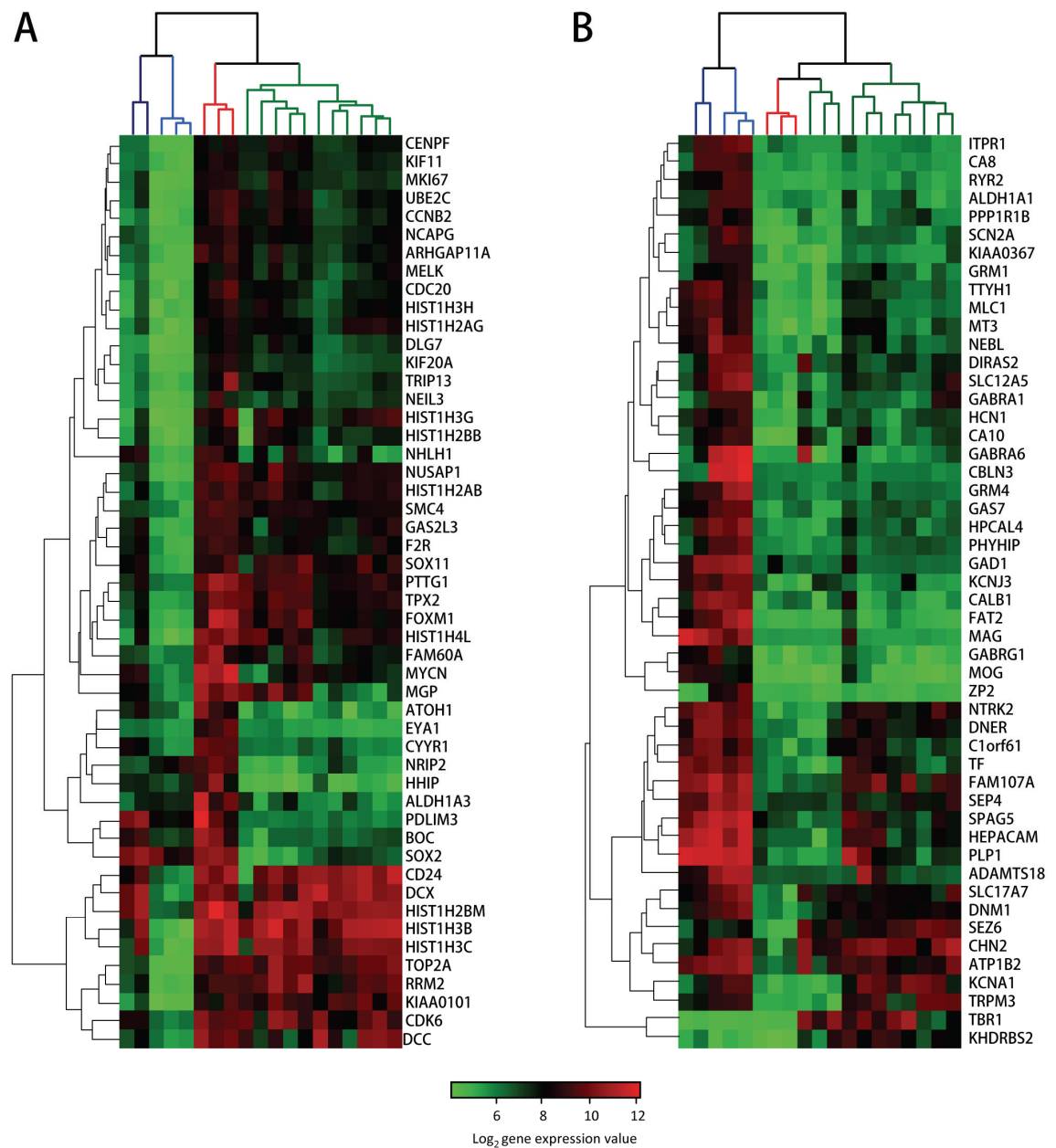
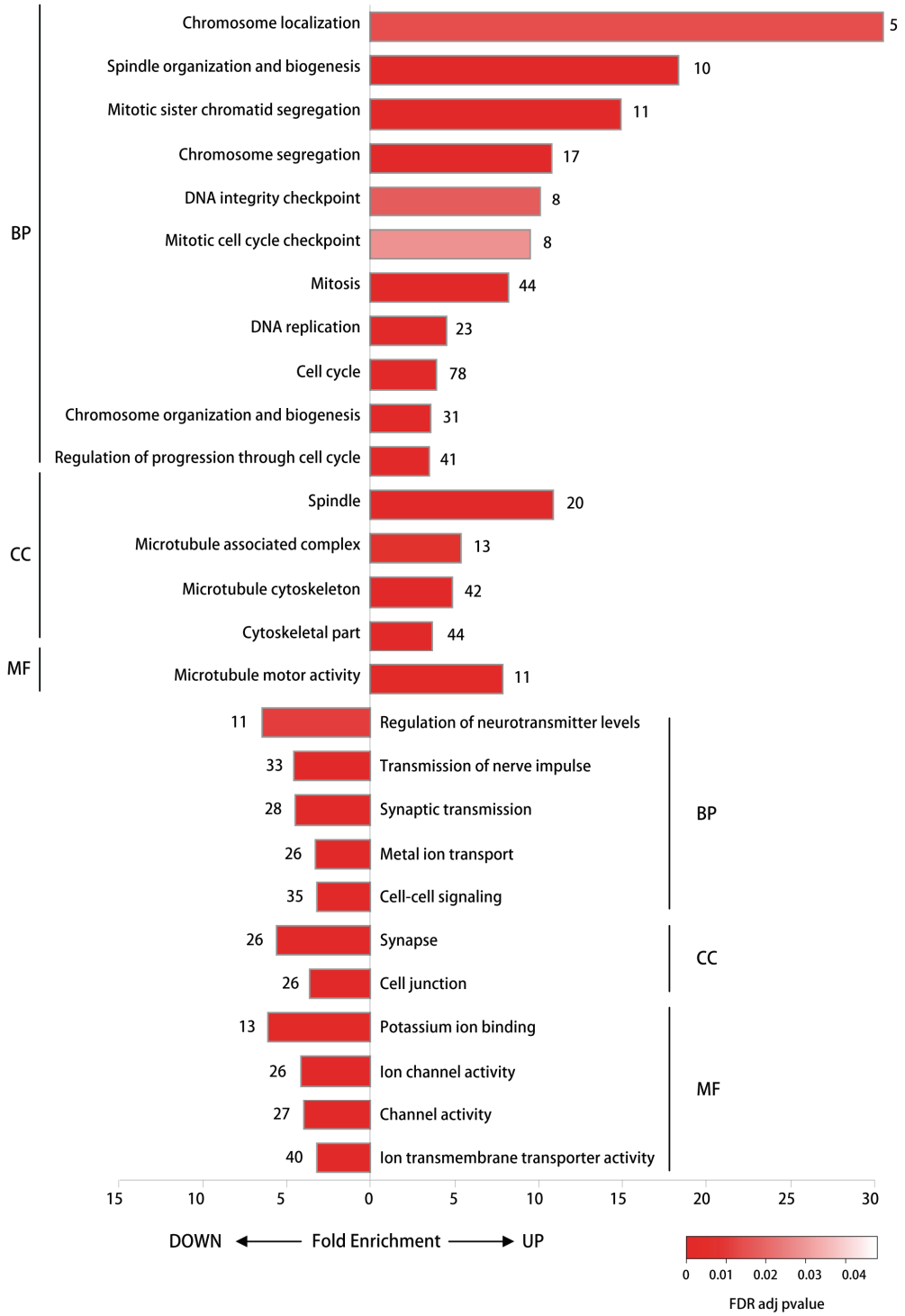


Figure 4.2. Top 50 genes up- and down-regulated in Shh-driven medulloblastomas.

Two heatmaps show the expression of the 50 most significantly up- (A) and down-regulated genes (B) in SHH tumours compared to the other sample groups. Both samples and genes were clustered according to their expression profiles and the corresponding dendrograms are shown to the top and to the left of the heatmaps, respectively. Samples subgroups are colour-coded as follows: dark blue, normal fetal CB; light blue, normal adult CB; red, SHH; green, MB2. A green-red colour palette was used to illustrate gene expression values, with green corresponding to low and red corresponding to high expression.

Figure 4.3. Functional enrichment analysis of Gene Ontology terms.

Gene Ontology (GO) annotation terms were used to perform functional enrichment analysis using the DAVID tools. Briefly, a statistical measure of the likelihood that any individual GO term would appear in the DEG list at the observed frequency (as compared to its frequency across the entire population of genes represented on the exon array) is calculated together with a p-value indicating the significance of the enrichment. Each bar represents a significantly enriched term and is colour-coded according to its corresponding p-value. The bar length represents the fold-enrichment, and the figure at the end of each bar refers to the number of DEGs described by that term. Genes up- and down-regulated in SHH tumours were analysed as separate gene lists and are depicted with bars pointing to the right and to the left, respectively. The three major GO categories are specified on the sides: BP, biological process; CC, cellular component; MF, molecular function.



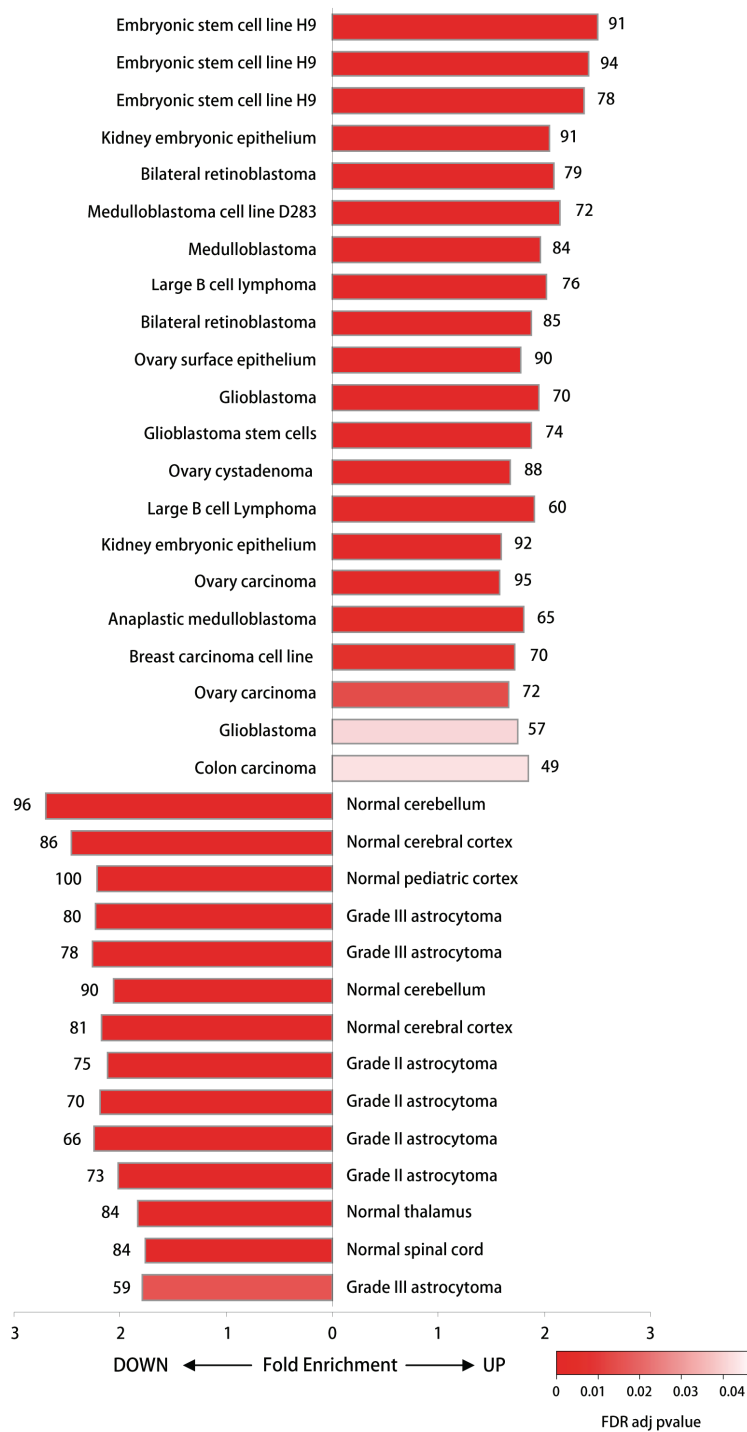


Figure 4.4. Functional enrichment analysis of tissue annotation.

DAVID tissue annotation category is based on the data obtained by Serial Analysis of Gene Expression (SAGE) of several normal and malignant tissues within the context of the Cancer Genome Anatomy Project (CGAP, <http://www.ncbi.nlm.nih.gov/ncicgap/>). A tissue annotation term is assigned to a gene if its expression level is higher in that given tissue as compared to the collection of all other tissues. Since several SAGE libraries are taken into account, the same annotation term can occur more than once. For a description of histogram features, see figure legend 4.3.

They also appeared to be expressed in brain tumours of glial origin, possibly indicating the presence of a smaller glial component in SHH tumour samples as opposed to the other profiled samples.

The DEGs identified in my study included genes differentially expressed in SHH tumours compared to either MB2 tumours or normal cerebella. Genes identified by medulloblastoma subset comparison are those which contribute to the Shh gene expression signature (*e.g. ATOH1, HHIP, BOC, etc.*); whereas genes selected in reference to normal samples are expected to be associated with a more general malignant cerebellar phenotype, and were indeed frequently expressed at a rather uniform level across all medulloblastoma samples. One of the most highly down-regulated genes obtained from the SHH *versus* MB2 comparison was *OTX2* (Appendix 3, page 242), which encodes a critical homeodomain-containing transcription factor implicated in brain morphogenesis [178]. Recurrent *OTX2* gene amplification and/or overexpression were observed both in medulloblastoma cell lines and primary tumours, particularly in those of anaplastic histology [179]. Interestingly, by performing genome-wide screening of differential gene expression, Kool *et al.* found a significant increase in *OTX2* expression levels in primary medulloblastomas that did not express a molecular signature of Shh pathway activation [92]. Further evidence of selective abnormal expression of *OTX2* in Shh-independent tumours came from Adamson *et al.*, who also associated gain of *OTX2* copy number with a worse prognosis for medulloblastoma patients and suggested a role for *OTX2* in promoting medulloblastoma progression by regulating *MYC* expression [180].

Compared to normal cerebella, SHH tumours expressed lower levels of several genes playing important roles in cerebellar development. Some interesting examples are *FAT2*, *GAS7* and *GABRA6* (Figure 4.2). The *FAT2* gene encodes a member of the well

conserved Fat subfamily of protochaderins, which are commonly involved in the regulation of cell-cell interactions during morphogenesis [181]. Within the subfamily, FAT2 is unique in its restricted expression pattern: in the developing cerebellum, the mouse Fat2 protein is specifically detected in non-proliferating granule neurons in the inner external germinal layer and in migrating granule neurons, but not in granule cell precursors in the outer external germinal layer. Fat2 protein levels peak in differentiated granule neurons during the third post-natal week and remain high throughout adulthood [182]. It has been suggested that *FAT2* could contribute to the regulation of granule cell axon organisation in the molecular layer of the cerebellar cortex through its engagement in homophilic interactions [182].

Growth arrest specific 7 (*GAS7*) is predominantly expressed in terminally differentiating neuronal cells in the mature cerebral cortex, hippocampus and cerebellum. It has putative roles in transcriptional regulation, neuronal differentiation and neurite formation [183]. *GAS7* maps to chromosome 17p, in the proximity of a highly unstable chromosomal region putatively involved in the formation of isochromosome 17q, the most common chromosomal aberration in medulloblastomas [25]. It has therefore been suggested that *GAS7* might represent a putative medulloblastoma tumour suppressor gene, which is disrupted as a result of i(17q) formation. However, *GAS7* gene expression has been detected independently of i(17q) in a series of childhood medulloblastomas [184] and its potential implication in medulloblastoma tumorigenesis remains uncertain.

GABRA6 encodes the $\alpha 6$ subunit of the GABA receptor. GABA is the major inhibitory neurotransmitter in the mammalian brain and the GABA receptor $\alpha 6$ subunit is primarily expressed in cerebellar granule neurons following their terminal

differentiation. Its expression is modulated by nuclear factor 1 as part of a neuronal lineage specification program [185].

Genes significantly up-regulated in the SHH tumour subtype will be discussed in the following section.

4.3. Selection of medulloblastoma-associated candidate genes

Alongside very well characterised genes which critically define the molecular signature of Shh-driven medulloblastomas (*e.g. ATOH1, FOXM1, MELK*; see Figure 3.8), I identified several other genes whose expression level was higher in tumour samples, particularly in the SHH tumour subset, and whose biological function suggested that they may represent interesting tumour candidate genes. Based on their expression profiles and on biological information retrieved from the literature, I selected 14 of these genes for further analysis (Figure 4.5). All of the 14 selected genes were expressed at higher levels in SHH tumours compared to normal adult cerebellar samples. Several candidate genes were equally overexpressed in all tumour samples (*e.g. PLK1, TROAP*), while others were significantly more expressed in the SHH tumour subgroup (*e.g. POU3F2, DLG7, BAZ1A*). In most cases, normal fetal cerebellar samples showed higher expression levels than their adult counterpart (*e.g. EZH2, PTTG1, TEAD2*).

Most of the selected genes encode spindle related proteins which are normally involved in regulating correct chromosome segregation during mitosis (*CHEK1, UBE2C, KIF4A, DLG7, CASC5, NUSAP1, PLK1, TROAP, and PTTG1*). Being involved in cell cycle specific processes, these genes typically show a characteristic expression profile in which their expression level peaks at the time when they are needed for their particular functions [186]. Regardless of whether their observed

overexpression in medulloblastoma simply reflects the high proliferation rate of tumour cells compared to differentiated normal cerebellar cells, or is actively contributing to the tumorigenesis process, these genes represent valuable candidates differentiating between normal and tumour cells and they are potential targets for clinical anticancer therapies that strategically aim to interfere with checkpoint signalling pathways [187-191].

Other selected genes encode transcription factors implicated in neuronal development (*POU3F2* and *TEAD2*) or chromatin-associated proteins participating in the chromatin-dependent regulation of transcription (*BAZ1A* and *EZH2*). Because processes that modulate gene expression within a cell ultimately control cell behaviour, defects in both transcription regulation and chromatin have been long associated with cancer and a considerable interest is emerging in the development of novel therapies targeting these key cellular processes [192, 193].

Finally, I selected candidate genes implicated in DNA replication and repair (*EXO1*, *CHEK1* and *KIF4A*). Alterations affecting DNA repair genes are major drivers of both hereditary and sporadic cancer [194]. Furthermore, since many of the existing chemo- and radiotherapy agents function through their ability to induce DNA damage, pharmacological inhibition of DNA repair mechanisms has been explored as a valuable approach to enhance drug sensitivity [187, 195].

More details of the selected genes' function and possible role in tumorigenesis can be found in Table 4.1.

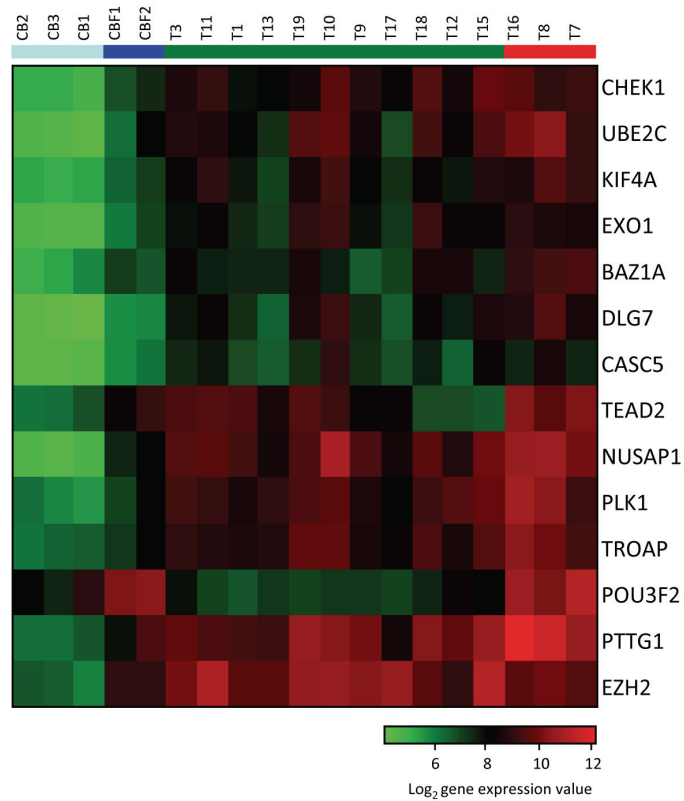


Figure 4.5. Selection of candidate genes up-regulated in Shh-driven medulloblastomas.

The heatmap show the expression of the 14 selected candidate genes. Samples subgroups are colour-coded as follows: dark blue bars, normal fetal CB; light blue bars, normal adult CB; red bars, SHH; green bars, MB2. A green-red colour palette was used to illustrate gene expression, with green corresponding to low and red corresponding to high expression values.

Table 4.1. Biological functions and potential tumorigenic roles of selected genes significantly up-regulated in Shh-driven medulloblastomas.

Gene Symbol	Description	Function(s)/ Role(s) in tumorigenesis	Reference(s)
CHEK1	Cell cycle checkpoint kinase	Regulatory component of cell cycle check points; DNA damage response. Potential drug target.	[187, 196]
UBE2C	Ubiquitin-conjugating enzyme	Required for the destruction of mitotic cyclins and for cell cycle progression. Overexpressed in several human cancers; associated with tumour progression.	[191, 197-199]
KIF4A	Microtubule-based motor protein	Maintenance of chromosome integrity during mitosis; DNA damage response.	[200, 201]
EXO1	5'-3' exonuclease	Implicated in DNA replication, recombination, and mismatch repair.	[202]
BAZ1A	ATP-dependent chromatin assembly factor subunit	Chromatin-dependent regulation of transcription.	[203]
DLG7	Microtubule-associated protein	Involved in microtubule polymerization and mitotic spindle stabilisation. Potential oncogenic target of Aurora-A.	[204-206]
CASC5	Kinetochore protein	Required for the localisation of outer kinetochore proteins and chromosome segregation.	[207]
TEAD2	Transcription factor	Contributes to neural tube closure; required for YAP-induced cell growth.	[208]
NUSAP1	Nucleolar-spindle associated protein	Mitotic spindle organization.	[209]
PLK1	Polo-like kinase	Involved in the control of spindle dynamics and chromosome segregation. Overexpressed in several human tumours.	[210, 211]
TROAP	Trophinin associated protein	Participates in early embryo implantation; required for spindle assembly during mitosis.	[212]
POU3F2	Transcription factor	Involved in Schwann cell development; regulator of melanocytic growth; neuronal-fate-inducing factor.	[213, 214]
PTTG1	Mitotic checkpoint securin	Prevents premature chromosome separation through inhibition of separase activity. Tumorigenic.	[190, 215]
EZH2	Member of the Polycomb-group family	Involved in the transcriptional silencing of differentiation genes. Potential role in tumorigenesis.	[216]

The table lists the 14 selected candidate genes together with a summary of their function in normal cells and their possible role in tumorigenesis.

4.4. In vitro culture of mouse cerebellar granule cell precursors

GCPs are the proposed cells of origin of Shh-driven medulloblastomas and an increasing number of studies have shown that genes which contribute to medulloblastoma pathogenesis are also implicated in GCP proliferation [163]. As a result, GCPs constitute the best characterized cell culture model to study the regulation and function of medulloblastoma candidate genes *in vitro* [45, 53, 54, 65, 166]. I therefore set up a mouse cerebellar granule cell precursor (GCP) culture model to investigate the possible role of Shh in regulating the expression of selected candidate genes (Figure 4.6). Cells isolated from mouse post-natal cerebellum initially include a mixture of mature granule neurons and GCPs at different stages of the cell cycle which are committed to differentiate unless their specific mitogen (Shh) is added to the cell culture medium [43]. I observed that the addition of ShhN (the biologically active NH₂-terminal peptide of Shh) induced a change in the overall culture morphology within 48 hours of plating, with cells visibly projecting fewer processes than their control counterparts and forming clumps of clonal expansion (Figure 4.6C). Cell clumping in GCP cultures has been previously described [69, 165], and in my experiments it was significantly accentuated in the presence of ShhN.

I assessed the activation of the Shh signalling pathway in ShhN-treated cultures by measuring the expression of well characterised Shh-associated genes (*Atoh1*, *Gli1*, *Foxm1* and *Melk*) by western blotting or RT-PCR. As expected, all of the analysed genes were expressed at remarkably higher levels in ShhN-treated cultures compared to the controls (Figure 4.7A-B).

Using a BrdU incorporation assay to label proliferating cells, I confirmed that the addition of ShhN maintained GCP proliferation at 48 hours after plating: whereas control cultures showed almost no positivity for BrdU, as measured both by

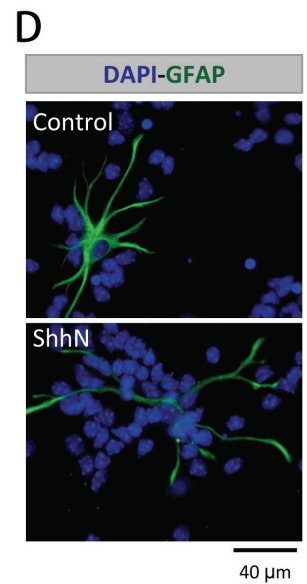
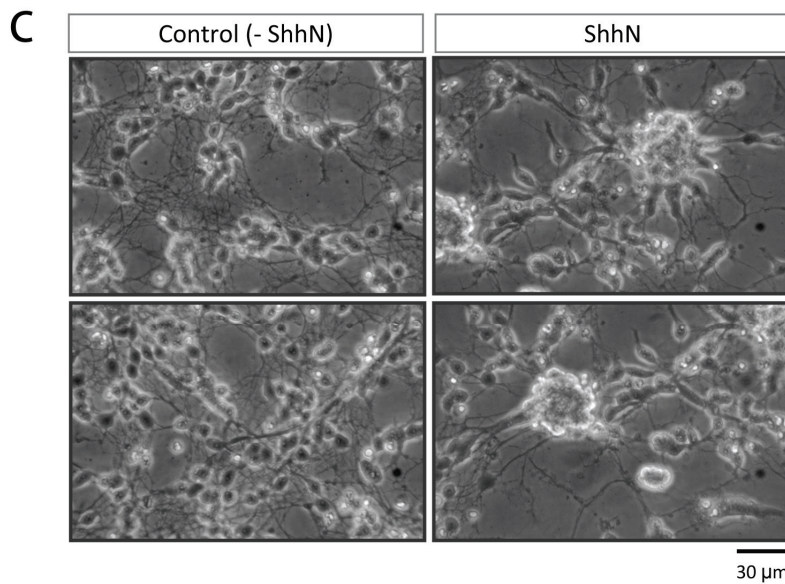
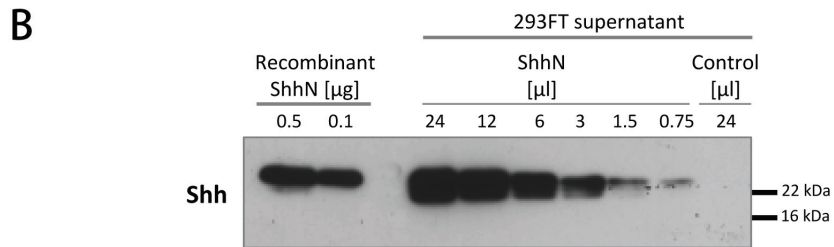
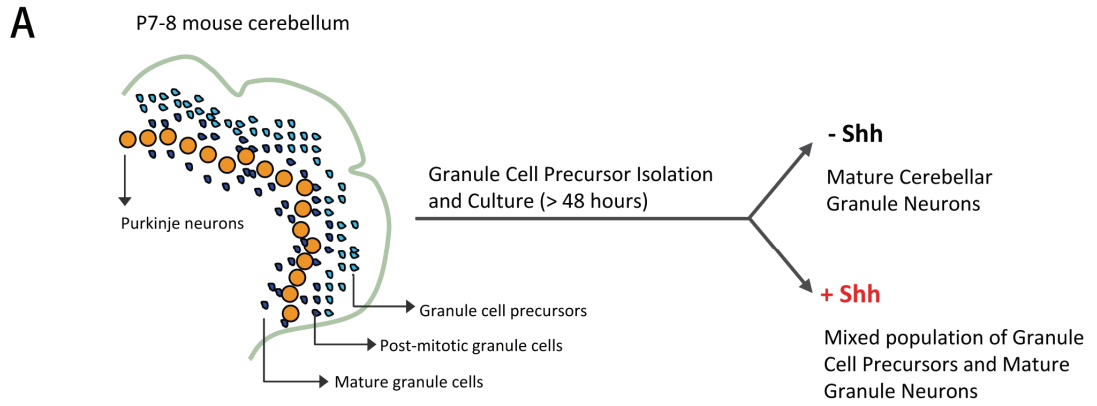
Figure 4.6. *In vitro* culture of mouse cerebellar granule cell precursors (GCPs).

(A) Schematic overview of *in vitro* GCP cultures. GCPs were isolated from mouse cerebella at post-natal days 7 or 8 and cultured for at least 48 hours in the presence or in the absence of Shh. Without Shh, GCPs begin to differentiate upon plating, so that within 48 hours the culture consists of a homogeneous population of post-mitotic, mature granule neurons. However, the addition of Shh to the culture medium prolongs GCP proliferation giving rise to a mixed population of precursors and mature granule neurons.

(B) Serial dilutions of the ShhN supernatant produced by transfecting 293FT cells were analysed by western blotting. The blot was probed with an anti-Shh antibody to confirm that the supernatant contained the ShhN polypeptide. Different amounts of recombinant ShhN were loaded as a control. Control supernatant did not generate any Shh signals.

(C) Phase contrast microscopy of cerebellar cell cultures (48 hours after plating). The two panels on the left show representative fields of mature granule neurons cultured in the absence of ShhN (control culture). On the right, two fields of cerebellar neuron cultures in the presence of ShhN are shown.

(D) Immunocytochemistry staining of astrocytes in cerebellar cell cultures. Forty-eight hours after plating, cells were stained with an antibody specific for astrocytes (GFAP).



immunocytochemistry and flow cytometry (Figure 4.7C-D), ShhN-treated cultures showed a considerably higher BrdU uptake, which further increased with prolonged BrdU pulses (Figure 4.7D). Interestingly, following a 15-hour BrdU incubation, the percentage of BrdU-positive cells in ShhN-treated cultures reached 64%, indicating that far more than half of the overall cell population consisted of proliferating GCPs.

To further validate the effects of ShhN-treatment on my GCP cultures, I carried out an immunocytochemistry assay using an antibody against NeuN, a nuclear antigen specifically expressed in post-mitotic neurons [217]. In line with previous reports, I found that cells cultured in the absence of ShhN were largely positive for NeuN, while a consistent proportion of ShhN-treated cells was NeuN-negative (Figure 4.8) [43, 218]. In addition, by performing NeuN and BrdU double staining, I verified that ShhN-cultures were a mixture of two distinct cell populations: NeuN-positive, BrdU-negative differentiated granule neurons coexisted with NeuN-negative, BrdU-positive granule cell precursors (Figure 4.8).

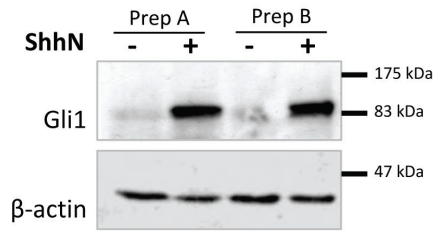
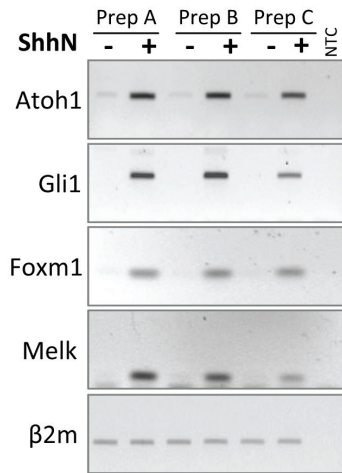
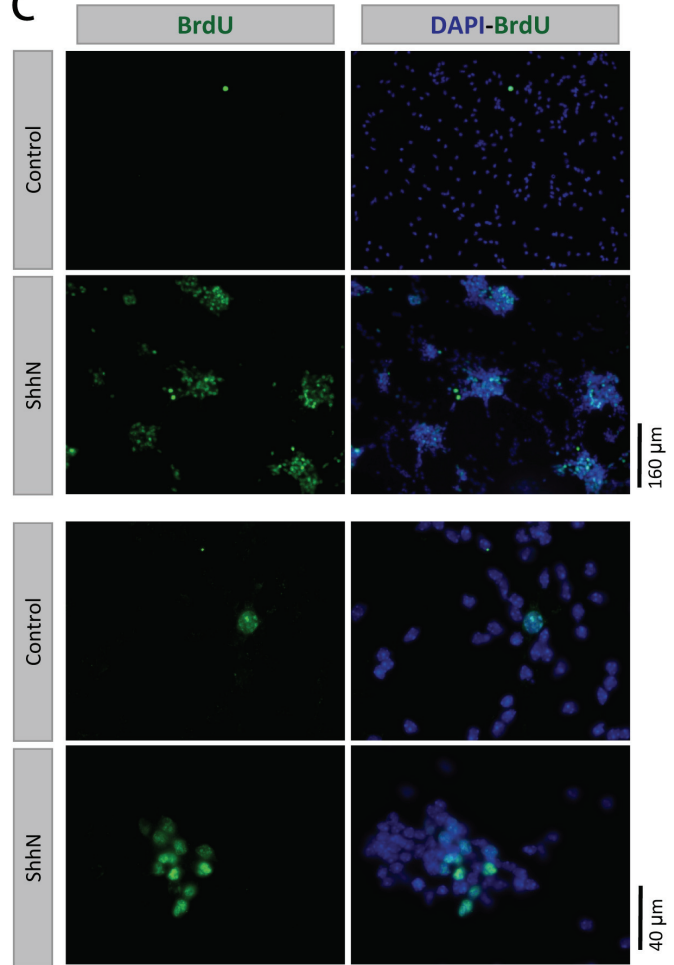
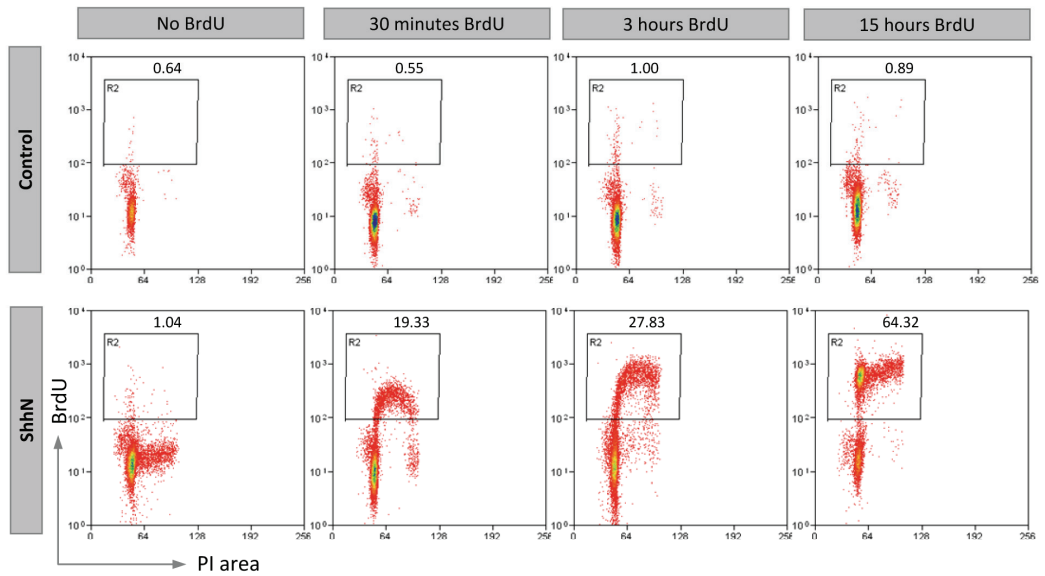
Although granule neurons and granule precursors represent the predominant cell populations in the early post-natal mouse cerebellum, other cell types are present during this period, including glial cells, such as astrocytes and oligodendrocytes, and Purkinje neurons. To minimise the contribution of non-granule neuronal types to the cell culture, the protocol for the generation of GCP cultures includes a Percoll gradient separation step [43, 164]. I confirmed that my GCP cultures were enriched in neuronal cell types by staining the cultures for glial fibrillary acidic protein (GFAP), a marker specific for astrocytes. I found that only a small minority of cells expressed GFAP (<1%). In addition, GFAP-positive cells were mostly located at the edges of the culture surface, perhaps as an effect of coverslip coating. Some examples of GFAP staining are shown in Figure 4.6D.

Figure 4.7. ShhN induces expression of granule precursor markers and proliferation of GCPs.

(A-B) Treatment of cerebellar cultures with ShhN for 48 hours induced the expression of well known markers of granule cell precursor state, as measured by western blotting (A) and RT-PCR (B). Preps A-C are independent GCP preparations. β -actin and β 2-microglobulin (β 2m) were used as housekeeping controls. NTC, non-template control.

(C) ShhN induction of BrdU uptake by GCPs measured by immunocytochemistry. Cells were incubated with BrdU for the last 3 hours of a 48-hour culture, then fixed and stained. Representative fields are shown at two different magnifications.

(D) ShhN induction of BrdU uptake by GCPs measured by flow cytometry. At the end of a 48-hour culture, cells were pulsed with BrdU for the indicated amount of time. They were then harvested, fixed and stained.

A**B****C****D**

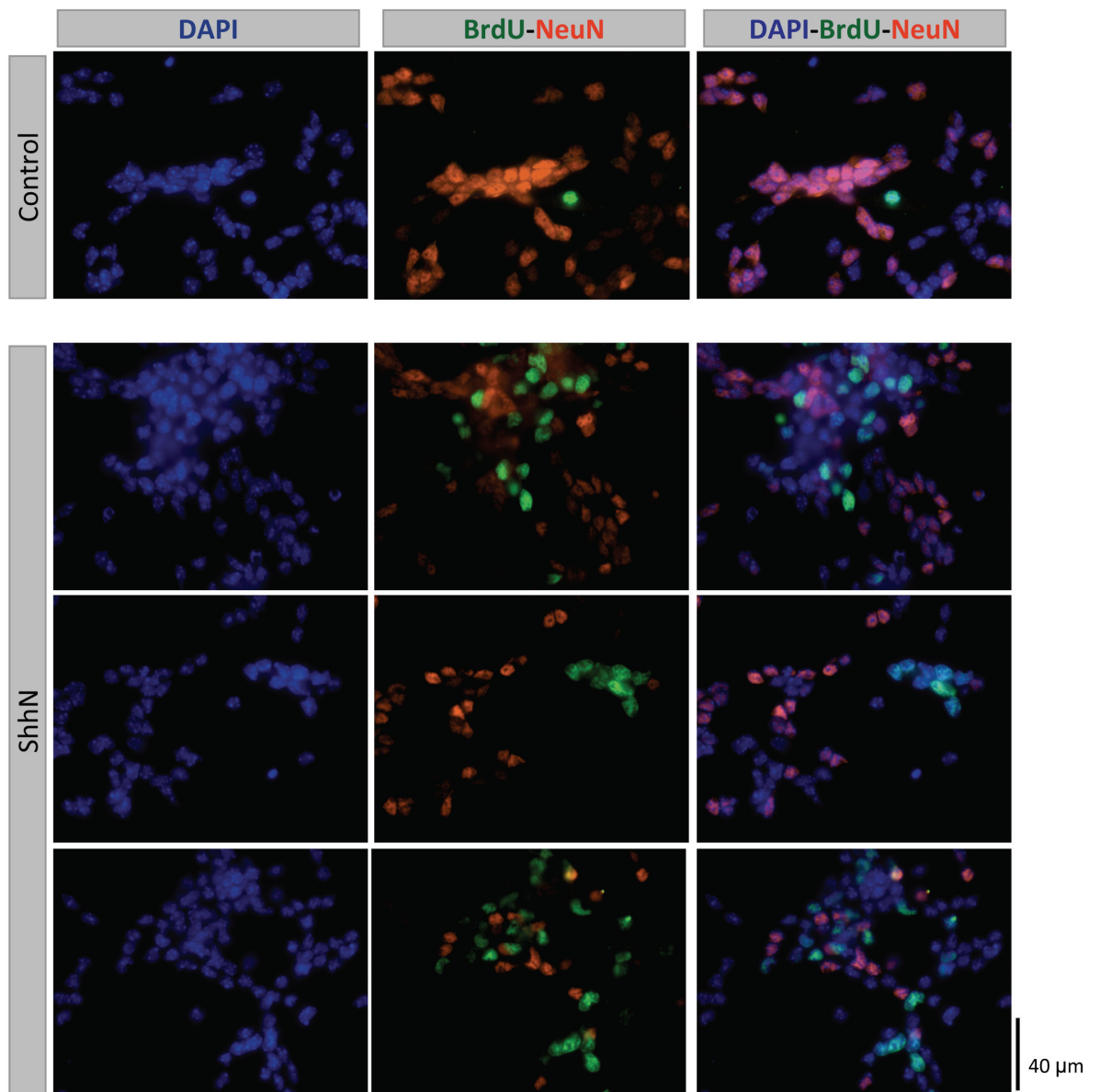


Figure 4.8. ShhN-treated cultures are a mixture of mature granule neurons and granule cell precursors.

Cerebellar cells were cultured for 48 hours in the absence or in the presence of ShhN, and pulsed with BrdU for the last 3 hours of culture. Cells were then fixed and double-stained with anti-NeuN and anti-BrdU antibodies.

4.5. Analysis of candidate gene expression in GCP cultures

Following the identification of a set of genes that were significantly overexpressed in SHH tumours (section 4.3), I was interested to test whether their expression levels were also modulated by Shh in cultured GCPs. To investigate this possibility, I performed semi-quantitative RT-PCR to measure gene expression in GCP cultures maintained in the presence or absence of ShhN for 48 hours. As shown in Figure 4.9, ShhN was able to induce a significant increase in the level of expression of the entire set of candidate genes. In most cases (*e.g. Dlg7, Kif4, Chek1*), I found minimal or no expression in control cultures, as opposed to a strong expression signal observed in ShhN-treated cultures. In a few other cases (*e.g. Ezh2, Pou3f2*), the difference in expression level between control and ShhN-treated cultures was more modest, but still significant (Figure 4.9).

For two genes, *Pou3f2* and *Ube2c*, I confirmed differential expression at the protein level by western blotting and immunofluorescence analysis (Figures 4.10 and 4.11). *Pou3f2* encodes a transcription factor implicated in the development of the nervous system. Targeted mutagenesis of *Pou3f2* in mouse embryonic stem cells resulted in the loss of specific neuronal lineages in the hypothalamus and mortality before post-natal day 10 [219]. Recently, *Pou3f2* was used in combination with two other transcription factors (*Ascl1* and *Myt1l*) to reprogramme mouse embryonic and post-natal fibroblasts into functional neuronal cells *in vitro* [213]. Besides being an important player in neuronal development, there is evidence that Pou3f2 plays a role in oncogenesis, and particularly in melanoma growth and survival [214]. In their study of the expression pattern of transcription factors in the mouse post-natal cerebellum, Schüller *et al.* observed widespread Pou3f2 protein expression in both the EGL and the IGL [220]. Accordingly, I found that *Pou3f2* was expressed both in ShhN-treated and in

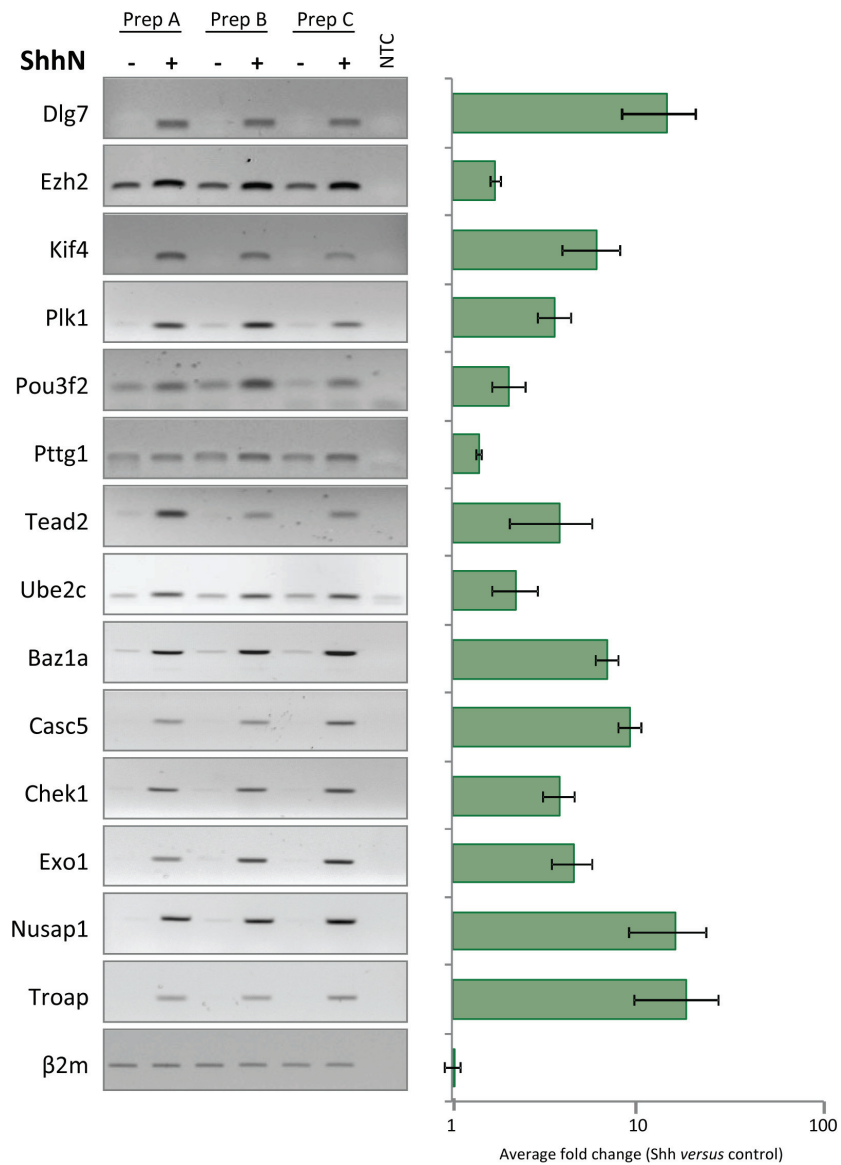


Figure 4.9. Genes overexpressed in Shh-driven medulloblastomas are also up-regulated in GCPs in the presence of Shh.

Treatment of cerebellar cultures with ShhN for 48 hours induced the expression of medulloblastoma-associated genes, as measured by RT-PCR. Preps A-C are independent GCP preparations. The housekeeping $\beta 2$ -microglobulin ($\beta 2m$) gene was used as a control. NTC, No-template control. The intensity of the agarose gel bands was quantified by densitometry. The bar chart shows average fold changes in gene expression between ShhN-treated and control cultures with 95% confidence intervals. All of the candidate genes examined were expressed at significantly higher levels in ShhN-treated cultures, while $\beta 2m$ gene expression did not differ between the two conditions (average fold change = 1.0; 95% CI 0.9, 1.1).

control GCP cultures, however its expression was significantly higher in the presence of ShhN (Figure 4.9). In the series of human samples used for my microarray experiment, the expression profile of *POU3F2* correlated extremely well with that of the *ATOHI* gene (correlation coefficient = 0.9), which suggested that they may be co-expressed in Shh-responsive cells.

To further test this hypothesis, I measured Pou3f2 protein expression in mouse GCP cultures. I found that Pou3f2 protein levels were more than four fold higher in ShhN-treated cultures compared to controls as measured by western blotting (p-value = 0.002, Figure 4.10A). Immunostaining for Pou3f2 showed the presence of a small number of positive cells in control cultures, whereas a much larger proportion of Pou3f2-expressing cells was observed in ShhN-treated cultures (Figure 4.10B). Typically, the cells which stained positive for Pou3f2 were NeuN-negative, suggesting that Pou3f2 expression was restricted to immature GCPs (Figure 4.10B).

Ube2c is a ubiquitin-conjugating enzyme responsible for the polyubiquitination and consequent destruction of mitotic cyclins prior to anaphase initiation and cell cycle progression. Its expression is modulated during the cell cycle, with *Ube2c* transcript levels increasing in mitosis and dropping during telophase and G₁. *Ube2c* was found to be expressed at relatively high levels in many different types of human cancer, including breast, lung, ovary and bladder carcinomas, and glioblastomas [191]. Its causative role in tumorigenesis has recently been established through the use of transgenic mice, in which *Ube2c* overexpression induced whole chromosome instability and spontaneous tumour formation [199].

I carried out western blotting to measure Ube2c protein levels in GCP cultures (Figure 4.11). In control cells, Ube2c was undetectable, as should be the case for differentiated neurons. However, in ShhN-treated GCPs the level of Ube2c expression

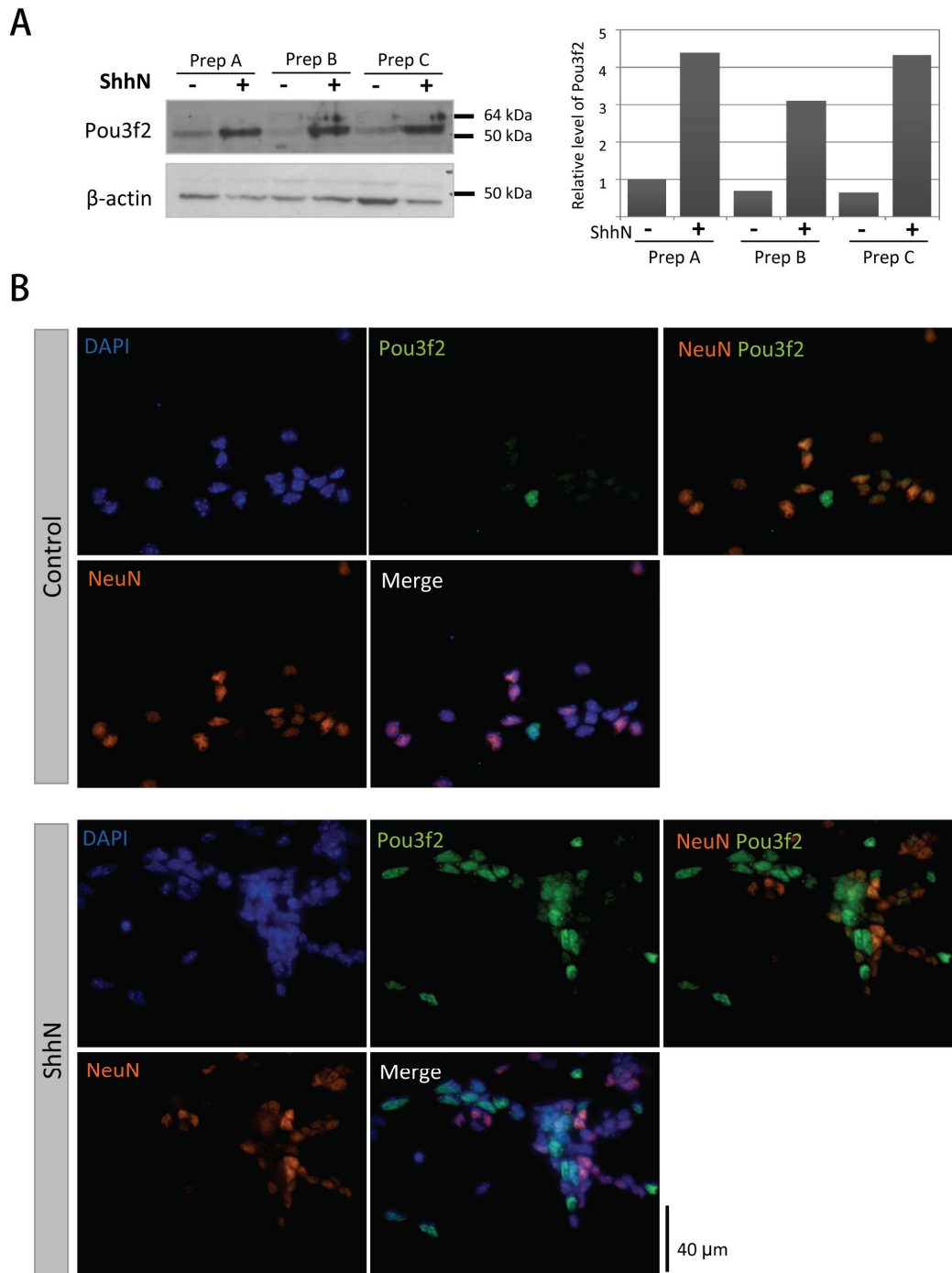


Figure 4.10. Shh induces the expression of Pou3f2 in GCP cultures.

(A) Western blot showing a significant increase in the level of the Pou3f2 protein in GCPs cultured for 48 hours in the presence of ShhN. β-actin was used as a loading control. A quantitation of the protein bands is shown to the right. Since basal levels of Pou3f2 were comparable across the three independent experiments, I normalised the intensity of each individual protein band to the same control band (Prep A).

(B) Analysis of Pou3f2 and NeuN expression by immunostaining.

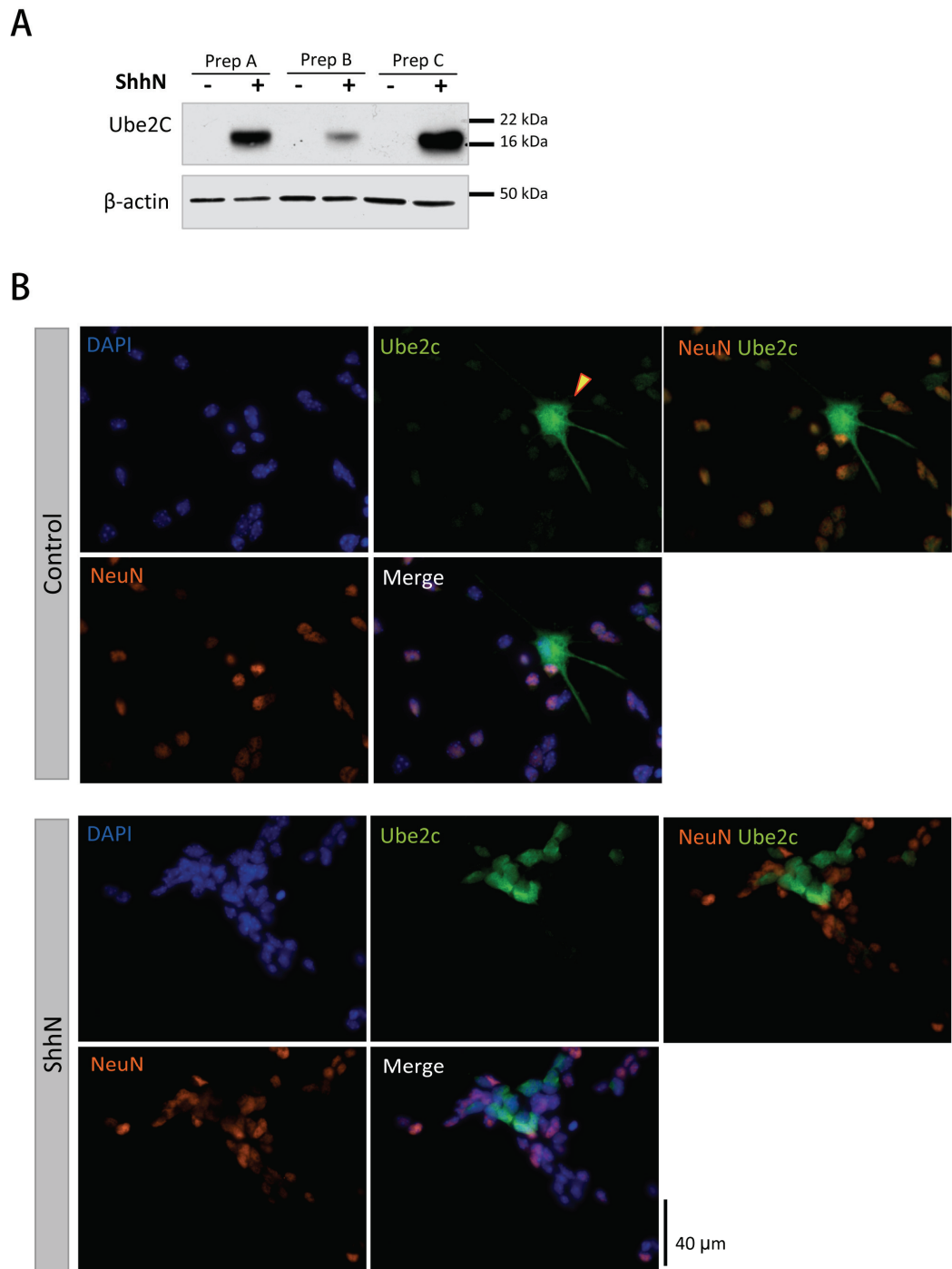


Figure 4.11. Shh induces the expression of Ube2c in GCP cultures.

(A) Western blot showing a very significant increase in Ube2c protein expression level in GCPs cultured for 48 hours in the presence of ShhN. β-actin was used as a loading control.

(B) Analysis of Ube2c and NeuN expression by immunostaining. In control cells Ube2c expression was extremely low, and the very few positive cells displayed glial cell morphology (arrow). In contrast, Ube2c was expressed at higher levels in ShhN-treated GCP cultures and its expression was specifically detected in NeuN-negative cells.

was remarkably higher (Figure 4.11A). A similar pattern of expression was observed in immunostaining experiments, in which the only positive cells in control GCP cultures clearly displayed a glial morphology, suggesting that they might be contaminating astrocytes or oligodendrocytes that maintained the ability to proliferate in culture (Figure 4.11B).

4.6. Analysis of candidate gene expression in human medulloblastoma cell lines

Human medulloblastoma cell lines have been successfully employed for the functional characterisation of putative tumour-associated genes. Aiming to address the possibility that some of the identified candidate genes were required to sustain tumour cell proliferation, I initially assessed candidate gene expression in three commonly used medulloblastoma cell lines, Daoy, D425 Med and UW228-2, by semi-quantitative RT-PCR. Three samples of normal adult cerebellum and two samples of normal fetal cerebellum were also analysed for comparison. The *FOXMI* gene, which is known to promote Shh-dependent cell cycle progression and is overexpressed in medulloblastomas [166], was used as a control. I also studied *MYC* gene expression as an additional control, because *MYC* is amplified in the D425 Med cell line.

As suggested from gene expression patterns in cultured GCPs and from the array analysis, most of the genes examined were expressed at higher levels in fetal cerebellar samples compared to adult cerebellar samples (Figure 4.12A). Importantly, the majority of genes also appeared to be expressed at considerably higher levels in the three medulloblastoma cell lines compared to both adult and fetal normal cerebellum. These genes included *FOXMI*, *UBE2C* (whose expression was also analysed at the protein level, Figure 4.12B) and many others. Only two genes, *POU3F2* and *TEAD2*, were expressed at similar levels in medulloblastoma cells and normal cerebellum (Figure

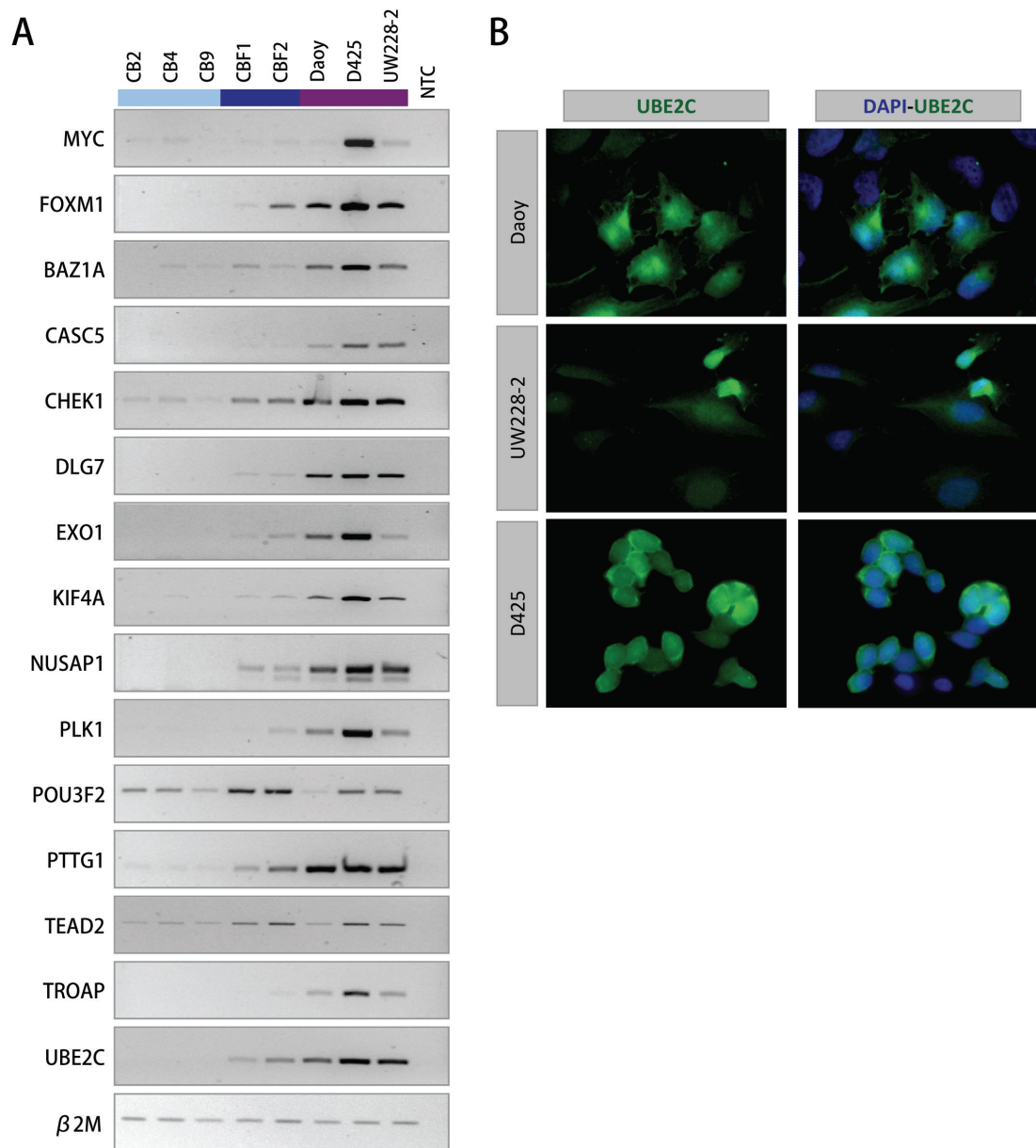


Figure 4.12. Expression of selected candidate genes in human medulloblastoma cell lines.

(A) Semi-quantitative RT-PCR analysis of candidate gene expression in adult normal cerebellum (light blue bar), fetal normal cerebellum (dark blue bar) and human medulloblastoma cell lines (Daoy, D425 Med and UW228-2, purple bar). The housekeeping β 2-microglobulin (β 2m) gene was used as a control. Gels are representative of at least two independent experiments. NTC, No-template control.

(B) Immunocytochemistry analysis of UBE2C expression in human medulloblastoma cell lines.

4.12A). In accordance with its amplification pattern, *MYC* transcript levels were much higher in D425 Med cells compared to all of the other samples. Overall, the RT-PCR results indicated that the medulloblastoma cell lines expressed all of the candidate genes identified in primary tumours and could be considered useful models for subsequent analysis.

4.7. Functional analysis of candidate genes by shRNA-mediated knockdown in medulloblastoma cell lines

To investigate the potential contribution of the selected candidate genes to medulloblastoma pathogenesis, and in particular their role in tumour growth and cell proliferation, I used shRNA expression constructs to inhibit their expression. ShRNAs have been widely used to knock down target genes in mammalian cells. Following transcription, shRNAs are cleaved by endogenous nucleases to generate short double stranded RNAs which are recognised by the RNA-induced silencing complex (RISC) and used to target complementary mRNAs for destruction [221]. ShRNAs can be easily delivered to target cells using viral vectors which are specifically designed to express the desired shRNA sequences [221]. In my experiments, I used the pGIPZ lentiviral vector system described in section 2.5.1.2, in which individual shRNAs are transcribed under the control of the CMV promoter and are co-expressed with the EGFP reporter gene and the gene encoding puromycin resistance [161]. Following viral transduction, I was therefore able to track and select for shRNA-expressing cells by monitoring EGFP expression and applying puromycin selection.

4.7.1. Initial characterisation of the shRNA expression system

Cells were inoculated with the appropriate viral preparation at a suitable MOI to obtain an efficiency of transduction in the range between 40% and 80% (unless otherwise stated, an MOI of 0.1 was used for both the Daoy and the UW228-2 cell lines). In general, for each target gene, three individual shRNAs were used which were complementary to different regions in the target mRNA. A scrambled shRNA sequence designed not to cause the specific degradation of any known human mRNAs was used in each experiment to control for non-specific changes in gene expression which may result from the shRNA delivery method. As shown in Figure 4.13A, at three days following transduction, the percentage of cells which expressed EGFP, and therefore the shRNA of interest, was measured by flow cytometry and cells were divided into two aliquots. One aliquot was subjected to a five-day puromycin selection protocol to remove all of the non-transduced cells (Figure 4.13B). Once a > 98% population of shRNA-expressing cells was obtained, total RNA and proteins were isolated for an assessment of shRNA-mediated gene knockdown efficiency by Real Time PCR or western blotting. The same cell population was also used to perform cell cycle analysis by BrdU or Propidium Iodide (PI) staining.

A second aliquot of transduced cells was maintained in culture for three to four weeks without applying any treatment. At every cell passage, the percentage of EGFP-positive cells was measured by flow cytometry. Any significant decrease in the proportion of EGFP-positive cells would indicate a growth disadvantage for the transduced cells relative to the non-transduced ones. This could be due to either a decrease in the cell proliferation rate or an increase in apoptosis or cellular senescence. In any case, by using scrambled shRNA-transduced cells as a reference, the screening would provide information about any alterations of the overall cell growth rate caused

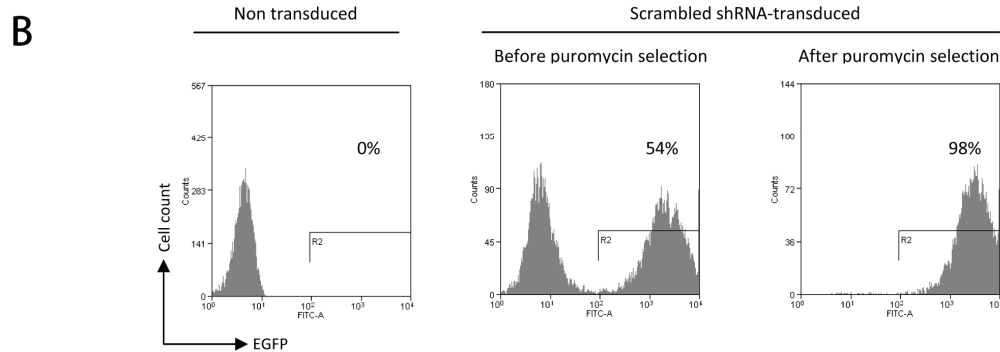
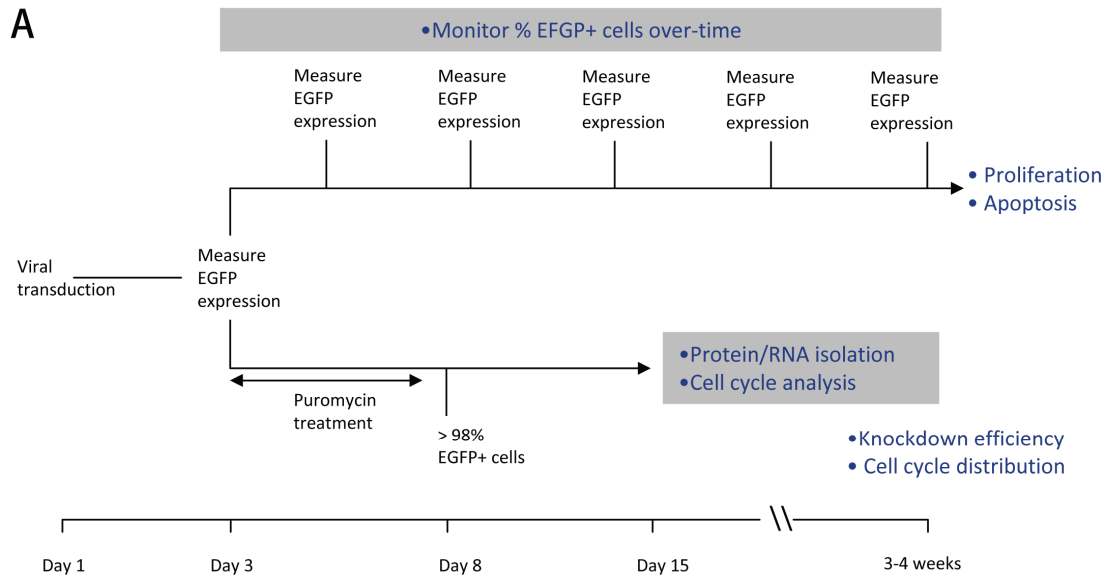


Figure 4.13. Experimental outline for the screening of candidate genes by shRNA silencing.

A) On day 1, medulloblastoma cells were inoculated with the appropriate viral preparations. Following the assessment of transduction efficiency, cells were divided into two aliquots. One aliquot was used to monitor changes in the proportion of EGFP-positive cells in culture, over a three to four-week time period. This would provide information about the effect of shRNA-mediated gene knockdown on cell proliferation/apoptosis. A second aliquot was put under puromycin selection to obtain a > 98% population of shRNA-expressing cells which would be used to assess the efficiency of shRNA-mediated gene knockdown and to perform cell cycle analysis.

B) A five-day puromycin selection period applied to a mixed population of < 100% transduced cells results in the restricted survival of transduced cells. Here I show an example of UW228-2 cells transduced with a scrambled shRNA-expressing lentiviral vector.

by the expression of gene-specific shRNAs. This technical approach has been successfully used by other groups in our department to identify putative tumour oncogenes in a variety of cell systems (unpublished data).

Before performing transduction experiments to knock down some of the putative target genes that I identified in my microarray study, I wanted to validate the overall approach by knocking down the expression of a control gene known to be important for medulloblastoma cell proliferation. I decided that the *BMII* gene, encoding a member of the Polycomb group of transcriptional repressor proteins, was an appropriate control gene. Polycomb group proteins are responsible for a variety of epigenetic programmes which regulate critical developmental mechanisms, including cell progenitor proliferation and stem cell self-renewal [222]. The *BMII* gene is expressed in the developing mouse and human cerebellum, where it regulates Shh-induced GCP proliferation [54], mainly through the repression of genes such as p16^{INK4a}, p19^{Arf} and p21^{Waf1/Cip1} [55]. *BMII* is also overexpressed in human and mouse medulloblastomas and is required for tumour formation in a mouse model of Shh-induced medulloblastoma [223]. In addition, a study by Wiederschain *et al.* showed that shRNA-mediated *BMII* knockdown in Daoy cells resulted in the inhibition of cell proliferation, as measured by MTS assay, as well as an increase in apoptotic cell death [224].

I transduced Daoy cells with three individual lentiviral shRNA constructs targeting the *BMII* mRNA. Levels of *BMII* mRNA and protein were significantly reduced by 70% to 90% in *BMII* shRNA-expressing Daoy cells compared to non-transduced Daoy cells or cells transduced with the control scrambled shRNA (Figure 4.14A-B). Despite causing a significant reduction in *BMII* protein levels, *BMII* knockdown did not seem to affect Daoy cell proliferation, as assessed by monitoring

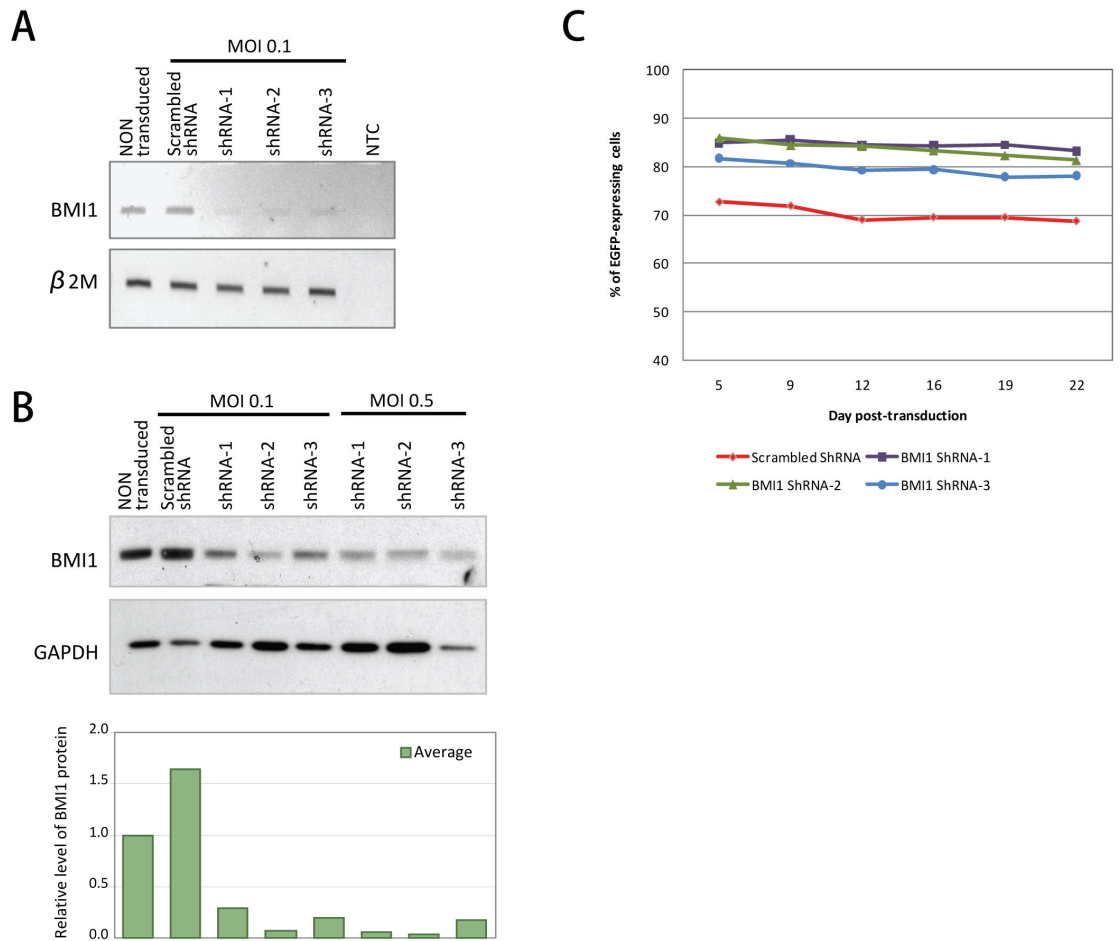


Figure 4.14. *BMI1* knockdown in Daoy cells.

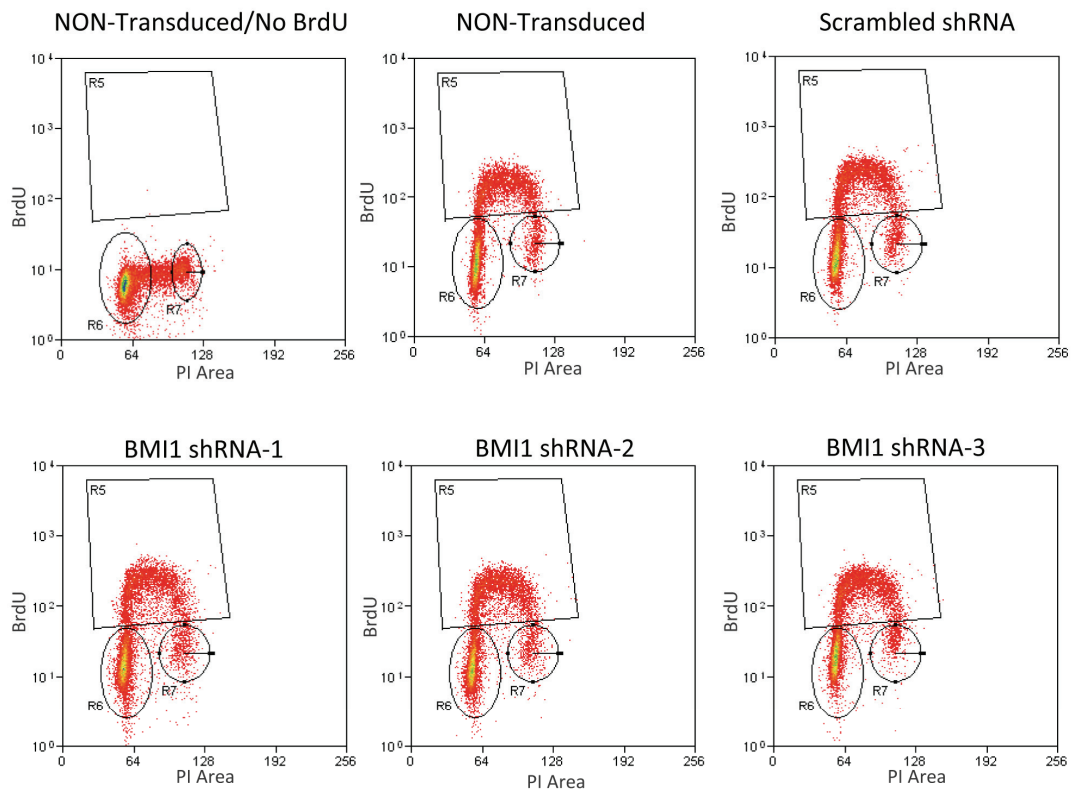
A-B) BMI-shRNAs efficiently reduced the levels of *BMI1* mRNA (A) and protein (B) in Daoy cells, as assessed by semiquantitative RT-PCR and western blotting. A scrambled shRNA was used as a control, and three individual shRNAs targeting the *BMI1* mRNA were tested (BMI1 shRNA 1-3). B, Protein bands were quantified by densitometry. The histogram shows GAPDH-normalised BMI1 protein levels as the averages of two experiments.

C) Percentage of EGFP-expressing Daoy cells, as assessed by flow cytometry analysis over a three-week time period following viral transduction.

EGFP-expression in transduced Daoy cell cultures over time (Figure 4.14C). In agreement with this result, cell cycle analysis by BrdU staining did not reveal any significant changes in the overall cell cycle distribution of BMI1-depleted Daoy cells relative to control cells (Figure 4.15A-B). My results contrasted with the *BMI1* knockdown effects I was expecting based on published data. One of the possible explanations is that the level of BMI1 protein knockdown I obtained was not good enough to elicit a biological effect. My decision to use an MOI of 0.1 for Daoy cell transduction experiments was intended to minimise the number of viral construct integration sites within the target cell genome. However, by increasing the MOI, I should obtain a better knockdown, and indeed BMI1 protein levels further decreased when I transduced Daoy cells with lentiviral shRNAs at the higher MOI of 0.5 (Figure 4.14B). In the future, it would also be interesting to perform additional assays to measure alternative biological readouts, as in my hands BMI1 might not be essential for cell proliferation but could affect other cellular functions. Importantly, *BMI1* knockdown in Daoy cells has been recently shown to alter cell adhesion and to favour the formation of cellular aggregates through the deregulation of the bone morphogenetic protein pathway, rather than affect cell proliferation or apoptosis (oral communication, [225]).

While this initial experiment was not completely conclusive, it did demonstrate that I could use shRNAs to target genes in the Daoy cell line. I therefore moved on to perform knockdown analysis of some of the medulloblastoma-associated candidate genes.

A



B

Gate	NON transduced	Scrambled ShRNA	BMI1 ShRNA-1	BMI1 ShRNA-2	BMI1 ShRNA-3
G1 (R6)	55.47	53.12	52.95	51.36	51.68
S (R5)	36.93	39.53	37.98	40.67	41.53
G2/M (R7)	6.02	5.94	6.01	6.13	4.79

Figure 4.15. Cell cycle analysis of Daoy cells transduced with BMI1 shRNAs.

A) Daoy cell lines expressing specific BMI1 shRNAs were obtained by lentiviral transduction followed by five days of puromycin selection. Following 1 hour of BrdU incubation, cells were harvested and stained with an anti-BrdU antibody and Propidium Iodide (PI). Cell cycle distribution was analysed by flow cytometry.

B) Percentage of cells in each cell cycle phase as determined by the flow cytometry analysis shown above.

4.7.2. Screening of candidate genes

I initiated a screening of medulloblastoma-associated candidate genes by looking at the effects of shRNA-mediated knockdown of four target genes: *DLG7*, *UBE2C*, *KIF4A* and *PLK1*. I performed *DLG7* knockdown analysis in Daoy cells only, whereas I analysed the other three genes in both the Daoy and the UW228-2 cell lines.

DLG7 is a microtubule-associated protein which plays a critical role in controlling mitotic spindle stability and dynamics throughout mitosis [204]. *DLG7* is phosphorylated by and shares a similar expression profile across a variety of normal and malignant human tissues with Aurora-A, a mitotic kinase with oncogenic properties [206]. It has been suggested that *DLG7* may represent a potential oncogenic target of Aurora-A [206]. Daoy cells expressing *DLG7* shRNAs showed a 45% to 85% decrease in *DLG7* mRNA levels compared to control cells, as measured by Real Time PCR (Figure 4.16A). This level of knockdown did not affect the overall cell growth rate, as confirmed by the steady proportion of EGFP-positive cells in transduced Daoy cell cultures, measured over a three-week time period (Figure 4.16B).

The ubiquitin-conjugating enzyme *UBE2C* has been the focus of an increasing number of studies in which *UBE2C* depletion in cancer cell lines was shown to inhibit cell proliferation and sensitise cells to apoptosis [191, 226, 227]. In my experiments, I obtained a modest *UBE2C* knockdown, with only one of the three *UBE2C* shRNAs tested being able to reduce *UBE2C* mRNA level by more than 50% in both the Daoy and the UW228-2 cell lines (Figure 4.17A). Possibly as a result of inefficient *UBE2C* silencing, I did not observe any changes in the growth rate of either Daoy or UW228-2 transduced cells (Figure 4.17B). Similarly, cell cycle analysis by PI staining did not reveal any differences in cell cycle distribution in *UBE2C* shRNA-expressing cells relative to non-transduced and scrambled shRNA-expressing control cells (Figure 4.18).

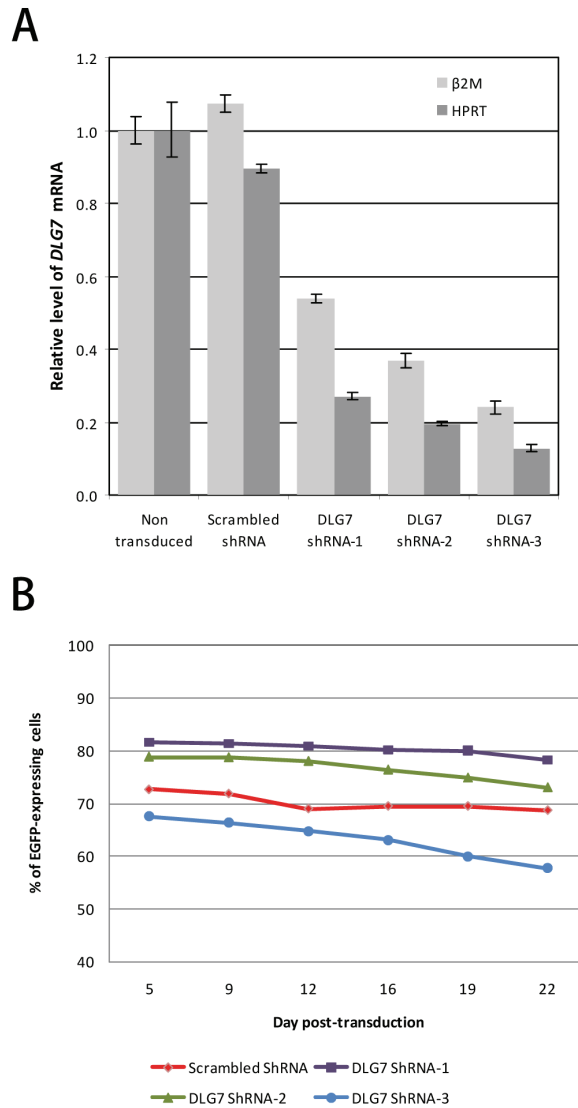


Figure 4.16. Analysis of *DLG7* knockdown in Daoy cells.

A) Real Time PCR analysis of *DLG7* gene expression in Daoy cells transduced with a scrambled shRNA or three individual shRNAs targeting the *DLG7* mRNA. The $\beta 2M$ and *HPRT* genes were used as housekeeping controls. The experiment was performed in triplicate. Bars correspond to averages \pm standard errors.

B) Percentage of EGFP-expressing Daoy cells over a three-week time period following viral transduction.

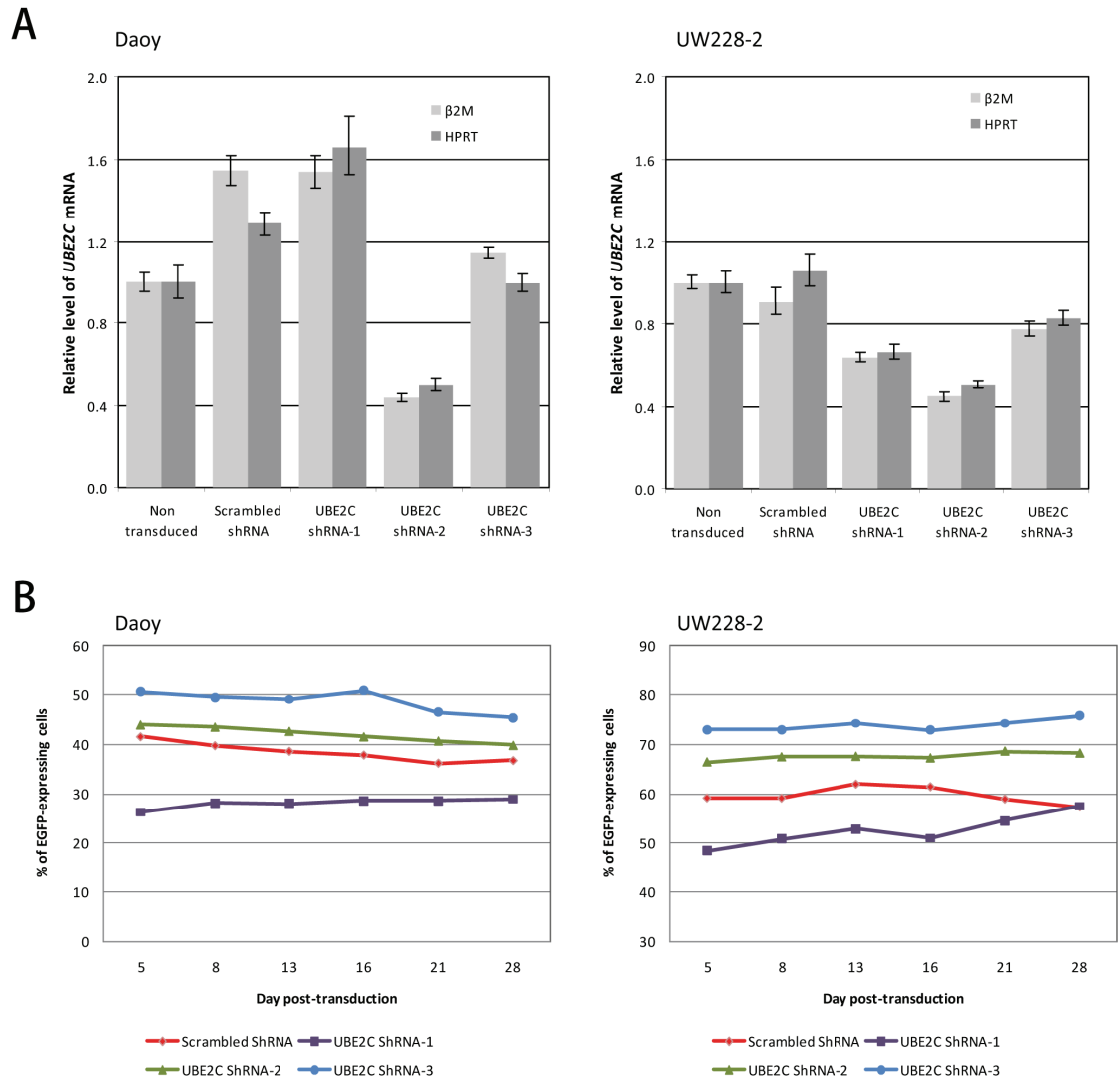


Figure 4.17. Analysis of *UBE2C* knockdown in Daoy and UW228-2 cells.

A) Real Time PCR analysis of *UBE2C* gene expression in Daoy (left) and UW228-2 (right) cells transduced with a scrambled shRNA or three individual shRNAs targeting the *UBE2C* mRNA. The $\beta 2M$ and *HPRT* genes were used as housekeeping controls. The experiment was performed in triplicate. Bars correspond to averages \pm standard errors.

B) Percentage of EGFP-expressing Daoy (left) and UW228-2 (right) cells over a four-week time period following viral transduction.

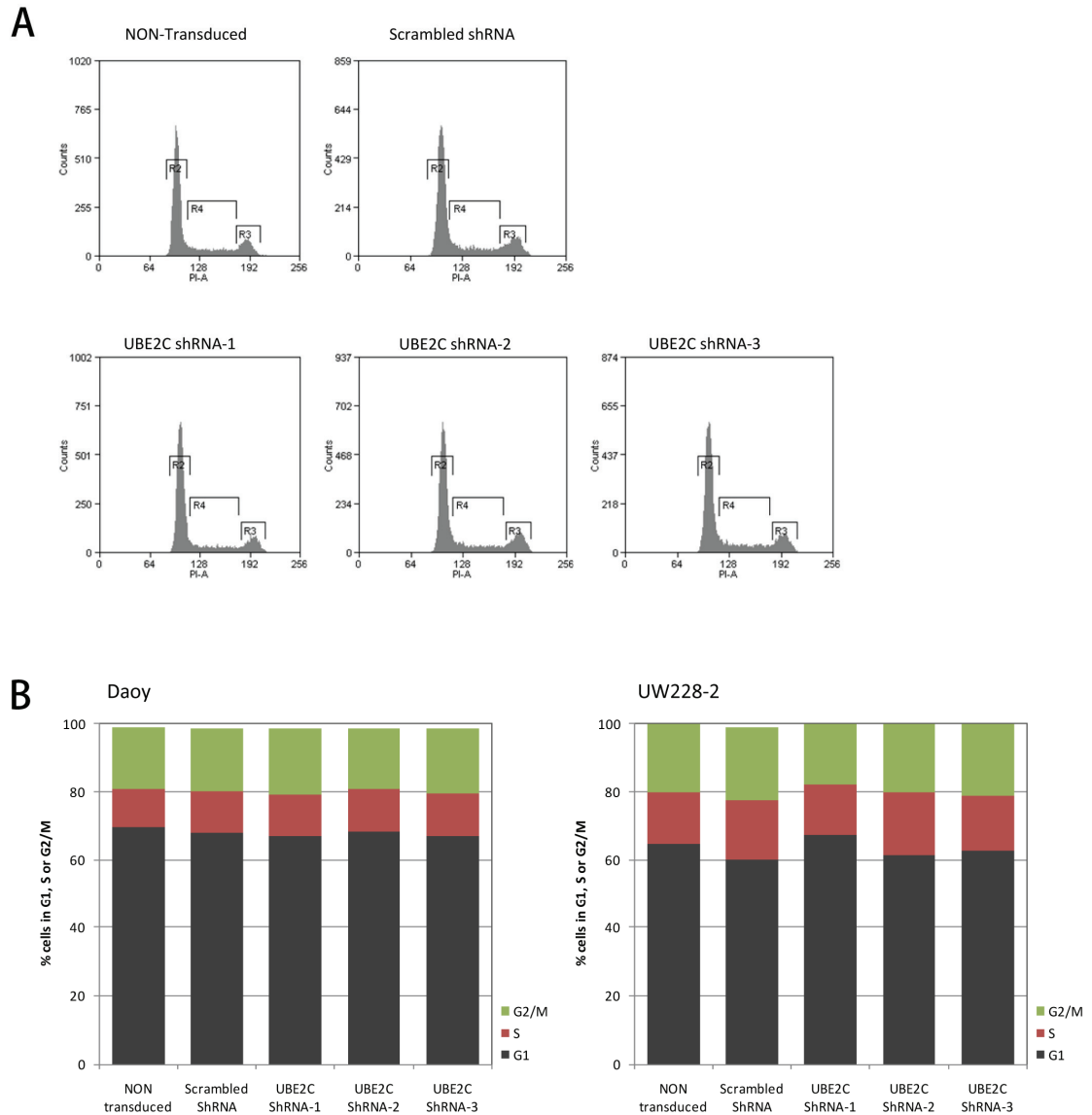


Figure 4.18. Cell cycle analysis of Daoy and UW228-2 cells transduced with UBE2C shRNAs.

A) Cell lines expressing UBE2C shRNAs were obtained by lentiviral transduction followed by five days of puromycin treatment. Cell cycle analysis was performed by flow cytometry using Propidium Iodide (PI) to label nuclear DNA. For each sample, gates were drawn to measure the proportion of cells in each cell cycle phase, based on PI signal area. Results of the analysis performed on UW228-2 cells are shown as an example.

B) Summary of cell cycle analysis by PI staining in Daoy and UW228-2 cells. The histograms show the proportion of cells in each cell cycle phase.

Kinesin family member 4A (KIF4A) is a microtubule-based motor protein implicated in chromosome condensation and segregation as well as in the regulation of cell cytokinesis [228, 229]. A role for KIF4A has also been described in modulating cell survival in post-mitotic neurons during brain development [230]. KIF4A has been found to be a prognostic biomarker in human lung cancer, with its overexpression being associated with increased patient mortality [231]. *In vitro* studies showed that KIF4A siRNA-mediated knockdown in lung cancer cell lines caused a significant decrease in cell viability [231]. I transduced the Daoy and UW228-2 cell lines with three individual viral shRNAs targeting human *KIF4A* mRNA and obtained a 40% to 70% decrease in *KIF4A* mRNA levels as measured by Real Time PCR (Figure 4.19A). However, neither Daoy nor UW228-2 KIF4A shRNA-expressing cells showed any significant changes in overall cell growth rate (Figure 4.19B), nor in cell cycle distribution (Figure 4.19C) relative to non-transduced and scrambled shRNA-expressing control cells.

PLK1 encodes a Polo-like kinase which plays multiple roles during mitosis, including regulating the G2/M transition, via the activating phosphorylation of the FOXM1 transcription factor [232, 233]. *PLK1* is overexpressed in several human tumour types and has therefore been proposed as a potential target in anticancer strategies [234]. *PLK1* depletion in human cancer cell lines has indeed shown an essential role for PLK1 in sustaining cancer cell proliferation and survival [189]. Daoy cells transduced with PLK1-specific viral shRNAs showed an extremely modest decrease in *PLK1* mRNA levels (15% to 40%, Figure 4.20A). *PLK1* knockdown was more efficient in UW228-2 cells, reaching up to 80% (Figure 4.20A). Nonetheless, I did not observe any important variations in the proportion of EGFP-expressing cells or in cell cycle distribution of either the Daoy or the UW228-2 medulloblastoma cells compared to control cells (Figure 4.20B and C).

Figure 4.19. Analysis of *KIF4A* knockdown in Daoy and UW228-2 cells.

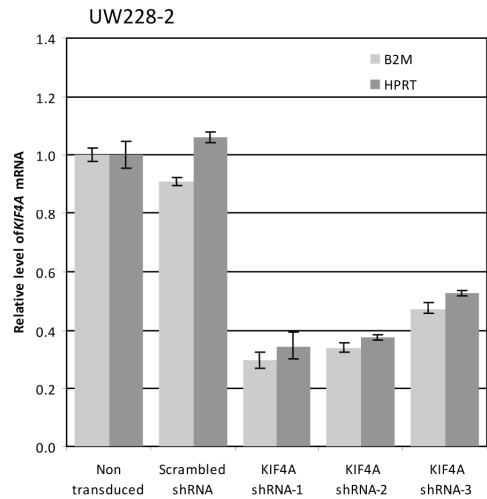
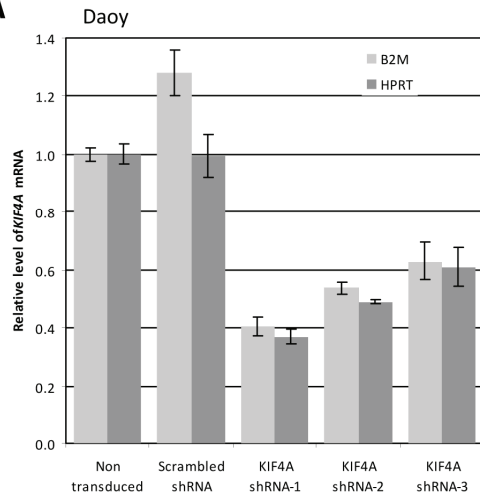
Daoy and UW228-2 cells were transduced with either a scrambled shRNA or three individual shRNAs targeting the *KIF4A* mRNA, at an MOI of 0.1. For the experiments shown in A and C, cells were treated with puromycin to obtain a homogeneous population of EGFP-expressing cells.

A) Real Time PCR analysis of *KIF4A* gene expression. The *β 2M* and *HPRT* genes were used as housekeeping controls. The experiment was performed in triplicate. Bars correspond to averages \pm standard errors.

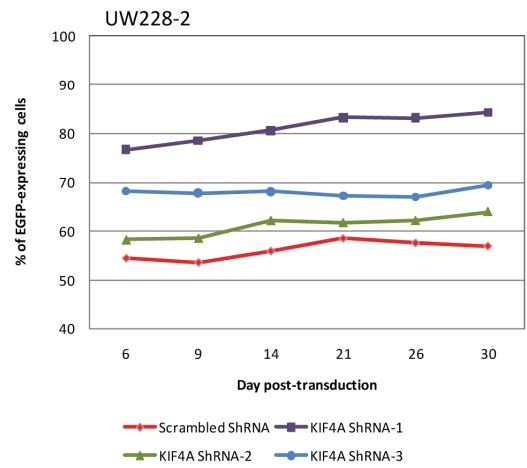
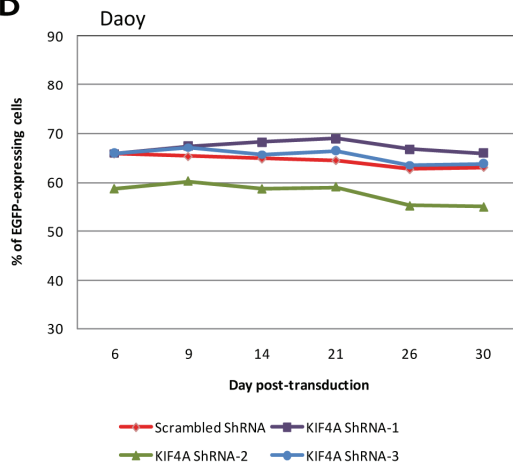
B) Percentage of EGFP-expressing cells over a four-week time period following viral transduction.

C) Cell cycle analysis by PI staining.

A



B



C

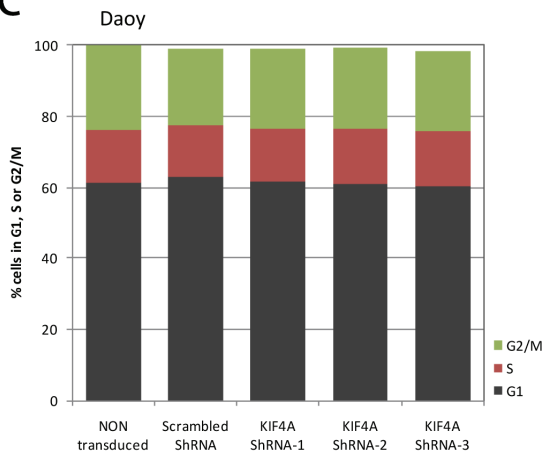


Figure 4.20. Analysis of *PLK1* knockdown in Daoy and UW228-2 cells.

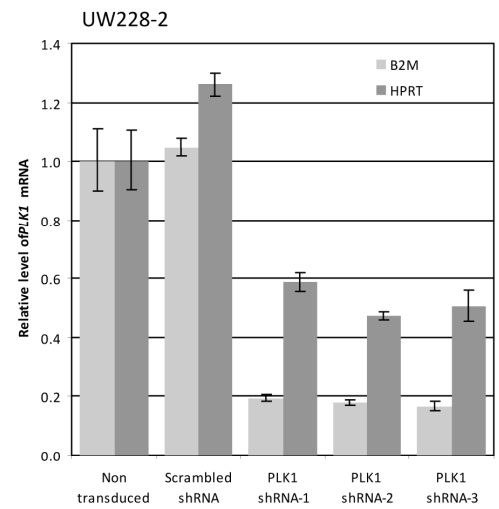
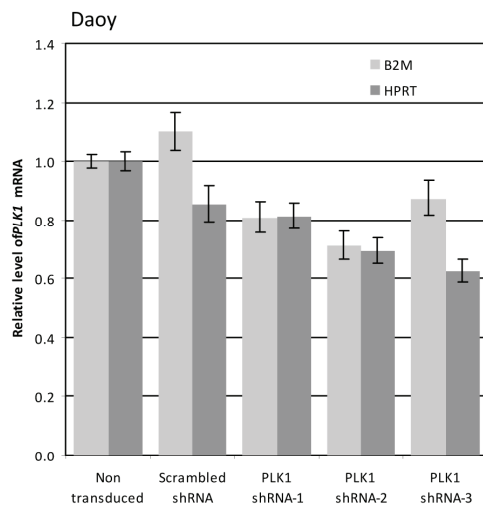
Daoy and UW228-2 cells were transduced with either a scrambled shRNA or three individual shRNAs targeting the *PLK1* mRNA, at an MOI of 0.1. For the experiments shown in A and C, cells were treated with puromycin to obtain a homogeneous population of EGFP-expressing cells.

A) Real Time PCR analysis of *PLK1* gene expression. The *β 2M* and *HPRT* genes were used as housekeeping controls. The experiment was performed in triplicate. Bars correspond to averages \pm standard errors.

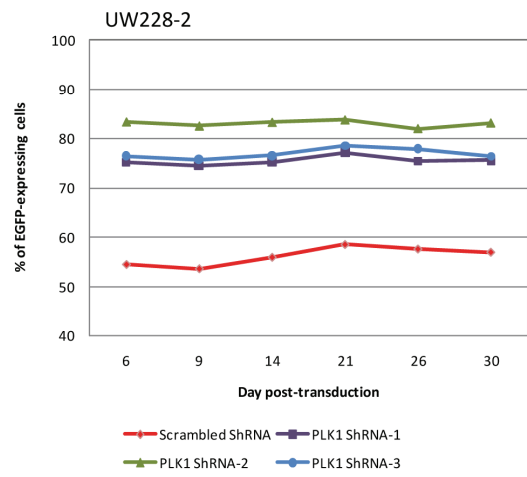
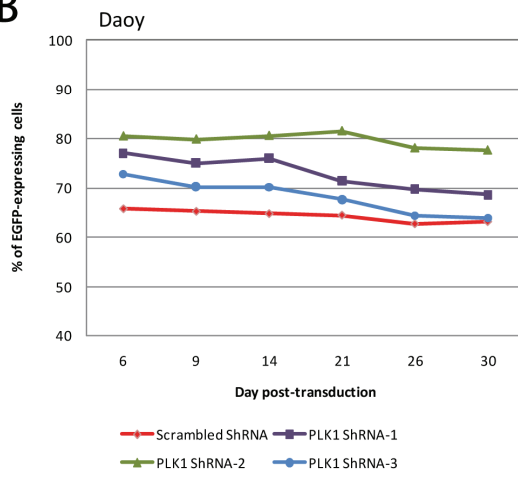
B) Percentage of EGFP-expressing cells over a four-week time period following viral transduction.

C) Cell cycle analysis by PI staining.

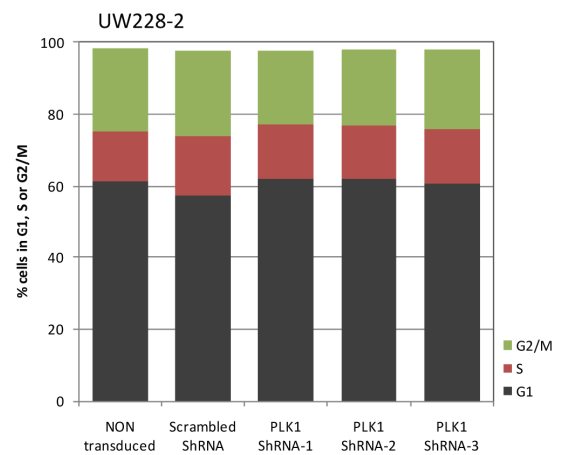
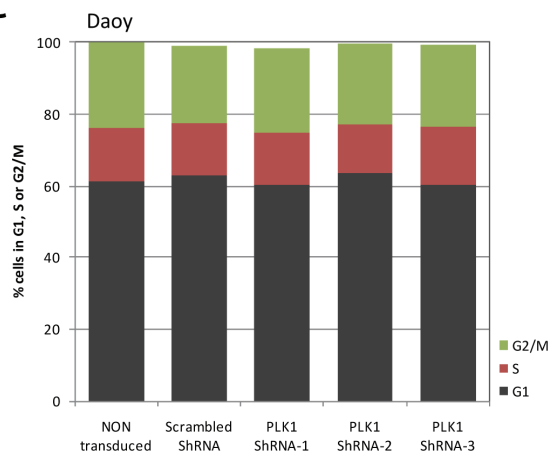
A



B



C



4.7.3. Optimisation of a viral transduction protocol for the D425 Med cell line

Unlike both the Daoy and UW228-2 medulloblastoma cell lines, which comprise large, polygonal-shaped adherent cells, D425 Med cells exhibit spheroid morphology, are semi-adherent in culture and display some of the structural abnormalities most commonly described in human medulloblastoma, such as isochromosome 17q and amplification of the *MYC* oncogene. Transduction of both the Daoy and UW228-2 cell lines using pGIPZ lentiviral constructs successfully induced long-term transgene expression, as monitored by flow cytometry analysis of EGFP-expressing cells. In contrast, when I transduced D425 Med cells with pGIPZ lentiviruses, I obtained extremely weak EGFP signal intensities, even when increasing the MOI, as shown in the upper panels of Figure 4.21. Importantly, the EGFP signal intensity further decreased over time, suggesting that the CMV promoter, which drives the expression of the EGFP gene as well as the puromycin resistance gene and the shRNA included in the pGIPZ vector, was inactivated, possibly as a consequence of epigenetic regulation [235, 236]. To optimise the expression of these sequences in D425 Med cell, I replaced the CMV promoter region in the pGIPZ vector with the SFFV-LTR promoter sequence. The lower panels in Figure 4.21 show flow cytometry analysis of EGFP expression achieved by transducing D425 Med cells with the modified pGIPZ-SFFV vector: by plotting cell count *versus* EGFP signal intensity, I could distinguish two discrete subpopulations of EGFP-positive and negative cells, corresponding to transduced and non-transduced cells respectively.

To confirm that the pGIPZ-SFFV viral construct could be used for the successful delivery of gene-specific shRNAs to target cells, I transduced D425 Med cells with pGIPZ-SFFV lentiviral constructs expressing an shRNA targeting the *GAPDH* mRNA, which had been used in previous experiments in our department to

induce at least a 40% decrease in *GAPDH* mRNA in human tumour cell lines. I also transduced cells with a scrambled shRNA as a control. D425 med cells expressing the *GAPDH* shRNA displayed a 40% decrease in *GAPDH* transcript levels compared to control cells. By increasing the MOI, the reduction in the level of *GAPDH* expression increased to 60% (Figure 4.22). These results confirmed the usefulness of modified pGIPZ-SFFV lentiviruses as an efficient tool to achieve target gene knockdown in the D425 Med cell line.

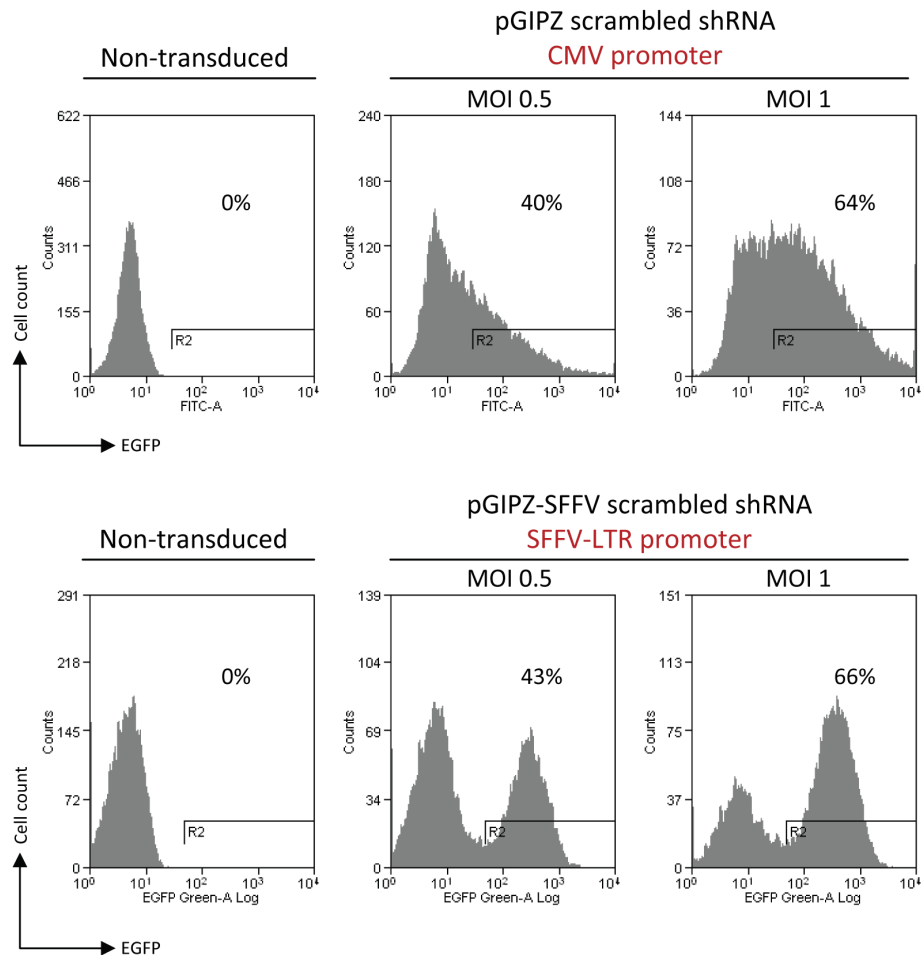


Figure 4.21. Transduction of D425 Med cells with different lentiviral constructs.

D425 Med cells were transduced with either the original pGIPZ lentiviral construct (CMV promoter, top panels), or the modified pGIPZ-SFFV lentiviral construct (SFFV-LTR promoter, bottom panels). In both cases two MOIs of 0.5 and 1 were tested.

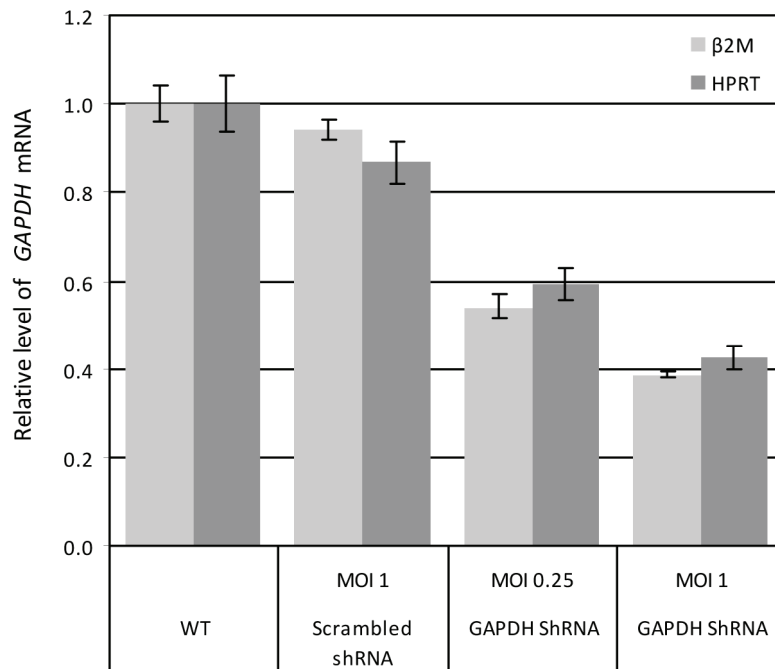


Figure 4.22. *GAPDH* knockdown in D425 Med cells.

Real Time PCR analysis of *GAPDH* gene expression in D425 Med cells transduced with a scrambled shRNA or an shRNA targeting the *GAPDH* mRNA. The *β2M* and *HPRT* genes were used as housekeeping controls. The experiment was performed in triplicate. Bars correspond to averages \pm standard errors.

4.8. Discussion

In recent years, the advent of high-resolution microarray platforms has allowed a significant improvement in our understanding of the tumour transcriptome. Genome-wide studies of human medulloblastomas have revealed an increasing number of putative cancer-associated genes whose deregulation during cerebellar development could contribute to the origin and growth of cerebellar malignancies [20, 92, 99-103, 107, 237]. Similarities in gene expression profiles between normal and tumour cerebellar tissues have provided additional support to the notion that GCPs represent the cell of origin of a molecular subset of medulloblastomas [20, 92, 105, 107]. Although little is known about the possible alternative origins of the remaining medulloblastoma subgroups, the investigation of the mechanisms and pathways which drive normal cerebellar development has proven to be an indispensable approach for the understanding of medulloblastoma pathogenesis [27, 28, 163, 238].

In this part of my project, I used the exon array data described in the previous chapter to perform a statistical analysis of differential gene expression between normal cerebellum and different medulloblastoma molecular subgroups. I identified a total of 278 and 300 unique genes as being respectively up- and down-regulated in Shh-driven tumours relative to either normal cerebellum or Shh-independent medulloblastoma samples. Several of the differentially expressed genes which I identified had already been described in association with medulloblastoma in general, such as *TOP2A* [101], *MELK* [239], or with Shh-driven medulloblastomas specifically, including *MYCN*, *BOC*, *HHIP* [20, 92], *NHLHI* [44], *FOXMI* [166].

I also identified a number of less characterised medulloblastoma candidate genes, many of which are implicated in spindle organisation, cell cycle control, epigenetic modification of chromatin structures and neuronal specification. I selected a

number of candidate genes which were overexpressed in Shh-driven tumours and showed that their level of expression also increased in the presence of Shh in primary cultures of mouse GCPs. These genes represent interesting candidates which may play a role in precursor cell proliferation as well as in medulloblastoma formation and maintenance. I therefore wanted to explore their role in sustaining cell proliferation and survival by using human medulloblastoma cell lines as *in vitro* models of medulloblastoma pathogenesis.

I decided to investigate the effects of target gene depletion by transducing medulloblastoma cell lines with lentiviral constructs designed to express gene-specific shRNAs. In preliminary experiments, I showed that pGIPZ lentiviruses could transduce the Daoy and UW228-2 medulloblastoma cell lines, leading to the expression of the EGFP reporter gene. I could also specifically select for the transduced cells by treating cell cultures with puromycin to obtain a uniform population of shRNA-expressing cells.

As an initial step, I performed shRNA-based knockdown analysis on four of the selected candidate genes: *DLG7*, *UBE2C*, *KIF4A* and *PLK1*. All four genes have been critically implicated in the survival and expansion of different types of human cancer cell lines and represent promising targets for anticancer therapies. Despite obtaining efficient transductions, I found that in most cases, shRNA-based target gene knockdown was not optimal. In addition, I did not observe any significant biological effects of gene-specific shRNA-expression in the tested medulloblastoma cell lines, such as changes in cell growth rate and cell cycle distribution.

One of the main technical problems with my experiments was that, in general, I did not achieve a high level of target mRNA knockdown, which could explain why there were no clear effects in the functional assays. In most of the studies that I reviewed from the literature, target gene knockdown was obtained by siRNA

transfection [189, 191, 226, 231]. Typically siRNAs can achieve more efficient reductions in mRNA/protein levels but they only allow transient *in vitro* studies. To improve shRNA-based gene silencing the MOI could be increased. Indeed, I obtained a more significant reduction in the level of target gene expression by performing higher MOI transductions. I could also increase the selection pressure on shRNA-expressing cells by increasing puromycin concentration, selecting only those transduced cells that expressed the transgenes at higher levels, including the puromycin resistance gene. The disadvantage of these approaches is that they cause an increase in the number of viral particles that integrate in the host cell DNA, raising the possibility of toxicity due to multiple integration sites. In my experiments, I used individual shRNA-expressing constructs to knock down candidate genes in medulloblastoma cell lines. It would be useful to transduce cells with a pool of two or more shRNA-constructs directed against the same target gene, as different shRNAs can act synergistically to significantly improve the efficiency of gene knockdown.

An alternative approach to the use of shRNAs is the overexpression of dominant negative mutant forms of the proteins of interest. For example, a dominant negative form of the UBE2C protein has been developed, in which the catalytic cysteine is converted into a serine. This single amino acid change disrupts UBE2C ubiquitination activity and prevents the destruction of cyclins during mitosis [240]. When transfected into mammalian cells, mutant UBE2C was shown to arrest cells in mitosis, consistent with other reports in which UBE2C was depleted by siRNA-mediated gene silencing [191]. It will be interesting to test whether expression of the UBE2C dominant negative protein in medulloblastoma cell lines induces growth arrest and triggers tumour-specific TRAIL-mediated cell killing, as has been described for other tumour cell lines [191]. Dominant negative forms have also been described for the DLG7 and PLK1 proteins

[206, 241]. In both cases, overexpression of the mutant forms in human cancer cell lines impaired their ability to grow and in some tumour cell lines was enough to induce tumour-specific cell death [241].

In my initial experiments I decided to evaluate the potential role of candidate genes in sustaining medulloblastoma cell growth. In the same plate, I co-cultured transduced cells expressing gene-specific shRNAs and non-transduced cells. Any changes in the relative proportions of the two cell subpopulations in culture would be indicative of a difference in their growth rates. This assay has the potential to detect very subtle changes in the ability of target cells to survive and proliferate. I also performed cell cycle analysis by flow cytometry to detect any differences in cell cycle distribution. However, it will be necessary to perform additional assays for a comprehensive investigation of the biological consequences of target gene knockdown. Cell colony forming and neurosphere assays are commonly used to test the ability of cancer cells to self renew [174, 242]. In some cases migration and invasion assays could be used to study the possible role of target genes in regulating tumour cell migration and invasiveness [176, 243]. Furthermore, I will set up gene-specific functional assays to confirm the efficiency of gene knockdown. For example, a significant reduction in the level of the UBE2C protein causes an increase in the level of cyclin B protein [191, 240]. Therefore by measuring cyclin B protein expression I would get an indication of residual UBE2C activity.

The efficient silencing of any individual target gene might induce different cell responses in different medulloblastoma cell lines. In agreement with the literature, my own experiments showed that the three human medulloblastoma cell lines that I used differed in terms of morphology, gene expression and in their biological response to viral transduction. While the Daoy and the UW228-2 cell lines strongly expressed

transgenes which were under the transcriptional control of the CMV promoter, I had to develop an alternative transduction protocol to be able to successfully express lentiviral shRNAs in the D425 Med cell line. It will be interesting to study any cell-specific effect of target gene depletion, which may be related to the specific gene signature of the three individual cell lines, such as the *MYC* oncogene amplification in the D425 Med cells.

The use of medulloblastoma cell lines as a model of tumour pathogenesis is rather controversial [171]. Several commercially available human cell lines have been extensively used in studies that have investigated the effect of putative medulloblastoma-associated genes in sustaining tumour growth and survival. However, these cells have been shown to be no longer responsive to Shh [58], and evidence has suggested that propagation of tumour cells in culture irreversibly inhibits Shh pathway activity [171]. These observations raise the issue of whether the available medulloblastoma cell lines represent an adequate tool for the study of the biological role of candidate genes whose level of expression is regulated by the Shh signalling pathway.

An appropriate investigation of the effects of Shh-dependent genes in a pathological context requires the use of an *in vitro* system in which cells retain their ability to respond to stimuli which enhance or antagonise the Shh signalling pathway. There is scarce evidence of the level of activity of the Shh pathway in human medulloblastoma cell lines. However, it has been reported that cyclopamine, a plant-derived Shh antagonist which acts at the level of the Smoothed receptor [244], induces a decrease in the level of expression of the *GLI1* gene, which is a direct target of Shh signalling, and increases apoptosis in DAOY and UW228 medulloblastoma cells [245]. Given more time, I would like to further investigate how the manipulation of the Shh signalling pathway can affect the survival and proliferation of human

medulloblastoma cell lines in order to assess whether they represent appropriate models of Shh-dependent medulloblastomas and, eventually, whether *SMO* or *GLII* could be used as control genes in my knockdown experiments.

Murine medulloblastoma allograft cell lines have been used to model Shh-mediated proliferation events and represent a useful alternative to commercially available tumour cell lines. Berman *et al.* described the generation of the PZp53MED medulloblastoma cell lines from allografts grown in athymic mice following the subcutaneous injection of tumour cells obtained from *Ptc^{+/-}*; *p53^{-/-}* mice [246]. Following a 72 hour-long treatment with cyclopamine, the authors observed a 60 to 80% reduction in cell proliferation [246]. Moreover, addition of cyclopamine to the cell culture induced a significant decrease in the expression level of genes typically regulated by Shh, including *Mycn* and *Cyclins D1* and *D2*, whereas the expression of *NeuroD1*, a marker of post-mitotic granule cells, increased. The effects of cyclopamine could be reversed by over-expressing the Shh effector *Gli1* [246]. It would be interesting to test whether human medulloblastoma allograft cell lines could be established in the same way. This cell model could be readily manipulated *in vitro* to silence the genes of interest. Any resulting changes in the ability of cells to progress through the cell cycle would be compared to the effects of cyclopamine treatment (*i.e.* inactivation of the Shh pathway) or *Gli1* gene knockdown.

Finally, mouse GCP primary cultures could be used to investigate the potential role of Shh-related genes in promoting cell proliferation during normal cerebellar development. In my future experiments, I would like to use lentiviral vectors to overexpress some of the selected medulloblastoma candidate genes in GCPs cultured in the presence or absence of ShhN. Measuring BrdU incorporation as a read-out for cell proliferation, I could assess whether the forced expression of candidate genes leads to

an increase in the cellular response to ShhN, and if it is sufficient to promote cell cycle progression in the absence of the ShhN stimulus. In this setting, overexpression of the *Mycn* gene would represent a valid control, as its role in mediating Shh-dependent GCP proliferation has been clearly established [45, 48]. Conversely, I could inactivate a gene of interest by expressing its dominant negative mutant form in ShhN-treated GCPs. A decrease in the proportion of proliferating cells would suggest a role for the candidate gene in the positive regulation of the cell cycle.

Chapter 5

Analysis of differential splicing in paediatric medulloblastoma

5.1. Introduction

Alterations in mRNA splicing are commonly found in a variety of human cancer types and can result in the production of novel transcript variants or in an imbalance between normal mRNA isoforms. In both cases the global protein expression within a cell can be altered in ways that have the potential to sustain tumour growth [116, 118, 119]. Individual candidate gene approaches have been used to characterise alternative transcript variants whose expression is enriched in cancer and which may display oncogenic potential (reviewed in [117, 118]). However, these studies can only reveal a minority of the splicing aberrations which occur during oncogenesis. During the past few years, an increasing number of computational and microarray-based studies have been carried out to explore genome-wide patterns of differential splicing between cancer tissues and their normal counterparts (reviewed in [117]). These studies demonstrated that the comprehensive analysis of cancer splicing patterns could improve cancer diagnostic classification and provide useful prognostic markers [247-250].

Since their development four years ago, Affymetrix exon arrays have been used in a variety of studies for the unsupervised discovery of alterations in the global patterns of alternative splicing (AS) associated with a range of conditions, including human cancer. In the first published exon array analysis of cancer-associated differential splicing, Gardina *et al.* identified nine genes undergoing differential splicing between paired tumour-normal colon cancer samples [148]. Interestingly, several of these genes were implicated in cell-cell interactions and cytoskeleton organisation, suggesting that

splicing alterations in colon cancer may affect cell mobility and extracellular interactions. French *et al.* applied exon array technology for the identification of splice variants whose expression differed between histological subgroups of glial tumours [249]. Through the unsupervised analysis of exon expression levels, the authors were able to classify glioma subgroups according to their histological appearance. In addition, they identified splice variants that appeared to be differentially regulated between low and high grade gliomas, and a collection of novel exons which were expressed as part of well annotated mRNAs but had not been previously described in the NCBI Reference Sequence (RefSeq) database. More recently, Dutertre *et al.* performed an exon array analysis of mouse primary mammary tumours with different metastatic potentials [248]. They identified several differentially expressed exons, many of which corresponded to genes implicated in cell migration and morphology. They also validated a selection of the candidate exons as being differentially expressed in human primary breast cancers associated with different metastatic capabilities, suggesting that alterations in splicing patterns were often conserved between mouse and human. Finally, they were able to associate the expression pattern of a subset of tumour-associated splice variants with poor prognosis in a large cohort of breast cancer patients. Overall these findings emphasise the important role that splicing programmes may play during oncogenesis and the increasing value of differential splice form expression in the clinical management of cancer.

Medulloblastoma originates from the cerebellum, which is known to undergo extensive splicing regulation [251, 252]. A few studies of human medulloblastomas have described alternative splice forms of individual genes which are associated with specific molecular subsets of medulloblastoma [128], normal cerebellar development [131] or tumour recurrence [130]. I wanted to explore on a wider scale whether changes

in splicing patterns occurred frequently in medulloblastomas and if such changes could be related to defects in the normal development of the cerebellum.

5.2. Identification of tumour-associated splicing events

To identify splicing patterns associated with either medulloblastoma in general or SHH tumours specifically, I compared exon/gene expression ratios between different sample subgroups, as illustrated in Figure 5.1. A total of 1,262 genes containing at least one potential differentially spliced exon were identified.

Probe set expression plots were used to evaluate the likelihood that candidate events represented true positive hits (as an example, expression plots for the *TJPI* and *DAAMI* genes are shown in Figure 5.2). Probe sets with very high or very low expression across all samples were discarded as they were suggestive of cross-hybridising probes or non-expressed exons respectively (*e.g.* probe set 3329727 mapping to exon 1 of the *MADD* gene, Figure 5.3). In a few cases, inspection of candidate gene expression plots allowed the identification of probe sets whose profile was indicative of differential splicing even though they did not meet the requirements for statistical significance (*e.g.* probe set 2680331 mapping to exon 15 of the *MAGII* gene, Figure 5.3). I therefore considered these probe sets as false negatives and retained them for subsequent analysis.

Following the filtering of strong candidate events based on expression profiles, I used the X:Map database to inspect probe set location in annotated transcript structures and to verify whether they mapped to known alternatively spliced exons. I was able to classify candidate events into a variety of AS mechanisms, including alternative starting or ending of the transcript and mutually exclusive exon usage (Figure 5.4). However, I chose to initially focus on cassette exon events as they could be more easily validated

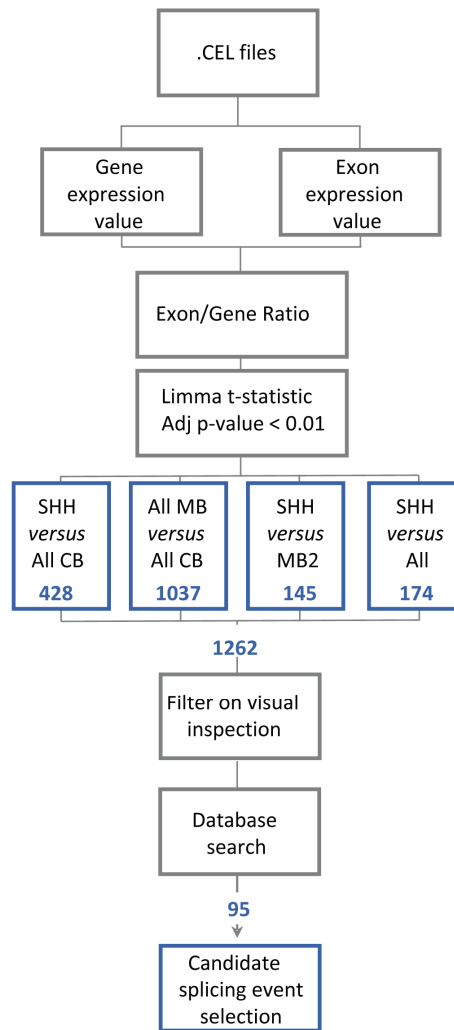


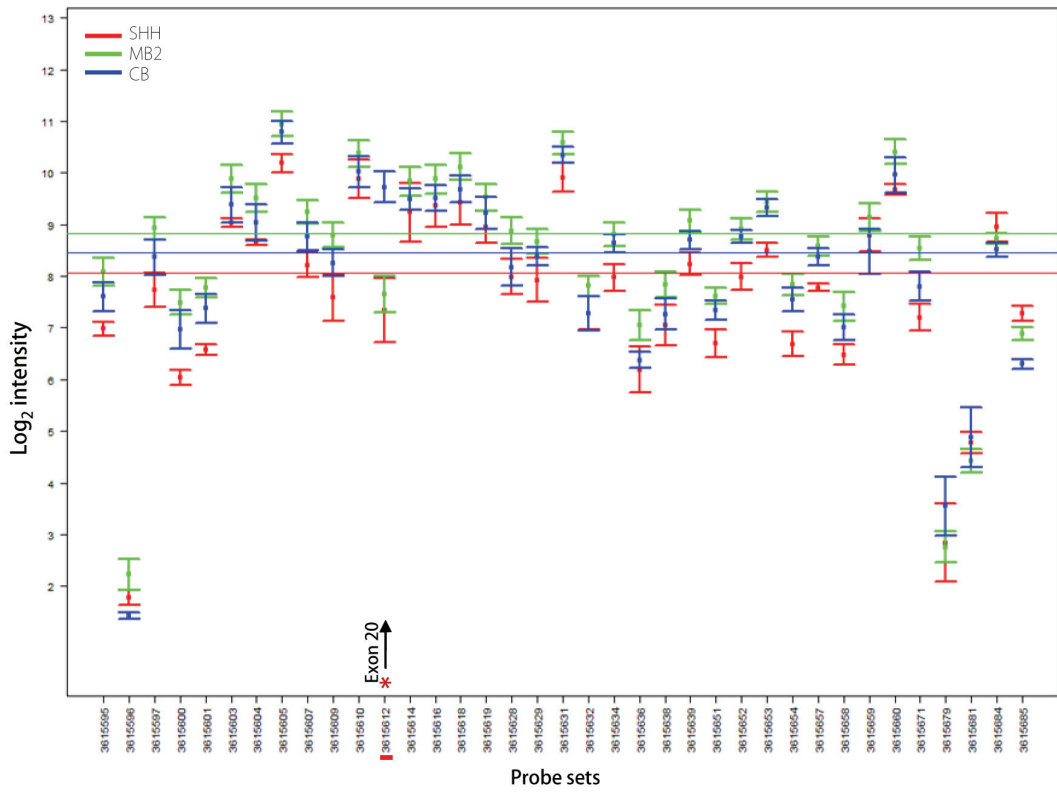
Figure 5.1. Schematic overview of exon-level analysis.

Exon- and gene-level signal estimates were generated through the Robust Multichip Average (RMA) algorithm using the Expression Console software. To identify differential splicing events, gene-level normalized intensity values (exon signal / gene signal) were calculated for each individual exon and compared across sample subgroups through the LIMMA moderated t-statistic and FDR multiple testing correction. Several comparisons were carried out as shown in the figure. Numbers in boxes refer to the number of genes containing at least one exon with differential inclusion rate across different sample subgroups. In total, 1,262 unique genes were predicted to generate splice variants associated with specific sample subgroups. The possibility that these genes represented true positive hits was investigated using expression plots and annotation databases and a collection of 95 strong candidate genes was obtained, from which a smaller set of events was selected for further analysis. SHH, SHH tumours; MB, medulloblastomas (including SHH and MB2); CB, normal cerebella (including adult and fetal samples).

Figure 5.2. *TJPI* and *DAAMI* probe set expression plots.

Expression plots show the signal distribution of each core probe set mapping to the *TJPI* gene (top graph) or the *DAAMI* gene (bottom graph). Each whisker plot represents the probe set average \log_2 expression in each subgroup with standard error bars. Probe sets are sorted by genomic location. Horizontal lines represent the average gene expression signal within each sample subgroup. Red asterisks indicate differentially expressed probe sets identified by statistical analysis. Black arrows point to the probe sets that I selected for RT-PCR validation. Probe set 3615612 mapping to exon 20 in the *TJPI* gene appeared to be significantly overexpressed in normal cerebella (CB) compared to medulloblastomas (SHH and MB2 tumours), suggesting differential splicing of exon 20 between the two sample subgroups (*i.e.* preferential retention of exon 20 in CB samples and skipping in MB2 and SHH samples). Similarly, the expression pattern of probe set 3538263 mapping to the *DAAMI* gene was indicative of *DAAMI* exon 16 being more frequently skipped in SHH tumours compared to all of the other samples examined.

Exon plot for TJP1



Exon plot for DAAM1

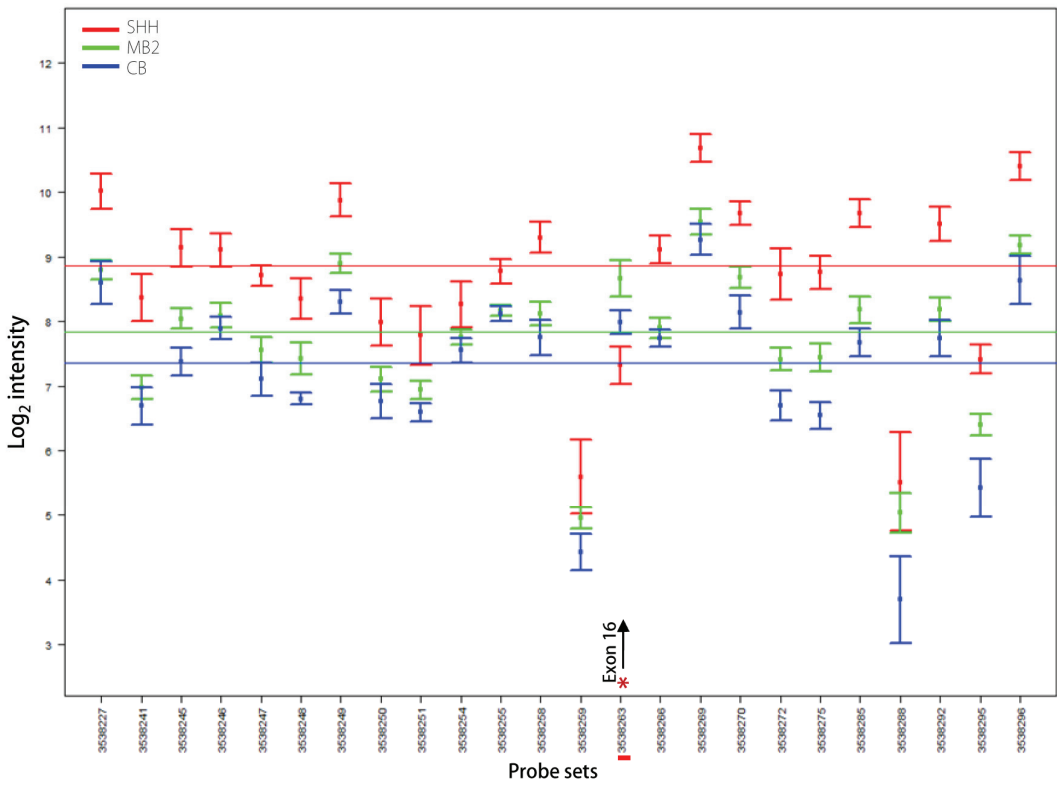
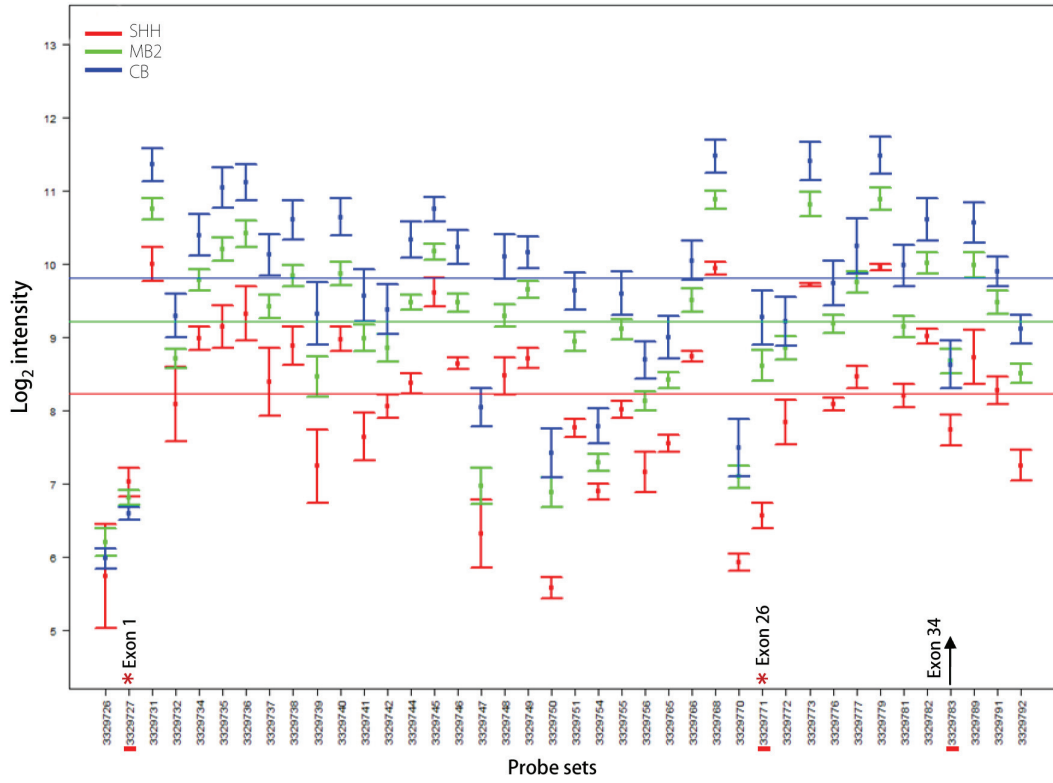


Figure 5.3. *MADD* and *MAGII* probe set expression plots.

Expression plots were drawn as described in figure legend 5.2. Probe set 3329727 mapping to exon 1 in the *MADD* gene is an example of a probe set discarded upon visual inspection of expression plots: its expression profile is suggestive of non-responsive/uniformly non-expressed probes. Despite not passing the statistical significance filter, probe sets 3329783 mapping to exon 34 of the *MADD* gene and 2680331 mapping to exon 15 of the *MAGII* gene were selected for RT-PCR analysis because their profile was indicative of differential expression between sample subgroups.

Exon plot for MADD



Exon plot for MAGI1

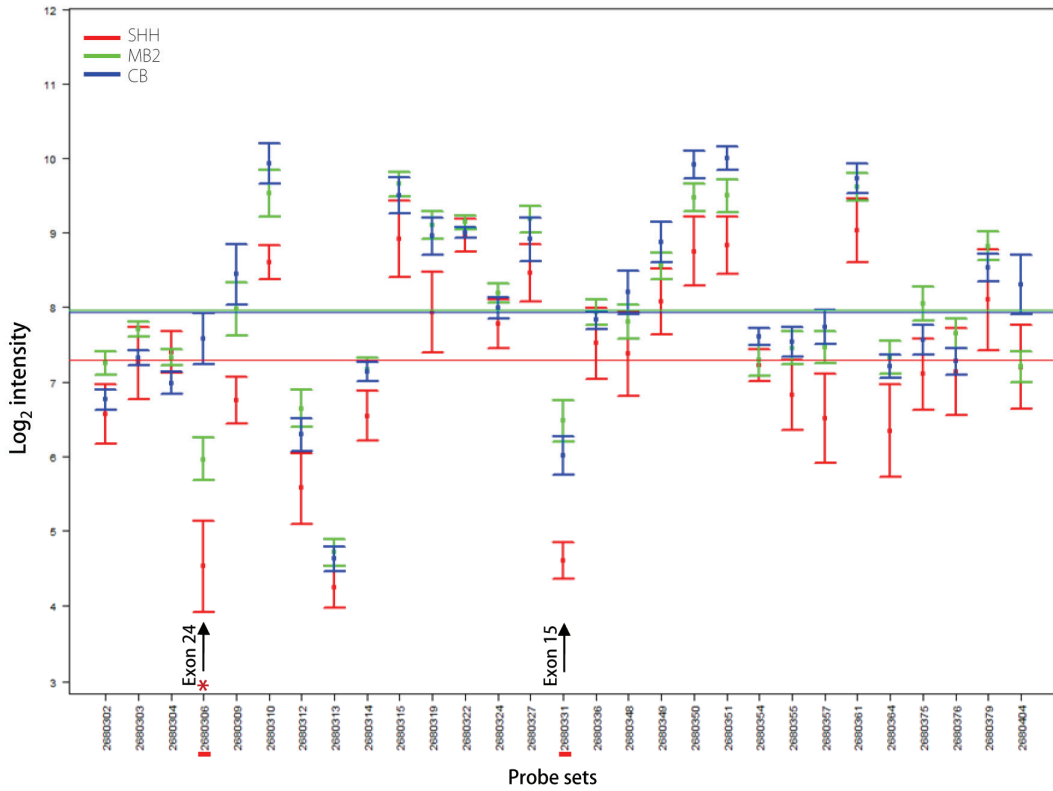


Figure 5.4. Differential splicing of the *WHSC1*, *TRRAP* and *WASF3* genes.

Heatmaps summarise probe set expression profiles across the sample set: expression values were normalised first on gene signals and then on the average probe set expression across all samples. Normalised values were then averaged for each sample subgroup: normal cerebella (CB), Shh-driven medulloblastomas (SHH), and Shh-independent medulloblastomas (MB2). A green-red colour palette illustrates normalised probe set expression values, with green corresponding to low and red corresponding to high expression. Probe sets are sorted by genomic location, with red asterisks underlying putative differentially spliced probe sets as identified by statistical analysis. Schematic representations of alternative transcript exon structures are shown for each gene, with red and grey boxes corresponding to protein coding exons and untranslated regions, respectively. Transcript IDs refer to Ensembl release 56.

A) Alternative splicing of the *WHSC1* gene generates splice forms with alternative 3' ends. Exon array analysis suggested that medulloblastomas, and particularly SHH tumours, expressed more of the longest transcript form (top transcript), as opposed to normal cerebellar samples which predominantly expressed the two shorter forms (middle and bottom transcripts).

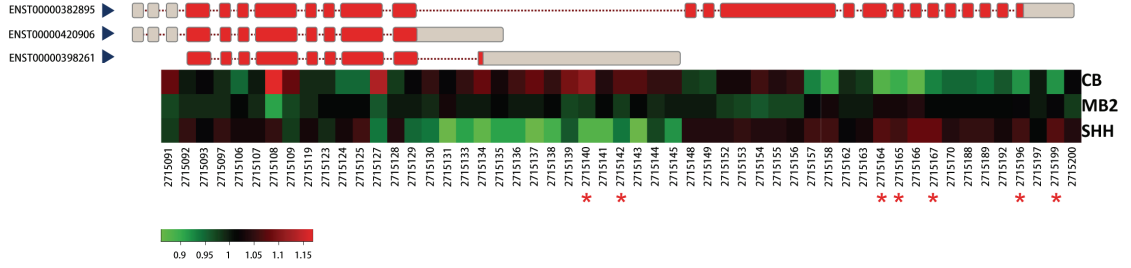
B) Alternative splicing of the *TRRAP* gene generates splice forms with alternative exon inclusion. Probe set 3014461 maps to a cassette exon in the *TRRAP* gene which is predicted to be skipped in SHH tumour transcripts, as opposed to normal cerebella and MB2 tumours.

C) Alternative splicing of the *WASF3* gene generates splice forms with mutually exclusive exons. One pair of alternative exons, 7A and 7B, is found in the *WASF3* gene; they are spliced in a mutually exclusive manner. Compared to medulloblastomas, normal cerebellar samples appeared to express significantly higher levels of the transcript form containing exon 7B (bottom transcript).

A

Alternative transcription start/end sites

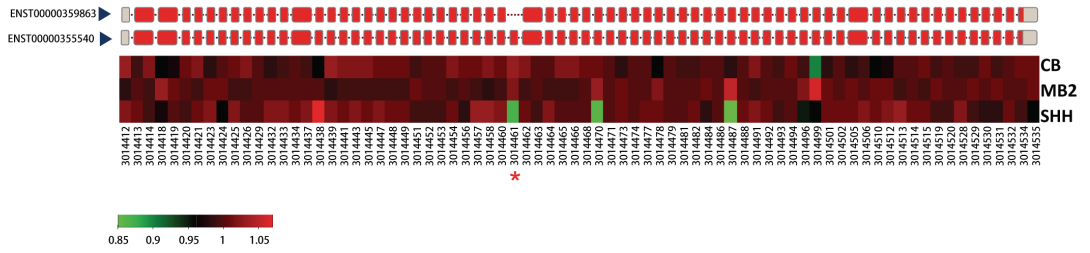
WHSC1



B

Alternative exon inclusion (cassette type)

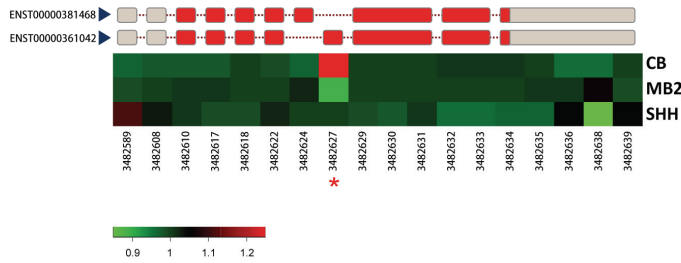
TRRAP



C

Mutually exclusive exons

WASF3



by RT-PCR. In total, 14 cassette exon splicing events were selected to be validated on a representative subset of the profiled samples (training set). Primers were designed to match constitutive exons flanking the candidate cassette exon, so as to generate PCR products of different sizes depending on the inclusion or exclusion of the target exon from the spliced transcript. For 11 of the 14 examples examined I observed amplification of both transcript forms (as confirmed by sequence analysis), indicating that the corresponding exons were genuinely undergoing alternative splicing (Figure 5.5). In the three non-confirmed cases, only one PCR product was detected, suggesting that only one transcript form was expressed. These events were not analysed further.

I quantified alternative PCR product intensities and calculated differences in their \log_2 ratios between sample subgroups to confirm the presence of significant differential splicing (Table 5.1). As predicted by the array analysis, three of the 11 experimentally validated genes (*DAAMI*, *EHBPI* and *TRRAP*) generated splicing patterns which distinguished between SHH tumours and all of the other samples (Figure 5.5 and Table 5.1). In all of the remaining cases, all of the medulloblastomas shared similar splicing patterns which differed from those of normal adult cerebellar samples. Interestingly, normal fetal cerebellar samples generally produced splicing patterns which were more similar to the tumours than to the normal adult samples (Figure 5.5).

To efficiently visualise patterns of differential splicing I performed hierarchical cluster analysis using Splicing Indicator values calculated for each one of the 11 validated events (the Splicing Indicator formula is summarised in Figure 5.6A). In cases where more than two transcript forms were amplified, the two most prominent were taken into account. Tumour and normal adult cerebellar samples were divided into two discrete clusters, with the latter mostly expressing splice forms retaining the candidate exons. An exception to this was the *MADD* gene, whose exon 34 appeared to be evenly

underexpressed in adult cerebella compared to medulloblastomas. One of the two fetal cerebellar samples (CBF1) clustered together with SHH tumours, while the second one (CBF2) subgrouped with the normal adult cerebella, but clearly exhibited an intermediate profile between normal and tumour samples (Figure 5.6B). This suggested the possibility that tumours retained splicing patterns characteristic of an undifferentiated cerebellar phenotype.

Table 5.1. Genes alternatively spliced in medulloblastoma identified by exon array analysis and validated by RT-PCR

Probe set ID	Gene Symbol	Probe set Location†	Transcript ID	Comparison‡	Exon Array		RT-PCR validation**		
					Adj p-value	Probe set FC§	Gene FC	Training set	Test set
3464995	<i>ATP2B1</i>	Ex 20	ENST00000359142	MB vs CB	0.003	-3.73	1.44	< 0.001	< 0.001
3329783	<i>MADD</i>	Ex 34	ENST00000311027	MB vs CB	> 0.01*	1.57	-1.74	0.01	< 0.001
2680306	<i>MAG11</i>	Ex 24	ENST00000330909	MB vs CB	< 0.001	-3.61	-1.09	< 0.001	< 0.001
3323129	<i>NAV2</i>	Ex 6	ENST00000360655	MB vs CB	0.009	-5.50	-3.42	0.02	0.008
2507435	<i>R3HDM1</i>	Ex 15	ENST00000264160	MB vs CB	0.004	-1.86	-1.12	0.04	< 0.001
3615612	<i>TJP1</i>	Ex 20	ENST00000346128	MB vs CB	0.002	-5.13	1.15	0.007	< 0.001
3789479	<i>WDR7</i>	Ex 17	ENST00000254442	MB vs CB	< 0.001	-5.46	-1.14	< 0.001	< 0.001
2680331	<i>MAG11</i>	EX 15	ENST00000330909	SHH vs CB	> 0.01*	-1.70	-1.56	0.03	0.004
3538263	<i>DAAM1</i>	Ex 16	ENST00000351081	SHH vs CB & MB2	0.009	-5.17	1.96	0.01	< 0.001
2485003	<i>EHBP1</i>	Ex 8	ENST00000263991	SHH vs CB & MB2	0.005	-8.88	1.11	0.003	0.006
3014461	<i>TRRAP</i>	Ex 22	ENST00000456197	SHH vs CB & MB2	0.003	-2.62	-1.10	0.004	< 0.001

† Exons are numbered according to the Ensembl transcripts listed to the right (Ensembl release 56). ‡ In several cases probe sets were identified as differentially spliced for more than one comparison. Here I report the comparison that generated the most significant difference. § Fold change in gene-normalised probe set signal values. || Fold change in gene signal values. ** P-values were calculated on the log₂ ratio between skipped and retained transcript forms as quantified from the agarose gels. MB, medulloblastoma (including both SHH and MB2); SHH, Shh-driven medulloblastoma; MB2, Shh-independent medulloblastoma, CB, normal cerebellum. * Events with an adjusted p-value > 0.01 but a profile suggestive of AS (Figure 5.3).

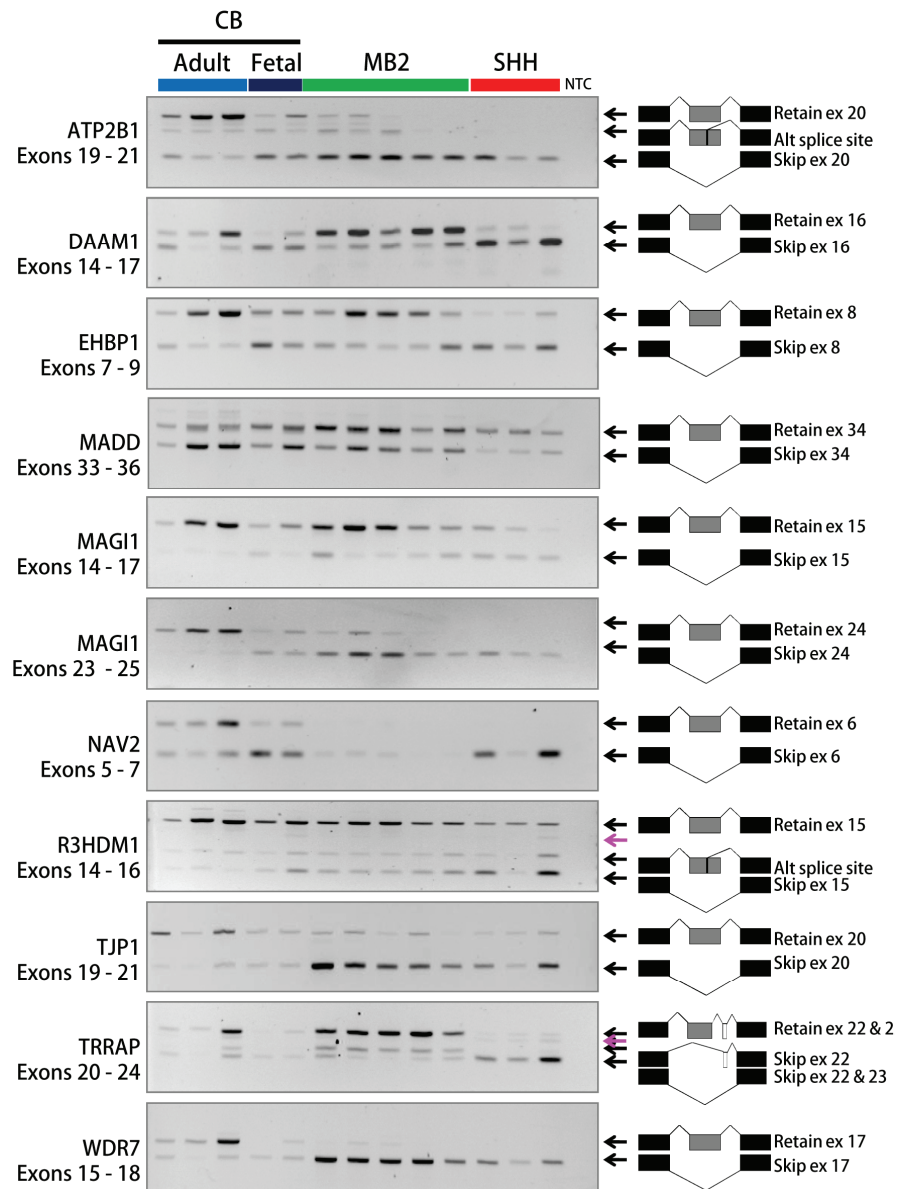


Figure 5.5. RT-PCR validation of differentially spliced cassette exons.

RT-PCR validation of candidate splicing events was performed on 13 of the 19 original samples profiled using exon arrays. PCR amplicons are listed below gene names. Exon structures corresponding to each amplified band are shown to the right of each gel. Pink arrows point to heteroduplexes of alternatively spliced forms. NTC, No-template control.

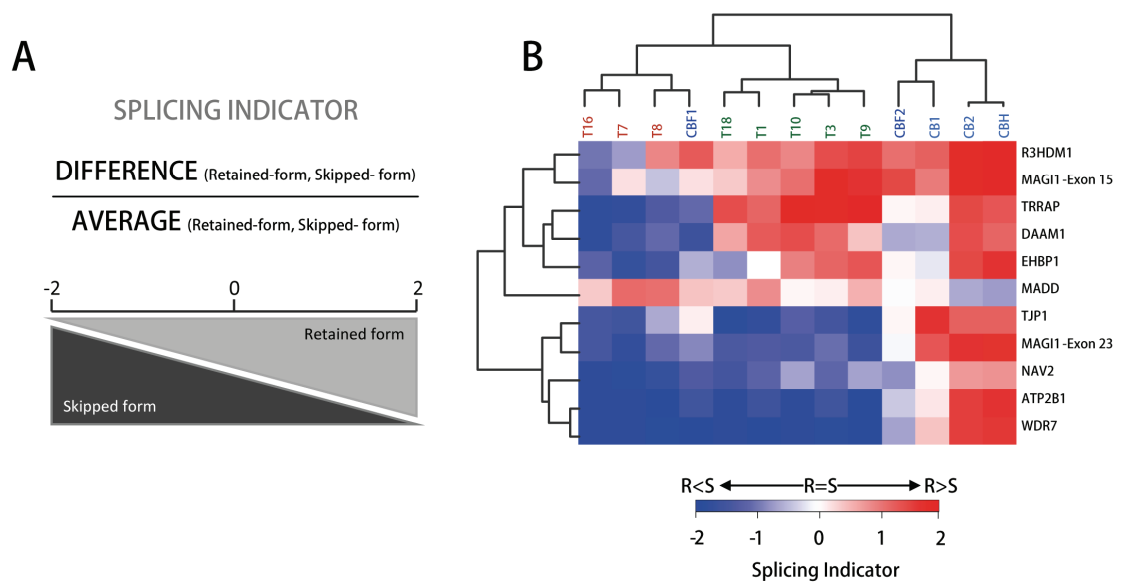


Figure 5.6. Visualisation of splicing patterns using the Splicing Indicator formula.

A) The Splicing Indicator formula was used to better visualise patterns of differential splicing. It corresponds to the ratio between difference and average of the signal intensities of the two alternative splice forms. Splicing Indicator values range between -2 and 2, where -2 and 2 correspond to exclusive amplification of the skipped exon isoform or the retained exon splice form respectively.

B) Cluster analysis was performed on the Splicing Indicator values corresponding to the 11 splicing events analysed by RT-PCR (see Figure 5.5). The Euclidean distance metric was used as a measure of distance between genes/samples. A blue-red colour palette was used to represent Splicing Indicator values, with blue corresponding to negative values (*i.e.* exon skipping, S); and red corresponding to positive values (*i.e.* exon retention, R). Sample subgroups are colour-coded as follow: light blue = adult normal cerebellum; dark blue = fetal normal cerebellum, green = MB2 tumours, red = SHH tumours.

5.3. Identification of novel splice forms

For some genes, I observed additional PCR products to those predicted by the exon array analysis. In two cases (*ATP2B1* and *R3HDM1*) I found that an extra transcript variant was generated via an alternative 5' splice site located within the candidate cassette exon (*ATP2B1* sequence analysis is shown in Figure 5.7A). Both novel transcript forms have been eventually annotated in Ensembl release 56 (September 2009). In the case of the *TRRAP* gene, the unexpected PCR product corresponded to a previously unreported splice form in which exon 22 is excluded and exon 23 is retained (see Figure 5.5 for a schematic illustration of exon structures). I also identified a novel 9 nucleotide-long exon inserted upstream of cassette exon 34 in the *MADD* gene (Figure 5.7B). Direct sequencing showed that this novel mini-exon was heterogeneously expressed across the sample-set.

All of the other extra bands detected corresponded to heteroduplexes forming between alternative PCR products (also described in [148, 250]), as confirmed by PCR subcloning and sequencing.

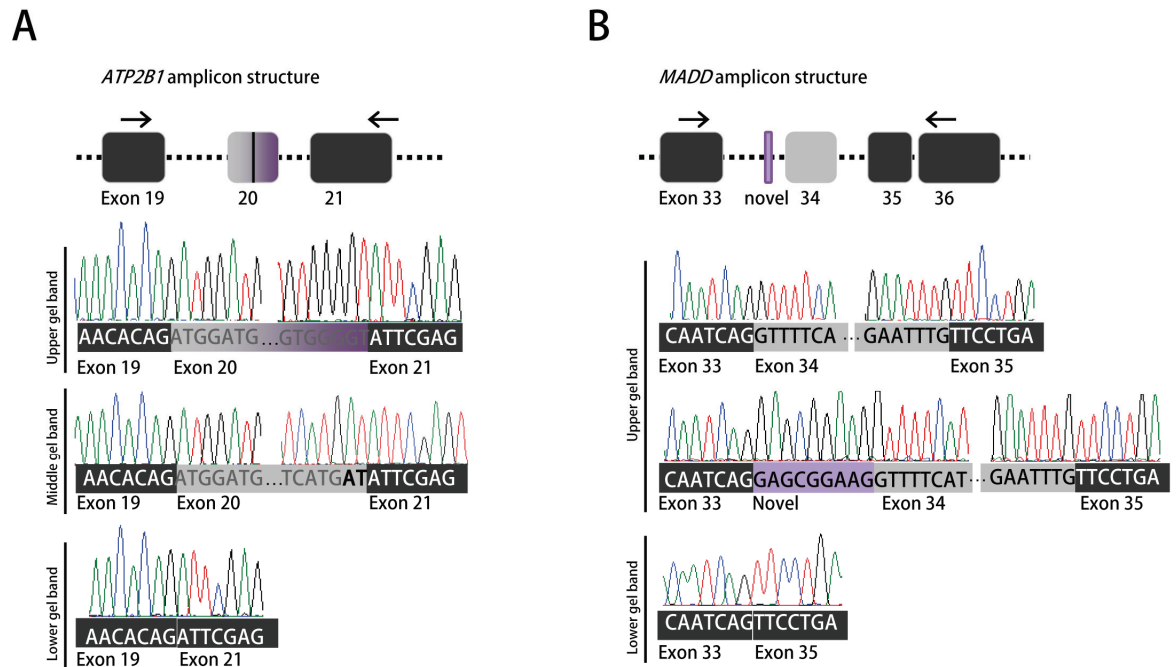


Figure 5.7. Examples of splice variant sequence analysis.

A) Sequence analysis of *ATP2B1* exons 19-21 PCR products. Amplification of the *ATP2B1* amplicon generated PCR products corresponding to three alternative splice forms. The upper and the lower gel bands corresponded to the transcript forms in which *ATP2B1* exon 20 is retained and skipped, respectively; the middle gel band corresponded to an additional transcript variant generated via an alternative 5' splice site within cassette exon 20.

B) Sequence analysis of *MADD* exons 33-35 PCR products. Sequencing of several PCR subclones of the *MADD* upper gel band revealed the presence, in most cases, of an additional 9 nucleotide-long exon located upstream of the candidate cassette exon.

5.4. Validation of differential splicing in an independent set of primary medulloblastomas and in medulloblastoma cell lines

To confirm that the splicing patterns of the selected genes were characteristic of medulloblastoma in general, I performed RT-PCR analysis of the 11 experimentally validated splice events using an independent set of ten normal cerebella and 20 medulloblastoma samples (test set). The clinical features of this novel sample series are presented in Table 5.2. The tumour samples had been previously classified into either the SHH or the MB2 subgroup according to whether or not they showed a gene expression signature indicative of Shh signalling pathway activation [92]. The novel independent set of samples replicated the same patterns of splicing identified in the initial set of samples (Figure 5.8), as confirmed by statistically significant differences in \log_2 ratios of transcript forms between sample subgroups (Table 5.1). It was interesting to see that the three genes previously shown to generate SHH-tumour specific splice forms (*DAAMI*, *EHBPI* and *TRRAP*) were also undergoing differential splicing in the SHH-tumours of the novel sample series, with only one exception (Figure 5.8).

I also analysed splicing patterns in three human medulloblastoma cell lines (Daoy, D425 Med and UW228-2) and found that they were similar to those of primary medulloblastomas, with the cell lines highly expressing tumour-associated transcript forms, including those characteristic of SHH-tumours (Figure 5.8).

To effectively visualise alternative transcript expression, I performed an unsupervised cluster analysis using Splicing Indicator values generated for each individual sample analysed by RT-PCR, including both training and test sets shown in Figure 5.5 and 5.8, respectively. Most of the adult normal cerebellar samples formed a homogeneous cluster and predominantly expressed transcript forms in which the candidate exons were retained. An exception to this was the CB1 sample, which showed

Table 5.2. Patients and tumour features of the sample series used for independent validation of differential splicing.

Medulloblastoma samples					Normal cerebellar samples				
Sample Id	Sex	Age at diagnosis (years)	Pathology	Shh Status	Sample Id	Sex	Age (years)	Source	Notes
T20	M	5.3	CLA	-	CB4	F/M	22-68	Clontech	pool of 10 individuals
T23	M	10.4	CLA	-	CB5	M	22	BioChain	
T24	M	4.9	CLA	-	CB6	M	26	BioChain	
T25	M	4.7	CLA	-	CBF3	M	Fetus	BioChain	26 weeks
T26	M	19.8	CLA	-	CB7	F	68	QSBB	Breast cancer
T27	F	9.7	CLA	-	CB8	M	38	QSBB	Gastric cancer
T28	F	6.5	CLA	-	CB9	M	43	QSBB	Heart attack
T29	F	9.8	LCA	-	CB10	M	76	QSBB	Lung cancer
T30	M	8.9	LCA	-	CB11	F	53	QSBB	Intra-cerebral haemorrhage
T32	M	14.0	CLA	-	CB14	M	63	QSBB	Congestive heart disease
T33	M	8.0	CLA	-					
T34	M	3.7	CLA	-					
T35	F	8.6	CLA	-					
T21	F	35.0	CLA	+					
T22	F	43.0	CLA	+					
T31	M	8.3	D	+					
T36	F	1.3	D	+					
T37	F	39.6	D	+					
T38	M	0.2	D	+					
T39	F	1.4	D	+					

The table illustrates the major clinical features of medulloblastoma (left) and normal cerebellar samples (right) used for the independent validation of differential splicing. Pathology: CLA, classic; LCA, large cell/anaplastic; D, desmoplastic. Sex: F, female; M, male. QSBB, Queen Square Brain Bank. In the note section, patients' cause of death is reported for samples obtained from QSBB.

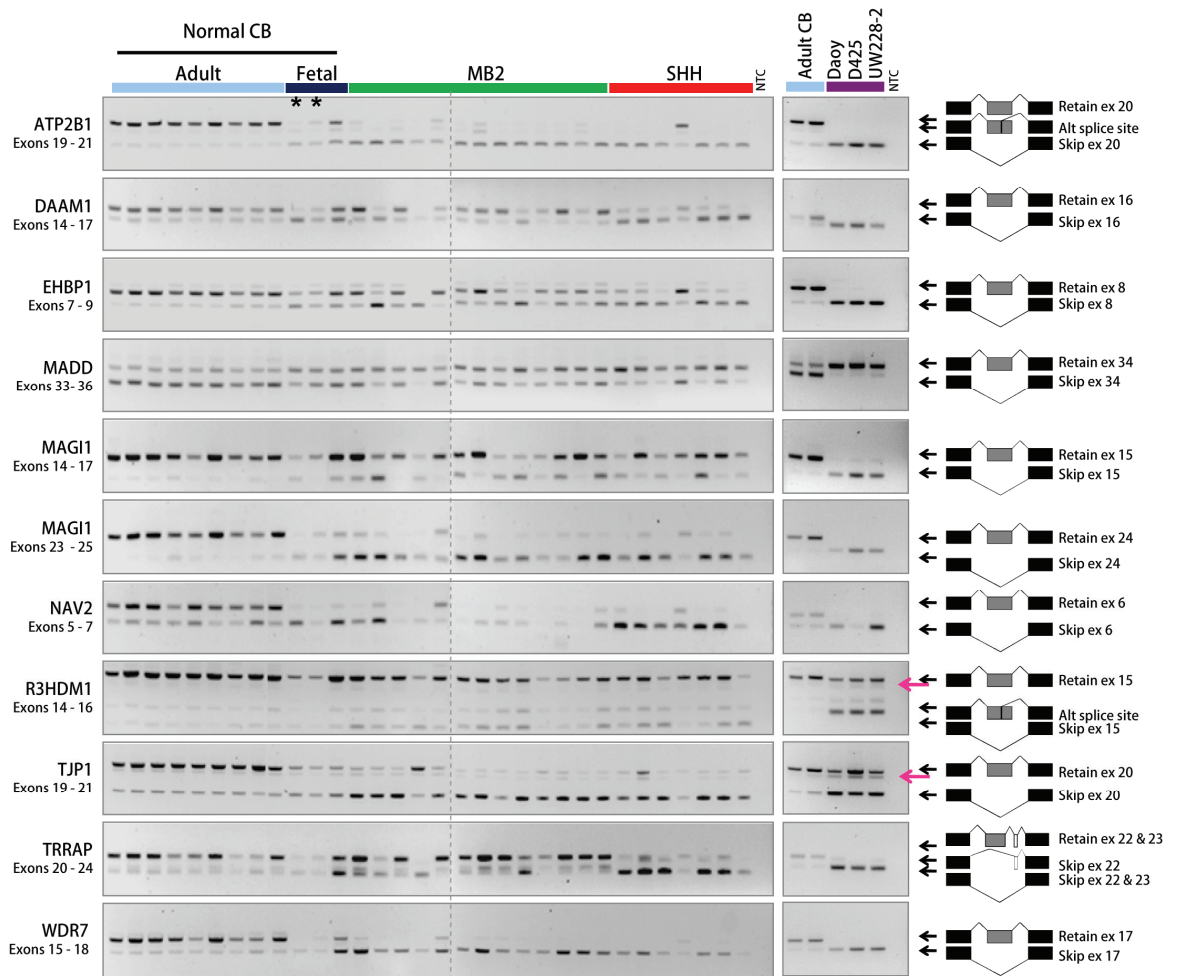


Figure 5.8. RT-PCR analysis of differential splicing in an independent set of samples and in medulloblastoma cell lines.

Left panel gels show RT-PCR results for an independent set of ten normal cerebellar and 20 medulloblastoma samples, including seven samples belonging to the SHH subgroup (red bar). Asterisks indicate two normal fetal cerebellar samples that were included in the initial validation (CBF1 and CBF2). Right panel gels show RT-PCR results for two adult normal cerebellar samples (light blue bar) and three human medulloblastoma cell lines (purple bar). PCR amplicons are listed below gene names. Exon structures corresponding to each amplified band are shown to the right of each gel. Pink arrows point to heteroduplexes of alternatively spliced forms. NTC, No-template control.

a splicing profile more similar to fetal cerebellar samples, and therefore slightly related to medulloblastomas. The CB1 tissue sample was obtained from a juvenile patient with a cerebellar glial tumour, so it may be that either the age of the patient or the undetected presence of a minor contamination of tumour cells could have contributed to the results.

Interestingly, the majority of SHH tumours shared similar splicing patterns, including a unique profile for those genes which were initially identified as undergoing SHH-associated splicing (*DAAMI*, *EHBPI* and *TRRAP*). As observed in Figure 5.8, only one SHH-tumour sample (T36) did not match this profile. Because sample T36 was also the only tumour sample which appeared to generally express transcript forms characteristic of normal adult cerebellum, it could be that the original tissue specimen from which RNA was isolated contained a large proportion of normal tissue which eventually affected the RT-PCR analysis. Furthermore, three tumour samples classified as MB2 tumours shared their overall splicing profiles with SHH-tumours. One of these samples was originally classified as a SHH-tumour on the basis of unsupervised clustering of gene expression; however, it did not show aberrant activation of the Shh signalling pathway and was therefore reclassified as a Shh-independent tumour (personal communication by Prof. Steve Clifford). As for the other two samples, they genuinely belonged to the Shh-independent molecular subgroup. It would be interesting to explore whether these ‘irregular’ splicing profiles could be informative of specific tumour characteristics or indicative of mis-classification.

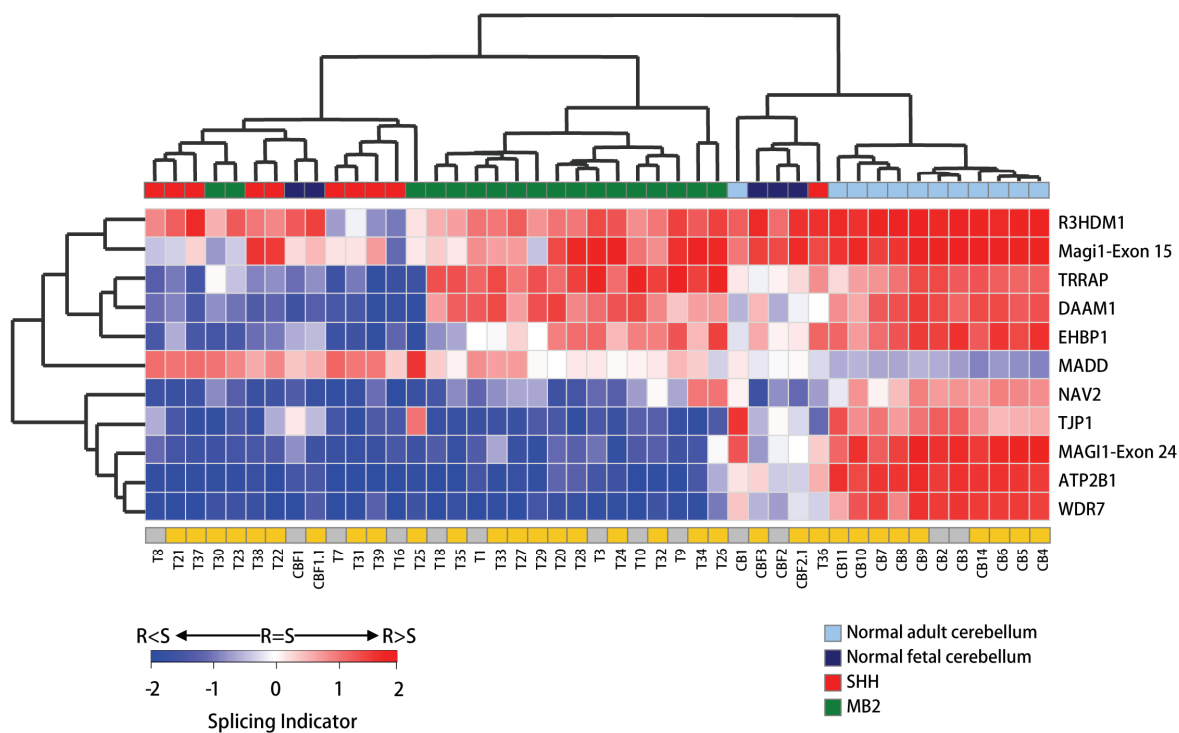


Figure 5.9. Cluster analysis of normal and tumour samples based on splicing patterns.

Unsupervised hierarchical clustering was performed on the Splicing Indicator values generated for each of the 45 individual samples analysed by RT-PCR (13 samples from the training set, 30 samples from the test set and CBF1 and CBF2 replicates, indicated above as CBF1.1 and CBF2.1) and using the Euclidean distance metric. Grey and yellow boxes at the bottom indicate samples analysed in the first (training set) and second (test set) RT-PCR validation experiments, respectively. S, Skipped exon splice form; R, Retained exon splice form.

5.5. Tumour-associated splicing patterns are observed during the normal development of mouse cerebellum

Cerebellar GCPs are the proposed cells of origin of Shh-driven medulloblastomas. I therefore investigated whether transcripts which showed characteristic splicing patterns in medulloblastomas were also differentially spliced in cultured GCPs. I analysed splicing variations in GCP cultures for seven of the candidate genes whose genomic organization was conserved between human and mouse (according to the X:Map database version 2.4, Table 5.3). In the presence of Shh, the splicing patterns for five out of the seven genes analyzed by RT-PCR (*Damml*, *Ehbp1*, *Magi1*, *Trrap* and *Wdr7*) recapitulated the patterns observed in the human tumour samples (Figure 5.10). That is, Shh caused a decrease in candidate exon inclusion rate, similarly to what I observed in medulloblastoma when compared to normal adult cerebellum. In the two remaining cases (*Madd* and *Nav2*), both transcript forms were expressed independently of Shh treatment (Figure 5.10).

The analysis of different stages of early post-natal mouse cerebellar development showed that the switch between the two alternative transcript forms of the five validated mouse genes occurred between post-natal days 7 and 14, at the time when GCPs mature into post-mitotic neurons (Figure 5.10). Thus, during the post-natal development of the mouse cerebellum, the amount of cassette exon inclusion that occurs falls as the number of proliferating GCPs decreases.

Table 5.3. Mouse cassette exons analysed by RT-PCR and their human equivalents.

<i>Mus musculus</i>			<i>Homo sapiens</i>		
Gene Name	Exon	Ensembl Transcript ID	Gene Name	Exon	Ensembl Transcript ID
<i>Daam1</i>	Ex 16	ENSMUST00000085299	<i>DAAM1</i>	Ex 16	ENST00000351081
<i>Ehbp1</i>	Ex 7	ENSMUST00000045167	<i>EHBP1</i>	Ex 8	ENST00000263991
<i>Magi1</i>	Ex 21	ENSMUST00000055224	<i>MAGI1</i>	Ex 24	ENST00000330909
<i>Trrap</i>	Ex 31	ENSMUST00000094120	<i>TRRAP</i>	Ex 22	ENST00000456197
<i>Wdr7</i>	Ex 17	ENSMUST00000072726	<i>WDR7</i>	Ex 17	ENST00000254442
<i>Nav2</i>	Ex 5	ENSMUST00000050869	<i>NAV2</i>	Ex 6	ENST00000360655
<i>Madd</i>	Ex 33	ENSMUST00000077941	<i>MADD</i>	Ex 34	ENST00000311027

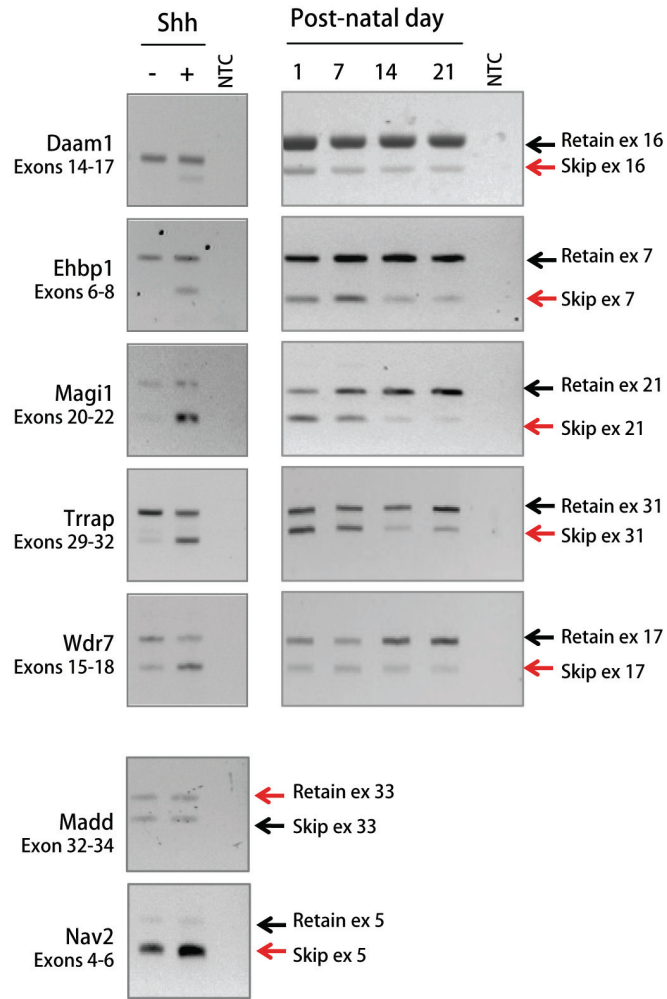
The table shows the mouse cassette exons analysed by RT-PCR and their human equivalent. Exons are numbered according to the corresponding Ensembl transcript IDs (Ensembl release 56).

Figure 5.10. Splicing variants characteristic of human medulloblastomas are expressed during normal mouse cerebellar development.

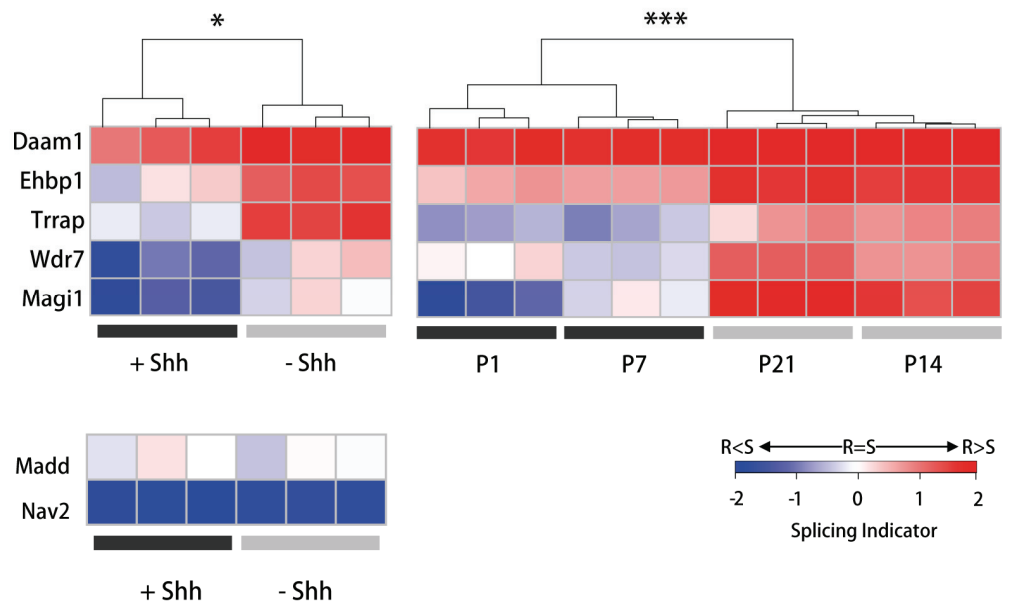
A) RT-PCR analysis of differential splicing in mouse GCP cultures maintained in the presence or in the absence of Shh for 48 hours (left panel) and in total mouse cerebellum during early post-natal development (right panel). Red arrows point to PCR bands corresponding to the predominant transcript forms observed in human medulloblastomas. Gels are representative of three independent experiments. NTC, No-template control.

B) Quantitation of transcript isoform ratios based on the Splicing Indicator formula. In both mouse systems, the top five represented genes were found to be differentially spliced, with medulloblastoma-associated variants being significantly more expressed in the presence of ShhN (left panel) and prior to GCP maturation in the post-natal cerebellum (P1-P7, right panel). In contrast, *Madd* and *Nav2* splice patterns were not modulated by ShhN in *in vitro* GCP cultures. *, ShhN-treated GCPs *versus* control, p-value , 0.05; ***, Total cerebellum at post-natal days 1-7 *versus* 14-21, p-value < 0.0001. S, Skipped exon splice form; R, Retained exon splice form.

A



B



5.6. Analysis of *MADD* differential splicing

The *MADD* gene (also known as *IG20*) encodes a death domain-containing adaptor protein which is believed to contribute to the propagation of apoptotic signals through its interaction with tumour necrosis factor receptor 1 (TNFR1). *MADD* has been implicated in cancer cell survival and apoptosis [253-256], as well as neurotransmission and neurodegeneration [257]. Evidence suggests that these contrasting effects are due to the differential expression of *MADD* alternative splice forms. Five different exons in the *MADD* gene are alternatively spliced to generate seven transcript forms (Figure 5.11), four of which (*IG20pa*, *MADD*, *IG20-SV2* and *DENN-SV*) have been reported to be commonly expressed across a variety of human tissues [255, 258]. In a series of papers published over the past ten years, Prabhakar *et al.* defined a critical role for the *DENN-SV* and *MADD* splice variants in promoting cell survival in HeLa and ovarian teratocarcinoma PA-1 cell lines, possibly via the activation of NF-kappa-B and of the Mitogen-Activated Protein Kinase (MAPK) cascade, respectively [254, 255, 259-261]. In contrast, expression of the *IG20pa* splice variant was shown to suppress cell replication and favour both spontaneous and drug-induced apoptosis in cancer cells [255]. Of interest, malignant tissues often express higher levels of the *MADD* and *DENN-SV* transcripts compared to the other two splice forms [255]. Recently, Li *et al.* described enriched expression of the *IG20-SV4* and *KIAA0358* splice forms in human neuronal tissues, and in neuroblastoma cell lines in particular [258]. Down-modulation experiments using splice form specific siRNAs showed that the two neuron-enriched transcripts elicited opposite cellular effects, with *KIAA0358* exerting potent anti-apoptotic functions and *IG20-SV4* enhancing caspase-8 activation and apoptosis.

In the RT-PCR validation experiments described in sections 5.4 and 5.5, I found that *MADD* exon 34 was expressed both in normal and in malignant cerebellum (Figures 5.5 and 5.8), in agreement with its expression being characteristic of neuronal cell types (*MADD* exon 34 is only retained in the two neuron-enriched splice forms *IG20-SV4* and *KIAA0358*, therefore it is not expressed in non-neuronal tissues). However I observed significantly higher inclusion rates of exon 34 in medulloblastoma samples compared to normal adult cerebellum. Since the analysis of exon 34 alone can not discriminate between all of the different splice variants of the *MADD* gene, I further investigated the alternative splicing profile of *MADD* exons 13L and 16 (Figure 5.12). Interestingly, medulloblastoma samples appeared to express high levels of the *DENN-SV* splice form, which is associated with cell survival. Fetal cerebellar samples shared a similar splicing profile (Figure 5.12A). In addition, several medulloblastoma samples showed preferential expression of both the *DENN-SV* and *MADD* anti-apoptotic splice forms. I also analysed splicing patterns of the *MADD* gene in the three human medulloblastoma cell lines Daoy, UW228-2 and D425 Med, and found that they exclusively expressed the *DENN-SV* and *MADD* isoforms (Figure 5.12B), following a pattern previously reported for other human cancer cell lines [253, 261].

Finally, I investigated the splicing pattern of mouse *Madd* exons 13L-16 in GCP cultures and during post-natal cerebellar development (Figure 5.12C). Previous analysis had shown that differential splicing of the *MADD* gene was not associated with the SHH tumour subgroup but rather with the medulloblastoma tumour set in general, and that the mouse equivalent of human *MADD* exon 34 was expressed independently of Shh treatment in GCP cultures (Figure 5.10). Here I confirmed that the different *Madd* gene transcript isoforms were not differentially expressed upon Shh treatment in mouse GCP cultures. I did however find modest but significant changes in the relative

expression levels of *Madd* gene transcript variants during mouse post-natal cerebellar development (P1-7 *versus* P14-21), with the early post-natal cerebellum expressing more of the *MADD* isoform compared to its mature counterpart.

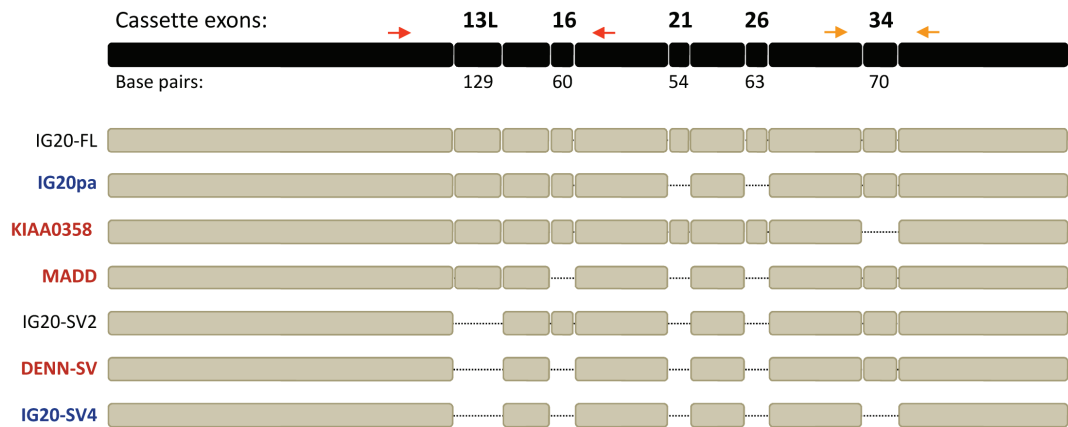


Figure 5.11. *MADD/IG20* splice forms.

Schematic representation of the human *MADD/IG20* gene and its transcript variants generated by alternative mRNA splicing. Exons 13L, 16, 21, 26 and 34, spliced in different combinations, generate seven different splice forms. Red and yellow arrows indicate the location of primer sets for the amplification of *MADD* exons 13L-16 and 34, respectively. Splice forms are defined as follows: blue, splice forms that have been shown to increase susceptibility to pro-apoptotic stimuli; red, splice forms associated with apoptosis resistance and cancer cell survival.

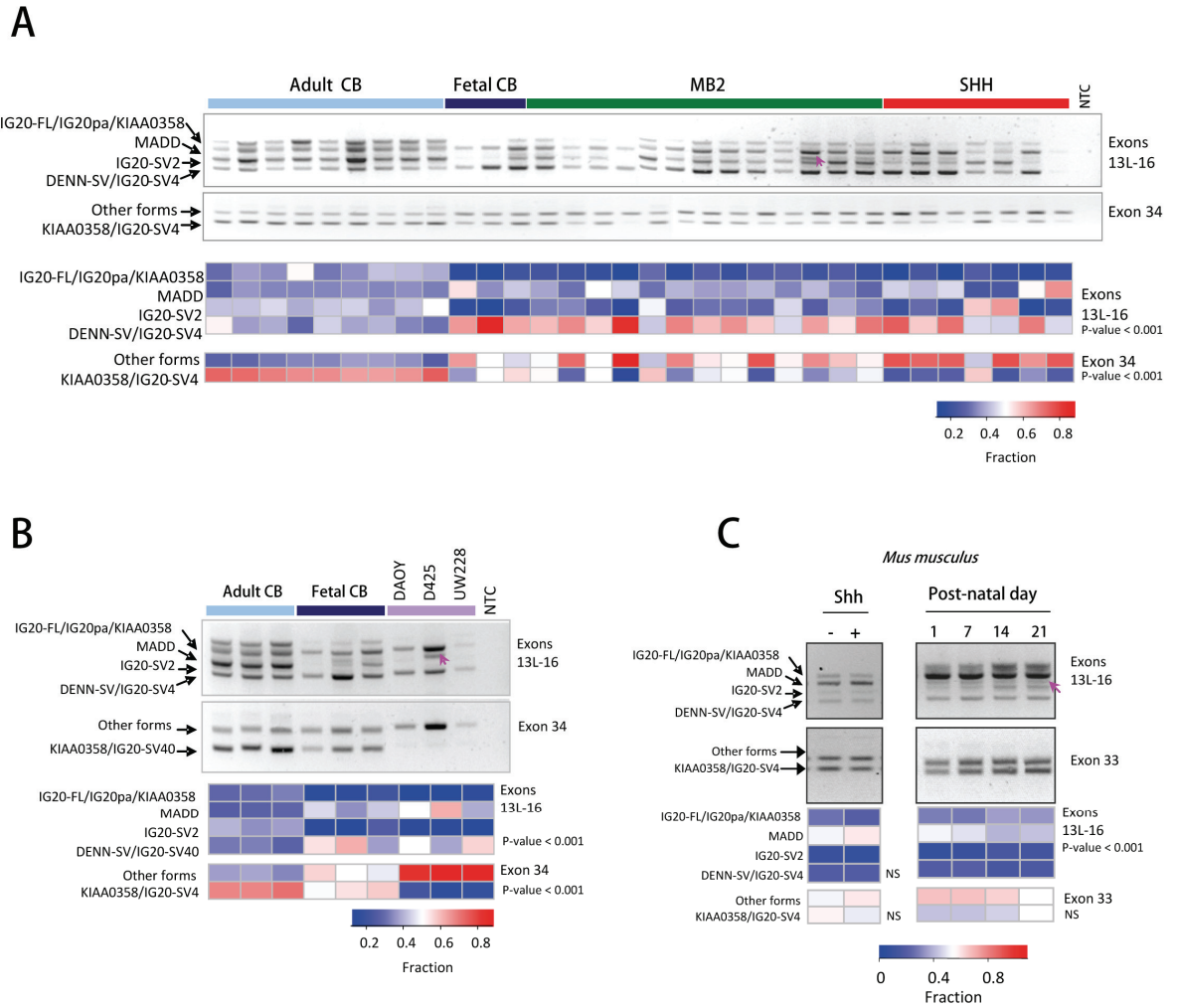


Figure 5.12. Analysis of *MADD/IG20* mRNA splicing in human medulloblastomas and during mouse cerebellar development.

Two primer sets were used to study the splicing patterns of exons 13L-16 and 34. Transcript variants corresponding to each PCR band are listed to the left of each gel. Pink arrows indicate heteroduplexes. A quantitation of individual PCR bands is represented at the bottom of the gels. The relative abundance of each transcript variant was measured as the fraction of the intensity of its PCR band against the total intensity for all of the bands amplified within the same sample. Splice variant fraction values were compared between sample subgroups using the Student's *t*-test. The resulting *p*-values are shown. NS, non significant.

A-B) RT-PCR analysis of *MADD/IG20* splice forms in normal cerebellum, primary human medulloblastomas (A) and human medulloblastoma cell lines (B).

C) RT-PCR analysis of *Madd* splice forms in mouse GCP cultures maintained in the presence or in the absence of Shh for 48 hours (left panel) and in total mouse cerebellum during early post-natal development (right panel).

5.7. An example of alternative transcript termination sites: analysis of *QKI* differential splicing

QKI (quaking) belongs to a family of RNA binding proteins that contain a nuclear ribonucleo-protein K homology (KH) domain and which are implicated in the regulation of mRNA splicing and stability, and protein translation. The mouse *Qk* gene was isolated as a candidate gene for the mouse neurological condition known as quaking, which affects the maturation of myelinating oligodendrocytes in the central nervous system [262]. As well as in oligodendrocytes, the QKI protein is also expressed in the heart, testis, lung and in other glial cell types throughout the brain [263, 264]. QKI expression in neuronal cell types has not been reported. The mammalian *QKI* gene undergoes alternative splicing generating at least three major transcript forms of 5, 6 and 7 kb: *QKI5*, *QKI6* and *QKI7* [264], whose expression is modulated during development. *QKI5* is the prevalent form during embryogenesis and its expression decreases after birth. Conversely, *QKI6* and *QKI7* are expressed during late embryogenesis, peak at mouse post-natal days 14-16, the time of myelination, and remain high into adulthood. The three forms differ in their C-terminal domain, which affects their subcellular localisation. The *QKI5* C-terminus contains a non-canonical nuclear import signal which allows its translocation to the nucleus. The other two protein forms are predominantly localised in the cytoplasm [263, 264]. *In silico* analysis of QKI binding sites in the mouse genome identified several putative QKI target mRNAs implicated in development and morphogenesis, cell-cell adhesion, cell growth and differentiation, therefore suggesting a critical role for QKI proteins in regulating cell fate and proliferation [265]. Interestingly, a conserved QKI binding sequence was described downstream of *MAGII* exon 24 [266], which I found to be differentially spliced between normal cerebellum and medulloblastoma (Figure 5.9).

In my exon array analysis, *QKI* appeared to be differentially spliced between normal cerebellum and medulloblastoma. Its probe set expression plot was indicative of alternative transcript termination, and in particular it suggested that normal cerebellar samples expressed relatively higher levels of *QKI7* compared to tumour samples, as shown schematically in Figure 5.13. This resulted in an increase in the *QKI5/QKI7* ratio in medulloblastomas (Figure 5.14A).

Of note, a recent paper by Lauriat *et al.* showed a positive correlation between *QKI6* and *QKI7* expression and the inclusion rate of *MAGII* exon 24 in the human prefrontal cortex [267]. Because of the interesting biological implications of QKI protein isoforms and of their role in modulating alternative splicing, I decided to validate differential splicing of the *QKI* gene in medulloblastoma. I performed Real Time PCR analysis to measure the fold change in expression between the *QKI5* and *QKI7* splice forms. Initially, I validated *QKI5/QKI7* expression ratios in a subset of the samples analysed by exon array and showed that the Real Time PCR results replicated the exon array data (Figure 5.14B). I then analysed a larger set of independent samples and found a significant increase in the ratio between *QKI5* and *QKI7* splice forms in medulloblastomas compared to normal adult cerebella (p-value = 0.009, Figure 5.15).

Since there was no evidence that *QKI* was expressed in neuronal cell types, I wanted to verify whether neuronal expression could actually occur and confirm that the *QKI* expression signal detected in the human sample series I analysed was not produced by the cerebellar glial component. I therefore analysed the expression of the mouse *Qk* gene in GCP cultures, as they are almost exclusively neurons. I found strong *Qk* expression in both Shh-treated and control cultures. In addition, a significant 50% increase in the ratio between *QKI5* and *QKI7* expression levels occurred when Shh was added to the culture (Figure 5.16A). Accordingly, the *QKI5/QKI7* ratio decreased in the

mouse cerebellum between post-natal days 7 and 14 (Figure 5.16B), in agreement with the literature [264].

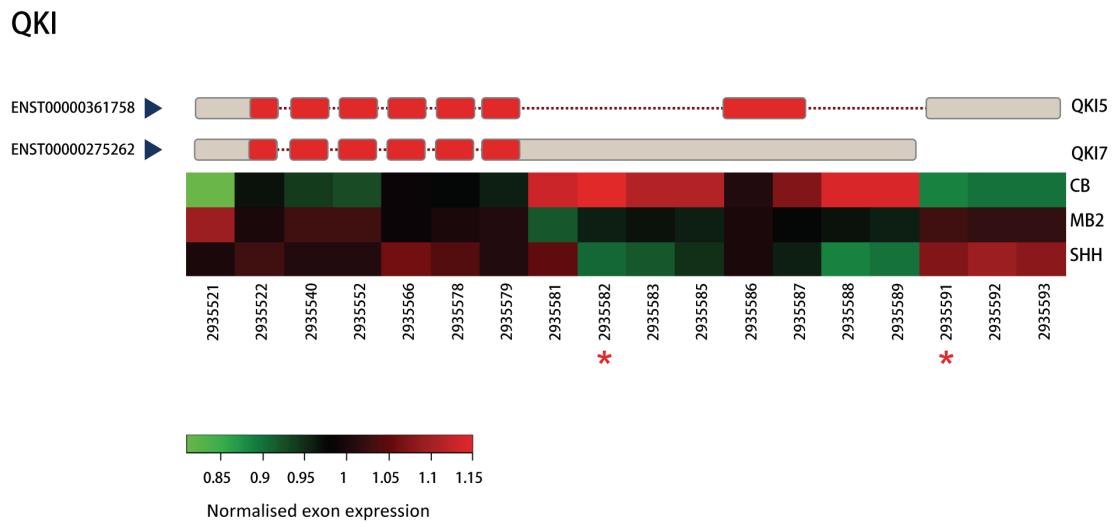


Figure 5.13. *QKI* probe set expression profile.

The heatmap summarises *QKI* probe set expression profiles across the sample set as described in figure legend 5.4. Probe sets are sorted by genomic location, with red asterisks underlying putative differentially spliced probe sets as identified by statistical analysis. Exon structures for the two alternative splice forms of interest (*QKI-5* and *QKI-7*) are shown at the top, with red and grey boxes corresponding to protein coding exons and untranslated regions, respectively. Transcript IDs refer to EnSEMBL release 56.

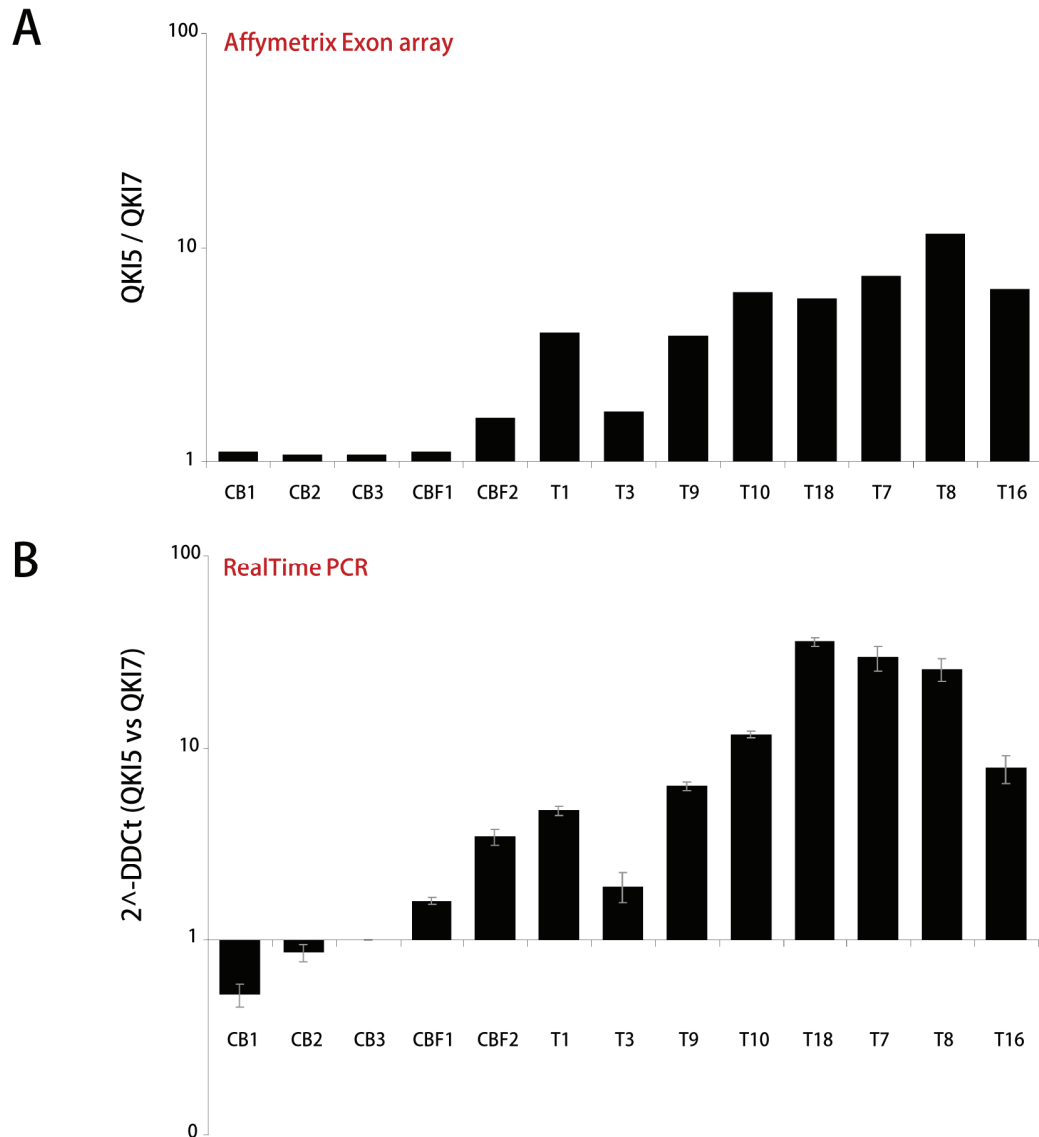


Figure 5.14. *QKI5/QKI7* expression ratio assessed by exon arrays and Real Time PCR.

A) Exon array data. *QKI5/QKI7* expression ratio was calculated as the ratio between the intensity of *QKI* probe set 2935591 mapping to the 3' end of *QKI5* transcript variant and the average signal value of all of *QKI* probe sets exclusively mapping to the 3' end of *QKI7* transcript variant.

B) Real Time PCR. *QKI5/QKI7* expression ratio was calculated using the $2^{-\Delta\Delta C_t}$ relative quantitation method. Real Time PCR replicated exon array expression ratios between the two alternative *QKI* isoforms (correlation coefficient = 0.77). The experiment was performed in triplicate. Bars correspond to averages +/- standard errors.

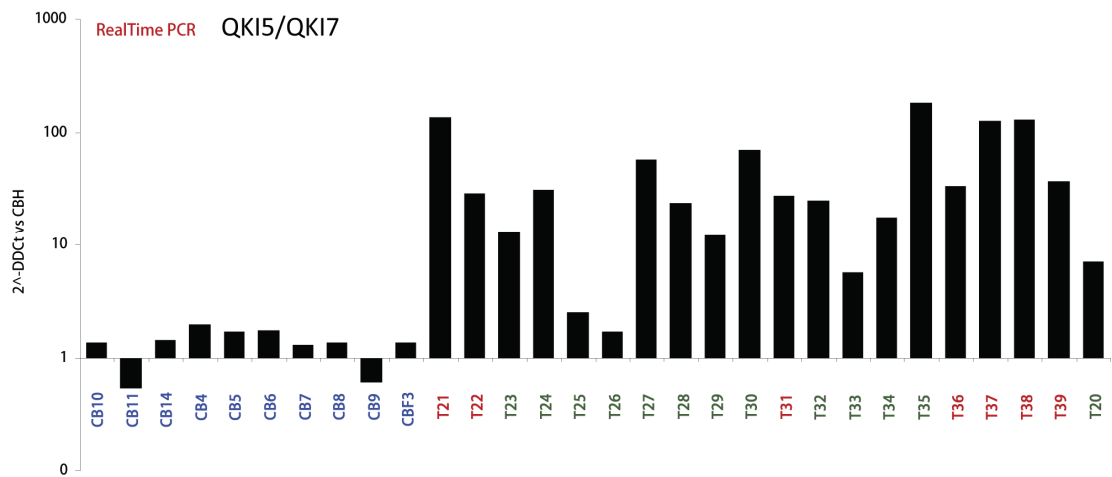


Figure 5.15. Validation of *QKI* differential splicing in an independent set of samples.

Real Time PCR validation of *QKI* differential splicing between normal cerebellum and primary medulloblastoma. *QKI5/QKI7* expression ratio was calculated using the $2^{-\Delta\Delta C_t}$ relative quantitation method in an independent set of ten normal cerebellar samples (in blue) and 20 primary medulloblastomas (SHH tumours in red and MB2 tumours in green).

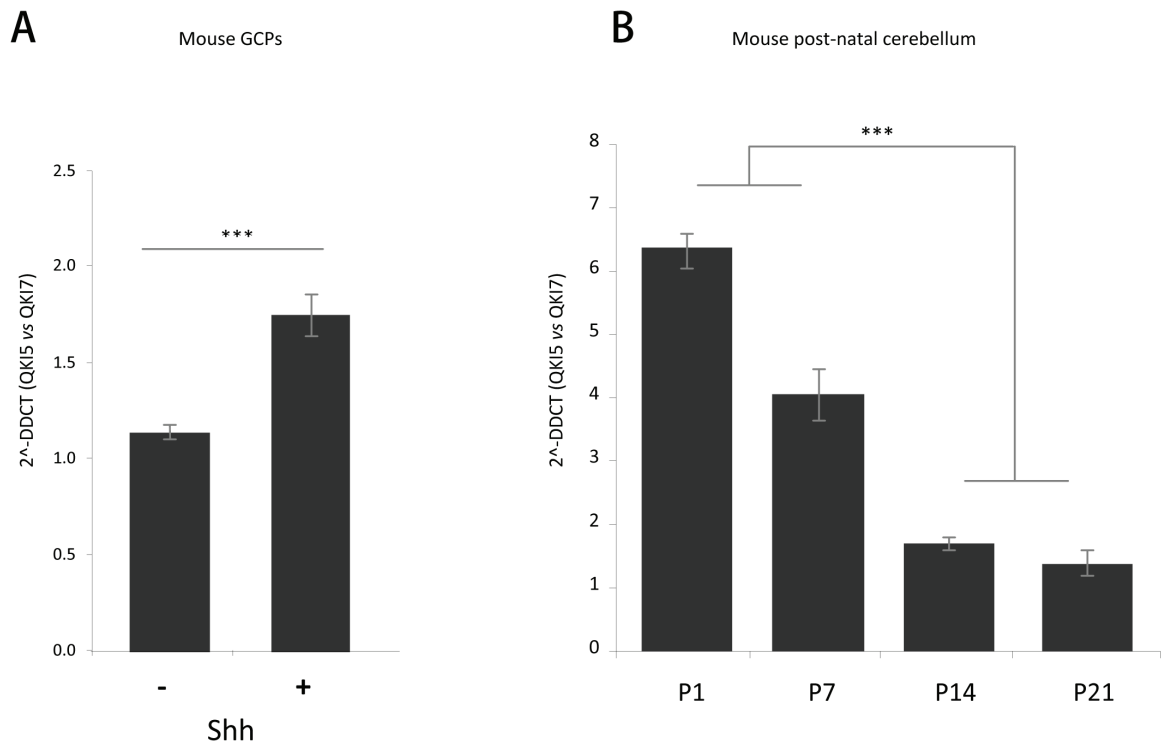


Figure 5.16. *QKI5* and *QKI7* splice variants are differentially expressed during normal mouse cerebellar development.

A) Mouse GCP primary cultures. Real Time PCR analysis of mouse *Qk* splice variants showed a significant 50% increase in the ratio between splice variants *QKI5* and *QKI7* when GCPs were cultured in the presence of ShhN (p-value < 0.0001). Histograms illustrate averages and standard errors of four independent experiments.

B) Mouse post-natal cerebellum. A significant decrease in the ratio between mouse splice forms *QKI5* and *QKI7* was observed between post-natal days 7 and 14 (p-value < 0.0001). Histograms illustrate averages and standard errors of three independent experiments.

5.9. Discussion

Alternative pre-mRNA splicing makes a major contribution to the generation of protein variety in a tissue- and development-specific manner. Alterations in the normal pathways of AS have been associated with the growth and maintenance of several tumour types, and have been indicated as candidate bio-markers of tumour progression, metastasis and patient survival [117, 118, 120]. I applied genome-wide exon array technology to identify splicing variations that distinguish between medulloblastoma and normal cerebellum. I identified 1,262 unique genes containing at least one candidate exon whose inclusion rate differed between sample subgroups. As opposed to the analysis of differential gene expression, the statistical analysis of alternative splicing appeared to be particularly prone to the generation of false positives. This has been reported in the literature [148, 149] and required a manual inspection of each individual candidate event by using probe set expression plots and taking advantage of annotation databases. As a result, I discarded a large part of the selected events aiming at the selection of only the most promising candidates. Thanks to the rapid development of novel statistical tools specifically designed for the investigation of splicing changes, it will be possible in the near future to apply optimised algorithms which not only compare exon expression levels between sample subgroups, but also take into account the relative location of each individual probe set in reference to the corresponding transcript cluster, therefore generating more accurate prediction of differential splicing.

Following the analysis of candidate event expression plots and gene structure annotation, I selected 14 cassette exons for experimental validation by RT-PCR and successfully confirmed differential splicing in 11 cases. All of the validated cassette exons encoded an in-frame polypeptide which would be included in the final protein product and did not contain stop codons.

Although in most cases the functional significance of AS has not yet been clarified, many of the validated genes have been previously implicated in key biological processes, such as neuronal differentiation and cancer progression. Several of the splicing events that I experimentally validated occurred in genes involved in cytoskeleton remodelling, cell morphology regulation and cell-cell interaction. DAAM1, EHBP1 and NAV2 all contain actin binding domains and have been suggested to mediate extensive reorganisation of actin structures likely affecting basic cellular functions, such as neurite growth and endocytic trafficking [268-270]. MAGI1 and TJP1 (also known as ZO-1) have been described as tight junction proteins co-localising in the apical region of polarised epithelial cells [271]. However, they are both expressed in non-epithelial cells, particularly in neuronal cell types, where they may be involved in different cell processes, such as regulation of gene expression [271, 272]. Interestingly, the two cassette exons of the *MAGI1* gene that I studied are almost exclusively expressed in the brain, and it has been suggested that they might be important for neuronal specification [271].

TRRAP is a highly conserved, large nuclear adaptor protein commonly found in histone acetyltransferase multi-protein complexes. It is thought to be necessary for the regulation of key chromatin processes, including DNA replication and repair, and MYC and E2F-mediated transcription [273]. TRRAP has recently been reported to be necessary for the maintenance of a stem cell phenotype in embryonic and hematopoietic stem cells [274, 275] as well as for the tumorigenic potential of brain cancer initiating cells [276]. I observed a specific pattern of splicing for the *TRRAP* gene, with Shh-driven medulloblastomas and medulloblastoma cell lines preferentially excluding the candidate cassette exon 22 (Figure 5.9). Also, more skipping of the equivalent mouse exon was seen in Shh-treated GCPs compared to controls and in the early stages of

mouse post-natal cerebellar development as opposed to the more mature cerebellum (Figure 5.10). It will be interesting to further investigate how insertion/exclusion of this exon alters the functioning of the TRRAP protein and whether it might affect the proliferation of granule cell precursors.

MADD encodes a death domain-containing adaptor protein which contributes to the propagation of apoptotic signals by modulating death receptor signalling. Five different exons in the *MADD* gene are alternatively spliced to generate seven transcript forms, which have been shown to elicit opposite cell responses, with at least two major splice forms promoting cancer cell survival and proliferation and another one associated with apoptosis (Figure 5.11) [253, 255, 261]. In my study I observed that, compared to normal adult cerebellum, primary medulloblastomas as well as the three medulloblastoma cell lines tested generally expressed higher levels of the two *MADD* splice forms associated with increased cell survival, namely the MADD and DENN-SV forms (Figure 5.12). To test whether these two forms contribute to the survival of medulloblastoma cells, it would be interesting to knockdown both of them or the MADD splice form exclusively (by targeting exon 13L) in medulloblastoma cell lines using shRNA silencing technology. It would also be interesting to express the exogenous IG20-pa splice variant and see if this sensitises medulloblastoma cells to spontaneous and drug-induced apoptosis.

The *QKI* gene encodes an RNA binding protein involved in RNA nuclear translocation, stability and processing and which affects both gene expression and splicing [265]. *QKI* is itself alternatively spliced to generate three major protein isoforms which differ in their C-terminal domain. Although little is known about the potential differences in the biological activity of the three QKI proteins, evidence has shown that both timing and subcellular compartmentalisation might regulate the access

of the different QKI proteins to their mRNA targets [263]. Exon array analysis showed that the relative expression ratio between the *QKI5* and *QKI7* splice forms was significantly higher in primary medulloblastomas as compared to normal cerebellum (Figure 5.15). *QKI5* is known to be expressed during early embryogenesis, as opposed to *QKI7*, whose expression levels peak soon after birth and remain high throughout adulthood, following an expression pattern which I validated in mouse cerebellum. Possibly, QKI5 specific target genes could be implicated in the maintenance of an undifferentiated phenotype. Interestingly, among QKI target genes, as predicted from *in silico* analysis of QKI binding sites, there are genes which I found to be overexpressed in primary tumours compared to control samples, such as *EYAI*, *NHLH1* and *EZH2* [265]. Future experiments should investigate the possible role of the *QKI5* splice form in regulating gene expression in GCPs and medulloblastomas.

In conclusion, by profiling exon expression in normal and malignant cerebellum, I identified splice variants generally enriched in medulloblastomas or specifically associated with the Shh-driven medulloblastoma molecular subgroup. I experimentally validated a selection of candidate events by RT-PCR or Real Time PCR in an independent set of normal and tumour samples, confirming that the initial sample set could be used to predict splicing profiles of a larger cohort of samples. For each validated event both alternative splice forms were detectable in the normal cerebellar samples, clearly suggesting that rather than novel splice forms, medulloblastomas expressed a significantly unbalanced ratio between transcript variants normally generated through AS in the cerebellum. Interestingly, I observed that the expression of transcript variants characteristic of human primary medulloblastomas, and in particular of the SHH tumour subgroup, often depended upon Shh in *in vitro* cultures of mouse

GCPs and during mouse normal cerebellar development. It is therefore plausible that the splicing pattern of at least some of the candidate genes identified through the exon array analysis was associated with a failure of cerebellar precursor cells to undergo neuronal differentiation, as a consequence of the aberrant activation of oncogenic pathways, such as the Shh signalling pathway.

Chapter 6

General discussion and future directions

Medulloblastoma is an embryonal tumour of the cerebellum and the most common malignant brain cancer in childhood [2]. Current treatments, which involve surgical resection, chemotherapy and radiotherapy, successfully cure only ~ 70% of patients, and are often associated with severe neurological deficits in long-term survivors [3]. There is, therefore, a great need for better therapies which are likely to derive from improvements in our understanding of the molecular pathways that drive medulloblastoma tumorigenesis [7].

During the past decade, integrative approaches for the study of the molecular abnormalities associated with malignant cerebellar phenotypes have revealed that medulloblastoma is a heterogeneous disease and that the characterisation of distinctive tumour molecular fingerprints has the potential to have an impact on the clinical management of medulloblastoma patients [7-9]. In particular, at least four medulloblastoma molecular subgroups have been described based on transcriptional and genomic data, including the WNT and SHH groups which display abnormalities indicative of inappropriate activation of the Wnt and Shh signalling pathways, respectively [20, 92]. Whereas increasing evidence indicates that SHH medulloblastomas originate from granule cell precursors (GCPs) in the developing cerebellum, the lineage of origin for the remaining medulloblastomas has not yet been elucidated [97].

In our group, we were interested in profiling gene expression patterns in a cohort of medulloblastoma patients treated at GOSH, and to generate a novel expression data set that would provide an additional level of analysis of the molecular complexity of human medulloblastoma. I therefore used the Affymetrix exon array platform to compare profiles of gene and exon expression within a series of medulloblastoma and normal cerebellar samples. In contrast to traditional array platforms, the exon array probe design allows two levels of analysis: at the gene level, it provides robust estimates of global gene expression; at the exon level, it allows the measurement of differential exon usage, for the investigation of tumour-associated splicing patterns [143].

Following array hybridisation and an initial assessment of experiment performance, I looked for the presence within my data set of samples expressing one of the well characterised medulloblastoma gene signatures. In agreement with previous reports, 21% of the tumours displayed a gene expression pattern indicative of Shh signalling pathway activation (SHH tumours) [20, 92, 107]. However, no tumours matching any of the other medulloblastoma molecular signatures described in the literature were found in my cohort. It will be useful to integrate gene expression data with candidate gene mutation and cytogenetic analyses to enhance the strength of molecular classification. Still, it was interesting to perform statistical analysis of changes in gene/exon expression levels to identify putative tumour-related genes whose transcriptional profiles specifically changed in SHH tumours compared to the other samples, as they might be implicated in the regulation of Shh-dependent cerebellar development and tumorigenesis.

Gene-level analysis of differential expression confirmed that Shh-driven medulloblastomas expressed higher levels of transcripts known to be directly or

indirectly regulated by Shh. Similarly, genes which are typically expressed in mature granule neurons were down-regulated in tumours compared to the normal cerebellum. In addition, I identified several novel genes whose expression was associated with SHH tumours, or with medulloblastomas in general (Figure 4.5). Interestingly, many of them appeared to be implicated in the regulation of mitotic spindle organisation and chromosome segregation during mitosis (*e.g. UBE2C, KIF4A, DLG7* and *PTTG1*). In normal cells, when even a single chromosome is not properly attached to the mitotic spindle, a mitotic checkpoint signalling cascade is initiated which results in cell cycle arrest [188]. Significant changes in the relative abundance of mitotic checkpoint proteins can lead to aneuploidy, a major molecular feature of tumour cells [188]. Whereas it is reasonable to consider the overexpression of genes regulating cell division as an index of the increased mitotic rate which typically characterises tumour tissues as opposed to the normal mature brain, these genes do represent appealing targets for a developing field of anti-cancer therapies designed to interfere with the mitotic checkpoint [277].

To test whether the level of expression of a selection of the candidate genes significantly up-regulated in SHH tumours was genuinely induced in response to Shh stimulation, I measured gene expression in *in vitro* cultures of mouse GCPs maintained in the presence or absence of Shh. When Shh was added to the cell culture, all of the candidate genes examined showed a significant increase in their transcript levels, suggesting that the Shh pathway regulates their activity to promote GCP progression through the cell cycle (Figure 4.9). It will be interesting in the future to investigate possible mechanisms by which Shh signalling may sustain candidate gene expression and whether any of the selected genes would be able to at least partially substitute for Shh in inducing cell proliferation both in normal and pathological conditions. Indeed,

transgenic mice overexpressing the *Ube2c* gene develop a variety of spontaneous tumours, following the disruption of the mitotic checkpoint and the accumulation of chromosomal abnormalities [199]. Similarly, overexpression of the *Pttg1* gene induces cell transformation *in vitro* and tumour formation in immuno-compromised mice, possibly by causing chromosomal instability and aneuploidy [190].

To determine whether the identified candidate genes regulated tumour cell proliferation, I wanted to investigate the effect of their down-regulation in human medulloblastoma cell lines. For this purpose, I set up an experimental system for the long-term silencing of target genes in the Daoy, UW228-2 and D425 Med cell lines through the delivery of gene-specific shRNAs by lentiviral transduction. In preliminary experiments, the targeting of a small selection of the candidate genes failed to induce any relevant changes in cell proliferation rate or cell cycle distribution, as described in section 4.8. Given more time, I would like to optimise the transduction protocol and improve target gene knockdown efficiency, introduce more specific biological read-outs as well as explore alternative ways of inhibiting the target genes, such as the use of dominant negative mutant proteins. I would also like to better investigate the level of activity of the Shh pathway in the three medulloblastoma cell lines, to assess whether they represent an appropriate model to study Shh-driven medulloblastomas. Alternatively, I could explore the potential role of Shh-related genes in promoting cell proliferation during normal cerebellar development using primary cultures of mouse GCPs, in which I would overexpress candidate genes or their dominant negative mutant forms.

The second part of my project involved an analysis of differential expression at the individual exon-level, which enabled me to identify splice variants significantly enriched in specific sample subgroups. Since the technology to perform comprehensive

analyses of alternative splicing patterns has been available only recently, the contribution of inappropriate splicing to tumour formation and growth is still not well understood [117-119]. However, multiple studies have shown that aberrant mRNA processing occurs frequently in human cancers and can directly contribute to the development of the disease (reviewed in [114, 115]). By comparing the normalised expression of individual exons between normal cerebellum and the subgroup of Shh-driven tumours or the entire set of medulloblastomas, I identified a large number of genes undergoing differential splicing. I then selected a small subset of these events to be validated by RT-PCR. Interestingly, I was able to confirm changes in exon inclusion rates for most of the cases examined (11 out of 14 cases), both in a subset of the profiled samples, and, more importantly, in a completely independent set of normal cerebellar and medulloblastoma tissues (Figure 5.8). In most cases the biological significance of the amino acid variation between the alternative splice forms has not yet been clarified, however many of the differently spliced exons are known to be predominantly expressed in the mature brain. Furthermore, for all of the events that I verified, the two alternative transcripts were detectable in the normal cerebellum, which indicates that rather than novel splice forms, medulloblastomas expressed unbalanced ratios between transcript variants normally generated through alternative splicing (AS) in the cerebellum. I observed that the expression of transcript variants characteristic of human primary medulloblastomas, and in particular of the SHH tumour subgroup, often depended upon Shh in *in vitro* cultures of mouse GCPs and during the normal development of the mouse cerebellum (Figure 5.10).

These findings clearly support the well established connection between cerebellar development and tumorigenesis, and provide an additional perspective to the analysis of the molecular similarities between GCPs and Shh-dependent

medulloblastomas. It is not surprising that programmes of alternative splicing are shared between Shh-dependent tumours and normal precursor cells, however, the more general splicing similarities between GCPs and all of the medulloblastomas under study are less clear. It is intriguing to hypothesise that these splicing patterns are characteristic of an even more immature progenitor cell in the cerebellum that then gives rise to the granule neuron lineage and SHH tumours as well as to alternative lineages, which in turn may follow divergent pathogenesis processes. It will also be interesting to investigate whether subgroup-specific patterns of differential splicing occur in the medulloblastoma subgroup with activation of the WNT signalling pathway, or any of the other discrete molecular subgroups.

The analysis of alternative splicing in medulloblastoma and normal cerebellum suggested that disruption of the correct balance between alternative transcript forms can be associated with a malignant phenotype. It will be important to explore the possible role of Shh and of other key signalling pathways that function in the developing brain in regulating programmes of alternative splicing. Lee *et al.* recently applied a genome-wide approach for the identification of genes directly regulated by Gli1 in GCPs and primary medulloblastomas derived from *Ptch*^{+/-} mice [278]. Interestingly, they found that several of the Gli1 target genes encode proteins implicated in mRNA processing and stability [278], suggesting that the Shh signalling pathway regulates splicing mechanisms in the developing cerebellum and in tumorigenesis. Consistent with these findings, when analysing changes in the level of expression of more than 300 genes encoding trans-acting splicing factors, I found a significant number of genes to be differentially expressed between normal adult cerebellum and medulloblastomas (Figure 6.1). Importantly, these include a few major regulators of splicing in the CNS, such as *NOVA1*, *PTBPI* and *A2BPI* [279-281].

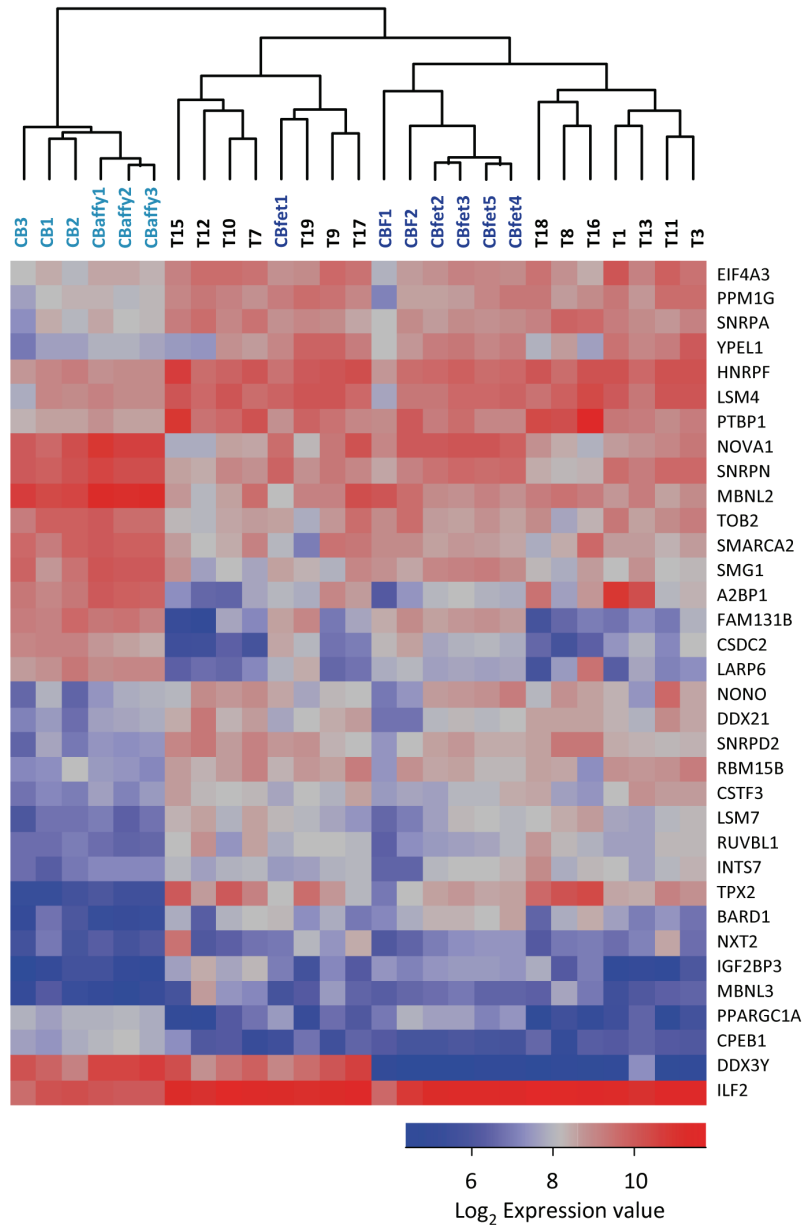


Figure 6.1. Gene-level expression analysis for genes encoding splicing factors.

The moderated t-statistic of the LIMMA package was used to compare the levels of expression of genes encoding splicing factors between medulloblastomas and normal cerebellar samples. The data set consisted of 27 total samples analysed by exon arrays, including the 19 samples analysed in my exon array experiment, three normal adult cerebellar samples from the Affymetrix human tissue public dataset (available from <http://www.affymetrix.com>) and five additional normal fetal cerebellar samples from Johnson *et al.* [282] (GEO dataset accession number GSE133344). Only genes with a fold change in expression higher or lower than 2 in medulloblastomas relative to normal adult cerebella are shown in the heatmap (FDR adjusted p-value < 0.05). Samples are colour-coded as follows: light blue, normal adult cerebellum; blue, normal fetal cerebellum, black, medulloblastoma.

Recent evidence has shown that one of the neuron-specific mechanisms for the inclusion of brain-enriched exons in transcripts involves the expression of microRNA miR-124 [280]. MiR-124 was able to trigger neuronal differentiation in neuroblastoma cell lines by directly targeting the mRNA of the *PTBPI* gene, one of the best characterised negative regulators of neuron-specific AS. In the developing brain, PTBPI activity is gradually lost, partly through negative regulation at the post-transcriptional level by miR-124 whose expression increases in the adult brain [280, 283]. This involves a major switch in the splice forms that are expressed in the adult brain as compared to the developing brain, with many neuron-specific exons (*e.g.* *DAAMI* exon 16) being incorporated into the mature mRNAs, and eventually resulting in the neuronal differentiation of progenitor cells into post-mitotic neurons [280] [284]. Remarkably, miR-124 was reported to be significantly down-regulated in human medulloblastomas compared to normal adult cerebellum [107, 285, 286], whereas the level of expression of the *PTBPI* gene was more than 2-fold higher in tumours compared to controls in my array data set (Figures 6.1 and 6.2). Moreover, *Ptbpl* was identified as one the Gli1 target genes in the study by Lee *et al.* [278]. Future experiments will investigate whether the characteristic patterns of differential cassette exon exclusion that I recognised in human medulloblastomas may be related to a failure in the neuron-specific AS programmes regulated by miR-124 via the down-regulation of *PTBPI*, or other key signalling pathways, such as the Shh pathway, which may control the overall activity of the splicing machinery in the developing cerebellum.

In conclusion, I performed a genome-wide analysis of gene expression in normal and malignant cerebellum and identified a subset of tumour samples expressing the molecular signature of Shh-dependent medulloblastomas. Statistical analysis of

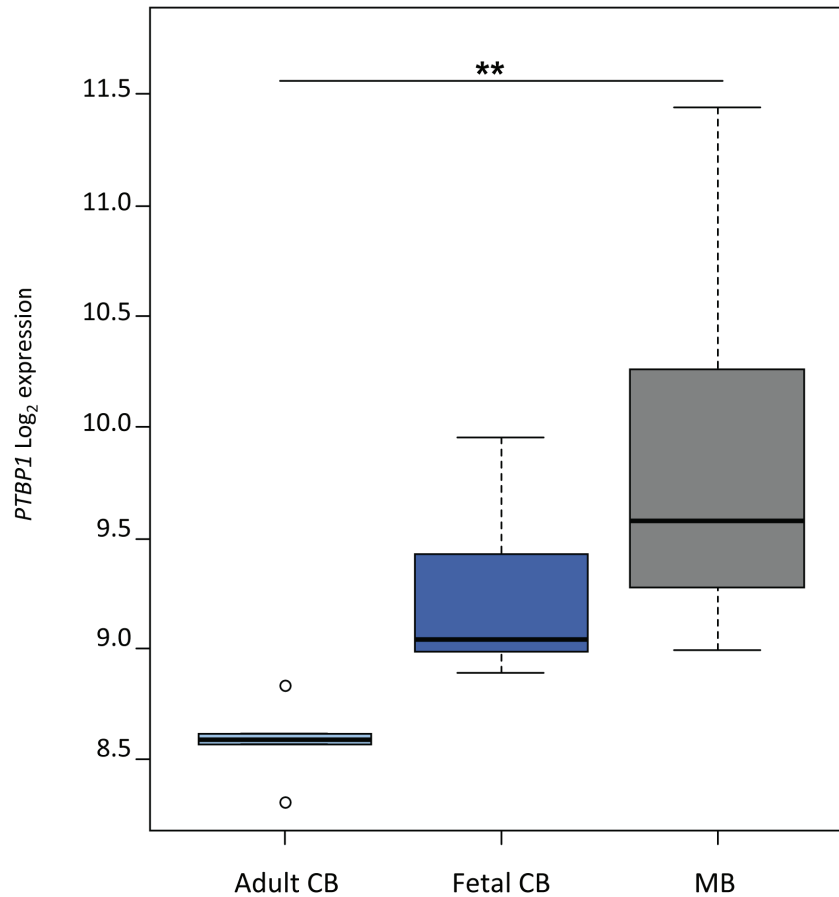


Figure 6.2. *PTBP1* is over-expressed in medulloblastomas compared to normal adult cerebella.

Box plots showing *PTBP1* gene expression in a set of 27 samples profiled by exon arrays. Box plots efficiently describe differences in gene signal distribution between sample subgroups within a data set. The bottom and top edges of the box correspond to the 25th percentile and 75th percentile, respectively. The median value is shown as a line across the box. Whiskers extend to 1.5 times the inter-quartile range (defined as the difference between the 75th and 25th percentiles), and outliers are marked with circles. The *PTBP1* gene is expressed at a significantly higher level in medulloblastomas compared to normal adult cerebellar samples (FDR adjusted p-value <0.001).

differential expression at the gene-level identified an interesting set of tumour-associated genes implicated in the regulation of the mitotic checkpoint, neuronal transcriptional programmes and DNA replication and repair. These genes were also overexpressed in GCPs cultured *in vitro* in the presence of Shh and in human medulloblastoma cell lines. Their role in sustaining the growth of precursor and tumour cells will be investigated in future experiments.

Changes in expression at the exon-level, which are indicative of differential splicing, were frequently found in association with medulloblastoma. Interestingly human primary tumours, particularly Shh-driven medulloblastomas, shared patterns of splicing with mouse GCPs, further supporting the idea that they have a common origin. The observation that CNS-specific exons were down-regulated and several trans-acting splicing factors differentially expressed in tumour tissues in comparison to the normal cerebellum, suggests that the disruption of AS programmes in the developing cerebellum might be associated with a failure of precursor cells to undergo neuronal differentiation as a consequence of the aberrant activation of oncogenic pathways, such as the Shh signalling pathway. The possible casual relationship between inappropriate splicing and medulloblastoma pathogenesis will be the subject of future investigation.

References

1. Crawford, J.R., T.J. MacDonald, and R.J. Packer, Medulloblastoma in childhood: new biological advances. *Lancet Neurol*, 2007. **6**(12): p. 1073-85.
2. Louis, D.N., et al., The 2007 WHO classification of tumours of the central nervous system. *Acta Neuropathol*, 2007. **114**(2): p. 97-109.
3. Packer, R.J., et al., Long-term neurologic and neurosensory sequelae in adult survivors of a childhood brain tumor: childhood cancer survivor study. *J Clin Oncol*, 2003. **21**(17): p. 3255-61.
4. Zeltzer, P.M., et al., Metastasis stage, adjuvant treatment, and residual tumor are prognostic factors for medulloblastoma in children: conclusions from the Children's Cancer Group 921 randomized phase III study. *J Clin Oncol*, 1999. **17**(3): p. 832-45.
5. McNeil, D.E., et al., Incidence and trends in pediatric malignancies medulloblastoma/primitive neuroectodermal tumor: a SEER update. *Surveillance Epidemiology and End Results. Med Pediatr Oncol*, 2002. **39**(3): p. 190-4.
6. Packer, R.J., Brain tumors in children. *Arch Neurol*, 1999. **56**(4): p. 421-5.
7. Ellison, D.W., Childhood medulloblastoma: novel approaches to the classification of a heterogeneous disease. *Acta Neuropathol*, 2010. **120**(3): p. 305-16.
8. Pfister, S., et al., Outcome prediction in pediatric medulloblastoma based on DNA copy-number aberrations of chromosomes 6q and 17q and the MYC and MYCN loci. *J Clin Oncol*, 2009. **27**(10): p. 1627-36.
9. Pizer, B.L. and S.C. Clifford, The potential impact of tumour biology on improved clinical practice for medulloblastoma: progress towards biologically driven clinical trials. *Br J Neurosurg*, 2009. **23**(4): p. 364-75.
10. Ellison, D., Classifying the medulloblastoma: insights from morphology and molecular genetics. *Neuropathol Appl Neurobiol*, 2002. **28**(4): p. 257-82.
11. McManamy, C.S., et al., Nodule formation and desmoplasia in medulloblastomas-defining the nodular/desmoplastic variant and its biological behavior. *Brain Pathol*, 2007. **17**(2): p. 151-64.
12. Gulino, A., A. Arcella, and F. Giangaspero, Pathological and molecular heterogeneity of medulloblastoma. *Curr Opin Oncol*, 2008. **20**(6): p. 668-75.
13. Rutkowski, S., et al., Medulloblastoma in young children. *Pediatr Blood Cancer*, 2010. **54**(4): p. 635-7.
14. Brown, H.G., et al., "Large cell/anaplastic" medulloblastomas: a Pediatric Oncology Group Study. *J Neuropathol Exp Neurol*, 2000. **59**(10): p. 857-65.
15. Eberhart, C.G., et al., Histopathologic grading of medulloblastomas: a Pediatric Oncology Group study. *Cancer*, 2002. **94**(2): p. 552-60.

16. Northcott, P.A., et al., Multiple recurrent genetic events converge on control of histone lysine methylation in medulloblastoma. *Nat Genet*, 2009. **41**(4): p. 465-72.
17. Bigner, S.H., et al., Structural chromosomal abnormalities in human medulloblastoma. *Cancer Genet Cytogenet*, 1988. **30**(1): p. 91-101.
18. Lamont, J.M., et al., Combined histopathological and molecular cytogenetic stratification of medulloblastoma patients. *Clin Cancer Res*, 2004. **10**(16): p. 5482-93.
19. Clifford, S.C., et al., Wnt/Wingless pathway activation and chromosome 6 loss characterize a distinct molecular sub-group of medulloblastomas associated with a favorable prognosis. *Cell Cycle*, 2006. **5**(22): p. 2666-70.
20. Thompson, M.C., et al., Genomics identifies medulloblastoma subgroups that are enriched for specific genetic alterations. *J Clin Oncol*, 2006. **24**(12): p. 1924-31.
21. Reardon, D.A., et al., Extensive genomic abnormalities in childhood medulloblastoma by comparative genomic hybridization. *Cancer Res*, 1997. **57**(18): p. 4042-7.
22. Bayani, J., et al., Molecular cytogenetic analysis of medulloblastomas and supratentorial primitive neuroectodermal tumors by using conventional banding, comparative genomic hybridization, and spectral karyotyping. *J Neurosurg*, 2000. **93**(3): p. 437-48.
23. Bigner, S.H., et al., Amplification of the c-myc gene in human medulloblastoma cell lines and xenografts. *Cancer Res*, 1990. **50**(8): p. 2347-50.
24. Aldosari, N., et al., MYCC and MYCN oncogene amplification in medulloblastoma. A fluorescence in situ hybridization study on paraffin sections from the Children's Oncology Group. *Arch Pathol Lab Med*, 2002. **126**(5): p. 540-4.
25. Northcott, P.A., J.T. Rutka, and M.D. Taylor, Genomics of medulloblastoma: from Giemsa-banding to next-generation sequencing in 20 years. *Neurosurg Focus*, 2010. **28**(1): p. E6.
26. Fogarty, M.P., J.D. Kessler, and R.J. Wechsler-Reya, Morphing into cancer: the role of developmental signaling pathways in brain tumor formation. *J Neurobiol*, 2005. **64**(4): p. 458-75.
27. Grimmer, M.R. and W.A. Weiss, Childhood tumors of the nervous system as disorders of normal development. *Curr Opin Pediatr*, 2006. **18**(6): p. 634-8.
28. Marino, S., Medulloblastoma: developmental mechanisms out of control. *Trends Mol Med*, 2005. **11**(1): p. 17-22.
29. Leiner, H.C., A.L. Leiner, and R.S. Dow, Cognitive and language functions of the human cerebellum. *Trends Neurosci*, 1993. **16**(11): p. 444-7.
30. Goldowitz, D. and K. Hamre, The cells and molecules that make a cerebellum. *Trends Neurosci*, 1998. **21**(9): p. 375-82.
31. Apps, R. and M. Garwicz, Anatomical and physiological foundations of cerebellar information processing. *Nat Rev Neurosci*, 2005. **6**(4): p. 297-311.

32. ten Donkelaar, H.J., et al., Development and developmental disorders of the human cerebellum. *J Neurol*, 2003. **250**(9): p. 1025-36.
33. Sillitoe, R.V. and A.L. Joyner, Morphology, molecular codes, and circuitry produce the three-dimensional complexity of the cerebellum. *Annu Rev Cell Dev Biol*, 2007. **23**: p. 549-77.
34. Wang, V.Y. and H.Y. Zoghbi, Genetic regulation of cerebellar development. *Nat Rev Neurosci*, 2001. **2**(7): p. 484-91.
35. Chizhikov, V. and K.J. Millen, Development and malformations of the cerebellum in mice. *Mol Genet Metab*, 2003. **80**(1-2): p. 54-65.
36. Oliver, T.G., et al., Loss of patched and disruption of granule cell development in a pre-neoplastic stage of medulloblastoma. *Development*, 2005. **132**(10): p. 2425-39.
37. Lee, A., et al., Isolation of neural stem cells from the postnatal cerebellum. *Nat Neurosci*, 2005. **8**(6): p. 723-9.
38. Goodrich, L.V., et al., Altered neural cell fates and medulloblastoma in mouse patched mutants. *Science*, 1997. **277**(5329): p. 1109-13.
39. Pietsch, T., et al., Medulloblastomas of the desmoplastic variant carry mutations of the human homologue of *Drosophila* patched. *Cancer Res*, 1997. **57**(11): p. 2085-8.
40. Raffel, C., et al., Sporadic medulloblastomas contain PTCH mutations. *Cancer Res*, 1997. **57**(5): p. 842-5.
41. Ruiz i Altaba, A., V. Palma, and N. Dahmane, Hedgehog-Gli signalling and the growth of the brain. *Nat Rev Neurosci*, 2002. **3**(1): p. 24-33.
42. Corrales, J.D., et al., Spatial pattern of sonic hedgehog signaling through Gli genes during cerebellum development. *Development*, 2004. **131**(22): p. 5581-90.
43. Wechsler-Reya, R.J. and M.P. Scott, Control of neuronal precursor proliferation in the cerebellum by Sonic Hedgehog. *Neuron*, 1999. **22**(1): p. 103-14.
44. De Smaele, E., et al., An integrated approach identifies *Nhlh1* and *Insm1* as Sonic Hedgehog-regulated genes in developing cerebellum and medulloblastoma. *Neoplasia*, 2008. **10**(1): p. 89-98.
45. Oliver, T.G., et al., Transcriptional profiling of the Sonic hedgehog response: a critical role for N-myc in proliferation of neuronal precursors. *Proc Natl Acad Sci U S A*, 2003. **100**(12): p. 7331-6.
46. Zhao, Q., et al., Identification of genes expressed with temporal-spatial restriction to developing cerebellar neuron precursors by a functional genomic approach. *Proc Natl Acad Sci U S A*, 2002. **99**(8): p. 5704-9.
47. Kenney, A.M. and D.H. Rowitch, Sonic hedgehog promotes G(1) cyclin expression and sustained cell cycle progression in mammalian neuronal precursors. *Mol Cell Biol*, 2000. **20**(23): p. 9055-67.

48. Kenney, A.M., M.D. Cole, and D.H. Rowitch, Nmyc upregulation by sonic hedgehog signaling promotes proliferation in developing cerebellar granule neuron precursors. *Development*, 2003. **130**(1): p. 15-28.
49. Knoepfler, P.S., P.F. Cheng, and R.N. Eisenman, N-myc is essential during neurogenesis for the rapid expansion of progenitor cell populations and the inhibition of neuronal differentiation. *Genes Dev*, 2002. **16**(20): p. 2699-712.
50. Thomas, W.D., et al., Patched1 deletion increases N-Myc protein stability as a mechanism of medulloblastoma initiation and progression. *Oncogene*, 2009. **28**(13): p. 1605-15.
51. Swartling, F.J., et al., Pleiotropic role for MYCN in medulloblastoma. *Genes Dev*, 2010. **24**(10): p. 1059-72.
52. Heine, V.M., et al., Dexamethasone destabilizes Nmyc to inhibit the growth of hedgehog-associated medulloblastoma. *Cancer Res*, 2010. **70**(13): p. 5220-5.
53. Yun, J.S., et al., A novel role of the Mad family member Mad3 in cerebellar granule neuron precursor proliferation. *Mol Cell Biol*, 2007. **27**(23): p. 8178-89.
54. Leung, C., et al., Bmi1 is essential for cerebellar development and is overexpressed in human medulloblastomas. *Nature*, 2004. **428**(6980): p. 337-41.
55. Subkhankulova, T., et al., Bmi1 directly represses p21(Waf1/Cip1) in Shh-induced proliferation of cerebellar granule cell progenitors. *Mol Cell Neurosci*, 2010.
56. Parathath, S.R., et al., Insulin receptor substrate 1 is an effector of sonic hedgehog mitogenic signaling in cerebellar neural precursors. *Development*, 2008. **135**(19): p. 3291-300.
57. Waters, S.B., K. Yamauchi, and J.E. Pessin, Functional expression of insulin receptor substrate-1 is required for insulin-stimulated mitogenic signaling. *J Biol Chem*, 1993. **268**(30): p. 22231-4.
58. Hartmann, W., et al., Insulin-like growth factor II is involved in the proliferation control of medulloblastoma and its cerebellar precursor cells. *Am J Pathol*, 2005. **166**(4): p. 1153-62.
59. Fernandez, L.A., et al., YAP1 is amplified and up-regulated in hedgehog-associated medulloblastomas and mediates Sonic hedgehog-driven neural precursor proliferation. *Genes Dev*, 2009. **23**(23): p. 2729-41.
60. Gazit, R., V. Krizhanovsky, and N. Ben-Arie, Math1 controls cerebellar granule cell differentiation by regulating multiple components of the Notch signaling pathway. *Development*, 2004. **131**(4): p. 903-13.
61. Flora, A., et al., Deletion of Atoh1 disrupts Sonic Hedgehog signaling in the developing cerebellum and prevents medulloblastoma. *Science*, 2009. **326**(5958): p. 1424-7.
62. Massague, J., How cells read TGF-beta signals. *Nat Rev Mol Cell Biol*, 2000. **1**(3): p. 169-78.
63. Alder, J., et al., Generation of cerebellar granule neurons in vivo by transplantation of BMP-treated neural progenitor cells. *Nat Neurosci*, 1999. **2**(6): p. 535-40.

64. Krizhanovsky, V. and N. Ben-Arie, A novel role for the choroid plexus in BMP-mediated inhibition of differentiation of cerebellar neural progenitors. *Mech Dev*, 2006. **123**(1): p. 67-75.
65. Zhao, H., et al., Post-transcriptional down-regulation of *Atoh1/Math1* by bone morphogenic proteins suppresses medulloblastoma development. *Genes Dev*, 2008. **22**(6): p. 722-7.
66. Rios, I., et al., *Bmp2* antagonizes sonic hedgehog-mediated proliferation of cerebellar granule neurones through *Smad5* signalling. *Development*, 2004. **131**(13): p. 3159-68.
67. Reuss, B. and O. von Bohlen und Halbach, Fibroblast growth factors and their receptors in the central nervous system. *Cell Tissue Res*, 2003. **313**(2): p. 139-57.
68. Yaguchi, Y., et al., Fibroblast growth factor (FGF) gene expression in the developing cerebellum suggests multiple roles for FGF signaling during cerebellar morphogenesis and development. *Dev Dyn*, 2009. **238**(8): p. 2058-72.
69. Fogarty, M.P., et al., Fibroblast growth factor blocks Sonic hedgehog signaling in neuronal precursors and tumor cells. *Proc Natl Acad Sci U S A*, 2007. **104**(8): p. 2973-8.
70. Ortega, S., et al., Neuronal defects and delayed wound healing in mice lacking fibroblast growth factor 2. *Proc Natl Acad Sci U S A*, 1998. **95**(10): p. 5672-7.
71. Di Marcotullio, L., et al., *REN(KCTD11)* is a suppressor of Hedgehog signaling and is deleted in human medulloblastoma. *Proc Natl Acad Sci U S A*, 2004. **101**(29): p. 10833-8.
72. Argenti, B., et al., Hedgehog antagonist *REN(KCTD11)* regulates proliferation and apoptosis of developing granule cell progenitors. *J Neurosci*, 2005. **25**(36): p. 8338-46.
73. Hahn, H., et al., Mutations of the human homolog of *Drosophila patched* in the nevoid basal cell carcinoma syndrome. *Cell*, 1996. **85**(6): p. 841-51.
74. Johnson, R.L., et al., Human homolog of *patched*, a candidate gene for the basal cell nevus syndrome. *Science*, 1996. **272**(5268): p. 1668-71.
75. Gorlin, R.J., Nevoid basal cell carcinoma (Gorlin) syndrome. *Genet Med*, 2004. **6**(6): p. 530-9.
76. Ellison, D.W., et al., What's new in neuro-oncology? Recent advances in medulloblastoma. *Eur J Paediatr Neurol*, 2003. **7**(2): p. 53-66.
77. Lam, C.W., et al., A frequent activated smoothed mutation in sporadic basal cell carcinomas. *Oncogene*, 1999. **18**(3): p. 833-6.
78. Taylor, M.D., et al., Mutations in *SUFU* predispose to medulloblastoma. *Nat Genet*, 2002. **31**(3): p. 306-10.
79. Corcoran, R.B. and M.P. Scott, A mouse model for medulloblastoma and basal cell nevus syndrome. *J Neurooncol*, 2001. **53**(3): p. 307-18.

80. Kim, J.Y., et al., Medulloblastoma tumorigenesis diverges from cerebellar granule cell differentiation in patched heterozygous mice. *Dev Biol*, 2003. **263**(1): p. 50-66.
81. Hatton, B.A., et al., The Smo/Smo model: hedgehog-induced medulloblastoma with 90% incidence and leptomeningeal spread. *Cancer Res*, 2008. **68**(6): p. 1768-76.
82. Marino, S., et al., Induction of medulloblastomas in p53-null mutant mice by somatic inactivation of Rb in the external granular layer cells of the cerebellum. *Genes Dev*, 2000. **14**(8): p. 994-1004.
83. Shakhova, O., et al., Lack of Rb and p53 delays cerebellar development and predisposes to large cell anaplastic medulloblastoma through amplification of N-Myc and Ptch2. *Cancer Res*, 2006. **66**(10): p. 5190-200.
84. Wetmore, C., D.E. Eberhart, and T. Curran, Loss of p53 but not ARF accelerates medulloblastoma in mice heterozygous for patched. *Cancer Res*, 2001. **61**(2): p. 513-6.
85. Zindy, F., et al., Genetic alterations in mouse medulloblastomas and generation of tumors de novo from primary cerebellar granule neuron precursors. *Cancer Res*, 2007. **67**(6): p. 2676-84.
86. Balordi, F. and G. Fishell, Hedgehog signaling in the subventricular zone is required for both the maintenance of stem cells and the migration of newborn neurons. *J Neurosci*, 2007. **27**(22): p. 5936-47.
87. Hemmati, H.D., et al., Cancerous stem cells can arise from pediatric brain tumors. *Proc Natl Acad Sci U S A*, 2003. **100**(25): p. 15178-83.
88. Singh, S.K., et al., Identification of human brain tumour initiating cells. *Nature*, 2004. **432**(7015): p. 396-401.
89. Sutter, R., et al., Cerebellar stem cells act as medulloblastoma-initiating cells in a mouse model and a neural stem cell signature characterizes a subset of human medulloblastomas. *Oncogene*, 2010. **29**(12): p. 1845-56.
90. Yang, Z.J., et al., Medulloblastoma can be initiated by deletion of Patched in lineage-restricted progenitors or stem cells. *Cancer Cell*, 2008. **14**(2): p. 135-45.
91. Schuller, U., et al., Acquisition of granule neuron precursor identity is a critical determinant of progenitor cell competence to form Shh-induced medulloblastoma. *Cancer Cell*, 2008. **14**(2): p. 123-34.
92. Kool, M., et al., Integrated genomics identifies five medulloblastoma subtypes with distinct genetic profiles, pathway signatures and clinicopathological features. *PLoS One*, 2008. **3**(8): p. e3088.
93. Ciani, L. and P.C. Salinas, WNTs in the vertebrate nervous system: from patterning to neuronal connectivity. *Nat Rev Neurosci*, 2005. **6**(5): p. 351-62.
94. Thomas, K.R. and M.R. Capecchi, Targeted disruption of the murine int-1 proto-oncogene resulting in severe abnormalities in midbrain and cerebellar development. *Nature*, 1990. **346**(6287): p. 847-50.
95. Schuller, U. and D.H. Rowitch, Beta-catenin function is required for cerebellar morphogenesis. *Brain Res*, 2007. **1140**: p. 161-9.

96. Fan, X. and C.G. Eberhart, Medulloblastoma stem cells. *J Clin Oncol*, 2008. **26**(17): p. 2821-7.
97. Gilbertson, R.J. and D.W. Ellison, The origins of medulloblastoma subtypes. *Annu Rev Pathol*, 2008. **3**: p. 341-65.
98. Michiels, E.M., et al., Genes differentially expressed in medulloblastoma and fetal brain. *Physiol Genomics*, 1999. **1**(2): p. 83-91.
99. MacDonald, T.J., et al., Expression profiling of medulloblastoma: PDGFRA and the RAS/MAPK pathway as therapeutic targets for metastatic disease. *Nat Genet*, 2001. **29**(2): p. 143-52.
100. Pomeroy, S.L., et al., Prediction of central nervous system embryonal tumour outcome based on gene expression. *Nature*, 2002. **415**(6870): p. 436-42.
101. Boon, K., et al., Comparison of medulloblastoma and normal neural transcriptomes identifies a restricted set of activated genes. *Oncogene*, 2003. **22**(48): p. 7687-94.
102. Park, P.C., et al., Transcriptional profiling of medulloblastoma in children. *J Neurosurg*, 2003. **99**(3): p. 534-41.
103. Neben, K., et al., Microarray-based screening for molecular markers in medulloblastoma revealed STK15 as independent predictor for survival. *Cancer Res*, 2004. **64**(9): p. 3103-11.
104. Velculescu, V.E., et al., Serial analysis of gene expression. *Science*, 1995. **270**(5235): p. 484-7.
105. Kho, A.T., et al., Conserved mechanisms across development and tumorigenesis revealed by a mouse development perspective of human cancers. *Genes Dev*, 2004. **18**(6): p. 629-40.
106. Sara, H., O. Kallioniemi, and M. Nees, A decade of cancer gene profiling: from molecular portraits to molecular function. *Methods Mol Biol*, 2010. **576**: p. 61-87.
107. Northcott, P.A., et al., The miR-17/92 polycistron is up-regulated in sonic hedgehog-driven medulloblastomas and induced by N-myc in sonic hedgehog-treated cerebellar neural precursors. *Cancer Res*, 2009. **69**(8): p. 3249-55.
108. Nilsen, T.W. and B.R. Graveley, Expansion of the eukaryotic proteome by alternative splicing. *Nature*, 2010. **463**(7280): p. 457-63.
109. Matlin, A.J., F. Clark, and C.W. Smith, Understanding alternative splicing: towards a cellular code. *Nat Rev Mol Cell Biol*, 2005. **6**(5): p. 386-98.
110. Lander, E.S., et al., Initial sequencing and analysis of the human genome. *Nature*, 2001. **409**(6822): p. 860-921.
111. Venter, J.C., et al., The sequence of the human genome. *Science*, 2001. **291**(5507): p. 1304-51.
112. Wang, E.T., et al., Alternative isoform regulation in human tissue transcriptomes. *Nature*, 2008. **456**(7221): p. 470-6.

113. Rino, J. and M. Carmo-Fonseca, The spliceosome: a self-organized macromolecular machine in the nucleus? *Trends Cell Biol*, 2009. **19**(8): p. 375-84.
114. Ward, A.J. and T.A. Cooper, The pathobiology of splicing. *J Pathol*, 2010. **220**(2): p. 152-63.
115. Wang, G.S. and T.A. Cooper, Splicing in disease: disruption of the splicing code and the decoding machinery. *Nat Rev Genet*, 2007. **8**(10): p. 749-61.
116. Venables, J.P., Aberrant and alternative splicing in cancer. *Cancer Res*, 2004. **64**(21): p. 7647-54.
117. Skotheim, R.I. and M. Nees, Alternative splicing in cancer: noise, functional, or systematic? *Int J Biochem Cell Biol*, 2007. **39**(7-8): p. 1432-49.
118. Srebrow, A. and A.R. Kornblihtt, The connection between splicing and cancer. *J Cell Sci*, 2006. **119**(Pt 13): p. 2635-41.
119. Pajares, M.J., et al., Alternative splicing: an emerging topic in molecular and clinical oncology. *Lancet Oncol*, 2007. **8**(4): p. 349-57.
120. Brinkman, B.M., Splice variants as cancer biomarkers. *Clin Biochem*, 2004. **37**(7): p. 584-94.
121. Omenn, G.S., A.K. Yocum, and R. Menon, Alternative splice variants, a new class of protein cancer biomarker candidates: findings in pancreatic cancer and breast cancer with systems biology implications. *Dis Markers*, 2010. **28**(4): p. 241-51.
122. Cheng, C., M.B. Yaffe, and P.A. Sharp, A positive feedback loop couples Ras activation and CD44 alternative splicing. *Genes Dev*, 2006. **20**(13): p. 1715-20.
123. DiFeo, A., J.A. Martignetti, and G. Narla, The role of KLF6 and its splice variants in cancer therapy. *Drug Resist Updat*, 2009. **12**(1-2): p. 1-7.
124. Planque, C., et al., Alternative splicing variant of kallikrein-related peptidase 8 as an independent predictor of unfavorable prognosis in lung cancer. *Clin Chem*, 2010. **56**(6): p. 987-97.
125. Chen, L.L., et al., A mutation-created novel intra-exonic pre-mRNA splice site causes constitutive activation of KIT in human gastrointestinal stromal tumors. *Oncogene*, 2005. **24**(26): p. 4271-80.
126. Mazoyer, S., et al., A BRCA1 nonsense mutation causes exon skipping. *Am J Hum Genet*, 1998. **62**(3): p. 713-5.
127. Karni, R., et al., The gene encoding the splicing factor SF2/ASF is a proto-oncogene. *Nat Struct Mol Biol*, 2007. **14**(3): p. 185-93.
128. Ferretti, E., et al., Alternative splicing of the ErbB-4 cytoplasmic domain and its regulation by hedgehog signaling identify distinct medulloblastoma subsets. *Oncogene*, 2006. **25**(55): p. 7267-73.

129. Uchikawa, H., et al., Brain- and heart-specific Patched-1 containing exon 12b is a dominant negative isoform and is expressed in medulloblastomas. *Biochem Biophys Res Commun*, 2006. **349**(1): p. 277-83.
130. Li, X.N., et al., Differential expression of survivin splice isoforms in medulloblastomas. *Neuropathol Appl Neurobiol*, 2007. **33**(1): p. 67-76.
131. Glassmann, A., et al., Developmental expression and differentiation-related neuron-specific splicing of metastasis suppressor 1 (Mtss1) in normal and transformed cerebellar cells. *BMC Dev Biol*, 2007. **7**: p. 111.
132. Yarden, Y. and M.X. Sliwkowski, Untangling the ErbB signalling network. *Nat Rev Mol Cell Biol*, 2001. **2**(2): p. 127-37.
133. Gilbertson, R., et al., Novel ERBB4 juxtamembrane splice variants are frequently expressed in childhood medulloblastoma. *Genes Chromosomes Cancer*, 2001. **31**(3): p. 288-94.
134. Elenius, K., et al., A novel juxtamembrane domain isoform of HER4/ErbB4. Isoform-specific tissue distribution and differential processing in response to phorbol ester. *J Biol Chem*, 1997. **272**(42): p. 26761-8.
135. Altieri, D.C., Survivin, versatile modulation of cell division and apoptosis in cancer. *Oncogene*, 2003. **22**(53): p. 8581-9.
136. Caldas, H., et al., Survivin splice variants regulate the balance between proliferation and cell death. *Oncogene*, 2005. **24**(12): p. 1994-2007.
137. Fangusaro, J.R., et al., Survivin, Survivin-2B, and Survivin-deltaEx3 expression in medulloblastoma: biologic markers of tumour morphology and clinical outcome. *Br J Cancer*, 2005. **92**(2): p. 359-65.
138. Nagao, K., et al., Detecting tissue-specific alternative splicing and disease-associated aberrant splicing of the PTCH gene with exon junction microarrays. *Hum Mol Genet*, 2005. **14**(22): p. 3379-88.
139. Mattila, P.K., et al., Mouse MIM, a tissue-specific regulator of cytoskeletal dynamics, interacts with ATP-actin monomers through its C-terminal WH2 domain. *J Biol Chem*, 2003. **278**(10): p. 8452-9.
140. Callahan, C.A., et al., MIM/BEG4, a Sonic hedgehog-responsive gene that potentiates Gli-dependent transcription. *Genes Dev*, 2004. **18**(22): p. 2724-9.
141. Rodriguez, F.J., et al., Histopathologic grading of adult medulloblastomas. *Cancer*, 2007. **109**(12): p. 2557-65.
142. Affymetrix Technical Note. Gene Chip Human Exon 1.0 ST Array and GeneChip WT Sense Target Labeling Assay for Genome-Wide, Exon-Level Expression Analysis. Available from: http://media.affymetrix.com/support/technical/technotes/human_exon_wt_target_technote.pdf.
143. Affymetrix Datasheet. Exon Array System. Available from: http://media.affymetrix.com/support/technical/datasheets/exon_arraydesign_datasheet.pdf.

144. Affymetrix Technical note. Guide to Probe Logarithmic Intensity Error (PLIER) Estimation. Available from:
http://media.affymetrix.com/support/technical/technotes/plier_technote.pdf.
145. Smyth, G.K., Linear models and empirical bayes methods for assessing differential expression in microarray experiments. *Stat Appl Genet Mol Biol*, 2004. **3**: p. Article3.
146. Dennis, G., Jr., et al., DAVID: Database for Annotation, Visualization, and Integrated Discovery. *Genome Biol*, 2003. **4**(5): p. P3.
147. Irizarry, R.A., et al., Summaries of Affymetrix GeneChip probe level data. *Nucleic Acids Res*, 2003. **31**(4): p. e15.
148. Gardina, P.J., et al., Alternative splicing and differential gene expression in colon cancer detected by a whole genome exon array. *BMC Genomics*, 2006. **7**: p. 325.
149. Shah, S.H. and J.A. Pallas, Identifying differential exon splicing using linear models and correlation coefficients. *BMC Bioinformatics*, 2009. **10**: p. 26.
150. Affymetrix technical note. Identifying and validating alternative splicing events. Available from:
http://media.affymetrix.com/support/technical/technotes/id_altsplicingevents_technote.pdf.
151. Yates, T., M.J. Okoniewski, and C.J. Miller, X:Map: annotation and visualization of genome structure for Affymetrix exon array analysis. *Nucleic Acids Res*, 2008. **36**(Database issue): p. D780-6.
152. Jacobsen, P.F., D.J. Jenkyn, and J.M. Papadimitriou, Establishment of a human medulloblastoma cell line and its heterotransplantation into nude mice. *J Neuropathol Exp Neurol*, 1985. **44**(5): p. 472-85.
153. Keles, G.E., et al., Establishment and characterization of four human medulloblastoma-derived cell lines. *Oncol Res*, 1995. **7**(10-11): p. 493-503.
154. Graham, F.L., et al., Characteristics of a human cell line transformed by DNA from human adenovirus type 5. *J Gen Virol*, 1977. **36**(1): p. 59-74.
155. Naldini, L., et al., Efficient transfer, integration, and sustained long-term expression of the transgene in adult rat brains injected with a lentiviral vector. *Proc Natl Acad Sci U S A*, 1996. **93**(21): p. 11382-8.
156. Rozen, S. and H. Skaletsky, Primer3 on the WWW for general users and for biologist programmers. *Methods Mol Biol*, 2000. **132**: p. 365-86.
157. Ginzinger, D.G., Gene quantification using real-time quantitative PCR: an emerging technology hits the mainstream. *Exp Hematol*, 2002. **30**(6): p. 503-12.
158. Silva, J.M., et al., Second-generation shRNA libraries covering the mouse and human genomes. *Nat Genet*, 2005. **37**(11): p. 1281-8.
159. Demaison, C., et al., High-level transduction and gene expression in hematopoietic repopulating cells using a human immunodeficiency [correction of imunodeficiency]

- virus type 1-based lentiviral vector containing an internal spleen focus forming virus promoter. *Hum Gene Ther*, 2002. **13**(7): p. 803-13.
160. Stegmeier, F., et al., A lentiviral microRNA-based system for single-copy polymerase II-regulated RNA interference in mammalian cells. *Proc Natl Acad Sci U S A*, 2005. **102**(37): p. 13212-7.
 161. Open Biosystems website. GIPZ Lentiviral shRNAmir [cited 06/04/2010]; Available from: <http://www.openbiosystems.com/RNAi/shRNAmirLibraries/GIPZLentiviralshRNAmir/>.
 162. Huse, J.T. and E.C. Holland, Targeting brain cancer: advances in the molecular pathology of malignant glioma and medulloblastoma. *Nat Rev Cancer*, 2010. **10**(5): p. 319-31.
 163. Behesti, H. and S. Marino, Cerebellar granule cells: insights into proliferation, differentiation, and role in medulloblastoma pathogenesis. *Int J Biochem Cell Biol*, 2009. **41**(3): p. 435-45.
 164. Hatten, M.E., Neuronal regulation of astroglial morphology and proliferation in vitro. *J Cell Biol*, 1985. **100**(2): p. 384-96.
 165. Messer, A., The maintenance and identification of mouse cerebellar granule cells in monolayer culture. *Brain Res*, 1977. **130**(1): p. 1-12.
 166. Schuller, U., et al., Forkhead transcription factor FoxM1 regulates mitotic entry and prevents spindle defects in cerebellar granule neuron precursors. *Mol Cell Biol*, 2007. **27**(23): p. 8259-70.
 167. Trojanowski, J.Q., et al., In vivo and in vitro models of medulloblastomas and other primitive neuroectodermal brain tumors of childhood. *Mol Chem Neuropathol*, 1994. **21**(2-3): p. 219-39.
 168. Voskoglou-Nomikos, T., J.L. Pater, and L. Seymour, Clinical predictive value of the in vitro cell line, human xenograft, and mouse allograft preclinical cancer models. *Clin Cancer Res*, 2003. **9**(11): p. 4227-39.
 169. Friedman, H.S., et al., Establishment and characterization of the human medulloblastoma cell line and transplantable xenograft D283 Med. *J Neuropathol Exp Neurol*, 1985. **44**(6): p. 592-605.
 170. McAllister, R.M., et al., Establishment of a human medulloblastoma cell line. *Int J Cancer*, 1977. **20**(2): p. 206-12.
 171. Sasai, K., et al., Shh pathway activity is down-regulated in cultured medulloblastoma cells: implications for preclinical studies. *Cancer Res*, 2006. **66**(8): p. 4215-22.
 172. Kongkham, P.N., et al., The SFRP family of WNT inhibitors function as novel tumor suppressor genes epigenetically silenced in medulloblastoma. *Oncogene*, 2010. **29**(20): p. 3017-24.
 173. Rao, J.S., et al., MMP-9 short interfering RNA induced senescence resulting in inhibition of medulloblastoma growth via p16(INK4a) and mitogen-activated protein kinase pathway. *Cancer Res*, 2007. **67**(10): p. 4956-64.

174. Sanchez-Diaz, P.C., et al., Musashi1 modulates cell proliferation genes in the medulloblastoma cell line Daoy. *BMC Cancer*, 2008. **8**: p. 280.
175. von Bueren, A.O., et al., RNA interference-mediated c-MYC inhibition prevents cell growth and decreases sensitivity to radio- and chemotherapy in childhood medulloblastoma cells. *BMC Cancer*, 2009. **9**: p. 10.
176. Osawa, H., et al., The role of the membrane cytoskeleton cross-linker ezrin in medulloblastoma cells. *Neuro Oncol*, 2009. **11**(4): p. 381-93.
177. El-Sheikh, A., et al., Inhibition of Aurora Kinase A enhances chemosensitivity of medulloblastoma cell lines. *Pediatr Blood Cancer*, 2010. **55**(1): p. 35-41.
178. Acampora, D., et al., Otx genes in brain morphogenesis. *Prog Neurobiol*, 2001. **64**(1): p. 69-95.
179. Di, C., et al., Identification of OTX2 as a medulloblastoma oncogene whose product can be targeted by all-trans retinoic acid. *Cancer Res*, 2005. **65**(3): p. 919-24.
180. Adamson, D.C., et al., OTX2 is critical for the maintenance and progression of Shh-independent medulloblastomas. *Cancer Res*, 2010. **70**(1): p. 181-91.
181. Tanoue, T. and M. Takeichi, New insights into Fat cadherins. *J Cell Sci*, 2005. **118**(Pt 11): p. 2347-53.
182. Nakayama, M., et al., MEGF1/fat2 proteins containing extraordinarily large extracellular domains are localized to thin parallel fibers of cerebellar granule cells. *Mol Cell Neurosci*, 2002. **20**(4): p. 563-78.
183. Ju, Y.T., et al., gas7: A gene expressed preferentially in growth-arrested fibroblasts and terminally differentiated Purkinje neurons affects neurite formation. *Proc Natl Acad Sci U S A*, 1998. **95**(19): p. 11423-8.
184. Ebinger, M., et al., Expression of GAS7 in childhood CNS tumors. *Pediatr Blood Cancer*, 2006. **46**(3): p. 325-8.
185. Wang, W., et al., A role for nuclear factor I in the intrinsic control of cerebellar granule neuron gene expression. *J Biol Chem*, 2004. **279**(51): p. 53491-7.
186. Whitfield, M.L., et al., Identification of genes periodically expressed in the human cell cycle and their expression in tumors. *Mol Biol Cell*, 2002. **13**(6): p. 1977-2000.
187. Bucher, N. and C.D. Britten, G2 checkpoint abrogation and checkpoint kinase-1 targeting in the treatment of cancer. *Br J Cancer*, 2008. **98**(3): p. 523-8.
188. Kops, G.J., B.A. Weaver, and D.W. Cleveland, On the road to cancer: aneuploidy and the mitotic checkpoint. *Nat Rev Cancer*, 2005. **5**(10): p. 773-85.
189. Liu, X. and R.L. Erikson, Polo-like kinase (Plk)1 depletion induces apoptosis in cancer cells. *Proc Natl Acad Sci U S A*, 2003. **100**(10): p. 5789-94.
190. Vlotides, G., T. Eigler, and S. Melmed, Pituitary tumor-transforming gene: physiology and implications for tumorigenesis. *Endocr Rev*, 2007. **28**(2): p. 165-86.

191. Wagner, K.W., et al., Overexpression, genomic amplification and therapeutic potential of inhibiting the UbcH10 ubiquitin conjugase in human carcinomas of diverse anatomic origin. *Oncogene*, 2004. **23**(39): p. 6621-9.
192. Karamouzis, M.V., V.G. Gorgoulis, and A.G. Papavassiliou, Transcription factors and neoplasia: vistas in novel drug design. *Clin Cancer Res*, 2002. **8**(5): p. 949-61.
193. Brock, M.V., J.G. Herman, and S.B. Baylin, Cancer as a manifestation of aberrant chromatin structure. *Cancer J*, 2007. **13**(1): p. 3-8.
194. Negrini, S., V.G. Gorgoulis, and T.D. Halazonetis, Genomic instability--an evolving hallmark of cancer. *Nat Rev Mol Cell Biol*, 2010. **11**(3): p. 220-8.
195. Helleday, T., et al., DNA repair pathways as targets for cancer therapy. *Nat Rev Cancer*, 2008. **8**(3): p. 193-204.
196. Dai, Y. and S. Grant, New insights into checkpoint kinase 1 in the DNA damage response signaling network. *Clin Cancer Res*, 2010. **16**(2): p. 376-83.
197. Okamoto, Y., et al., UbcH10 is the cancer-related E2 ubiquitin-conjugating enzyme. *Cancer Res*, 2003. **63**(14): p. 4167-73.
198. Summers, M.K., et al., The unique N terminus of the UbcH10 E2 enzyme controls the threshold for APC activation and enhances checkpoint regulation of the APC. *Mol Cell*, 2008. **31**(4): p. 544-56.
199. van Ree, J.H., et al., Overexpression of the E2 ubiquitin-conjugating enzyme UbcH10 causes chromosome missegregation and tumor formation. *J Cell Biol*, 2010. **188**(1): p. 83-100.
200. Kurasawa, Y., et al., Essential roles of KIF4 and its binding partner PRC1 in organized central spindle midzone formation. *Embo J*, 2004. **23**(16): p. 3237-48.
201. Lee, Y.M., et al., Human kinesin superfamily member 4 is dominantly localized in the nuclear matrix and is associated with chromosomes during mitosis. *Biochem J*, 2001. **360**(Pt 3): p. 549-56.
202. Tran, P.T., et al., EXO1-A multi-tasking eukaryotic nuclease. *DNA Repair (Amst)*, 2004. **3**(12): p. 1549-59.
203. Collins, N., et al., An ACF1-ISWI chromatin-remodeling complex is required for DNA replication through heterochromatin. *Nat Genet*, 2002. **32**(4): p. 627-32.
204. Wong, J. and G. Fang, HURP controls spindle dynamics to promote proper interkinetochore tension and efficient kinetochore capture. *J Cell Biol*, 2006. **173**(6): p. 879-91.
205. Wong, J., et al., Aurora A regulates the activity of HURP by controlling the accessibility of its microtubule-binding domain. *Mol Biol Cell*, 2008. **19**(5): p. 2083-91.
206. Yu, C.T., et al., Phosphorylation and stabilization of HURP by Aurora-A: implication of HURP as a transforming target of Aurora-A. *Mol Cell Biol*, 2005. **25**(14): p. 5789-800.

207. Cheeseman, I.M., et al., KNL1 and the CENP-H/I/K complex coordinately direct kinetochore assembly in vertebrates. *Mol Biol Cell*, 2008. **19**(2): p. 587-94.
208. Zhao, B., et al., TEAD mediates YAP-dependent gene induction and growth control. *Genes Dev*, 2008. **22**(14): p. 1962-71.
209. Raemaekers, T., et al., NuSAP, a novel microtubule-associated protein involved in mitotic spindle organization. *J Cell Biol*, 2003. **162**(6): p. 1017-29.
210. Golsteyn, R.M., et al., Cell cycle regulation of the activity and subcellular localization of Plk1, a human protein kinase implicated in mitotic spindle function. *J Cell Biol*, 1995. **129**(6): p. 1617-28.
211. Eckerdt, F., J. Yuan, and K. Strebhardt, Polo-like kinases and oncogenesis. *Oncogene*, 2005. **24**(2): p. 267-76.
212. Yang, S., et al., Tustin is required for bipolar spindle assembly and centrosome integrity during mitosis. *Faseb J*, 2008. **22**(6): p. 1960-72.
213. Vierbuchen, T., et al., Direct conversion of fibroblasts to functional neurons by defined factors. *Nature*, 2010. **463**(7284): p. 1035-41.
214. Cook, A.L. and R.A. Sturm, POU domain transcription factors: BRN2 as a regulator of melanocytic growth and tumorigenesis. *Pigment Cell Melanoma Res*, 2008. **21**(6): p. 611-26.
215. Tfelt-Hansen, J., D. Kanuparthi, and N. Chattopadhyay, The emerging role of pituitary tumor transforming gene in tumorigenesis. *Clin Med Res*, 2006. **4**(2): p. 130-7.
216. Simon, J.A. and C.A. Lange, Roles of the EZH2 histone methyltransferase in cancer epigenetics. *Mutat Res*, 2008. **647**(1-2): p. 21-9.
217. Mullen, R.J., C.R. Buck, and A.M. Smith, NeuN, a neuronal specific nuclear protein in vertebrates. *Development*, 1992. **116**(1): p. 201-11.
218. Lin, X. and R.F. Bulleit, Insulin-like growth factor I (IGF-I) is a critical trophic factor for developing cerebellar granule cells. *Brain Res Dev Brain Res*, 1997. **99**(2): p. 234-42.
219. Nakai, S., et al., The POU domain transcription factor Brn-2 is required for the determination of specific neuronal lineages in the hypothalamus of the mouse. *Genes Dev*, 1995. **9**(24): p. 3109-21.
220. Schuller, U., et al., Cerebellar 'transcriptome' reveals cell-type and stage-specific expression during postnatal development and tumorigenesis. *Mol Cell Neurosci*, 2006. **33**(3): p. 247-59.
221. Manjunath, N., et al., Lentiviral delivery of short hairpin RNAs. *Adv Drug Deliv Rev*, 2009. **61**(9): p. 732-45.
222. Rajasekhar, V.K. and M. Begemann, Concise review: roles of polycomb group proteins in development and disease: a stem cell perspective. *Stem Cells*, 2007. **25**(10): p. 2498-510.

223. Michael, L.E., et al., Bmi1 is required for Hedgehog pathway-driven medulloblastoma expansion. *Neoplasia*, 2008. **10**(12): p. 1343-9, 5p following 1349.
224. Wiederschain, D., et al., Contribution of polycomb homologues Bmi-1 and Mel-18 to medulloblastoma pathogenesis. *Mol Cell Biol*, 2007. **27**(13): p. 4968-79.
225. Merve, A., X. Zhang, and S. Marino, Bmi-1 gene silencing causes BMP pathway activation and deregulation of cell adhesion in medulloblastoma cell lines. *Neuropathology and Applied Neurobiology*, 2010. **36**: p. 6.
226. Jiang, L., et al., Knockdown of ubiquitin-conjugating enzyme E2C/UbcH10 expression by RNA interference inhibits glioma cell proliferation and enhances cell apoptosis in vitro. *J Cancer Res Clin Oncol*, 2010. **136**(2): p. 211-7.
227. Lin, J., et al., Expression and effect of inhibition of the ubiquitin-conjugating enzyme E2C on esophageal adenocarcinoma. *Neoplasia*, 2006. **8**(12): p. 1062-71.
228. Mazumdar, M., S. Sundareshan, and T. Misteli, Human chromokinesin KIF4A functions in chromosome condensation and segregation. *J Cell Biol*, 2004. **166**(5): p. 613-20.
229. Zhu, C., et al., Functional analysis of human microtubule-based motor proteins, the kinesins and dyneins, in mitosis/cytokinesis using RNA interference. *Mol Biol Cell*, 2005. **16**(7): p. 3187-99.
230. Midorikawa, R., Y. Takei, and N. Hirokawa, KIF4 motor regulates activity-dependent neuronal survival by suppressing PARP-1 enzymatic activity. *Cell*, 2006. **125**(2): p. 371-83.
231. Taniwaki, M., et al., Activation of KIF4A as a prognostic biomarker and therapeutic target for lung cancer. *Clin Cancer Res*, 2007. **13**(22 Pt 1): p. 6624-31.
232. van Vugt, M.A. and R.H. Medema, Getting in and out of mitosis with Polo-like kinase-1. *Oncogene*, 2005. **24**(17): p. 2844-59.
233. Fu, Z., et al., Plk1-dependent phosphorylation of FoxM1 regulates a transcriptional programme required for mitotic progression. *Nat Cell Biol*, 2008. **10**(9): p. 1076-82.
234. Degenhardt, Y. and T. Lampkin, Targeting Polo-like kinase in cancer therapy. *Clin Cancer Res*, 2010. **16**(2): p. 384-9.
235. Grassi, G., et al., Inhibitors of DNA methylation and histone deacetylation activate cytomegalovirus promoter-controlled reporter gene expression in human glioblastoma cell line U87. *Carcinogenesis*, 2003. **24**(10): p. 1625-35.
236. Loser, P., et al., Reactivation of the previously silenced cytomegalovirus major immediate-early promoter in the mouse liver: involvement of NFkappaB. *J Virol*, 1998. **72**(1): p. 180-90.
237. Yokota, N., et al., Identification of differentially expressed and developmentally regulated genes in medulloblastoma using suppression subtraction hybridization. *Oncogene*, 2004. **23**(19): p. 3444-53.
238. Wechsler-Reya, R.J., Analysis of gene expression in the normal and malignant cerebellum. *Recent Prog Horm Res*, 2003. **58**: p. 227-48.

239. Nakano, I., et al., Maternal embryonic leucine zipper kinase (MELK) regulates multipotent neural progenitor proliferation. *J Cell Biol*, 2005. **170**(3): p. 413-27.
240. Townsley, F.M., et al., Dominant-negative cyclin-selective ubiquitin carrier protein E2-C/UbcH10 blocks cells in metaphase. *Proc Natl Acad Sci U S A*, 1997. **94**(6): p. 2362-7.
241. Cogswell, J.P., et al., Dominant-negative polo-like kinase 1 induces mitotic catastrophe independent of cdc25C function. *Cell Growth Differ*, 2000. **11**(12): p. 615-23.
242. Annabi, B., et al., Tumor environment dictates medulloblastoma cancer stem cell expression and invasive phenotype. *Mol Cancer Res*, 2008. **6**(6): p. 907-16.
243. Ranger, A., et al., The invasiveness of five medulloblastoma cell lines in collagen gels. *J Neurooncol*, 2010. **96**(2): p. 181-9.
244. Taipale, J., et al., Effects of oncogenic mutations in Smoothed and Patched can be reversed by cyclopamine. *Nature*, 2000. **406**(6799): p. 1005-9.
245. Bar, E.E., et al., Hedgehog signaling promotes medulloblastoma survival via Bc/II. *Am J Pathol*, 2007. **170**(1): p. 347-55.
246. Berman, D.M., et al., Medulloblastoma growth inhibition by hedgehog pathway blockade. *Science*, 2002. **297**(5586): p. 1559-61.
247. Zhang, C., et al., Profiling alternatively spliced mRNA isoforms for prostate cancer classification. *BMC Bioinformatics*, 2006. **7**: p. 202.
248. Dutertre, M., et al., Exon-based clustering of murine breast tumor transcriptomes reveals alternative exons whose expression is associated with metastasis. *Cancer Res*, 2010. **70**(3): p. 896-905.
249. French, P.J., et al., Identification of differentially regulated splice variants and novel exons in glial brain tumors using exon expression arrays. *Cancer Res*, 2007. **67**(12): p. 5635-42.
250. Thorsen, K., et al., Alternative splicing in colon, bladder, and prostate cancer identified by exon array analysis. *Mol Cell Proteomics*, 2008. **7**(7): p. 1214-24.
251. Wang, X., et al., Genome-wide prediction of cis-acting RNA elements regulating tissue-specific pre-mRNA alternative splicing. *BMC Genomics*, 2009. **10 Suppl 1**: p. S4.
252. de la Grange, P., et al., Splicing factor and exon profiling across human tissues. *Nucleic Acids Res*, 2010. **38**(9): p. 2825-38.
253. Lim, K.M., W.S. Yeo, and V.T. Chow, Antisense abrogation of DENN expression induces apoptosis of leukemia cells in vitro, causes tumor regression in vivo and alters the transcription of genes involved in apoptosis and the cell cycle. *Int J Cancer*, 2004. **109**(1): p. 24-37.
254. Al-Zoubi, A.M., et al., Contrasting effects of IG20 and its splice isoforms, MADD and DENN-SV, on tumor necrosis factor alpha-induced apoptosis and activation of caspase-8 and -3. *J Biol Chem*, 2001. **276**(50): p. 47202-11.

255. Efimova, E.V., et al., IG20, in contrast to DENN-SV, (MADD splice variants) suppresses tumor cell survival, and enhances their susceptibility to apoptosis and cancer drugs. *Oncogene*, 2004. **23**(5): p. 1076-87.
256. Subramanian, M., et al., Knockdown of IG20 gene expression renders thyroid cancer cells susceptible to apoptosis. *J Clin Endocrinol Metab*, 2009. **94**(4): p. 1467-71.
257. Miyoshi, J. and Y. Takai, Dual role of DENN/MADD (Rab3GEP) in neurotransmission and neuroprotection. *Trends Mol Med*, 2004. **10**(10): p. 476-80.
258. Li, L.C., et al., Regulation of apoptosis and caspase-8 expression in neuroblastoma cells by isoforms of the IG20 gene. *Cancer Res*, 2008. **68**(18): p. 7352-61.
259. Kurada, B.R., et al., MADD, a splice variant of IG20, is indispensable for MAPK activation and protection against apoptosis upon tumor necrosis factor-alpha treatment. *J Biol Chem*, 2009. **284**(20): p. 13533-41.
260. Mulherkar, N., K.V. Prasad, and B.S. Prabhakar, MADD/DENN splice variant of the IG20 gene is a negative regulator of caspase-8 activation. Knockdown enhances TRAIL-induced apoptosis of cancer cells. *J Biol Chem*, 2007. **282**(16): p. 11715-21.
261. Mulherkar, N., et al., MADD/DENN splice variant of the IG20 gene is necessary and sufficient for cancer cell survival. *Oncogene*, 2006. **25**(47): p. 6252-61.
262. Bockbrader, K. and Y. Feng, Essential function, sophisticated regulation and pathological impact of the selective RNA-binding protein QKI in CNS myelin development. *Future Neurol*, 2008. **3**(6): p. 655-668.
263. Chenard, C.A. and S. Richard, New implications for the QUAKING RNA binding protein in human disease. *J Neurosci Res*, 2008. **86**(2): p. 233-42.
264. Kondo, T., et al., Genomic organization and expression analysis of the mouse qkI locus. *Mamm Genome*, 1999. **10**(7): p. 662-9.
265. Galarneau, A. and S. Richard, Target RNA motif and target mRNAs of the Quaking STAR protein. *Nat Struct Mol Biol*, 2005. **12**(8): p. 691-8.
266. Sugnet, C.W., et al., Unusual intron conservation near tissue-regulated exons found by splicing microarrays. *PLoS Comput Biol*, 2006. **2**(1): p. e4.
267. Lauriat, T.L., et al., Developmental expression profile of quaking, a candidate gene for schizophrenia, and its target genes in human prefrontal cortex and hippocampus shows regional specificity. *J Neurosci Res*, 2008. **86**(4): p. 785-96.
268. Goode, B.L. and M.J. Eck, Mechanism and function of formins in the control of actin assembly. *Annu Rev Biochem*, 2007. **76**: p. 593-627.
269. Guilherme, A., et al., EHD2 and the novel EH domain binding protein EHP1 couple endocytosis to the actin cytoskeleton. *J Biol Chem*, 2004. **279**(11): p. 10593-605.
270. Peeters, P.J., et al., Sensory deficits in mice hypomorphic for a mammalian homologue of unc-53. *Brain Res Dev Brain Res*, 2004. **150**(2): p. 89-101.
271. Laura, R.P., et al., MAGI-1: a widely expressed, alternatively spliced tight junction protein. *Exp Cell Res*, 2002. **275**(2): p. 155-70.

272. Howarth, A.G., M.R. Hughes, and B.R. Stevenson, Detection of the tight junction-associated protein ZO-1 in astrocytes and other nonepithelial cell types. *Am J Physiol*, 1992. **262**(2 Pt 1): p. C461-9.
273. Murr, R., et al., Orchestration of chromatin-based processes: mind the TRRAP. *Oncogene*, 2007. **26**(37): p. 5358-72.
274. Fazio, T.G., J.T. Huff, and B. Panning, An RNAi screen of chromatin proteins identifies Tip60-p400 as a regulator of embryonic stem cell identity. *Cell*, 2008. **134**(1): p. 162-74.
275. Loizou, J.I., et al., Histone acetyltransferase cofactor Trrap is essential for maintaining the hematopoietic stem/progenitor cell pool. *J Immunol*, 2009. **183**(10): p. 6422-31.
276. Wurdak, H., et al., An RNAi screen identifies TRRAP as a regulator of brain tumor-initiating cell differentiation. *Cell Stem Cell*, 2010. **6**(1): p. 37-47.
277. Kops, G.J., D.R. Foltz, and D.W. Cleveland, Lethality to human cancer cells through massive chromosome loss by inhibition of the mitotic checkpoint. *Proc Natl Acad Sci U S A*, 2004. **101**(23): p. 8699-704.
278. Lee, E.Y., et al., Hedgehog pathway-regulated gene networks in cerebellum development and tumorigenesis. *Proc Natl Acad Sci U S A*, 2010. **107**(21): p. 9736-41.
279. Jelen, N., et al., Evolution of Nova-dependent splicing regulation in the brain. *PLoS Genet*, 2007. **3**(10): p. 1838-47.
280. Makeyev, E.V., et al., The MicroRNA miR-124 promotes neuronal differentiation by triggering brain-specific alternative pre-mRNA splicing. *Mol Cell*, 2007. **27**(3): p. 435-48.
281. Lee, J.A., Z.Z. Tang, and D.L. Black, An inducible change in Fox-1/A2BP1 splicing modulates the alternative splicing of downstream neuronal target exons. *Genes Dev*, 2009. **23**(19): p. 2284-93.
282. Johnson, M.B., et al., Functional and evolutionary insights into human brain development through global transcriptome analysis. *Neuron*, 2009. **62**(4): p. 494-509.
283. Cheng, L.C., et al., miR-124 regulates adult neurogenesis in the subventricular zone stem cell niche. *Nat Neurosci*, 2009. **12**(4): p. 399-408.
284. Calarco, J.A., et al., Regulation of vertebrate nervous system alternative splicing and development by an SR-related protein. *Cell*, 2009. **138**(5): p. 898-910.
285. Li, K.K., et al., miR-124 is frequently down-regulated in medulloblastoma and is a negative regulator of SLC16A1. *Hum Pathol*, 2009. **40**(9): p. 1234-43.
286. Uziel, T., et al., The miR-17~92 cluster collaborates with the Sonic Hedgehog pathway in medulloblastoma. *Proc Natl Acad Sci U S A*, 2009. **106**(8): p. 2812-7.

Appendix 1. Primer sets for PCR analysis of gene expression and alternative splicing.

Organism	Gene symbol/variant	Forward 5' - 3'	Reverse 5' - 3'	Assay
<i>Mm</i>	B2m	CTGACCGCCTGTATGCTAT	CAGTCTCAGTGGGGTGAAT	RT-PCR
<i>Mm</i>	Baz1a	TGCTGATGGAGAGACGATTG	TAGGTGGGTCATCAGGGAAG	RT-PCR
<i>Mm</i>	Casc5	ATTTTGAAACCCCAAGGAG	CTGAATTGGAGCACAAAGCA	RT-PCR
<i>Mm</i>	Chek1	CCAGAAAACCTCCTCTTGGA	AATTCTCCAGCCAACATTGC	RT-PCR
<i>Mm</i>	Dlg7	GGGAAGCTGGACCTGGACAT	TTGACCAACCGTTGTACGGATA	RT-PCR
<i>Mm</i>	Exo1	CAGGCTGTCATCACAGAGGA	CACGATATCGGGTTATTGG	RT-PCR
<i>Mm</i>	Ezh2	TTCGTGCCCTGTGTGATAGC	TGCACCGACATCCAGGAAA	RT-PCR
<i>Mm</i>	Foxm1	ACCTGGAGCAGAATCGGGTGA	ACAGAGTCTGCCAAGATGTTGA	RT-PCR
<i>Mm</i>	Gli1	CTTTCTGGTCTGCCCTTTTG	ATTACGGTTTGCAGGTCGAG	RT-PCR
<i>Mm</i>	Kif4	CCAGATGCTGGAGAGGATCATT	GCATGCCGCTGAGTTCT	RT-PCR
<i>Mm</i>	Math1	GGTGCAGCTGGACGCTTT	TCTGTCCATCATCGCTGT	RT-PCR
<i>Mm</i>	Melk	ATCCCTGGGTCATGCAAGATTA	AGGTGAGTCAAAGGAGTCTTGCTT	RT-PCR
<i>Mm</i>	Nusap1	GCTCACTGACCAAGACACCA	GCTTGTAGTTGAGGGGACGA	RT-PCR
<i>Mm</i>	Plk1	GGGTGCATCATGTATACCTTGCT	CTTGATCCGGAGGTAGGTCCTT	RT-PCR
<i>Mm</i>	Pou3f2	CAGCTGAGCTTCAAGAACATGTG	GAGGATGAGTCTGCCTCTTCCA	RT-PCR
<i>Mm</i>	Pttg1	CCGACCTTGACTGGGAAAAA	CATCAGGAGCAGGAACAGAAGT	RT-PCR
<i>Mm</i>	Tead2	TGCCTTCTCTCGTCAAGT	CAAAGGAGCAGACCTGGAG	RT-PCR
<i>Mm</i>	Troap	TAGCTCTGGGGATCAAATG	GGATTCTGGGAGCCAGGTAT	RT-PCR
<i>Mm</i>	Ube2c	ATCCTCATGACATCTGGTGACAAA	CCCCTTGAACAGTTGTCTGA	RT-PCR
<i>Mm</i>	Wdr7	TTGGCGATCACATGAAGAAG	GTCTGCCATCTTCGAGCTA	RT-PCR
<i>Mm</i>	Trrap	GCCTTCCCAAATCCTTC	GCTGGATCAGATGGAAAAG	RT-PCR
<i>Mm</i>	Daam1	GCCCTGAAATCCTCAACTG	TCATCAATGGCATCTGCTC	RT-PCR
<i>Mm</i>	Ehbp1	GATGACGAGAACCGTGTGAA	GCCAAGTCTTTTGTGCTC	RT-PCR
<i>Mm</i>	Magi1	GACGGCTCAGTCCCAGAATA	TGGGTAACCTGGACTCCAAGG	RT-PCR
<i>Mm</i>	Madd / exons 13L16	TGCCAGTGAAGTGGAGATTG	TCCTCAGGAAGTCTGGTT	RT-PCR
<i>Mm</i>	Madd / exon 34	GAGTTCCTGTGACGACAT	GCCATTGGCGTCTTGACTT	RT-PCR
<i>Mm</i>	Qk5	GCGGTGGCTACTAAAGTTCG	GCATGGTCAGGTCATATTG	Real Time PCR
<i>Mm</i>	Qk7	CTCACCAACTGCTGCAATA	GCAAGTCAATGGGCTGAAAT	Real Time PCR
<i>Hs</i>	B2M	GGCATTCTGAAGCTGACA	CGGCAGGCATACTCATCTT	RT-PCR
<i>Hs</i>	BAZ1A	GAAGTCTCCCTCCATCACA	GGTGGATCATCAGGAAGAA	RT-PCR
<i>Hs</i>	BMI1	CAGCAATGACTGTGATGCACT	GCCTGTCACTCCAGAGTC	RT-PCR
<i>Hs</i>	POU3F2	CACAAAATGCAGCTTCTGA	GGCTTCAACTCTCTCCGATG	RT-PCR
<i>Hs</i>	CASC5	TTCAAAAATGGATGGGGTGT	TCAAAGCATTGGATTCTGA	RT-PCR
<i>Hs</i>	CHEK1	CAGGGGTGGTTTATCTGCAT	TCCACAGGACCAAAACATCAA	RT-PCR
<i>Hs</i>	DLG7	ATGTTAAGCCAAGGGCAATG	TTGCTCGAACATCACTCTCG	RT-PCR
<i>Hs</i>	EXO1	GCTCCCTATGAAGCTGATGC	ACATTCCTAGCCGAGCTTGA	RT-PCR
<i>Hs</i>	FOXM1	CAACTCAGCCTCCAGGACTC	TCGAAGGCTCCTCAACCTTA	RT-PCR
<i>Hs</i>	KIF4A	CTGTTTTGGTTGCCCTGGAT	CACAAAGCCACCCTTTTGT	RT-PCR
<i>Hs</i>	MYC	GCTGCTTAGACGCTGGATT	CTGCTGCTGCTGGTAGAAGTT	RT-PCR
<i>Hs</i>	NUSAP1	AGCAACCAGGAAGAAGCTGA	CTGAGATCCTGGCTTCTCTG	RT-PCR
<i>Hs</i>	PLK1	GCCCTCACAGTCTCAATA	TACCAAGGCCGTACTTGTC	RT-PCR
<i>Hs</i>	PTTG1	GGACCCCTCAAACAAAACA	GAGAGGCACTCCACTCAAGG	RT-PCR
<i>Hs</i>	TEAD2	AGTTCTCAGCCTCTGTGGAA	TTGCCAAAAGAGCAGACCTT	RT-PCR
<i>Hs</i>	TROAP	CTCGTAAGCCATCATGACC	TCCCCAACATCTTTGTGAT	RT-PCR
<i>Hs</i>	UBE2C	TGGCGATAAAGGATTCTG	AGGGCAGACCACTTTTCCTT	RT-PCR
<i>Hs</i>	ATP2B1	GTGGCCAAATCTGTGGTTT	CCGGTTTTCTAACCTTCA	RT-PCR
<i>Hs</i>	DAAM1	CACAAATGCCCTGAAATCCT	TCATCAATGGCATCTGCTC	RT-PCR

<i>Hs</i>	EHBP1	ATGAAGCAGGCTGACATTGG	GCAGCATCAGGATCATCAAA	RT-PCR
<i>Hs</i>	MADD / exon 34	TGTGCAGGACCTGAAGACTG	TAGCCCCTCTCCATCAGCTA	RT-PCR
<i>Hs</i>	MADD / exons 13L16	CCTCTGACACATGCAGCACT	CACTAACGCCCTCCTGTTTC	RT-PCR
<i>Hs</i>	MADD / exon 21	CCAAAGGCTATGGCACAAC	CGCTGATCTGGGACTTTTTTC	RT-PCR
<i>Hs</i>	MADD / exon 26	AGAGACCCTTGAGCTGACA	GGTCCATACCCATCCCTTCT	RT-PCR
<i>Hs</i>	MAGI1 / exon 15	CCCAGTCCAGGAGCATGTAT	CACCCAGTGGTACGATGTGA	RT-PCR
<i>Hs</i>	MAGI1 / exon 24	GGAGACGGCTCAGTACCAGA	TGAAGATCGGGTGGGTAAC	RT-PCR
<i>Hs</i>	NAV2	CAGCAGTCAAAGCACAAGC	TGCGTCGGTTGTTAGCAGTA	RT-PCR
<i>Hs</i>	QKI-5	GCGGTGGCTACTAAAGTTCG	GCATGGTCAGGTCATCATTG	Real Time PCR
<i>Hs</i>	QKI-7	ACACATTGGCACCAGCTACA	AAAACAAAGGGTTGCACAG	Real Time PCR
<i>Hs</i>	R3HDM1	GGAAGCAGCAAAGCATAGG	GTCCAGGCACTGGGATCTA	RT-PCR
<i>Hs</i>	TJP1	GTCTGCCATTACACGGTCCT	GACTAACGGCTGGCTGTTTC	RT-PCR
<i>Hs</i>	TRRAP	GGCTCTCCCAAATTCCTTC	AGCAAAGGCTTCACCAAGTGT	RT-PCR
<i>Hs</i>	WDR7	CGTATCGTTTGGCCTCTTGT	GGCAGCATAACACAGTGCAT	RT-PCR

Appendix 2. List of genes significantly up-regulated in Shh-driven medulloblastomas.

Transcript ID	Gene Symbol	SHH-Ad CB		SHH- CB		SHH-MB2		Transcript ID	Gene Symbol	SHH-Ad CB		SHH- CB		SHH-MB2	
		FC	DEG	FC	DEG	FC	DEG			FC	DEG	FC	DEG	FC	DEG
2946215	HIST1H3B	6.7	DEG	4.9	--	0.5	--	3463112	E2F7	2.6	DEG	1.9	--	0.9	--
2899102	HIST1H3C	6.5	DEG	4.9	--	1.1	--	3490655	CKAP2	2.6	--	2.4	DEG	0.6	--
2947081	HIST1H4L	6.0	DEG	5.0	--	1.8	--	3673684	CDT1	2.5	--	2.3	DEG	0.9	--
3440598	FOXM1	5.7	--	4.8	DEG	1.9	--	2450345	KIF14	2.5	--	2.2	DEG	0.5	--
2470838	MYCN	5.7	DEG	4.5	DEG	3.8	DEG	3235789	MCM10	2.5	DEG	2.2	DEG	-0.3	--
3756193	TOP2A	5.2	DEG	4.1	DEG	-0.4	--	2859667	ADAMTS6	2.5	DEG	2.0	--	0.5	--
3590388	NUSAP1	5.2	DEG	4.1	DEG	1.0	--	3225855	ANGPTL2	0.6	--	0.5	--	2.5	DEG
2946369	HIST1H3G	5.1	DEG	4.3	--	0.9	--	3727449	TOM1L1	1.7	--	2.0	--	2.5	DEG
2900059	HIST1H2BM	4.9	DEG	3.4	--	1.0	--	3458783	CDK4	2.5	--	2.3	DEG	1.0	--
2469252	RRM2	4.7	DEG	3.6	--	-0.4	--	2980241	FBXO5	2.5	--	2.2	DEG	0.6	--
3587457	ARHGAP11A	4.7	DEG	3.9	DEG	1.4	--	3639031	PRC1	2.5	--	2.3	DEG	0.1	--
3629103	KIAA0101	4.7	--	3.8	DEG	-0.4	--	3903146	E2F1	2.5	DEG	2.0	DEG	0.0	--
3445741	MGP	4.7	DEG	3.7	--	2.7	--	4006280	NDP	-0.3	--	-0.5	--	2.5	DEG
2333136	CDC20	4.7	--	4.0	DEG	1.4	--	3288518	C10orf72	1.4	--	1.4	--	2.4	DEG
4035833	CD24	4.6	DEG	3.5	--	0.6	--	3861786	FBXO17	0.4	--	0.7	--	2.4	DEG
2745899	HHIP	2.3	--	2.1	--	4.6	DEG	2703902	BCHE	1.5	--	1.1	--	2.4	DEG
3887049	UBE2C	4.6	DEG	3.7	DEG	1.1	--	3676300	RPS2	2.4	DEG	2.4	--	1.4	--
3595979	CCNB2	4.5	DEG	3.9	DEG	1.2	--	2427619	KCNA3	0.7	--	0.8	--	2.4	DEG
3788560	DCC	4.5	DEG	3.8	--	1.3	--	2965739	C6orf167	2.4	--	1.9	DEG	1.0	--
3312490	MKI67	4.5	DEG	3.4	DEG	1.1	--	3750785	SPAG5	2.4	--	2.1	DEG	-0.1	--
3881443	TPX2	4.5	DEG	3.6	DEG	0.9	--	3703112	GINS2	2.4	--	2.2	DEG	-0.3	--
2838201	PTTG1	4.5	DEG	3.7	DEG	1.5	--	2894573	GCNT2	1.1	--	0.8	--	2.3	DEG
4018218	DCX	4.4	DEG	2.5	--	0.0	--	3720896	WIPF2	2.3	--	2.0	DEG	-0.5	--
3428268	GAS2L3	4.4	DEG	3.1	--	1.2	--	3890109	C20orf108	2.1	--	2.3	DEG	1.2	--
2654454	SOX2	1.4	--	0.8	--	4.4	DEG	2714955	TACC3	2.3	--	2.0	DEG	0.5	--
2720251	NCAPG	4.3	DEG	3.4	DEG	0.9	--	2780172	CENPE	2.3	--	2.1	DEG	0.6	--
2796951	PDLIM3	2.0	--	1.2	--	4.3	DEG	2569908	SEP10	2.3	--	1.7	--	2.3	DEG
2899756	HIST1H2AG	4.2	DEG	3.4	DEG	0.4	--	3454223	RACGAP1	2.3	--	2.0	DEG	-0.5	--
2736224	ATOX1	3.3	--	2.5	--	4.2	DEG	4021508	SUHW3	2.3	--	2.1	DEG	1.0	--
2900051	HIST1H3H	4.2	DEG	3.6	DEG	0.9	--	2540157	ODC1	2.3	--	1.9	DEG	-0.5	--
3440568	NRIP2	1.2	--	1.9	--	4.2	DEG	2373564	CRB1	-0.1	--	-0.2	--	2.3	DEG
2363128	NHLH1	4.2	DEG	2.6	--	2.3	--	3169331	ALDH1B1	2.3	--	2.1	DEG	0.5	--
2816459	F2R	4.2	DEG	2.9	--	1.2	--	2620256	KIF15	2.3	--	2.0	DEG	0.2	--
2946219	HIST1H2AB	4.1	DEG	3.4	DEG	0.9	--	3865568	SNRPD2	2.3	--	2.0	DEG	0.8	--
2798915	TRIP13	4.1	--	3.7	DEG	1.5	--	2783596	PDE5A	1.8	--	1.5	--	2.3	DEG
3565663	DLG7	4.1	DEG	3.6	DEG	0.9	--	2783715	MAD2L1	2.2	--	2.1	DEG	0.8	--
3449700	FAM60A	4.1	--	3.6	DEG	2.1	--	3197955	GLDC	1.1	--	0.7	--	2.2	DEG
2946225	HIST1H2BB	4.1	DEG	3.2	--	0.9	--	3130244	TEX15	2.2	--	1.8	DEG	2.1	DEG
3140037	EYA1	3.8	DEG	3.5	DEG	4.0	DEG	3983537	PABPC5	1.6	--	1.3	--	2.2	DEG
3927392	CYYR1	4.0	DEG	3.0	--	3.6	DEG	3527493	APEX1	2.2	--	1.9	DEG	0.8	--
2830638	KIF20A	4.0	--	3.4	DEG	1.3	--	3670772	CMIP	2.2	--	1.9	DEG	1.7	DEG
3611625	ALDH1A3	2.6	--	2.9	--	4.0	DEG	3563395	POLE2	2.2	DEG	1.8	DEG	0.2	--
3168508	MELK	4.0	DEG	3.3	DEG	0.7	--	3168938	POLR1E	2.2	--	2.0	DEG	1.2	--
2379863	CENPF	4.0	DEG	3.2	DEG	0.4	--	3342426	FLJ25416	2.2	--	2.0	DEG	0.4	--
2467855	SOX11	4.0	DEG	2.7	--	0.3	--	2970532	HDAC2	2.2	--	2.0	DEG	0.3	--
3258168	KIF11	4.0	DEG	3.3	DEG	0.8	--	3924573	PCNT	2.2	--	2.0	DEG	2.0	DEG
2650199	SMC4	3.8	--	3.3	DEG	0.9	--	3845365	TCF3	2.1	--	1.7	DEG	0.9	--
2752725	NEIL3	3.8	--	3.2	DEG	1.0	--	2633691	TMEM45A	2.1	--	1.8	--	1.6	DEG
3061319	CDK6	3.8	DEG	2.8	--	0.5	--	3427352	NEDD1	2.1	--	2.0	DEG	0.7	--
2636319	BOC	2.9	--	2.1	--	3.8	DEG	2522212	SGOL2	2.1	--	2.0	DEG	0.6	--

Transcript ID	Gene Symbol	SHH-Ad CB		SHH- CB		SHH-MB2		Transcript ID	Gene Symbol	SHH-Ad CB		SHH- CB		SHH-MB2	
		FC	DEG	FC	DEG	FC	DEG			FC	DEG	FC	DEG	FC	DEG
2604254	DKFZp762E1312	3.8	DEG	3.0	DEG	1.0	--	2617276	CTDSPL	0.5	--	0.4	--	2.1	DEG
3401804	DYRK4	3.7	--	3.5	DEG	1.5	--	3928070	CCT8	1.7	--	2.1	DEG	0.8	--
3653072	PLK1	3.7	--	3.2	DEG	1.0	--	2797393	FAT	-1.0	--	-0.8	--	2.1	DEG
3354799	CHEK1	3.6	DEG	2.9	DEG	0.4	--	2781138	LEF1	1.9	--	1.4	--	2.1	DEG
3855856	EDG4	3.6	DEG	2.3	--	0.6	--	2838656	HMMR	2.1	--	2.0	DEG	0.9	--
2378937	DTL	3.6	DEG	2.8	DEG	-0.2	--	2339786	PGM1	0.6	--	0.8	--	2.1	DEG
3736290	BIRC5	3.6	DEG	3.0	DEG	0.3	--	3680583	RSL1D1	2.0	--	2.1	DEG	1.1	--
2388219	EXO1	3.6	DEG	2.9	DEG	0.5	--	3619945	OIP5	2.1	--	1.9	DEG	0.2	--
3504617	C13orf3	3.6	--	3.0	DEG	0.6	--	2823551	MAN2A1	0.9	--	0.8	--	2.1	DEG
3728964	PRR11	3.6	--	3.0	DEG	0.7	--	2407191	GNL2	2.0	--	2.0	DEG	1.1	--
2740896	NDST3	1.1	--	1.0	--	3.6	DEG	2431112	NOTCH2	0.1	--	-0.2	--	2.0	DEG
3744263	AURKB	3.5	DEG	2.8	--	0.9	--	2589255	FKBP7	2.0	--	1.8	DEG	0.9	--
3599811	KIF23	3.5	DEG	2.9	DEG	0.6	--	2416218	ITGB3BP	2.0	--	1.9	DEG	0.7	--
2334098	KIF2C	3.5	DEG	3.0	DEG	0.9	--	2694817	PLXND1	2.0	--	1.9	DEG	1.9	DEG
3129149	PBK	3.5	DEG	2.9	--	0.7	--	4052881	FAM72A	2.0	--	2.0	DEG	0.8	--
2784113	CCNA2	3.4	--	2.9	DEG	0.9	--	3979659	MSN	1.0	--	0.8	--	2.0	DEG
2570616	BUB1	3.4	DEG	2.8	DEG	0.6	--	2698565	TFDP2	2.0	--	1.7	--	1.9	DEG
2449559	F13B	3.4	DEG	2.8	DEG	0.6	--	3845868	LSM7	2.0	--	1.9	DEG	0.6	--
3178583	CKS2	3.4	DEG	3.1	DEG	0.4	--	3983228	DACH2	2.0	--	1.9	--	1.8	DEG
2516023	CDCA7	3.4	DEG	2.9	--	0.6	--	3603408	PSMA4	1.7	--	2.0	DEG	0.5	--
2748198	KIAA0922	3.4	--	2.4	--	2.6	DEG	2687979	KIAA1524	2.0	--	1.7	DEG	0.4	--
3560711	BAZ1A	3.4	DEG	2.8	DEG	1.3	--	2827185	LMNB1	1.9	--	1.8	DEG	-0.2	--
2364438	NUF2	3.3	DEG	2.8	DEG	0.3	--	3200611	SCARNA8	1.8	--	1.9	DEG	1.1	DEG
2947100	HIST1H2AM	3.3	DEG	2.6	DEG	0.4	--	3561532	SLC25A21	1.9	--	1.9	DEG	1.9	DEG
3980560	KIF4A	3.3	DEG	2.8	DEG	0.7	--	2695941	TOPBP1	1.9	--	1.7	DEG	0.7	--
2914777	TTK	3.3	DEG	2.9	DEG	0.6	--	3164914	MTAP	1.9	--	1.8	DEG	1.5	--
3949055	GTSE1	3.3	DEG	2.6	DEG	0.5	--	3529908	NFATC4	1.5	--	1.4	--	1.9	DEG
2594089	SATB2	2.8	--	2.1	--	3.3	DEG	3523881	KDEL1	1.9	--	1.8	DEG	1.3	DEG
3850660	SPC24	3.2	DEG	2.6	--	0.2	--	3493391	C13orf34	1.8	--	1.9	DEG	0.8	--
2899772	HIST1H2AH	3.2	DEG	2.8	--	1.5	--	3721452	FKBP10	1.5	--	1.1	--	1.9	DEG
2494484	NCAPH	3.2	DEG	2.8	DEG	0.5	--	3974098	MID1IP1	1.2	--	1.4	--	1.9	DEG
3765580	BRIP1	3.2	DEG	2.5	DEG	-0.2	--	3821908	RNASEH2A	1.9	--	1.8	DEG	0.0	--
2947063	HIST1H2AK	3.2	DEG	2.5	--	0.8	--	3484641	BRCA2	1.8	--	1.5	DEG	0.0	--
3677969	SRL	3.2	--	3.0	DEG	3.2	DEG	3204534	FANCG	1.6	--	1.8	DEG	0.8	--
3867796	TEAD2	3.2	DEG	2.4	--	1.5	--	2911413	PRIM2A	1.8	--	1.7	DEG	0.3	--
2454444	NEK2	3.2	--	2.8	DEG	0.4	--	4001369	SCML2	1.8	--	1.5	DEG	0.9	--
2897899	SOX4	3.2	DEG	1.9	--	-1.0	--	4012299	PHKA1	0.8	--	0.8	--	1.8	DEG
2813414	CCNB1	3.2	--	3.0	DEG	1.0	--	2532699	INPP5D	1.3	--	1.2	--	1.8	DEG
3780334	MCSR	3.1	--	2.9	--	2.9	DEG	2727116	RASL11B	0.4	--	0.9	--	1.8	DEG
3590014	CASC5	3.1	DEG	2.5	DEG	0.4	--	3040897	CDCA7L	1.8	--	1.8	--	1.5	DEG
3883941	TGIF2	3.1	DEG	2.3	--	2.4	--	3879467	XRN2	1.8	--	1.8	DEG	0.7	--
3391653	DRD2	3.1	DEG	2.9	--	2.3	--	3565571	WDHD1	1.8	--	1.7	DEG	0.1	--
2858592	DEPDC1B	3.1	DEG	2.6	DEG	0.2	--	3996667	DKC1	1.7	--	1.8	DEG	0.3	--
3291435	PLEKHK1	3.1	DEG	2.5	DEG	0.3	--	2412799	ORC1L	1.7	--	1.5	DEG	0.3	--
3248289	CDC2	3.1	DEG	2.6	DEG	0.4	--	4007216	UXT	1.7	--	1.7	DEG	0.9	--
2520429	MYO1B	3.1	DEG	2.4	--	1.2	--	3367036	CCDC34	1.7	--	1.7	DEG	0.4	--
2652675	ECT2	3.1	DEG	3.0	DEG	1.0	--	3944147	MCM5	1.7	--	1.6	DEG	0.4	--
3776139	NDC80	3.1	DEG	2.6	DEG	0.6	--	3428845	C12orf48	1.7	--	1.5	DEG	0.5	--
2791419	C4orf18	1.5	--	1.6	--	3.0	DEG	3911814	SLMO2	1.4	--	1.7	DEG	0.3	--
2665572	SGOL1	3.0	--	2.6	DEG	0.7	--	3250055	DDX21	1.5	--	1.7	DEG	0.1	--
3607510	FANCI	3.0	--	2.7	DEG	0.9	--	2603987	NGEF	1.6	--	1.5	--	1.6	DEG
3413875	TROAP	3.0	--	2.6	DEG	0.8	--	3831260	ZNF146	1.6	--	1.6	DEG	0.5	--
3607698	C15orf42	3.0	DEG	2.2	--	1.0	--	3488942	NUDT15	1.6	--	1.6	DEG	0.3	--

Transcript ID	Gene Symbol	SHH-Ad CB		SHH- CB		SHH-MB2		Transcript ID	Gene Symbol	SHH-Ad CB		SHH- CB		SHH-MB2	
		FC	DEG	FC	DEG	FC	DEG			FC	DEG	FC	DEG	FC	DEG
2470805	MYCN	3.0	--	2.8	DEG	2.3	DEG	2409847	PTCH2	1.3	--	1.2	--	1.6	DEG
3302533	SFRP5	2.4	--	2.5	--	3.0	DEG	2332711	PPIH	1.6	--	1.5	DEG	0.8	--
2640855	MCM2	3.0	DEG	2.8	DEG	0.9	--	3463522	PAWR	1.5	--	1.3	--	1.6	DEG
2330773	CDCA8	3.0	--	2.6	DEG	1.1	--	2691798	IQCB1	1.4	--	1.6	DEG	0.8	--
3968303	SHROOM2	3.0	--	2.9	DEG	2.7	DEG	3421177	NUP107	1.4	--	1.6	DEG	0.5	--
2710599	CLDN1	2.9	--	2.8	--	2.8	DEG	3929038	C21orf45	1.6	--	1.5	DEG	0.8	--
2571457	IL1A	2.9	DEG	2.5	DEG	0.3	--	3852034	TRMT1	1.6	--	1.5	DEG	0.7	--
3910785	AURKA	2.9	--	2.7	DEG	1.0	--	4012142	FLJ20105	1.6	--	1.4	DEG	0.5	--
2918388	POU3F2	2.2	--	1.4	--	2.9	DEG	3485863	EXOSC8	1.6	--	1.5	DEG	0.5	--
3078348	EZH2	2.9	DEG	2.0	--	-0.5	--	2616166	CRTAP	1.1	--	1.2	--	1.6	DEG
2915571	C6orf117	1.2	--	1.6	--	2.9	DEG	2543066	C2orf43	1.6	--	1.4	DEG	-0.3	--
2451200	UBE2T	2.9	--	2.6	DEG	0.3	--	2340186	RAVER2	0.4	--	0.6	--	1.5	DEG
3333595	GNG3	-1.5	--	-1.6	--	2.8	DEG	3160773	RCL1	1.5	--	1.4	DEG	1.2	DEG
3587495	SCG5	-0.2	--	0.3	--	2.8	DEG	3877776	SNRPB2	1.5	--	1.5	DEG	0.4	--
2417528	DEPDC1	2.8	--	2.4	DEG	0.5	--	3838809	PRMT1	1.5	--	1.5	DEG	0.2	--
3367338	KIF18A	2.8	DEG	2.5	DEG	0.9	--	2593352	GTF3C3	1.4	--	1.5	DEG	0.5	--
3862167	DYRK1B	2.8	DEG	2.5	DEG	1.4	--	2741768	EXOSC9	1.3	--	1.5	DEG	0.7	--
2541523	MYCNOS	2.7	--	2.4	--	2.1	DEG	3875195	MCM8	1.3	--	1.5	DEG	0.5	--
3555300	CCNB1IP1	2.7	--	2.3	DEG	1.8	DEG	3167383	NUDT2	1.4	--	1.4	DEG	0.9	--
3884892	FAM83D	2.7	DEG	2.2	--	0.5	--	3246888	PRKG1	0.4	--	0.5	--	1.4	DEG
3576441	CCDC88C	2.7	DEG	1.8	--	0.5	--	3627363	NARG2	1.4	--	1.4	DEG	0.5	--
2451958	RPL21	1.0	--	1.0	--	2.7	DEG	3852691	DDX39	1.4	--	1.4	DEG	0.2	--
3400190	CCDC77	2.7	--	2.5	DEG	1.4	--	2805786	TARS	1.2	--	1.4	DEG	0.5	--
3420442	IRAK3	2.4	--	1.9	--	2.7	DEG	3257338	MPHOSPH1	1.4	--	1.4	DEG	0.3	--
2593796	RFTN2	-0.2	--	-0.3	--	2.7	DEG	2944068	DEK	1.2	--	1.4	DEG	0.3	--
3515965	DIAPH3	2.7	DEG	2.0	--	0.7	--	2645764	ATP1B3	0.9	--	1.0	--	1.3	DEG
3377423	CDCA5	2.7	--	2.3	DEG	0.6	--	3318009	RRM1	1.2	--	1.3	DEG	0.0	--
2654023	ACTL6A	2.6	--	2.7	DEG	0.9	--	3556924	PRMT5	1.3	--	1.3	DEG	0.4	--
2742985	PLK4	2.7	DEG	2.1	DEG	0.4	--	3373724	SSRP1	1.3	--	1.3	DEG	0.2	--
2584134	IFIH1	2.6	--	2.3	DEG	2.5	DEG	2893721	RIOK1	1.1	--	1.3	DEG	0.0	--
3402571	NCAPD2	2.6	--	2.3	DEG	0.8	--	3468261	NUP37	1.2	--	1.2	DEG	0.1	--
3063685	MCM7	2.6	DEG	2.0	--	0.3	--	2809885	SKIV2L2	1.1	--	1.2	DEG	0.4	--
2380590	TGFB2	0.8	--	0.6	--	2.6	DEG	2425118	SASS6	1.2	--	1.2	DEG	0.3	--
3635737	RKHD3	2.6	DEG	1.8	--	-0.2	--	3252170	ADK	1.1	--	1.2	--	1.1	DEG
3536336	CDKN3	2.6	--	2.5	DEG	0.1	--	3200689	RPS6	1.1	--	1.1	DEG	0.6	--
3258444	CEP55	2.6	--	2.3	DEG	0.9	--	3259503	DNTT	1.1	--	1.0	--	1.0	DEG

Ad CB, adult cerebellum; CB, cerebellum (including adult and fetal samples); FC, fold change in gene expression; DEG, differentially expressed gene.

Appendix 3. List of genes significantly down-regulated in Shh-driven medulloblastomas.

Transcript ID	Gene Symbol	SHH-Ad CB		SHH- CB		SHH-MB2		Transcript ID	Gene Symbol	SHH-Ad CB		SHH- CB		SHH-MB2	
		FC	DEG	FC	DEG	FC	DEG			FC	DEG	FC	DEG	FC	DEG
2838399	GABRA6	-7.4	DEG	-5.2	--	-1.2	--	2679406	CADPS	-2.0	--	-1.8	--	-3.2	DEG
3558270	CBLN3	-6.9	DEG	-4.2	--	-0.1	--	4054481	GABRD	-3.2	DEG	-1.9	--	-0.3	--
2882026	FAT2	-6.6	DEG	-5.8	DEG	-0.3	--	2833286	ARHGAP26	-3.2	--	-2.8	DEG	0.4	--
3985717	PLP1	-6.2	DEG	-6.3	--	-1.3	--	2842194	CPLX2	-3.1	--	-2.8	DEG	-0.4	--
3830320	MAG	-5.6	DEG	-6.2	DEG	-0.3	--	3779950	C18orf1	-3.1	DEG	-3.0	--	-2.4	--
2513471	SCN2A	-5.7	DEG	-4.4	DEG	-1.9	--	3841102	PRKCG	-3.1	--	-2.5	DEG	0.1	--
3887241	SLC12A5	-5.6	DEG	-4.4	--	-1.6	--	2587790	GPR155	-3.1	DEG	-2.8	--	-1.3	--
3762753	CA10	-5.6	DEG	-4.8	DEG	-2.9	--	2339139	INADL	-3.1	DEG	-2.1	--	-1.3	--
2678448	FAM107A	-5.5	DEG	-5.2	DEG	-2.5	--	3946944	CSDC2	-3.1	DEG	-2.8	DEG	-0.9	--
3662093	MT3	-5.4	--	-5.2	DEG	-2.0	--	2764004	LGI2	-3.1	DEG	-2.3	--	0.4	--
3280573	NEBL	-5.4	DEG	-4.7	DEG	-1.2	--	3260985	SFXN3	-3.1	--	-3.0	DEG	-2.9	DEG
3144033	CALB1	-5.4	DEG	-4.7	--	0.0	--	3528013	RPGRIP1	0.4	--	0.3	--	-3.1	DEG
3177111	NTRK2	-5.4	DEG	-5.3	DEG	-2.8	--	2975867	MAP3K5	-3.1	--	-2.9	DEG	-0.5	--
3396249	HEPACAM	-5.4	DEG	-5.3	--	-0.8	--	2715016	FGFR3	-3.1	--	-2.4	DEG	-0.4	--
3867842	SLC17A7	-5.4	--	-4.6	DEG	-3.3	DEG	2362469	CADM3	-3.1	--	-2.8	DEG	-2.1	DEG
2408041	HPCAL4	-5.3	DEG	-4.3	DEG	-0.7	--	2321466	KIAA1026	-3.1	--	-2.8	DEG	-0.2	--
2838416	GABRA1	-5.3	DEG	-3.9	--	-2.5	--	2829905	FBXL21	-0.3	--	-0.3	--	-3.0	DEG
2512752	TBR1	0.0	--	0.0	--	-5.2	DEG	3155901	KCNK9	-3.0	--	-2.6	DEG	1.1	--
3214227	DIRAS2	-5.2	DEG	-3.9	--	-2.1	--	3884793	SLC32A1	-3.0	DEG	-2.4	--	0.0	--
3700158	ADAMTS18	-4.9	DEG	-3.9	--	-0.7	--	3572929	ZDHHC22	0.0	--	-0.2	--	-3.0	DEG
2511153	KCNJ3	-4.8	--	-4.6	DEG	-0.6	--	3779207	GNAL	-3.0	DEG	-3.0	--	-2.4	--
2900940	MOG	-4.5	DEG	-4.8	DEG	-0.5	--	3189714	GARNL3	-3.0	DEG	-2.8	DEG	-1.7	--
3401994	KCNA1	-4.8	DEG	-3.6	--	-3.4	--	3693141	PLLP	-2.9	--	-3.0	DEG	-0.2	--
3744965	GAS7	-4.8	DEG	-4.1	DEG	-0.9	--	3901191	NAPB	-3.0	DEG	-2.1	--	-2.1	--
3190242	DNM1	-4.8	DEG	-4.1	DEG	-2.8	DEG	3384718	DLG2	-3.0	--	-2.9	DEG	-0.5	--
3965536	MLC1	-4.8	DEG	-4.7	DEG	-1.3	--	2398820	PADI2	-3.0	--	-2.7	DEG	-0.7	--
3751237	SEZ6	-3.1	--	-3.0	--	-4.8	DEG	3788097	MAPK4	-3.0	DEG	-2.5	--	-1.0	--
2950970	GRM4	-4.8	--	-3.9	DEG	0.0	--	3900545	NKX2-2	-3.0	--	-3.0	DEG	-0.1	--
3750767	SPAG5	-4.8	DEG	-4.2	--	-0.3	--	2906333	DAAM2	-3.0	--	-2.8	DEG	-0.7	--
3684007	ZP2	-4.7	DEG	-2.7	--	0.2	--	3267382	INPP5F	-3.0	DEG	-2.6	--	-2.2	--
3708938	ATP1B2	-4.7	DEG	-4.4	DEG	-2.8	--	3590498	TCEB1	-2.9	--	-2.5	DEG	-0.4	--
2994835	CHN2	-4.7	--	-3.5	--	-4.0	DEG	2999334	HECW1	-2.9	--	-2.9	DEG	-0.3	--
2438169	C1orf61	-4.6	--	-4.7	DEG	-2.0	--	3063035	TMEM130	-2.9	--	-2.8	DEG	-2.1	--
2602770	DNER	-4.6	DEG	-4.4	--	-1.7	--	2841699	CPEB4	-2.9	DEG	-2.8	--	-1.9	--
3210497	KIAA0367	-4.6	DEG	-3.5	--	-0.7	--	2997907	EPDR1	-2.9	DEG	-2.1	--	0.2	--
2643217	TF	-4.6	DEG	-4.6	--	-1.1	--	2475911	EHD3	-2.9	DEG	-2.2	--	0.2	--
2959039	KHDRBS2	-0.7	--	-1.1	--	-4.6	DEG	2578790	LRP1B	-2.9	--	-2.9	DEG	0.0	--
3841439	TTYH1	-4.5	--	-4.6	DEG	-1.1	--	3301782	TMEM10	-2.8	--	-2.7	DEG	0.5	--
3720322	PPP1R1B	-4.5	--	-4.1	DEG	-1.5	--	3957938	PISD	-2.8	DEG	-2.0	--	-1.1	--
3137120	CA8	-4.5	DEG	-3.8	DEG	-0.1	--	2324820	EPHA8	0.1	--	-0.3	--	-2.8	DEG
2767932	GABRG1	-4.5	--	-4.5	DEG	-0.8	--	3364878	ABCC8	-1.9	--	-2.0	--	-2.8	DEG
2608469	ITPR1	-4.5	DEG	-3.8	DEG	0.2	--	2980449	PIP3-E	-2.8	DEG	-1.9	--	-1.2	--
3127385	PHYHIP	-4.5	DEG	-3.4	--	-0.7	--	3457891	GLS2	-2.8	DEG	-1.8	--	-0.2	--
3209726	ALDH1A1	-4.5	DEG	-3.5	--	-0.4	--	2553262	PSME4	-2.8	--	-2.6	DEG	-0.3	--
2929571	GRM1	-4.5	DEG	-4.0	--	-1.9	--	3097701	SNTG1	-2.8	DEG	-2.4	DEG	-0.6	--
3209060	TRPM3	-4.5	DEG	-3.9	--	-3.1	--	3183604	ZNF462	-1.1	--	-1.3	--	-2.8	DEG
2387126	RYR2	-4.5	--	-4.0	DEG	-0.3	--	2693409	ALDH1L1	-2.3	--	-2.8	DEG	-0.2	--
2855963	HCN1	-4.4	DEG	-4.1	DEG	-1.9	--	3307851	AFAP1L2	-2.8	--	-2.4	DEG	-0.2	--

Trans ID	Symbol	SHH-Ad CB		SHH- CB		SHH-MB2		Trans ID	Symbol	SHH-Ad CB		SHH- CB		SHH-MB2	
		FC	DEG	FC	DEG	FC	DEG			FC	DEG	FC	DEG	FC	DEG
3764527	39329	-4.4	DEG	-3.8	DEG	-0.9	--	3961023	CBX7	-2.8	DEG	-2.0	--	-0.8	--
2514969	GAD1	-4.4	--	-3.9	DEG	0.4	--	2374926	TMEM58	-2.7	--	-2.7	DEG	-0.3	--
2707045	PEX5L	-2.4	--	-2.2	--	-4.4	DEG	2656146	MAP3K13	-1.7	--	-2.1	--	-2.7	DEG
3127352	LGI3	-4.3	DEG	-4.0	DEG	-0.2	--	2996563	BMPEP	-2.7	DEG	-2.1	--	0.0	--
2622970	DOCK3	-4.3	--	-4.2	DEG	-3.1	DEG	3872380	ZNF154	-2.4	--	-2.5	DEG	-2.7	DEG
3239667	GAD2	-4.3	DEG	-3.3	DEG	0.2	--	3423301	NAV3	-2.6	--	-2.7	DEG	-0.5	--
3362159	NRIP3	-4.3	DEG	-3.4	--	-0.7	--	2893562	RREB1	0.5	--	0.1	--	-2.7	DEG
2444899	TNR	-4.3	--	-4.1	DEG	-0.8	--	2600089	PTPRN	-2.7	--	-2.2	--	-2.2	DEG
3173673	PIP5K1B	-4.3	DEG	-3.5	DEG	-0.5	--	2704143	WDR49	-2.7	--	-2.5	DEG	-0.4	--
2736060	GRID2	-4.3	DEG	-4.2	DEG	0.1	--	3758692	MPP2	-2.7	--	-2.5	DEG	-2.5	DEG
2836242	GRIA1	-4.3	DEG	-4.3	DEG	-1.9	--	3706659	ASPA	-2.7	DEG	-2.5	DEG	-0.3	--
2361635	BCAN	-3.8	--	-4.3	DEG	-1.2	--	3190420	CEECAM1	-2.7	--	-2.5	DEG	-1.6	--
2888399	SNCB	-4.3	--	-3.9	DEG	-0.4	--	3901296	CST3	-2.5	--	-2.6	DEG	-0.9	--
2460296	AGT	-4.3	DEG	-3.7	--	-1.1	--	3043895	SCRN1	-2.6	DEG	-2.2	--	-0.5	--
2451261	SYT2	-4.3	--	-3.6	DEG	0.1	--	3337042	KIAA1394	-2.4	DEG	-2.6	DEG	0.0	--
3793827	CNDP1	-4.2	DEG	-3.1	--	-0.5	--	3219030	---	0.0	--	-0.5	--	-2.6	DEG
3710505	LOC284033	-4.2	DEG	-4.2	--	-1.4	--	2933175	ZDHC14	-2.6	--	-2.3	DEG	-0.4	--
3353640	GRAMD1B	-4.2	DEG	-3.5	--	-3.2	--	2511045	GALNT13	-2.6	DEG	-1.8	--	1.0	--
2512790	SLC4A10	-4.2	DEG	-3.7	DEG	-2.3	DEG	3467351	ANKS1B	-2.6	DEG	-2.5	--	-2.1	--
2323172	IGSF21	-3.1	--	-2.7	--	-4.2	DEG	3307939	ABLIM1	-2.6	DEG	-2.0	--	0.3	--
3529467	CPNE6	-4.2	DEG	-3.1	--	-2.1	--	3286211	RASGEF1A	-2.6	DEG	-2.0	--	-0.8	--
3566176	OTX2	1.4	--	0.8	--	-4.2	DEG	2715749	GRK4	-2.6	DEG	-2.3	DEG	-1.9	DEG
3411721	CNTN1	-4.2	DEG	-3.9	--	-3.2	--	2364016	NOS1AP	-2.6	--	-2.4	DEG	-1.8	DEG
2439960	KCNJ10	-4.1	--	-3.6	DEG	-0.8	--	2740067	ANK2	-2.6	DEG	-2.2	--	0.0	--
3507199	FLT3	-4.1	DEG	-2.6	--	0.0	--	3907934	ZNF334	-1.6	--	-1.9	--	-2.6	DEG
2385873	KCNK1	-4.1	DEG	-3.4	--	-1.0	--	3831975	ZNF540	-2.6	--	-2.3	--	-2.0	DEG
2955691	DSCR1L1	-4.1	DEG	-3.2	--	-2.0	--	3155489	FAM135B	-2.6	DEG	-2.2	--	-1.6	--
3353417	CRTAM	-4.1	DEG	-2.5	--	0.0	--	3417249	ERBB3	-2.4	--	-2.5	DEG	0.0	--
3672059	KIAA0513	-4.0	DEG	-3.2	--	-1.5	--	3124333	C8orf5	-2.4	--	-2.5	DEG	-2.3	DEG
3184925	---	-4.0	DEG	-3.2	--	-1.1	--	2623426	ABHD14A	-2.1	--	-1.6	--	-2.5	DEG
3222534	ASTN2	-3.3	--	-3.1	--	-4.0	DEG	2705266	TNIK	-2.0	--	-2.3	--	-2.5	DEG
3184896	ZNF483	-4.0	DEG	-2.9	--	-1.0	--	3456212	MAP3K12	-2.5	--	-2.2	DEG	-0.1	--
2949772	PRRT1	-4.0	DEG	-3.2	--	-1.1	--	3190558	SPTAN1	-2.5	DEG	-2.3	--	-2.1	DEG
2438016	PAQR6	-3.9	DEG	-4.0	DEG	-0.5	--	3665049	FLJ37464	-2.5	--	-2.3	DEG	-1.6	--
2375038	GPR37L1	-4.0	DEG	-3.2	--	-0.5	--	2321607	FLJ43806	-2.4	--	-2.4	DEG	-0.4	--
2842255	CPLX2	-4.0	--	-3.7	DEG	-0.7	--	3200762	SLC24A2	-2.4	DEG	-2.1	--	-0.4	--
3347431	ELMOD1	-4.0	DEG	-3.3	DEG	-1.1	--	3074912	DGKI	-2.4	DEG	-2.4	--	0.2	--
2975741	MAP7	-4.0	DEG	-3.4	--	-0.8	--	3945781	SYNGR1	-2.4	--	-2.0	DEG	-1.1	--
3217242	GABBR2	-4.0	DEG	-3.6	--	-2.7	--	2711225	ATP13A4	-2.4	--	-2.4	DEG	-0.4	--
2607568	CHL1	-3.8	DEG	-4.0	--	-3.5	--	2765590	CENTD1	-2.3	--	-2.4	DEG	-0.2	--
3555736	NDRG2	-4.0	--	-3.8	DEG	-1.4	--	3726569	SPATA20	-2.4	--	-2.0	--	-2.3	DEG
3448088	BHLHB3	-4.0	DEG	-3.2	--	-1.2	--	3764399	RNF43	-2.3	--	-2.2	DEG	0.4	--
2703836	SLITRK3	-4.0	DEG	-3.8	--	-2.1	--	3721956	TUBG2	-2.3	--	-2.0	DEG	-0.6	--
3684039	CRYM	-3.9	DEG	-2.5	--	-0.1	--	2458513	TMEM63A	-2.2	--	-2.3	DEG	0.2	--
2616596	ARPP-21	-3.9	--	-3.6	DEG	-1.3	--	3036565	MMD2	-2.1	--	-2.3	--	-2.2	DEG
2874920	ACSL6	-3.9	DEG	-3.4	DEG	-1.9	--	3071459	LRRC4	-2.3	--	-1.9	--	-2.3	DEG
3249369	LRRTM3	-3.8	--	-3.9	DEG	-0.8	--	3906062	ZHX3	-2.3	--	-2.1	DEG	-1.2	--
2452478	LEMD1	-0.8	--	-0.7	--	-3.9	DEG	3758615	DUSP3	-2.3	--	-2.1	--	-1.8	DEG
2610972	SYN2	-3.9	--	-3.3	DEG	-2.4	DEG	3901696	ACSS1	-2.3	--	-2.3	DEG	-0.1	--
3910360	BCAS1	-3.6	--	-3.9	DEG	-0.4	--	3868557	SYT3	-2.3	--	-2.0	DEG	-0.3	--
3936224	SLC25A18	-3.6	--	-3.9	DEG	-0.7	--	3230610	ABCA2	-2.3	--	-2.0	DEG	-0.5	--
3258713	LGI1	-3.9	DEG	-3.0	--	-2.4	--	3846076	TLE2	-2.0	--	-1.9	--	-2.3	DEG

Trans ID	Symbol	SHH-Ad CB		SHH- CB		SHH-MB2		Trans ID	Symbol	SHH-Ad CB		SHH- CB		SHH-MB2	
		FC	DEG	FC	DEG	FC	DEG			FC	DEG	FC	DEG	FC	DEG
3733238	KCNJ16	-3.8	DEG	-2.9	--	-0.6	--	3715368	NLK	-0.4	--	-0.4	--	-2.3	DEG
2750753	TLL1	-3.8	DEG	-3.5	--	-2.3	--	3678369	ROGDI	-2.2	--	-2.1	--	-2.2	DEG
2733360	FGF5	-3.6	--	-3.8	DEG	1.2	--	3101629	ADHFE1	-2.1	--	-2.2	DEG	0.0	--
3604287	IL16	-3.8	--	-2.9	DEG	-0.1	--	2777333	PPM1K	-2.2	--	-1.9	DEG	-0.1	--
2662698	ATP2B2	-3.8	--	-3.2	DEG	-0.9	--	3230932	C9orf75	-2.1	--	-2.1	DEG	-1.0	DEG
3633699	NRG4	-3.7	DEG	-2.4	--	-0.8	--	2875454	39333	-2.1	--	-1.8	DEG	-1.1	--
3322521	KCNC1	-3.7	--	-3.1	DEG	-1.4	--	2884727	ATP10B	-2.0	--	-2.1	DEG	-0.4	--
2868265	LIX1	-3.5	--	-3.7	DEG	-0.7	--	2786567	OSAP	-2.1	DEG	-1.3	--	0.2	--
3148871	FLJ20366	-3.7	--	-2.9	DEG	0.6	--	2567447	TBC1D8	-1.3	--	-1.0	--	-2.1	DEG
3726618	CACNA1G	-3.7	DEG	-3.5	--	-3.2	DEG	3980643	DLG3	-0.9	--	-1.0	--	-2.1	DEG
3369366	SLC1A2	-3.7	--	-3.6	DEG	-1.6	--	3830961	APLP1	-2.0	--	-2.1	--	-1.8	DEG
3750723	UNC119	-1.1	--	-1.1	--	-3.7	DEG	3632492	NPTN	-2.1	DEG	-1.6	--	-0.8	--
2397600	C1orf126	-3.6	--	-3.0	DEG	0.0	--	3226138	AK1	-2.0	--	-1.7	--	-2.1	DEG
2636483	SIDT1	-3.6	--	-2.9	DEG	-0.2	--	3094778	TACC1	-2.1	--	-2.1	DEG	-0.9	--
3223157	DBC1	-3.6	DEG	-3.6	DEG	-2.7	DEG	2493858	MAL	-1.9	--	-2.1	DEG	0.1	--
2708203	MAP6D1	-3.6	DEG	-3.1	DEG	-0.5	--	4012178	CITED1	-0.2	--	0.0	--	-2.1	DEG
2734270	CDS1	-3.6	DEG	-2.8	--	-0.9	--	3777470	PTPRM	-2.1	--	-2.0	DEG	0.0	--
2945129	PRL	1.7	--	1.5	--	-3.6	DEG	3709244	CHD3	-0.2	--	-0.8	--	-2.0	DEG
3758640	MPP3	-3.0	--	-2.7	--	-3.6	DEG	2376457	PCTK3	-1.6	--	-2.0	DEG	-0.5	--
3868768	KLK6	-3.5	--	-3.5	DEG	-0.5	--	2431877	---	-2.0	--	-1.9	DEG	-0.2	--
2450865	CSRP1	-3.5	--	-3.3	DEG	-0.8	--	2675801	PCBP4	0.2	--	0.1	--	-2.0	DEG
2607757	CNTN6	-3.5	DEG	-3.1	--	-1.3	--	3893973	MYT1	-1.4	--	-1.4	--	-1.9	DEG
3064361	ACHE	-3.5	--	-3.1	--	-3.1	DEG	3185498	SLC31A2	-1.9	--	-1.7	DEG	-0.4	--
3011180	GRM3	-3.5	--	-3.2	DEG	-0.1	--	2351121	FAM40A	-1.9	--	-1.8	DEG	-0.3	--
3876245	SNAP25	-3.5	DEG	-2.5	--	-0.9	--	2682436	RYBP	0.0	--	-0.3	--	-1.9	DEG
2463567	PLD5	-3.5	DEG	-3.5	DEG	-0.9	--	3567243	C14orf39	0.0	--	0.0	--	-1.8	DEG
3690747	CBLN1	-3.5	DEG	-3.1	--	-0.6	--	2327817	PTPRU	-1.8	--	-1.6	--	-1.7	DEG
3032647	DPP6	-3.5	DEG	-3.4	--	-2.6	--	3740367	SLC43A2	-1.8	--	-1.7	DEG	-1.4	DEG
3601931	CPLX3	-0.9	--	-0.3	--	-3.5	DEG	3947258	WBP2NL	-1.8	--	-1.8	DEG	-1.3	DEG
3886867	DBNDD2	-3.5	--	-3.0	DEG	-0.3	--	2711205	ATP13A4	-1.7	--	-1.8	DEG	-0.4	--
2880051	PPP2R2B	-3.5	--	-3.4	--	-3.1	DEG	3720695	THRA	-1.8	--	-1.8	--	-1.7	DEG
3124227	XKR6	-3.5	--	-3.3	DEG	-2.0	--	3872398	ZNF671	-1.6	--	-1.6	--	-1.7	DEG
2648991	KCNAB1	-3.4	DEG	-2.8	--	-1.1	--	3751323	TIAF1	-1.7	--	-1.5	--	-1.5	DEG
2941632	MAK	-0.2	--	-0.3	--	-3.4	DEG	3972657	IL1RAPL1	-1.4	--	-1.6	DEG	0.3	--
3884830	PPP1R16B	-3.3	DEG	-3.0	DEG	0.1	--	3221395	ALAD	-1.6	--	-1.4	--	-1.4	DEG
3545634	NRXN3	-3.2	DEG	-3.3	--	-1.3	--	3719210	MRM1	-1.1	--	-0.9	--	-1.6	DEG
2827299	MEGF10	-3.2	--	-3.3	DEG	-0.5	--	3553337	TRAF3	-0.9	--	-0.9	--	-1.5	DEG
3755790	NEUROD2	-2.6	--	-2.5	--	-3.3	DEG	2787459	INPP4B	-1.4	--	-1.5	DEG	0.2	--
3549605	KIAA1622	-3.3	DEG	-2.5	--	-0.3	--	2331213	MACF1	-1.4	--	-1.5	--	-1.4	DEG
3059258	PCLO	-3.3	--	-2.9	DEG	-1.8	--	3677612	ZNF597	-1.1	--	-0.9	--	-1.4	DEG
3029900	CNTNAP2	-2.8	DEG	-3.3	--	-1.4	--	2708720	EIF2S2	-0.9	--	-0.8	--	-1.4	DEG
3504213	GJB6	-3.3	--	-3.2	DEG	-0.2	--	3350775	SIDT2	-1.4	--	-1.4	DEG	-0.3	--
3300242	CPEB3	-3.3	DEG	-2.8	--	-1.9	--	3720402	ERBB2	-1.2	--	-1.4	--	-1.3	DEG
3173974	C9orf61	-3.0	--	-3.2	DEG	-0.6	--	3872370	---	-1.0	--	-1.1	--	-1.4	DEG
2725977	GABRB1	-3.2	DEG	-3.1	--	-1.1	--	2340819	TCTEX1D1	-1.1	--	-1.3	DEG	-0.1	--
2975014	SGK	-1.7	--	-2.0	--	-3.2	DEG	3189864	LRSAM1	-1.2	--	-1.1	--	-1.0	DEG
2672821	CSPG5	-2.1	--	-2.0	--	-3.2	DEG	3432798	SDSL	-0.1	--	-0.2	--	-1.2	DEG
3033127	HTR5A	-3.2	DEG	-2.3	--	-1.6	--	3770699	MIF4GD	-0.6	--	-0.7	--	-1.2	DEG
2865390	EDIL3	-2.6	--	-2.6	--	-3.2	DEG	3751121	FLOT2	-0.6	--	-0.5	--	-1.1	DEG
3989448	GRIA3	-3.2	DEG	-3.2	DEG	-0.3	--	3228621	SURF6	-0.4	--	-0.3	--	-1.1	DEG

Ad CB, adult cerebellum; CB, cerebellum (including adult and fetal samples); FC, fold change in gene expression; DEG, differentially expressed gene.